博士論文

Prediction for shallow landslides based on time history of tilting of slope surface

(斜面表層の傾斜の経時変化に基づく浅層すべりの予測)

By
Jiren Xie

謝　済仁

June, 2018

Department of Civil Engineering
The University of Toky

ABSTRACT

Landslide disasters, which are mainly caused by heavy rainfalls and strong earthquakes, are the major threat to human lives and infrastructures. Every year thousands of fatalities and billions in property are damaged by landslide disasters. The huge economic losses and casualties associated with landslide disasters led to research on prevention and mitigation of landslides. Nowadays, retaining walls and ground anchors which improve the factor of safety against failure, have been widely used as typical methods to prevent slope failures. However, these methods are highly cost, and not suitable for a large number of slopes with potential risk of failure. Currently, landslide early warning systems using inclinometers, tilt sensors, extensimeters, or other monitoring equipements, have been developed and considered as promising methods to reduce the risk of damage in human as well as properties caused by landslides. In these systems, the tilting of slope surface monitoring systems using tilt sensors with lower-cost and easier installation, are widely used in landslide monitoring. However, the method for landslide occurrence prediction based on tilting behavior of slope surface is still under consideration.

Nowadays, the most of landslide predicting methods are based on the relationship between the rate of displacement and duration time before failure, which was approached from the creep tests and model tests under constant rainfall intensity. In recent decades, from the existing monitoring data of slope surface measured by extensometers and tilt sensors respectively, a similar trend has been observed between surface displacement and tilting angle against time after the onset of slope sliding, but there is limited research have been done to explore this trend. This study attempts to investigate the relationship between the surface displacement and tilting angle, and then develop a new method for landslide occurrence prediction based on time history of tilting of slope surface. Laboratory model tests, with pre-defined slipe surfaces as well as with different testing materials, were conducted under different triggering factors for slope failure and using tilt sensors attached to various lengths of rods. In small-scaled model tests, the slope failure was induced by tilting the container or applying the

artificial rainfall. In the tests, the displacement and the tilting angle of the slope were measured. Additionally, field tests were also carried out. In field tests, the extensometers were used for the displacement monitoring and the tilting sensors with different length of steel rods were employed for measuring the tilting angle of slopes. The test results from the model tests and the field tests show that tilt sensors with no rods or short rods located above the slip surface will tilt backward while the tilt sensors will tilt forward if the rods of tilt sensors reaching the slip surface. Furthermore, a linear relationship between the displacement and tilting angle of slopes was found from the results in model tests as well as in field tests. By substituting the relationship between the displacement and tilting angle of slopes into the existing landslide prediction method based on the rate of displacement, a new method for landslide occurrence prediction is proposed utilizing the time history of tilting of slope. This new proposed method was validated by model tests as well as field tests. This method was also used for a real-time slope monitoring, and the result shows that this method has practical importance.

Keywords: Landslide monitoring; relationship; displacement; tilting; prediction.

ACKNOWLEDGEMENTS

I would like to express my greatest thanks to Uchimura sensei, my PhD research supervisor, who sacrificed a lot of spare time to guide me, and it is impossible to finish my PhD research without him. The well-directed research freedom provided by him always encouraged me to think out of the box and try innovative options. Our long and stimulating discussions not only helped me improve my research but also helped nourishing my critical thinking abilities. I still remember last year we spent 8 hours on our discussion from the morning to the the evening, and dear "Sensei", thank you very much from the core of my heart.

My appreciation and gratitude is extended to Koseki sensei, who gave me the chance to be a PhD student of Tokyo University and also gave me constructive comments and good suggestions on my research in general and this thesis in particular.

I would also express my gratitude to Kuwano sensei, Kiyota sensei and Wang sensei from Kyoto University, who gave me good suggestions on my research and took time out of their busy schedules to be part of the evaluation committee.

I want to show my appreciation to Dr. Huang Dong from Institute of Mountain Hazards and Environment, as well as Dr. Wang Lin from Chuo Kai Hatsu Corporation, thanks for your help and suggestions. I also want to thanks Sato sensei, Kyokawa sensei, Dr. Zhao Chuang, Dr. Yu Fangwei, Dr. Lin Wenli, Dr. Liu Weichen, Dr. Tao Shangning, and other memembers in the lab. Thanks for Hema san from Sri Lanka, Konno san from Saitama University, Dr. Shen Quan, Master Chen Pan, Master Liu Jiapeng, Master Xie Canrong, Dr. Lei Wenkai, Dr. Dong pengyuan and the other people gave me help in model tests or field tests. Great appreciation and gratitude also extended to my Host family, Miyazaki san, who gave me much help and encouragement in the past three years.

Finally, I want to thanks my family, expecially for my wife, He Libin. Without your

understanding and believing in me, I could not go through the long journey. Thanks for love, which motivates me to overcome the difficulties, and thanks for standing by my side, which give me the confidence and power to solve the problems I confronted. Thanks for my parents, grandparents, and other relatives, thanks for you unconditional love and care, which makes me what I am today.

The scholarship funded by the Chinese Scholarship Council (CSC) China for my research and life in past three years at the University of Tokyo, is also appreciated.

Contents

Lists of Figures

Lists of Tables

Chapter 1
DISSERTATION OVERVIEW

1.1. Introduction

Landslide disasters caused by heavy rainfall and strong earthquakes, are major threat to human lives and infrastructures, and mainly happen in Asian area, as shown in Fig. 1-1. Thousands of fatalities and billions in property losses are caused by landslide disasters (Petley 2012, Keefer et al. 1987, Lee 2009) every year. Fig. 1-2 and Fig. 1-3 show serious damage to human habitate and infrastructures, which was caused by landslides.

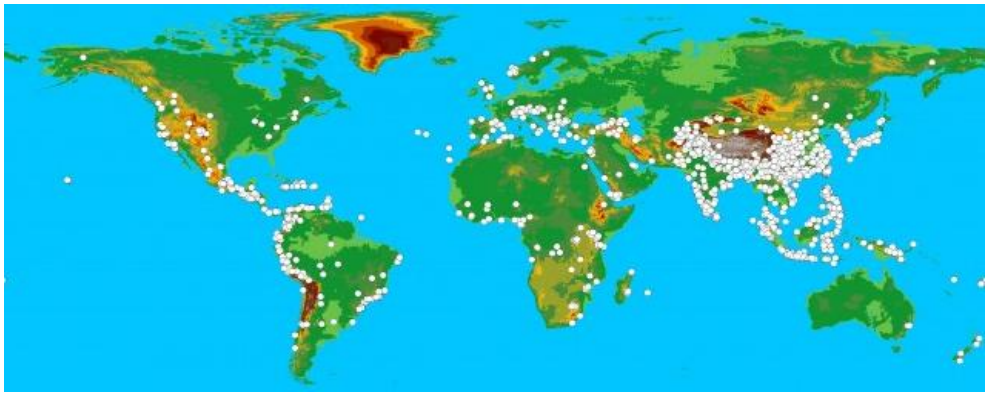

Fig. 1-1 The distribution of landslides happened during 2004 to 2012 (after Peltey, 2012)

Fig. 1-2 A landslides happened in Conchita, CA (after USGS, 2005)

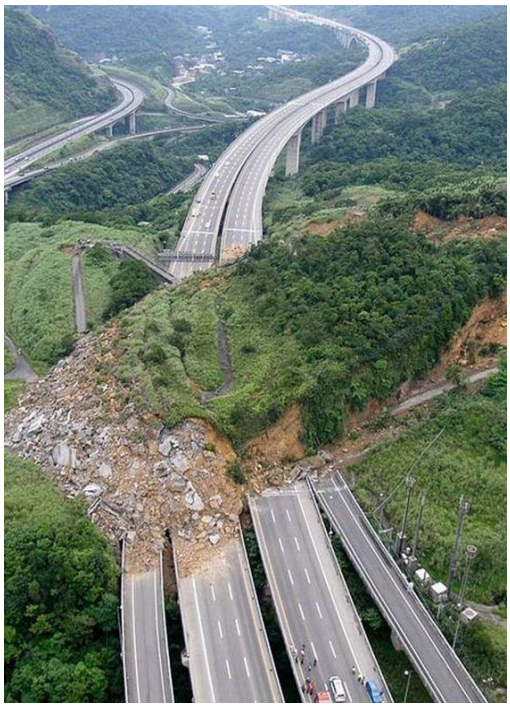

Fig. 1-3 Roads damaged by a massive landslide in Taiwan (after American Geophysical Union)

Huge economic losses and casualties associated with landslide disasters led to research on prevention and mitigation of landslides. Nowadays, typical counter-measures to prevent landslides, including retaining walls and ground anchors, which improve the factor of safety against failure, have been widely used (Uchimura et al. 2010). However, those methods are not suitable for some slopes with potential

risk of landslides due to the high cost.

In recent years, different types of early warning systems for landslides have been developed to avoid, or at least to minimize losses of human lives and damage to property. For example, based on a relation between rainfall intensity and landslides risks, some landslide warning systems were proposed to measure the precipitation or storm events in a large area(Keefer, 1987; Okada, 2001, Osanai et al., 2010), as shown in Fig. 1-4. These systems predict the likelihood of potential landslides in a region relatively well, but the systems are not effective to predict the slope failure for individual slope in the region because the relationship between rainfall intensity and risks of individual landslide are unclear.

Slope surface movement, or displacement, is one of the important items commonly monitored in individual slope. GPS and remote sensing with radar technology, such as InSar system, have beem employed in monitoring the long-term displacement on slope surface in wide areas (Casagli et al., 2010), as shown in Fig. 1-5.

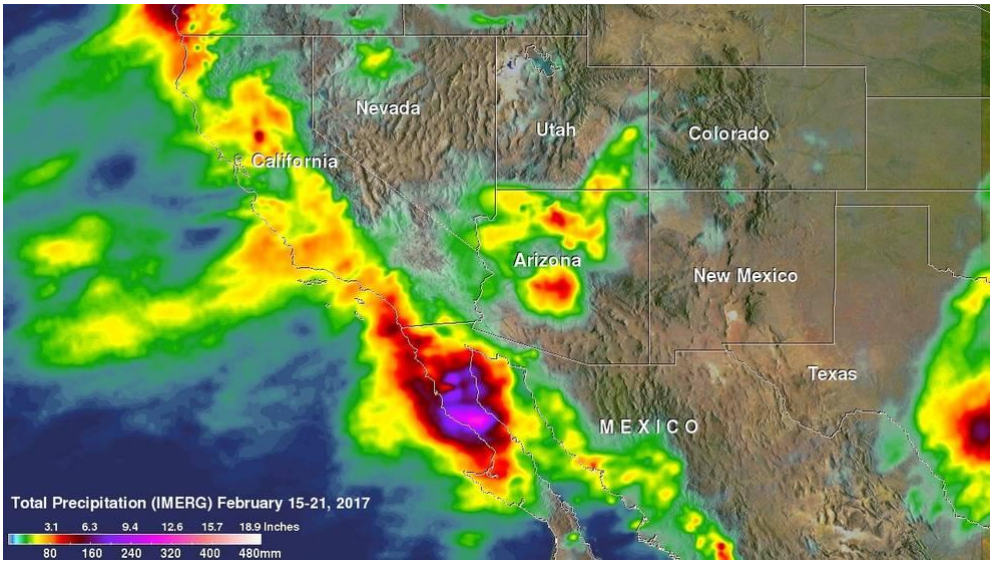

Fig. 1-4 The distribution of Precipitation (after IMERG)

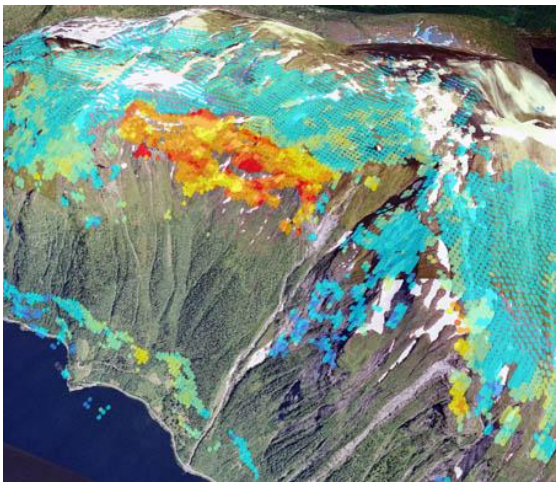

Fig.1-5 The surface displacement of slopes monitored by Satellite(after NGU, 2014)

However, those systems are with low resolution around 5-10mm, and are insufficient to detect pre-failure stage of landslides. Furthermore, those systems are high cost, and are also not suitable for some slopes with vegetation on the slope surfaces. Nowadays, extensometers are the widely-used equipment for monitoring the displacement along a slope surface(Fig. 1-6). Although extensometers are less costly than the typical counter-measures to prevent the slope failure and those surface displacement monitoring systems using satallites or radars, there are still some problems existed. For example, the stable part in slopes to install extensometers can not be decided exactly. In addition, skilled engineer are required for the installation and operation of the extensometers.

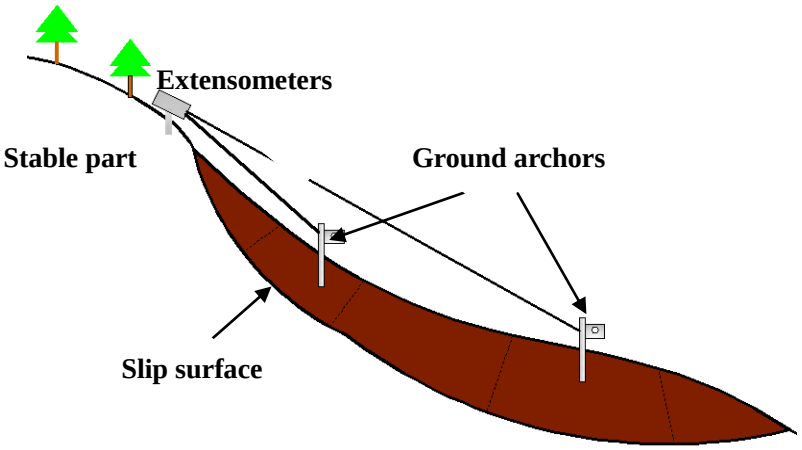

Fig.1-6 The illustration of extensometers exploited in slope monitoring

In last two decades, with the rapid development of sensing, computing, and communication technologies, simple monitoring systems using Micro Electro

Mechanical Systems (MEMS) technology have been designed to measure the tilt angles (rotations) in the unstable surface layer of slopes, and detect the pre-failure stages of slope failures in shallow landslides(Uchimura et al., 2008, Lee, 2009). The illustration of tilt sensors implication is presented in Fig. 1-7. The tilt sensors are inserted into slopes with steel rods ranging from 0.5 m to 1 m. Tilting angles of slopes observed by these tilt sensors are sent to a data logger continuously. It has been reported that the tilting angle monitoring systems can detect the pre-failure behaviour in some landslides(Towhata et al., 2005, Lee, 2009, Uchimura et al., 2015).

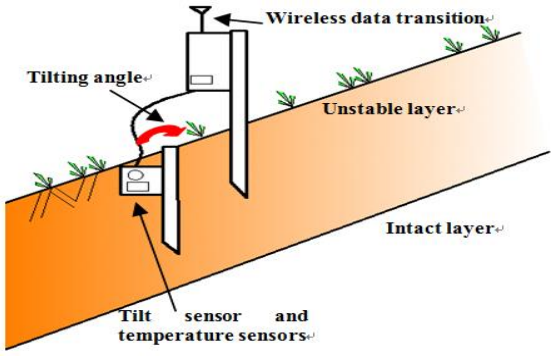

Fig. 1-7 The illustration of tilt sensors exploited in slope monitoring

1.2. Problem statement

It is reported that triggering factors for slope failure can not be identitied precisely for individual slope, and the surface deformation, comsisting of surface displacement and tilting of slope surface, which may be induced by various factors, such as ground water level change, pore water pressure change, or soil dilitancy along the slip surface of slopes and so on, are considered as important indexs in many slopes before the catastrophic failure.

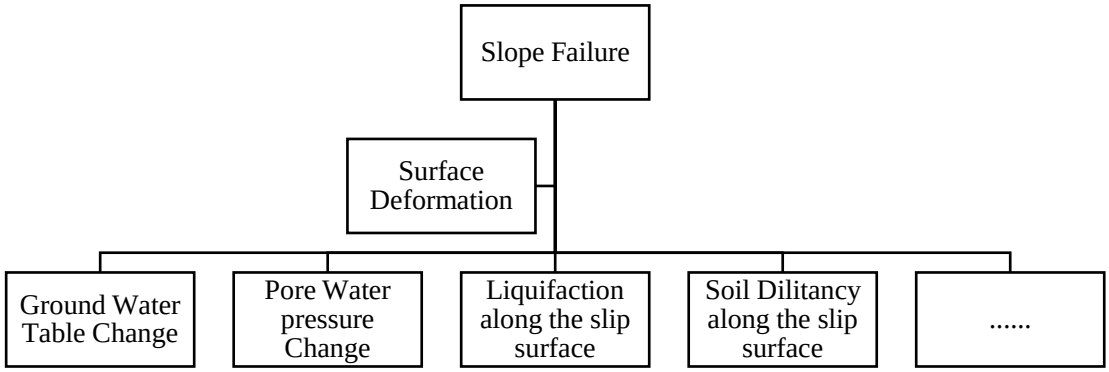

Fig. 1-8 The various triggering factors of landslides

In terms of surface displacement monitoring systems, the rate of displacement is often used as an index to define the threshold of warning, which varies for individual slope. Thresholds of warning for each slope determined by engineers based on their experiences, and the thresholds were set to be several mm/day for caution and mm/hour for evacuation (Maruyama and Kozima, 1994). The reliability of the thresholds for landslide warning is low due to the insufficient evidence and poor scientific background.

Instead of adopting threshold values of the rate of displacement for landslide early warning, Saito (1965), Fukuzono (1985), and Voight (1989) developed a more advanced empirical forecasting method to predict the timing of catastrophic failures based on the monitored time history of the displacement on the slope surface. Successful applications of these methods can be found in many literatures(Rose and Hungr, 2007, Casagli et al., 2009, and Gigli et al., 2011). The expression of this method is shown in equation 1-1,

$$\frac{d\Omega}{dt} = \left[A \cdot (\alpha - 1)\right]^{\frac{-1}{\alpha-1}} (t_R - t)^{\frac{-1}{\alpha-1}} \tag{1-1}$$

Where Ω is the surface displacement of slopes, $\frac{d\Omega}{dt}$ represents for the first derivatives of Ω . A and α are constant parameters, while t and t_R are the current time and rupture time respectively. Equation 1-1 can be rewritten as

$$\frac{dt}{d\Omega} = \left[A \cdot (\alpha - 1)\right]^{\frac{1}{\alpha-1}} (t_R - t)^{\frac{1}{\alpha-1}} \tag{1-2}$$

Equation 1-2 indicates that the relationship between inverse rate of displacement and duration time. Timming of landslides can be forecasted by plotting the inverse rate of displacement against time, as shown in Fig. 1-9. When the inverse rate is equal to 0, the slope failure time can be approached.

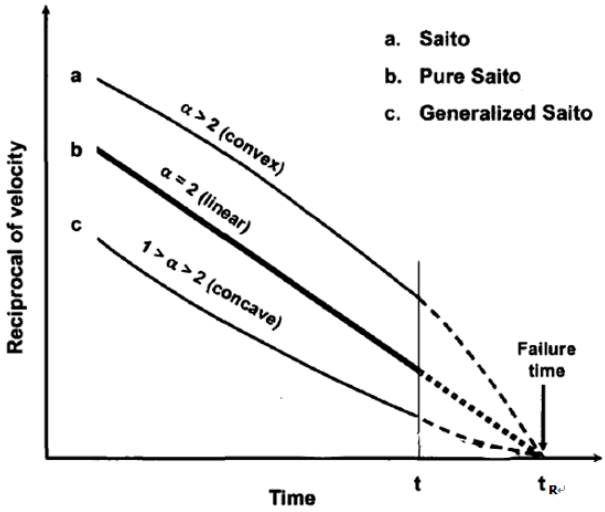

Fig. 1-9 The inverse rate of displacement against time(after Fukuzono, 1985)

On the other hand, as for the warning criteria for landslides using tilting angle monitoring systems, Uchimura proposed that the precaution of landslides should be issued when the tilting rate exceeds 0.01 ^{o}/h, while the warning should be issued when the tilting rate larger than 0.1 ^{o}/h. These special tilting rates for precaution and warning are proposed based on a limited number of cases, without considering the time history of tilting for individual slope(Uchimura et al., 2015). Additionally, this criteria for the early warning of landslide is conservative, and more studies should be carried out to investigate the slope failure using the tilting of slopes.

1.3. Objectives

Although tilting angle monitoring systems are with simple installation and lower-cost, the predicting methods for landslides using tilting angle are still under consideration. In this study, landslide predicting methods based on time history of tilting angle of slopes are explored. To propose a new landslide predicting method with tilting angle, three sub-objectives are investigated by labotary tests as well as field tests. These three sub-objectives are listed as below,

1) The tilting directions of tilt sensors are investigated.
2) The relationship between surface displacement of slopes and tilting angle are investigated.
3) A new method to forecast landslides based on time history of tilting of slopes is investigated.

1.4. Dissertation organization

This dissertation is organized into 8 chapters. The following briefly summarizes the content included in each of the remaining chapters.

Chapter 2 is an overview of past work related to the research topic: landslide hazard, landslide monitoring, and landslide prediction.

Chapter 3 presents details about soil materials and experimental set up.

Chapter 4 presents the methodology of labotary tests and field tests

Chapter 5 presents the test results about the tilting direction investigation

Chapter 6 presents the tests results about the relationship investigation between surface displacement and tilting angle of slope

Chapter 7 presents a new prediction method for shallow landslides based on time history of tilting of slope surface, and then the validation of this method against labotary tests as well as field tests is carried out. In addition, the the influence caused by rainfall intensity and other factors on this method, as well as the limitation of the new method are also discussed. Furthermore, a complementary method for landslide warning based on statistic study is also proposed.

Chapter 8 presents conclusions and recommendations for future research.

1.5. References

Casagli, N., Catani, F., Del Ventisette, C., Luzi, G. (2010). "Monitoring, prediction, and early warning using ground-based radar interferometry." Landslides, 7(3), 291–301.

Petley, D. N. (2012). "Global patterns of loss of life from landslides." Geology, 40,

927-930.

Fukuzono, T. (1985). "A new method for predicting the failure time of a slope." International Conference and Field Workshop on Landslides, Tokyo, 145-150.

Gigli, G., Fanti, R., Canuti, P., Casagli, N. (2011). "Integration of advanced monitoring and numerical modeling techniques for the complete risk scenario analysis of rockslides: the case of Mt. Beni (Florence Italy)." Engineering Geology, 120, 48-59.

Lee, J. M. S. (2009). "Real-time monitoring of landslides using wireless network." Doctor dissertation, The Ohio State University.

Keefer, D. K., Wilson, R. C., Mark, R. K., Brab, E. E., Brown, W. M., Ellen, S. D., Harp, E. L., Wieczorek, G. F., Alger, C. S. and Zatkin, R. S. (1987). "Real-time landslide warning during heavy rainfall." Science, 238, 921-925.

Maruyama, K., Kozima, S. (1994). "A proposal of the warning criterion for the landslide crisis depended on the observation data of sliding distance." J. Japan Landslide Soc., 31 (1), 45-51.(in Japanese)

Okada, K. (2001). "Soil water index." Sokko-Jiho, Japan Meteorological Agency, 69-567-100 .(in Japanese)

Osanai, N., Shimizu, T., Kuramoto, K., Kojima, S., & Noro, T. (2010). "Japanese early-warning for debris flows and slope failure using rainfall indices with Radial Basis Function Network." Landslides, 7(3), 325-338.

Rose, N. D., Hungr, O. (2007). "Forecasting potential rock slope failure in open pit mines using the inverse-velocity method." International Journal of Rock Mechanics and Mining Science, 44, 308-3

Saito M. (1965). "Forecasting the time of occurrence of a slope failure." Proceedings of the Sixth International Conference on Soil mechanics and Foundation Engineering, 537-541.

Towhata I., Uchimura T., Gallage C., On early detection and warning against rainfall-induced landslide, Proc. of The First General Assembly and The Fourth Session of Board of Representatives of the International Consortium on Landslides (ICL).Springer, Washington, DC (2005), pp. 133–139.

Uchimura T., Towhata I., Wang L., Nishie S., Yamaguchi H., Seko I. and Qiao J. (2015). "Precaution and early warning of surface failure of slopes by using tilt sensors." Soil and Foundation, 55(5), 1086-1099.

Uchimura T., Towhata I., Trinh T. L., Fukuda, J., Carlos, J. B. B., Lin, W., Seko, I., Uchida T., Matsuoka, A., Yosuke I., Onda, Y., Iwagami, S., Min-Seok K., Sakai, N. (2010). "Simple monitoring method for precaution of landslides watching tilting and water contents on slopes surface." Landslides, 7, 351-357.

Uchimura T., Towhata I., Wang L., Seko I. (2008). "Simple and low-cost wireless monitoring units for slope failure." Proc. of the First World Landslide Forum, International Consortium on Landslides (ICL), Tokyo, 611–614.

Voight, B. (1989). "A relation to describe rate-dependent material failure." Science, 246, 200-203.

CHAPTER 2

LITERATURE REVIEW

2.1. Introduction

In this chapter, a brief overview of published research works related to landslides is presented, and the definition of landslides, the triggering factors for the landslide disasters, as well as the mechanism of landslides are also discussed. Furthermore, the countermeasures to prevent the landslides, and the early-warning methods for slope failure to mitigate the risk of damage for lives as well as infrastructures are studied. Additionally, limitation of these methods are also discussed in the following sections. Then, the slope tilting angle monitoring systems which have been developed in recent decades, are introduced. Even though those monitoring systems have been used in slope failure monitoring due to the simple installation and low-cost, there are some problems existed, for example, how to predict the slope failure time based on the time history of tilting. The core of this study is to understand the pre-failure tilting behaviors of landslides, and develop a method for landslide predition based on the time history of tilting of slope surface.

2.2. Landslide definition and classification

The term landslide is widely used, which is known as a landslip, such as sliding of slopes. Landslide also has been used as an allinclusive term for almost all varieties of slope movements, including some that involve little or no true sliding(David, 1958).

Landslides can be classified in many ways with different emphasis on features

pertinent to recognition, avoidance, control, correction, and other purposes. Among these classifications, criteria for classifying the landslides is depending on type of movement, kind of material, rate of movement, geometry of the area of failure and the resulting deposit, age, causes, degree of disruption of the displaced mass, relation or lack of relation of slide geometry to geologic structure, degree of development, geographic locations, and state of activity(David, 1958). The primary types of landslides based on the slope movements can be divided into five groups, including falls, topples, slides, spreads and flows. In this study, the sliding slope failures, which have been subdivided into rotational slides and translational or planar slides, as shown in Fig. 2-1, are investigated.

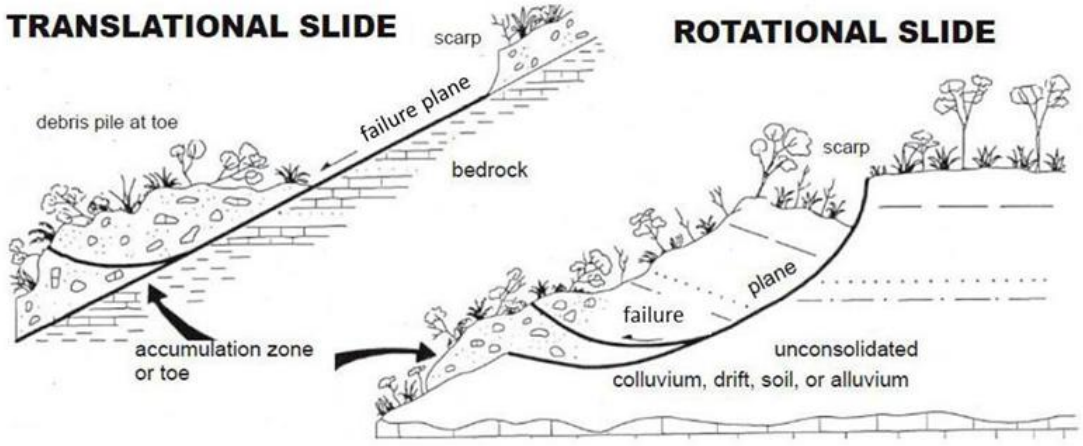

Fig. 2-1 Illustration for rotational and translational slope failure

The rotational landslides normally slide along the slip surface of a slope that is curved concavely upward, and in many rotational slope failure, the underlying slip surface of slope is always together with exposed spoon-shaped scarps, as shown in Fig. 2-2a. If the slide extends for a considerable distance along the slope perpendicular to the direction of movement, the unstable block is more or less rotational about an axis that is parallel to the slope (Fig. 2-2b).

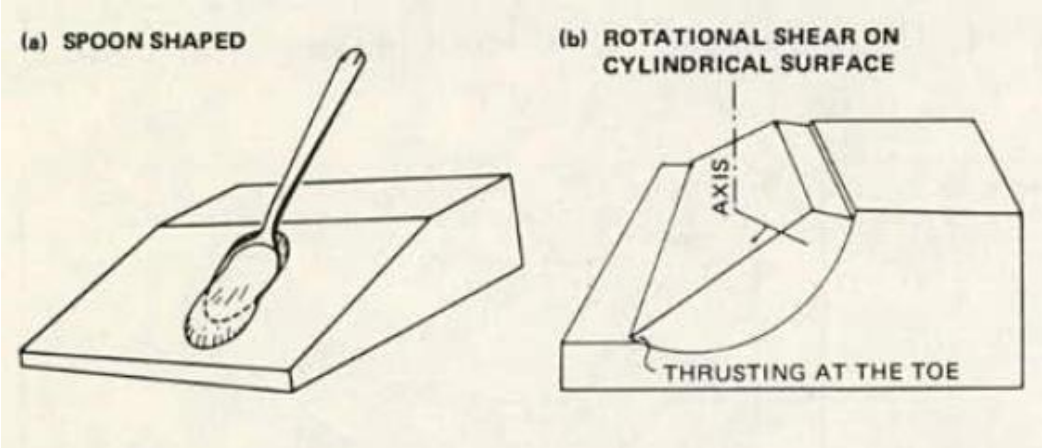

Fig. 2-2 Illustration of rotational slope failure (after David, 1958)

The rotational landslips occur most frequently in fairly homogeneous materials, such as hogomeneous slopes, constructed embankments as well as fills (Fig. 2-3).

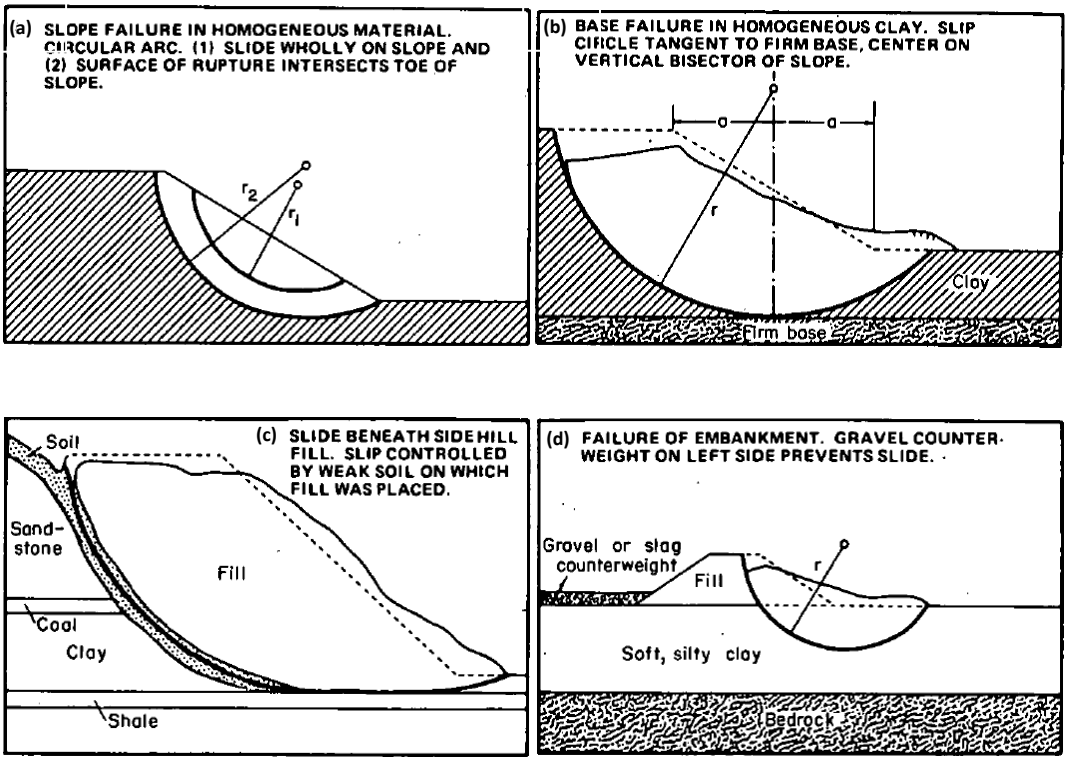

Fig. 2-3 Rotational landslides in homogeneous materials (after David, 1958)

On the other hand, in translational landslides, the unstable mass slides along a planar or gently undulatory surface with little rotary movement or tilting, and the sliding mass commonly moves out parallel to the original slope surface, which is distinctive to rotational landslides. The movement of translational slides is commonly controlled by weak layers, such as existing slip surfaces, faults, bedding planes, and so on.

Fig. 2-4 shows the field events of a translational landslides.

Fig. 2-4 Field events of translational landslides

2.3. The definition of slope failure

There are many definitions of slope failure. One concept is that slope failure can be defined as the beginning point of the accelerating stage of slope movement(Singh et al., 1969，Finn et al., 1973). However, this definition has not been approved by all means. For example, in cases of soil slopes, usually there remains a long duration time and large movement before failure after passing the point when slopes begin to move acceleratively. It is not reasonable to abandon the tertiary stage as failure zone.

Petley also proposed a concept to define the slope failure based on the variation of the factor of safety in a slope, as shown in Fig. 2-5.

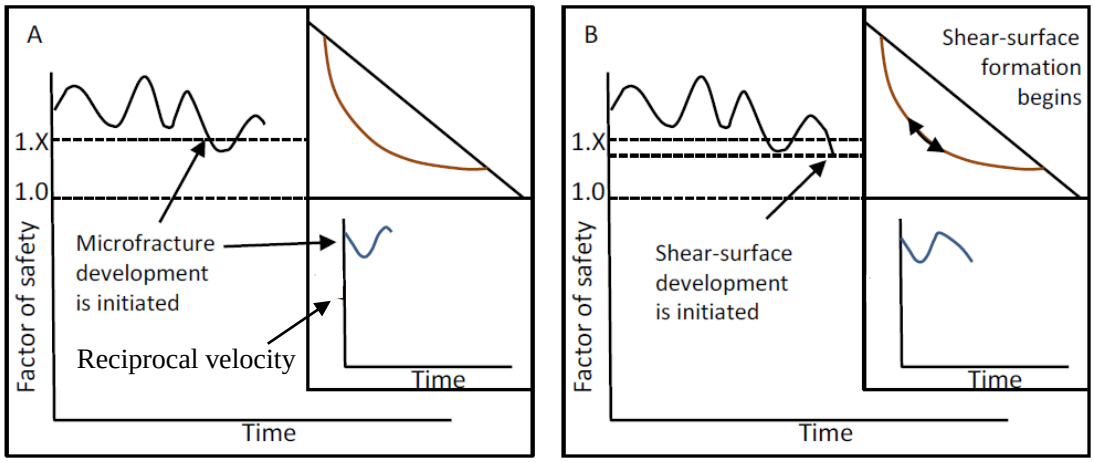

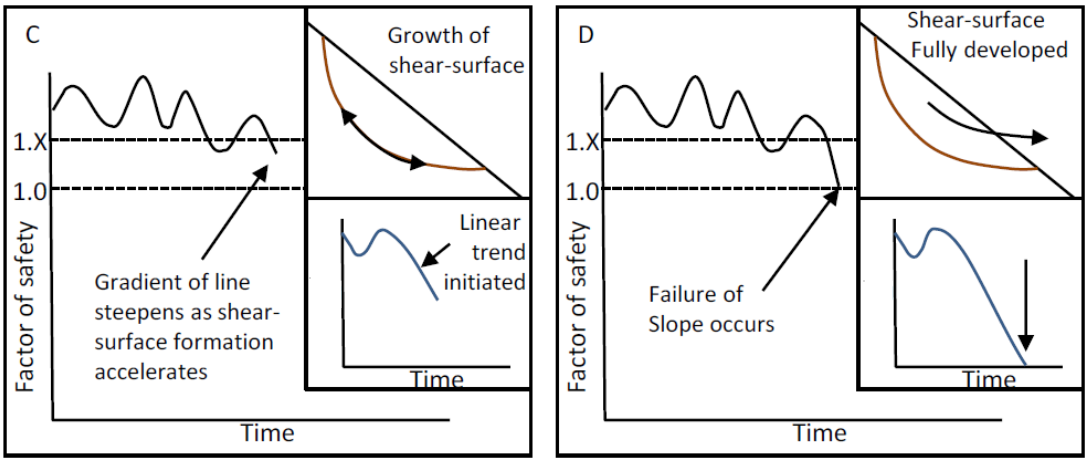

Fig. 2-5 Definition of slope failure considering the change in factor of safety (after Petley et al., 2005)

However, there is a contradiction existed in this definition. According to this definition, the factor of safety is larger than 1 after a linear trend between reciprocal velocity and time initiated (Fig. 2-5c), and the safety factor approaches to 1 when the reciprocal velocity close to 0. On the other hand, with the decrease of reciprocal velocity against time, the velocity increases, which results from the acceleration along the slip surface. The occurrence of acceleration is contradictory to the case that the factor of safety defined as the ratio between shear strength and shear stress along the slip surface of a slope, is always large than 1 in the whole slope failing process.

A very clear definition of slope failure which has been widely accepted is that, the slope failure is defined as the point when a slope slides at a very large velocity, as it is presented in Fig. 2-6,

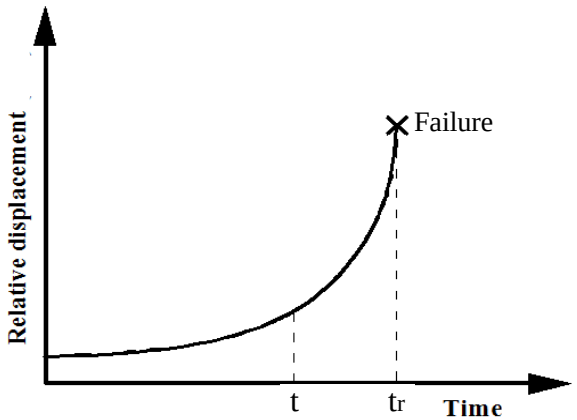

Fig. 2-6 Schematic representions of slope failure

2.4. Triggering factors of landslides

Landslides can be induced by many factors, such as earthquakes, heavy rainfall, volcano eruptions, and so on, among these factors, heavy rainfall is the major causative driving factor for the occurrence of landslides based on the statistical study on 19,035 cases of landslides between 1972 and 2007 in Japan (Osanai et al, 2009). In this statistical study, it was reported that 93% of those landslides were caused by heavy rainfall, and most of them were shallow surface landslides with a average deepth of slip surface less than 1.2 m.

For rainfall induced landslides, the infiltration of rainwater into steep and marginally static slopes which may consist of different types of soils, such as colluvial and residual soils, may be the main reason for slope failure(Tsukamoto et al., 1998). Landslides are produced when the balance between the shear strength of the slope material and the downslope component of the gravitational force imposed by the weight of slope material above a potential slip surface can not be sustained during the rainwater infiltration(Keefer et al., 1987). On the other hand, some researchers assume that, during or after several cycles of heavy rainfalls, the initial stress state in the slope may be quite close to failure, and even a small driving forece can cause failure. The stress state is governed by several numbers of factors such as slope angle, depth, unit weight of soil and so on(Anderson et al., 1991; Anderson et al., 1995).

2.5. Mechanism of rainfall-induced landslides

With a review of published research works related to the mechanism of rainfall-induced slope failure (Anderson et al., 1995; Farooq, et al., 2004; Brand, 1981), it is widely assumed that the slope failure induced by rainfall is because of reduction of matric suction with the water content of soil increasing during the rainwater infiltrating. The relationship between water content and matric suction is usually described by the soil-water characteristic curve(Fig. 2-7).

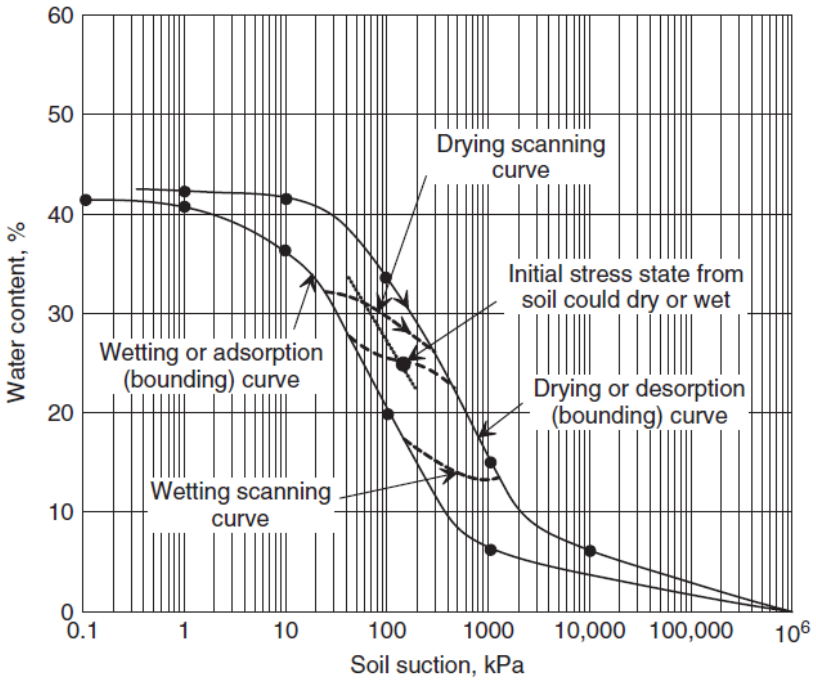

Fig. 2-7 Soil-Water characteristic curve (after Fredlund, 2003)

There are various fitting equations for this correlation between the water content and soil suction, and the formular presented by Van Genuchten (1980) has been widely used.

$$\frac{\theta}{\theta_s}=\left[\frac{1}{1+(\alpha\psi)^n}\right]^m \tag{2-1}$$

Where θ and θ_s are the water content and saturated water contents respectively; α, n and m are empirical parameters; ψ is the soil suction value.

The state of stress in unsaturated soil, which is fundamentally different from the state of stress in saturated soil, can be expressed by following equation,

$$\sigma'=(\sigma-u_a)-\chi(u_a-u_w) \tag{2-2}$$

Where σ' is the effective interparticle stress; σ is total stress; u_a and u_w are pore air pressure and pore water pressure respectively, and χ is a material property related to the degree of saturation or matric suction.

With the increase of saturation degree, the failure envelope will shrink in the Se-p-q space as shown in Fig. 2-8.

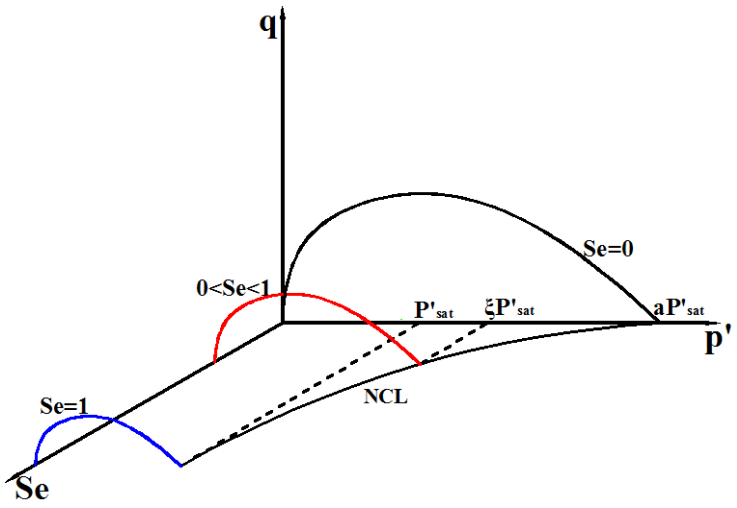

Fig. 2-8 The failure envelope for unsaturated soil in Se-p-q space

Where p' and q mean the effective normal stress and deviator stress. Se represents for the effective saturation, which is expressed by following equation:

$$S_e = \frac{\theta - \theta_r}{\theta_s - \theta_r} \tag{2-3}$$

Where θ and θ_s are the water content and saturated water contents, and θ_r is the resident soil water contents.

When the rainwater infiltrating into slope, shear strength of materials decreases with the increase of water content. Furthermore, the rainwater also makes the weight of unstable parts in slopes increase, which causes the shear stress acting on the potential slip surface of slopes rising. Once the stress balance at the slip surface can not be sustained, the slope will slides along the slip surface of slopes.

Some other researchers proposed that the triggering mechanism of rainfall-induced landslides on shallow hillslopes is attributed to the increase of positive pore water pressure(Terlien,1998). On a natural soil slope during the rainfall, the shear stress is approximately constant, while shear strength decreases due to the reduction of normal effective stress of the slope materials acting on a potential shear surface, which is caused by the increase of pore pressure as a result of rainfall infiltration progressively, and eventually the landslide is produced. This failure mode is also expressed by using the Mohr-Coulomb failure envelope (Fig. 2-9).

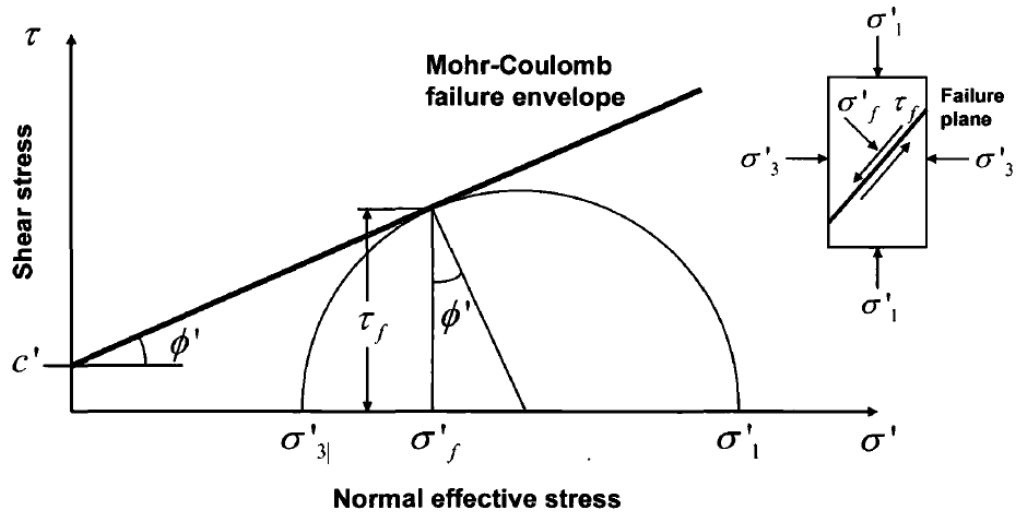

Fig. 2-9 Stress conditions at failure (after Craig, 1997)

2.6.Typical countermeasures for landslide disasters mitigation

Nowadays, typical countermeasures, such as retaining walls and ground anchors in Fig. 2-10 which improve the factor of safety against failure have been widely used to prevent slope failures.

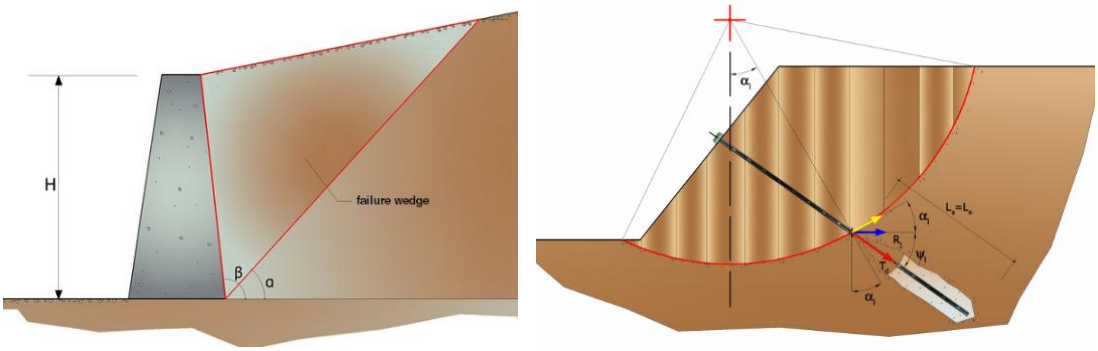

(a) Retaining walls (b) Ground anchors

Fig. 2-10 Typical countermeasures for slope failure prevention

However, these methods are only applicable for some important projects, and are not suitable for large number of slopes with potential risk because of the high cost.

2.7 Landslide prediction methods Based on Rainfall Thresholds

In recent decades, various ideas for the early-warning systems for landslides have been

developed and discussed (Zan et al., 2002; Intrieri et al., 2012; Thiebes et al., 2013). Those early-warning systems are generally based on rainfall thresholds, or deformation of slope surface. Rainfall thresholds, such as the rainfall quantity, duration or intensity of a storm are commonly used for landslide prediction. For example, in some cases, the accumulated amount of rainfall is considered as the index for landslide warning (Terlien, 1998; Rossi et al., 2012). In 1987, a real-time system based on the relation between rainfall intensity and landslides has been developed by Keefer. Japan Railway Company (JR-East) also developed a similar system based on the accumulated rainfall as well as the rainfall intensity for safe operation in railway systems to avoid landslide related accidents during rainfall. By analysing the relationship between accumulated rainfall (mm) and rainfall intensity (mm/hr.), the train service is regulated or even completely stopped on the way in case the present rainfall amount is expected to surpass the limit to cause slope failures, as schematically shown in Fig. 2-11. At the moment, the operation control values to predict slope failure are determined empirically by referring to the record of disaster.

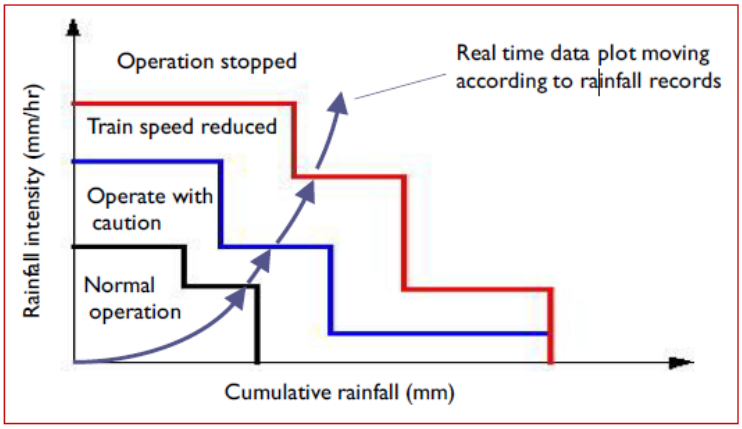

Fig. 2-11 Methodology used by Japan Railway Company in avoiding landslide related accidents (East Japan Railway)

In addition, Soil Moisture Index (SMI) developed by Japan Meteorological Agency is a much more appropriate index to represent the virtual moisture content in hill slopes. This index is calculated with a spatial resolution of 5 km and provided for local governments for the disaster mitigation. SMI has been adopted as a standard reference for early warning by Japanese local governments since 2008.

Although the early-warning methods based on rainfall thresholds are low cost and work well to predict the likelihood of potential landslides in a region, these methods are not suitable to evaluate the risk of individual slope because the relationship between rainfall intensity or accumulated amount of rainfwater and slope failure for particular slopes is still under consideration.

2.8. Landslide Prediction Based on Surface Displacement Monitoring

In past decades, prediction methods for landslide based on slope surface displacement monitoring derive from the results of laboratory creep tests which indicates the relationship between surface displacement or strain and the time before the failure, as shown in Fig. 2-12

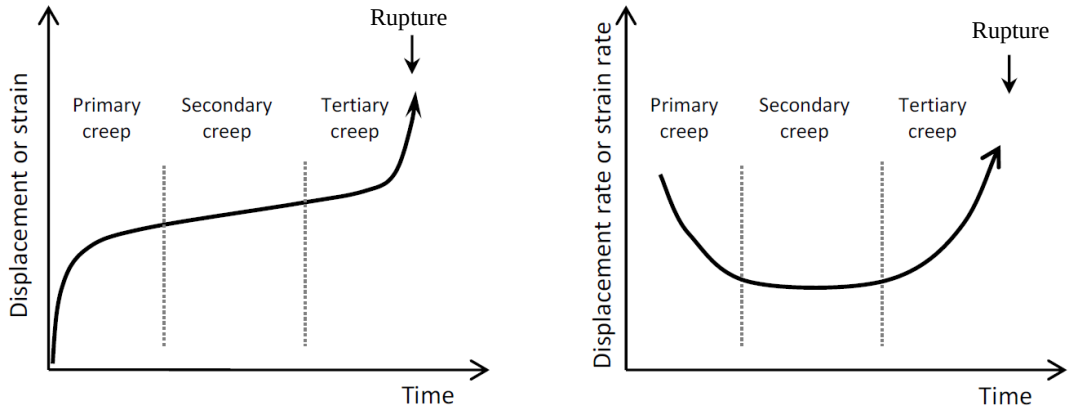

Fig. 2-12 Diagrammatic representation of creep behaviours for pre-failure

As shown in Fig. 2-12, three phases including primary creep, secondary creep and tertiary creep occure in creep tests, which have been explained in the light of damage mechanics and subcritical crack growth by Main in 2000 (Main, 2000). Main assumed that, the primary creep indicates the early stages of damage, dominated by the local hardening mechanism at the tip of the crack. Crack growth at this stage is decelerating because of the stress hardening on the samples. On the contrary, crack growth accelerating in the tertiary stages results from the damage with local softening feedback mechanisms. In terms of secondary creep, it is interpreted by the linear superposition of the local hardening and softening processes with a power law rheology.

The empirical equation for the accelerating behavior of material failure in tertiary creep was first proposed by Monkman in 1956 when studying the failure behaviour of mental, steel as well as ceramic under constanst stress in triaxial tests.

$$\frac{d\varepsilon}{dt}\cdot(t_R - t) = C \tag{2-4}$$

Where: $\frac{d\varepsilon}{dt}$ is strain rate, t_R is the failure time, $t_R - t$ is the duration time before failure and C is a constant related to material properties.

Saito developed a similar equation for slope failures based on the observation of an inversely proportional relationship between the strain rate and the duration time before failure in logarithm form:

$$0.916\cdot\log_{10}\frac{d\varepsilon}{dt} + \log_{10}(t_R - t) = 2.33 \tag{2-5}$$

Based on a statistical study using existing data from soil creep tests, slope model tests by applying rainfall, as well as the monitoring data from the field cases, equation 2-5 has been rewritten as

$$0.916\cdot\log_{10}\frac{d\varepsilon}{dt} + \log_{10}(t_R - t) = 2.33 \pm 0.59 \tag{2-6}$$

A successful prediction was performed for a landslide occurred on December14, 1960, along the Ooigawa railway line (Japan), with the application of this method. It was reported that the railroad traffic was interrupted 1 day before the slope collapse (Saito ,1965).

In 1985, Fukuzono developed an new prediction method based on the relationship between the inverse velocity and the failure time, which derived from the large-scale slope failure experiments induced by rainfall. By investigating the correlation between acceleration and velocity in tertiary stage of slope failure experiments, he found that for rapid failure the logarithm of accelerationi is proportional to the logarithm of the velocity of ground surface displacement (Fig. 2-13), which can be expressed by equation 2-7.

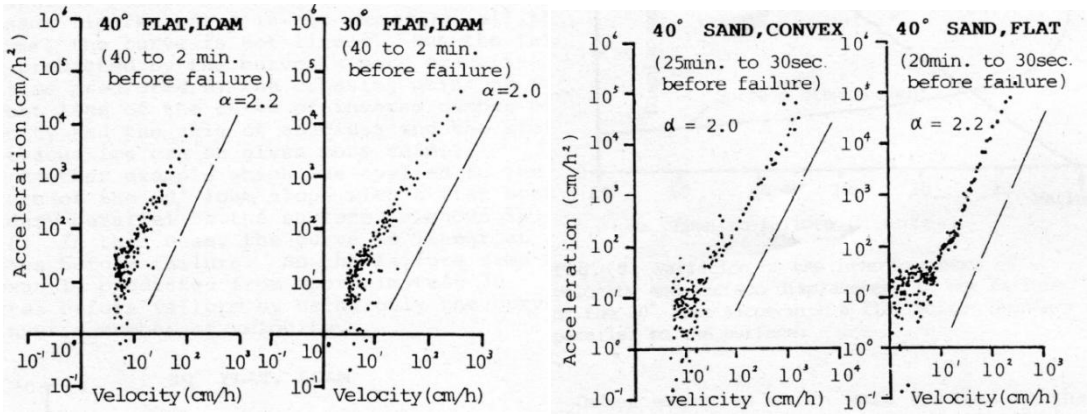

Fig.2-13 Relationship between acceleration and velocity (after Fukuzono,1985)

$$\frac{d^2x}{dt^2} = A \cdot \left(\frac{dx}{dt}\right)^{\alpha} \tag{2-7}$$

Where x is surface displacement, t is time, A and α are empirical constants. $\frac{d^2x}{dt^2}$ and $\frac{dx}{dt}$ represent the acceleration and velocity respectively.

By integrating equation (2-7) for the range of $\alpha > 0$, following equations can be achieved,

$$\frac{dx}{dt} = \left\{a \cdot (1-\alpha)\right\}^{\frac{1}{1-\alpha}} \cdot (t_1 + t)^{\frac{1}{1-\alpha}} \qquad (0 < \alpha < 1) \tag{2-8}$$

$$\frac{dx}{dt} = \exp\left\{a \cdot (t_2 + t)\right\} \qquad (\alpha = 1 \tag{2-9}$$

$$\frac{dx}{dt} = \left\{a \cdot (1-\alpha)\right\}^{\frac{-1}{1-\alpha}} \cdot (t_r - t)^{\frac{-1}{1-\alpha}} \qquad (\alpha > 1 \tag{2-10}$$

Where t_1, t_2, t_r are constants, and α are close to 2 in the model tests and element tests (Fukuzono, 1985; Voigt, 1989).

Equation (2-10) can be rewritten as

$$\frac{dt}{dx} = \left\{a \cdot (1-\alpha)\right\}^{\frac{1}{1-\alpha}} \cdot (t_r - t)^{\frac{1}{1-\alpha}} \qquad (\alpha > 1 \tag{2-11}$$

The plot for equation (2-11) is presented in Fig. 2-14. The failure time t_r can be predicted when the inverse velocity is equal to 0, which means the unstable slope

slipping at an infinite large speed. Fig. 2-14 also indicates that there are two forms existed for the relationship between reciprocal velocity and time. The linear form will occur when α=2, while it will be asymptotic under the condition $\alpha \neq 2$.

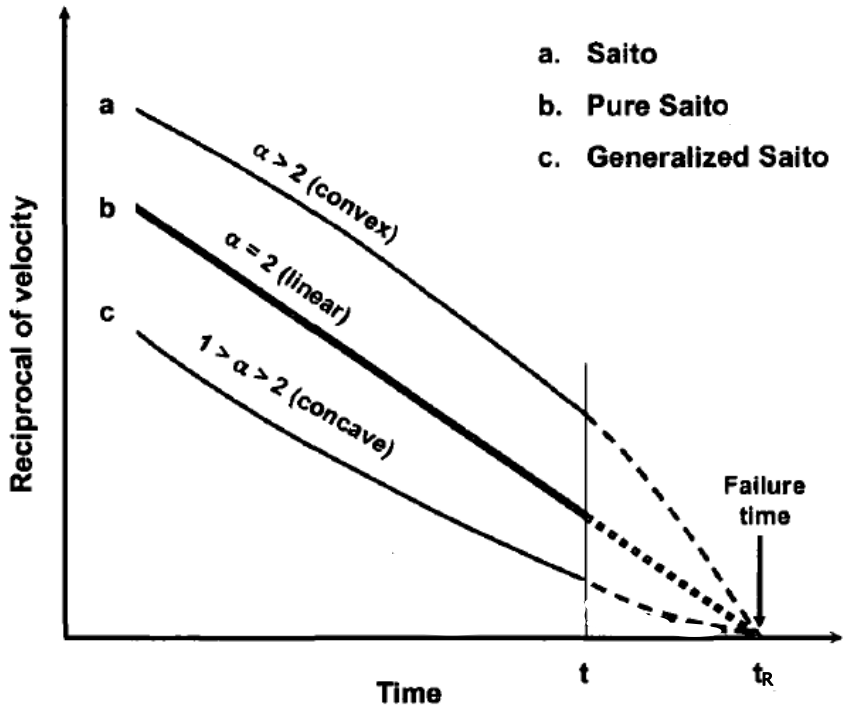

Fig.2-14 Relationship reciprocal of velocity of surface displacement and time to failure in the tertiary stage(after Fukuzono,1985)

Voight proposed a model similar to the equation (2-7),

$$\frac{d^2\Omega}{dt^2} = A \cdot \left(\frac{d\Omega}{dt} \right)^{\alpha} \tag{2-12}$$

Where Ω is an measurable parameter of deformation such as strain or displacement of soil materials, $\frac{d\Omega}{dt}$ and $\frac{d^2\Omega}{dt^2}$ are the first and second derivatives of Ω respectively, A and α are empirical constants.

Equation (2-12) was considered as a fundamental physical material science law by Voight (Voight, 1988; Voight, 1989). Futhermore, this equation appears to control both first-time and reactivated failure for various kinds of materials during the tertiary stage when the stress conditions are nearly constant. Voight also indicated that this

equation is successful in approaching the failure time of some geological phenomena (Voight, 1988), but the physical meaning and mechanisms for equation (2-12) is still poorly understood (Voight, 1989; Hutchinson, 2001; Federico et al, 2012).

There are some other empirical forms of failure time prediction methods in the tertiary creep stage as shown in Table 2-1.

Table 2-1 Reference and expression for failure-time prediction

Reference	Expression
Saito(1965)	$0.916 \cdot \log_{10} \frac{d\varepsilon}{dt} + \log_{10}(t_R - t) = A$
Yamaguchi(1978)	$\alpha \cdot \log_{10} \frac{d\varepsilon}{dt} + \log_{10}(t_R - t) = A$
Hayashi et al.(1988)	$\alpha \cdot \log_{10} \frac{d\varepsilon}{dt} + \log_{10}(t_R - t) = A + \alpha \cdot \log_{10} \varepsilon$
Fukuzono(1985),Voight(1988)	$(\alpha - 1) \cdot \log_{10} \frac{d\varepsilon}{dt} + \log_{10}(t_R - t) = -\log_{10}\{a \cdot (\alpha - 1)\}$
Mufundirwa et al.(2010)	$t \cdot \frac{d\varepsilon}{dt} = t_R \cdot \frac{d\varepsilon}{dt} - A$

It is easy to find that, even though empirical expressions developed by different researchers, most of them can be deduced from the equation first proposed by Fukuzono in 1985.

As it was reported by Federico et al. in 2012, even though these methods predicted some landslides events successfully (Saito,1965; Kennedy et al., 1969 and 1970; Hoek et al.,1977), the exactness of prediction of the actual date was merely a matter of coincidence, since the accuracy of prediction using these methods depends on a hand extrapolation beyond the last date of observation, which can lead to a number of other possible dates of failure, within a time span ranging from several seconds to months. Nevertheless, from an engineering point of view, even a prediction with an error of few weeks is acceptable and helps in taking the right decisions (Hoek et al.1977). As a consequence, one may state that one of the key issues for a good prediction is the correct choice and the subsequent good monitoring of the relevant physical parameters.

The other limitation of these landslide prediction methods is that, these methods are only applicable for the landslides with clear tertiary stage when the unstable slope sliding acceleratively. Even though the tertiary stage observed in some landslide events from model tests and field cases, there are some other landslide moving without a clear accelerating stage, which was reported by Petley et al. in 2005 (Fig. 2-15), and limited researches have been carried out to investigate the various moving pattern of slopes.

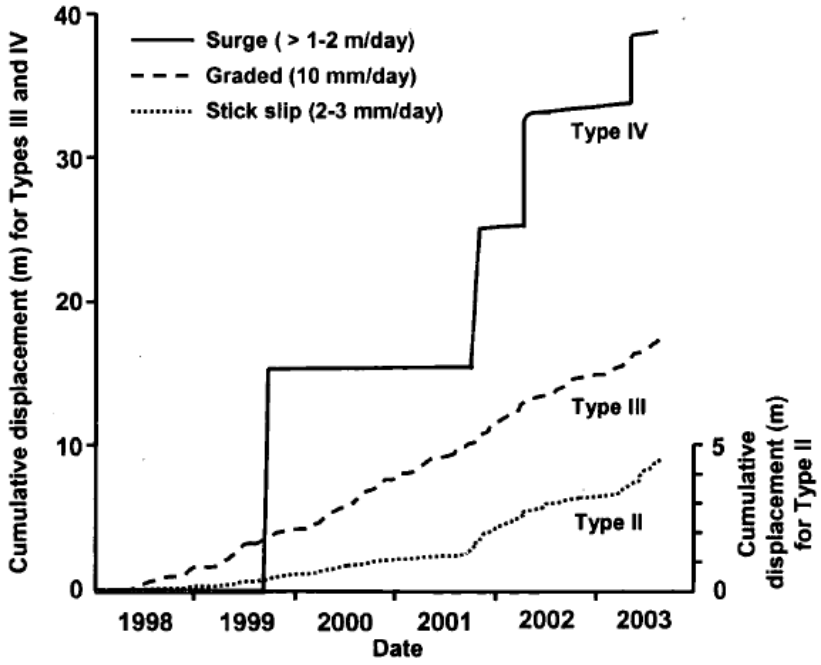

Fig. 2-15 Types of landslides movement without clear acceleration stage (after Petley et al.,2005)

For the moving patterns as shown in Fig. 2-15, the definition of failure for these kinds of landslides is still under consideration.

2.9. Landslide Prediction Based on Tilting Behaviour Monitoring

Iverson et al. (2000) conducted laboratory tests to investigate surface displacement as well as the tilting behaviour of landslides. In the tests, two ground-surface extensometers and tiltmeters were exploited simultaneously to measure landslide movement. The test results, as shown in Fig. 2-16, present that as surface displacements increased, tilt characteristics also showed increasing rates of movement,

and also indicate that, tilt movement could be used as an indication of a landslide failure.

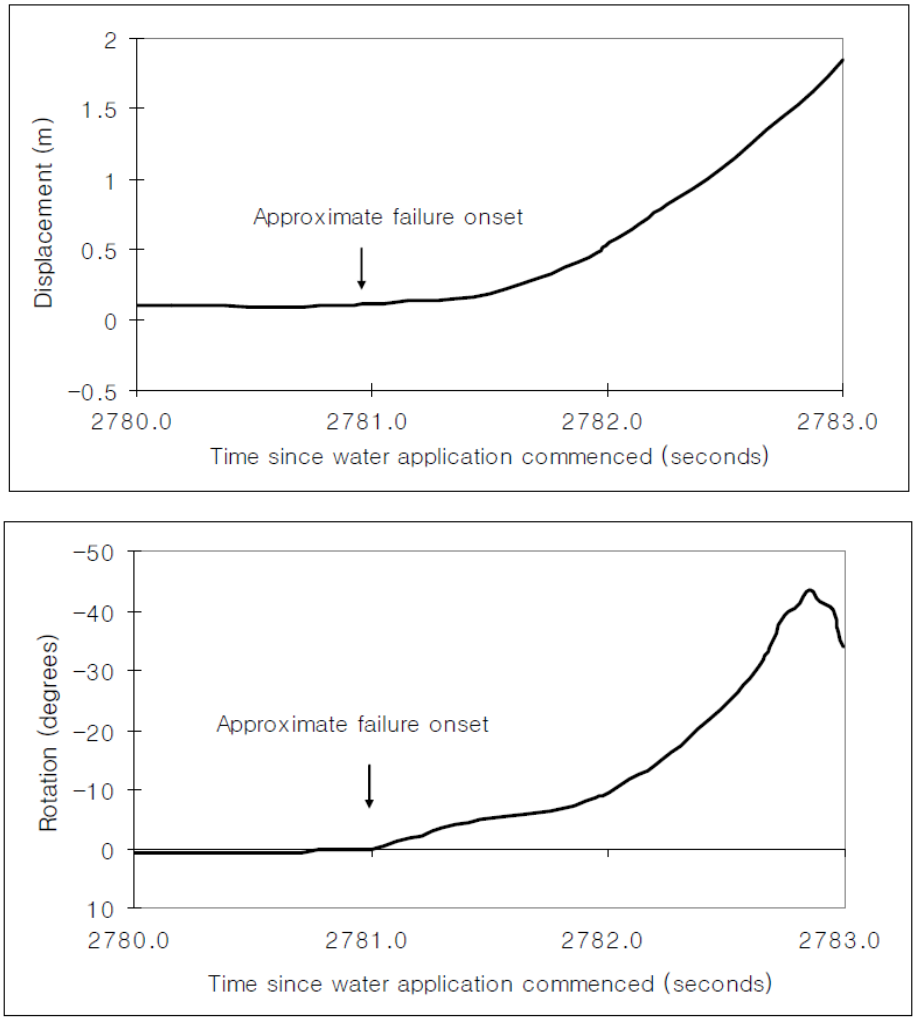

Fig. 2-16 Displacement and tilting angle against time (after Iverson et al., 2000)

Additionally, a similar trend has been found between surface displacement and tilting angle against time after the initiation of slope failure from the existing monitoring data using extensometers and tilt sensors (Fig. 2-17).

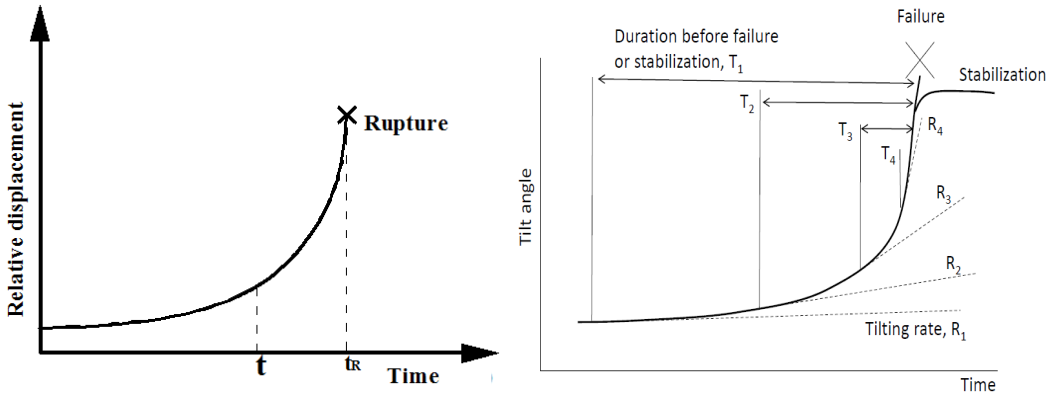

Fig.2-17 A similar trend between displacement and tilt angle against time

2.9.1 Development of slope tilting angle monitoring system

Even though extensometers are with lower costs compared with the retaining walls and ground anchors, there are still several problems to be overcome. The first one is that it is often difficult to distinguish the exact boundaries between the stable regions and unstable regions in a slope, hence the location for monitoring sensors installation can not be decided accurately. Furthermore, the installation or operation of extensometers requires skilled engineers, which will result in a considerable cost increase.

Considering the contexts mentioned above, low-cost monitoring systems with MEMS (Micro Electro Mechanical Systems) technology to measure the tilt angles (rotations) of slopes in the surface have been developed (Towhata et al., 2005; Lee, 2009; Uchimura et al., 2010). As shown in Fig. 2-18, These units are assembled with a Micro Electro Mechanical Systems (MEMS) tilt sensor which can measure rotation angles of the surface layer of slopes and a temperature sensor used for temperature compensation for the tilt sensor. Each sensor unit is powered by batteries and a solar panel, which can last for more than one year. The collected data from every single unit is transmited to a gateway unit by wireless communication using a data server on the Internet through a cell phone network, a schematic diagram wireless monitoring is presented in Fig. 2-19.

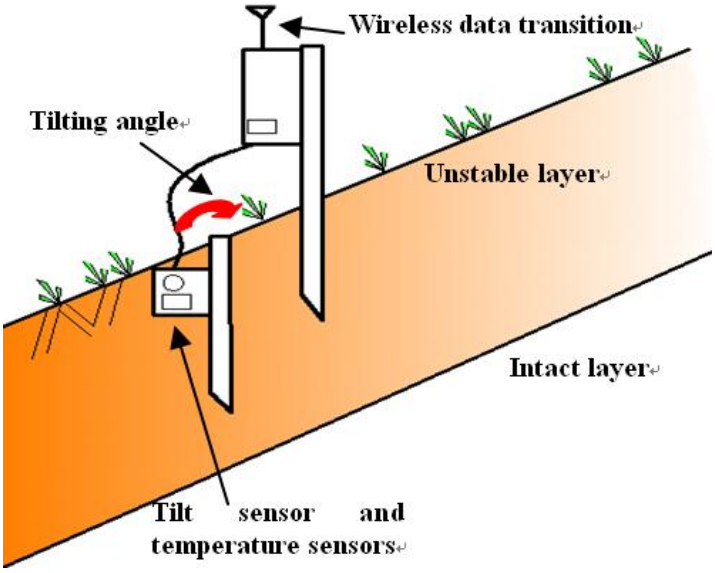

Fig. 2-18 Wireless unit with tilt sensors and temperature sensor

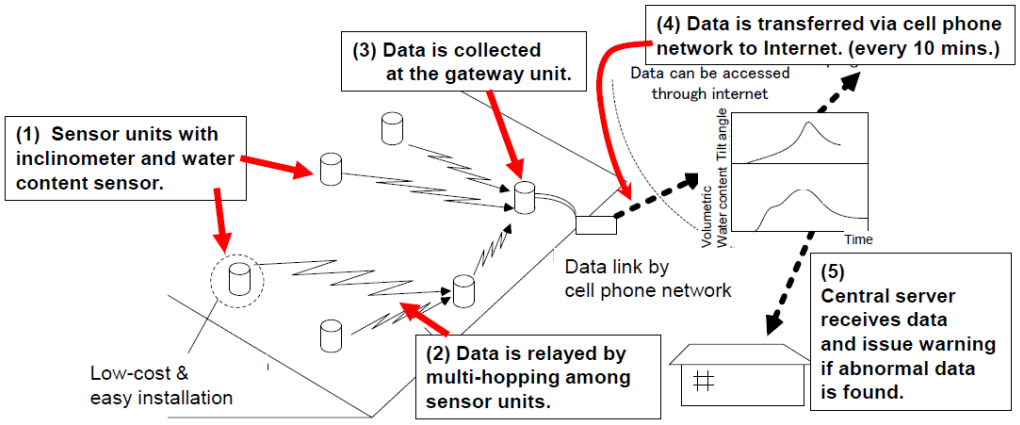

Fig. 2-19 A schematic illustration of wireless monitoring (after Uchimura, 2015)

The slope tilting angle system is used to monitor abnormal tilting behaviors of slope surface and this system has been validated against some laboratory tests as well as a field artificial rainfall test (Uchimura et al. 2015).

By imitating the method developed by Saito, in which the relationship between surface displacement rate and remaining time before failure was proposed for slope failure time prediction, the data of the tilting rates and the duration before slope failure or stability was presented in Fig. 2-20. The criterion value of tilting rates for precaution and warning was determined to be 0.01 degrees per hour and 0.1 degrees per hour respectively, for a conservative decision (Uchimura T.et al.2015).

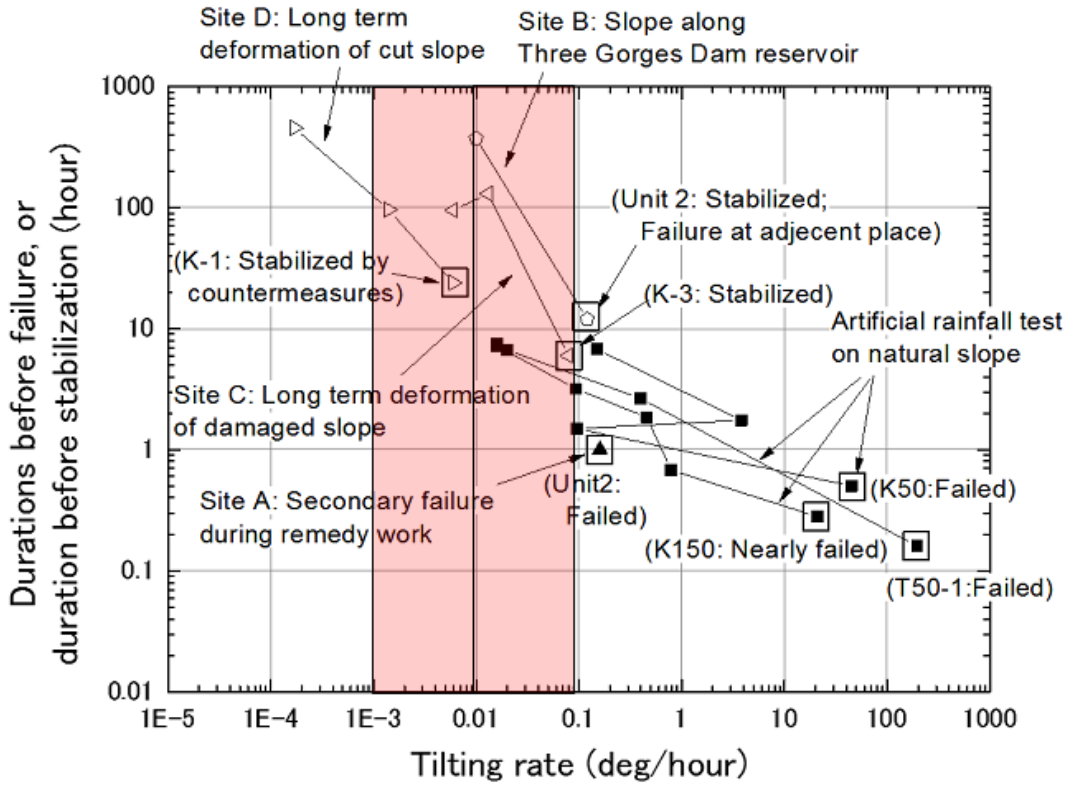

Fig. 2-20 Data of tilting angle rate against durations before failure and stability(after Uchimura,2015)

Although these tilting anr monitoring systems for landslides are with simple installation and lower-cost, there are still some problem to overcome. The first one is that, some sensors tilted forward, while other sensors tilted backward. The tilting directions of these tilt sensors are inconsistent. Secondly, Even though a similar trend has been observed between the time history of displacement and tilting angle in the pre-failure stage of slope failure, the relationship between the surface displacement and tilting angle of slope in the pre-failure stage is unclear. Further, there are limited researches have been carried out to explore the landslide prediction methods using the time history of tilting of slopes.

2.10. SUMMARY

In this chapter, the definition of landslides and failure, landslide early warning systems using rainfall thresholds, and prediction method using surface displacement is summaried. In addition, the tilting angle monitoring system using MEMS is introduced, and the advantages as well as disadvantages of this system is discussed

briefly. In following chapters, the study on the tilting behaviour of tilt sensors, the correlation between surface displacement and tilting angle of slopes, as well as the new prediction method based on the time history of tilting of slopes will be investigated by laborary tests and field tests.

2.11. References

Anderson, S., Sitar, N. (1991). "Influence of stress path on soil strength parameters and analysis of rainfall induced slope failures." Proceedings: Symp.Eng.Geol.Geotech. Eng, 21-26.

Anderson, S., Sitar, N. (1995). "Analysis of rainfall-induced debris flows." Journal of Geotechnical Engineering, 121(7), 544-552.

Brand, E. W. (1981). "Some Thoughts on Rain-Induced Slope Failures." Proc. of 10th International Conference on Soil Mechanics and Foundation Engineering, 3, 373-376.

Craig, R.F. (1997). "Soil Mechanics." Spon Press, London, 485.

Farooq, K., Orense, R., Towhata, I. (2004). "Response of Unsaturated Sandy Soils under Constant Shear Stress Drained Condition." Soils and foundations, 44(2), 1-13.

Finn, W. D. L., Snead, D. (1973). "Creep and creep rupture of an undisturbed sensitive clay." Proc. Eighth Int. Conf. on Soil Mech. And Found. Eng'g, Moscow, 1(1), 135-142.

Fredlund, D. G. , Rahardjo, H. (1993). "Soil mechanics for unsaturated soils." John Wiley & Sons, New York.

Fukuzono, T. (1985). "A new method for predicting the failure time of a slope." Proc. IV, International Conference and Field Workshop on Landslides, Tokyo, 145-150.

Hoek E., Bray J. (1977). "Rock slope engineering." The Institution of Mining and Metallurgy, London.

Hutchinson, J. N. (1988). "Morphological and geotechnical parameters of landslides in relation to geology and hydrology, general report,in: Landslides." Proceedings of the 5th International Symposium on Landslides, Rotterdam, Netherlands, 1, 3–35.

Intrieri, E., Gigli, G., Mugnai, F., Fanti, R., Casagli, N. (2012). "Design and Implementation of a Landslide Early Warning System." Engineering Geology, 147(148), 124-136.

Iverson, R. M., Reid, M. E., Iverson, N. R., Husen, R. G., Logan, M., Mann, J. E. and Brien, D. L. (2000). "Acute Sensitivity of Landslide Rates to Initial Soil Porosity." Science, 290, 513-516.

Lee, J. M .S. (2009). "Real-time monitoring of landslides using wireless network." Doctor dissertation, The Ohio State University.

Keefer, David K., Wilson, Raymond C., Mark, Robert K., Brabb, E. E., Brown, W. M., Ellen, Stephen, D., Harp, E. L., Wieczorek, G. F., Alger, C. S.,Zatkin, R. S. (1987). "Real-time landslide warning during heavy rainfall." Science, 238(4829), 921–925.

Kennedy B. A., Niermeyer, K. E., Fahm, B. A. (1969). "A major slope failure at the Chuquicamata Mine, Chile." Min Eng AIME, 12(12), 60.

Kennedy B. A., Niermeyer, K. E. (1970). "Slope monitoring system used in the prediction of a major slope failure at the Chuquicamata Mine, Chile." Proceedings of symposium on planning open pit mines, Johannesburg, 215–225.

Main, I. G. (2000). "A damage mechanics model for power-law creep and earthquake

aftershock and foreshock sequences." Geophysical Journal International, 142, 151–161.

Osanai, N., Shimizu, T., Kuramoto, K., Kojima, S., Noro, T. (2010). "Japanese early-warnig for debris flows and slope failure using rainfall indices with radial basis function network." Landslides, 7(3), 325–338.

Petley, D. N., Petley, D. J., Bulmer, M. H., Carey, J. (2005). "Development of progressive landslide failure in cohesive materials." Geology, v.33(3), pp.201-204.

Petley, D. N., Mantovani, F., Bulmer, M. H., Zannoni, A. (2005). "The use of surface monitoring data for the interpretation of landslide movement patterns." Geomorphology, 66, 133–147.

Rossi, M., Peruccacci, S., Brunetti, M., Marchesini, I., Luciani, S., Ardizzone, F., Fiorucci, F. (2012). "Sanf: National Warning System for Rainfall-Induced Landslides in Italy." Proceedings: Proceeding of the 11th International Symposium on Landslides (ISL) and the 2nd North American Symposium on Landslides (NASL).

Saito M. (1965). "Forecasting the time of occurrence of a slope failure." proceedings of the Sixth International Conference on Soil mechanics and Foundation Engineering, 537-541.

Singh, A., Mitchell, J. K. (1969). "Creep potential and creep rupture of soils." Proc. Seventh Int. Conf. on Soil Mech. and Found. Eng'g, Mexico City, 1,379-384.

Terlien, M.T. (1998). "The determination of statistical and deterministic hydrological landslide-triggering thresholds." Environmental Geology, 35(2-3), 124-130.

Thiebes, B., Bell, R., Glade, T., Jäger, S., Mayer, J., Anderson, M., & Holcombe, L.

(2014). "Integration of a Limit-Equilibrium Model into a Landslide Early Warning System." Landslides., 11, 859-875.

Towhata I., Uchimura T., Gallage C. (2005). "On early detection and warning against rainfall-induced landslide." Proc. of The First General Assembly and The Fourth Session of Board of Representatives of the International Consortium on Landslides (ICL).Springer, Washington, DC, 133–139.

Tsukamoto Y., Ishihara K., Nosaka Y. (2002). "On the initiation of rainfall induced soil failure." Maric, Lisac, Szavits-Nossan (eds) Geotechnical hazards. Balkema, Rotterdam, 883– 890.

Van, G. M. T. (1980). "A Closed-form Equation for Predicting the Hydraulic Conductivity of Unsaturated Soils." SOIL SCI. SOC. AM. J., 44, 892-898.

Voight, B. (1989), "A relation to describe rate-dependent material failure." Science, 246, 200-203.

Voight, B. (1988). "A method for prediction of volcanic eruptions." Nature, 332, 125-130.

Zan, L., Latini, G., Piscina, E., Polloni, G., & Baldelli, P. (2002). "Landslides Early Warning Monitoring System." Proceedings: Geoscience and Remote Sensing Symposium, 188-190.

Uchimura, T., Towhata, I.,Trinh, T. L., Fukuda, J., Carlos, J. B. B., Lin, W., Seko, I., Uchida T., Matsuoka, A., Yosuke I., Onda, Y., Iwagami, S., Min-Seok K., Sakai, N. (2010). "Simple monitoring method for precaution of landslides watching tilting and water contents on slopes surface." Landslides, 7, 351-357.

Uchimura T., Towhata I., Wang L., Nishie S., Yamaguchi H., Seko I. and Qiao J. (2015). "Precaution and early warning of surface failure of slopes by using tilt sensors." Soil and Foundation, 55(5), 1086-1099.

CHAPTER 3

MATERIALS AND EXPERIMENTAL SETUP

3.1. Introduction

For the purpose to have a better understanding of the tilting behaviour of landslides, laboratory model tests as well as field tests, which have been regarded as the most reliable methods for studying the rainfall-triggered landslide, were conducted. In this chapter, the materials employed in the tests, including Silica number 7 sand as well as Edosaki sand, and the apparatus are discussed.

3.2. Test Materials

In this study, Silica sand # 7 and Edosaki sand were used in laboratory tests. Silica sand # 7 is a economical research material, and has a similar soil particle distribution as Toyoura sand which has been regarded as japanese standard sand and widely used as research material in Japan. The other kind of materials employed in the model tests is Edosaki sand. The Edosaki sand, with brown-yellowish color, is procured from a natural slope in Ibaraki prefecture of Japan. The soil for the field tests is weak expansive clay, which is widely distributed in Guangxi Province, China.

3.2.1 Physical properties of Silica number 7 sand

3.2.1.1 Particle size distribution of Silica number 7 sand

Sieve analysis tests were carried out on Silica sand to find fine particle size distribution, and the particle size distribution curves of Silica sand # 7 is given in Fig.

3-1. The mean grain size, the coefficient of uniformity and coefficient of gradation are provided in Table 3-1.

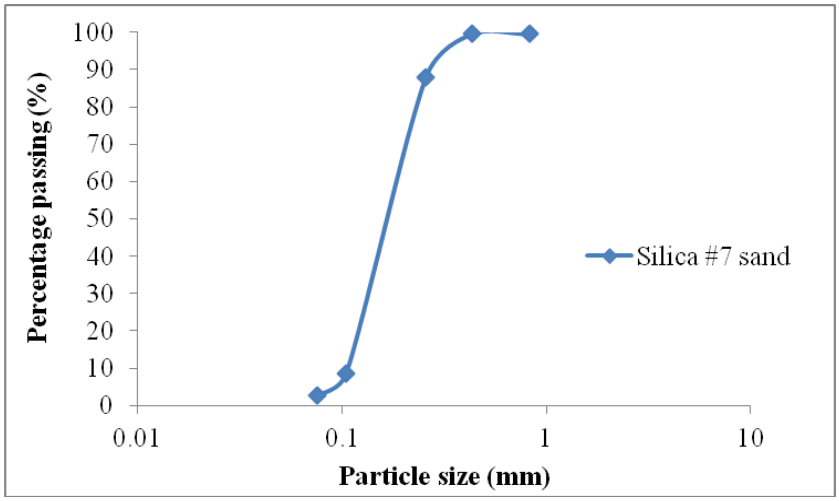

Fig. 3-1 Particle size distribution curve of Silica sand # 7

Table 3-1 Physical properties of Silica sand # 7

Properties	**Silica No 7 sand**
Grain size at 60% fine (mm)	0.19
Mean grain size or Grain size at 50% fine (mm)	0.18
Grain size at 30% fine (mm)	0.14
Grain size at 10% fine (mm)	0.11
Coefficient of uniformity, $C_u=D_{60}/D_{10}$	1.72
Coefficient of gradation, $C_c=(D_{30})^2/(D_{10}*D_{60})$	1.00
Minimum void ratio	0. 743
Maximum void ratio	1.243

3.2.1.2 Specific gravity of soil solids

Density bottle method, as shown in Fig. 3-2, was used to determine the specific gravity of soil solids (G_s) according to Japanese standards, and results of the test are given in Table 3-2.

Fig. 3-2 Density bottle method to Determine the Gs

Table 3-2 Test result of specific gravity of soil solid

Items	**Silica No 7 sand**		
Specimen Number	1	2	3
Density Bottle Number	81	68	77
Weight of density bottle = W_1(g)	57.656	55.956	53.181
W_1 + Dry soil = W_2(g)	82.206	80.255	74.636
W_2 + Water = W_3(g)	180.887	172.253	164.572
W_1 + Water = W_4(g)	165.628	157.231	151.294
Specific Gravity	2.64	2.62	2.62
Average Value	2.63		

3.2.1.3 Compaction curve of Silica number 7 sand

Compaction characteristics of Silica number 7 sand were obtained by Standard Proctor Compaction method, and the result is given in Fig. 3-3. The maximum dry density ($(\gamma_d)_{max}$) and optimum moisture content (W_{opt}) are found to be 1.61 g/cm^3 and 11.6% respectively.

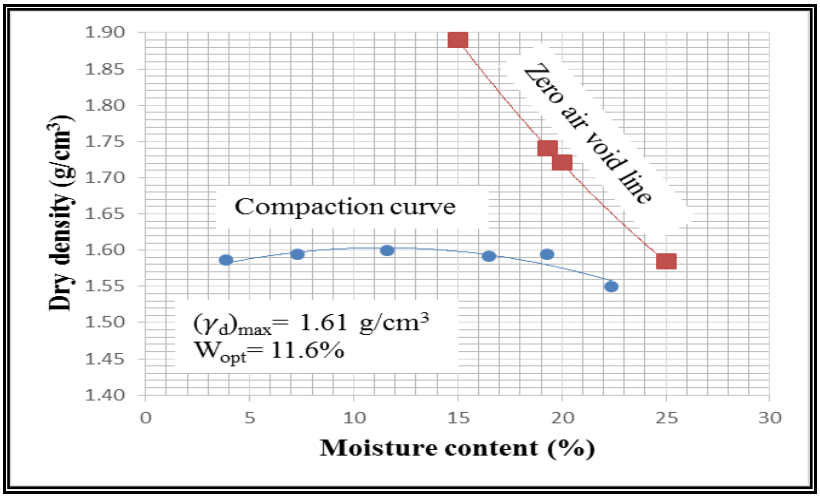

Fig. 3-3 Compaction curve of Silica No 7 sand(after Hema,2017)

3.2.1.4 Soil water characteristic curve(SWCC) of Silica sand # 7

Soil-Water Characteristic curve (SWCC) of Silica sand # 7 was measured using pressure plate apparatus at Geotechnical laboratory by Zamsyar in 2016, and the experimental data of SWCC for Silica number 7 sand at the relative density equavalent to 50% (Dr=50%), is shown in Fig. 3-4.

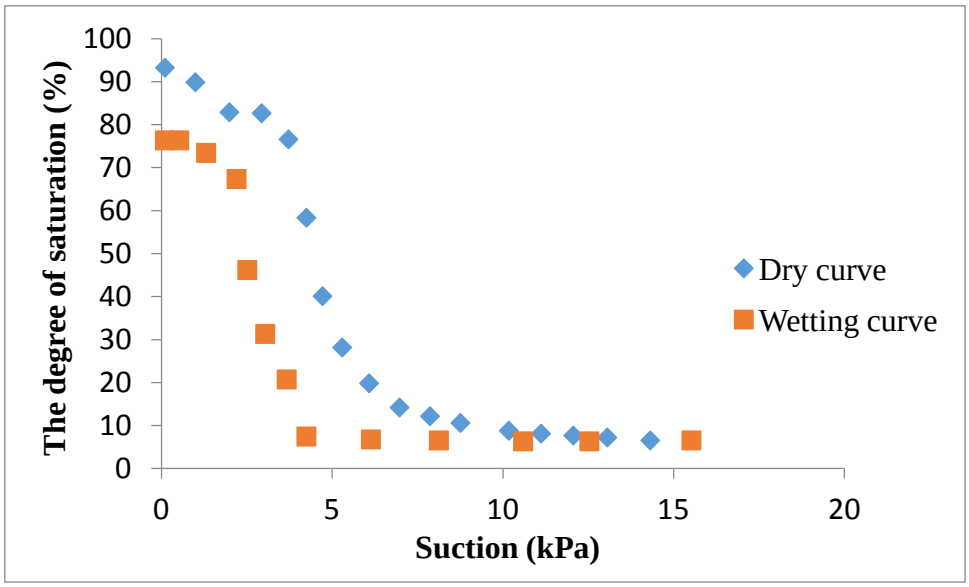

Fig. 3-4 SWCC for Silica No 7 sand, Dr=50% (after Zamsyar,2016)

3.2.2 Physical properties of Edosaki sand

3.2.2.1 Particle size distribution of Edosaki sand

Unlike Silica sand # 7, the Edosaki sand was procured from a natural slope in Ibaraki prefecture (Japan) containing a high percentage of fine particle, and it is classified as

silty sand according to the unified soil classification system (USCS) (Chaminda, 2006).

The Edosaki sand contains a high precentage of fine particle, around 17%, so the sieve analysis as well as hydrometer analysis were conducted to obtain its particle-size distribution curve presented in Fig. 3-5. Additionally, physical properties of Edosaki sand, including specific gravity of soil solids, mean particle diameter and so on, which are determined by the corresponding laboratory tests according to Japanese Geotechnical Society (JGS) standards, is described in Table 3-3.

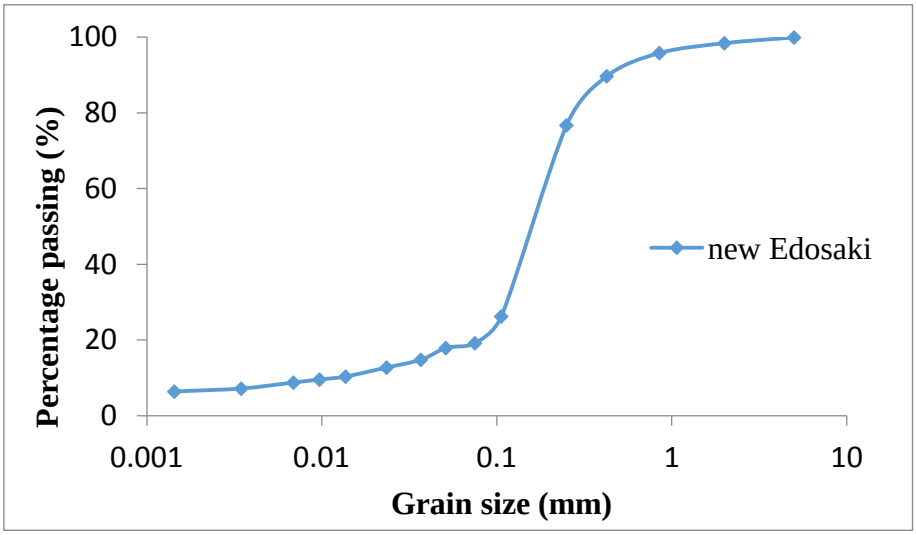

Fig. 3-5 Particle size distribution curve of Edosaki sand

Table 3-3 Physical properties of Edosaki sand

Properties	Edosaki sand
Specific gravity, Gs	2.68
Minimum void ratio	0.83
Maximum void ratio	1.36
Fines(%)	17
Coefficient of uniformity, $C_u=D_{60}/D_{10}$	15.8
Coefficient of gradation, $C_c=(D_{30})^2/(D_{10}*D_{60})$	6.31

3.2.2.2 Compaction curve of Edosaki sand

Compaction characteristics of Edosaki sand is presented in Fig. 3-6 following Irfan

(Irfan, 2014). The maximum dry density ($(\gamma_d)_{max}$) and optimum moisture content (W_{opt}) are found to be 1.762 g/cm^3 and 14.6% respectively.

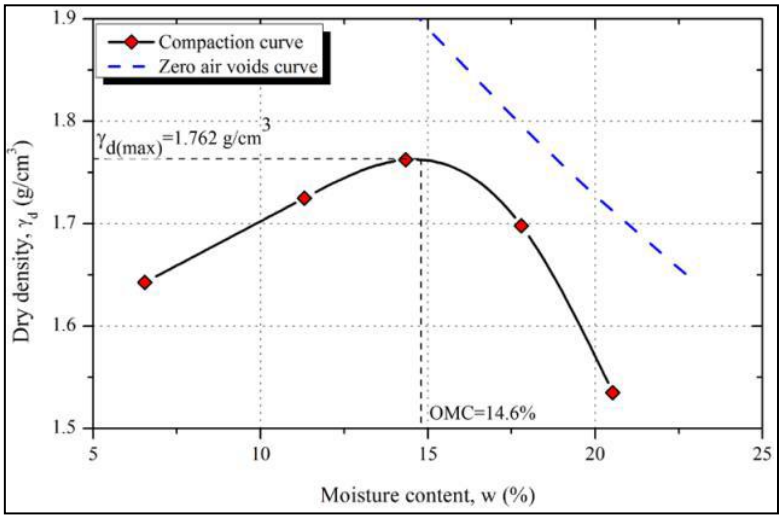

Fig. 3-6 Compaction curve of Edosaki sand(after Irfan,2014)

3.2.2.3 Soil water characteristic curve(SWCC) of Edosaki sand

To approach the SWCC of Edosaki sand, a modified triaxial apparatus was served as a measurement apparatus, and the test results with different relative density are presented in Fig. 3-7 and Fig. 3-8. Fig. 3-7 shows test results of a preliminary test conducted on Edosaki sand with the dry density around 1.25 g/cm^3 under net normal stress 10 kPa, while Fig. 3-8 presents the results with the dry density around 1.38 g/cm^3 under the same net normal stress (Irfan, 2014).

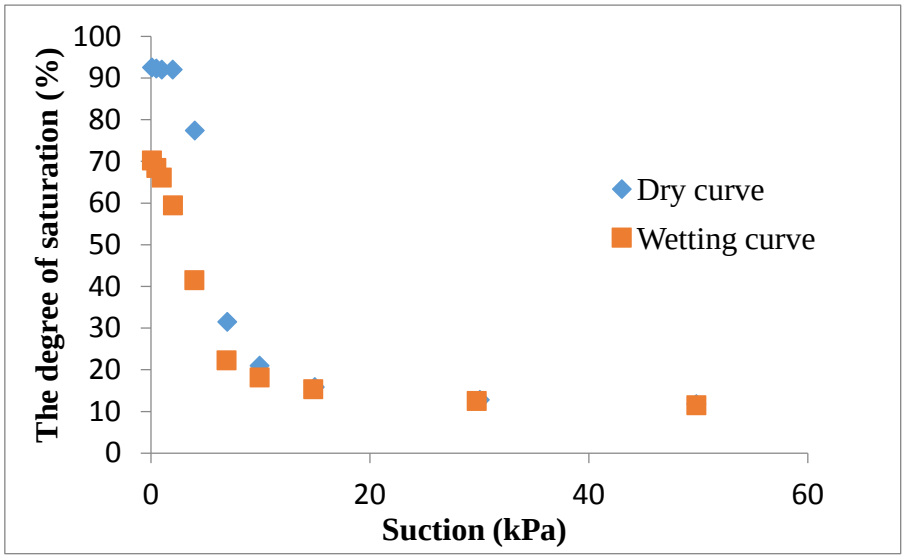

Fig. 3-7 SWCC for Edosaki sand, Dry density 1.25g/cm^3 (after Irfan,2014)

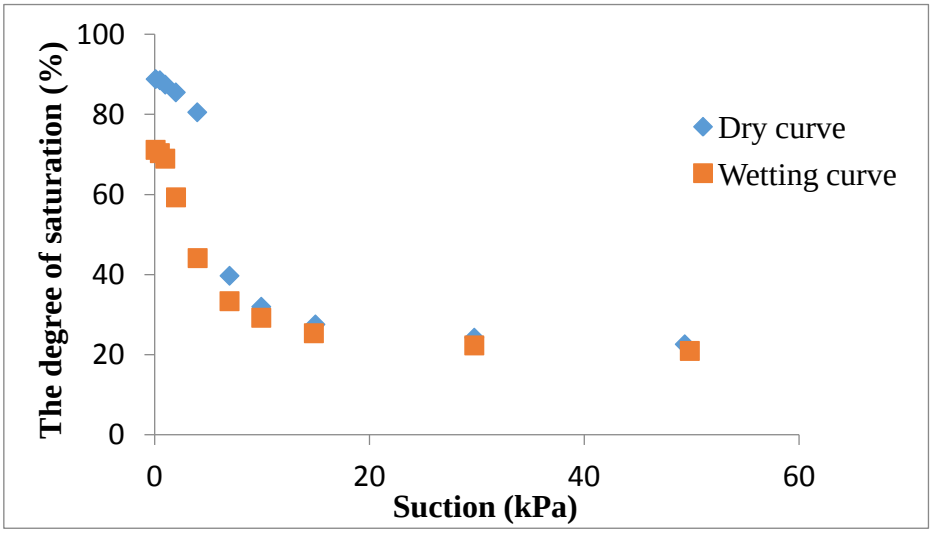

Fig. 3-8 SWCC for Edosaki sand, Dry density 1.38g/cm^3 (after Irfan,2014)

3.2.2.4 The relationship between void ratio and mean effective stress (e-p curve) of Edosaki sand

The e-p curve, which can reflect the correlation between stress and deformation of materials, is determined by drained consolidation tests with the specific dry density, around 1.25 g/cm^3 of Edosaki sand, and the results of these tests is shown in Fig. 3-9. Fig. 3-9 indicates the relationships between void rate and effective normal pressure when loading or unloading in the consolidation.

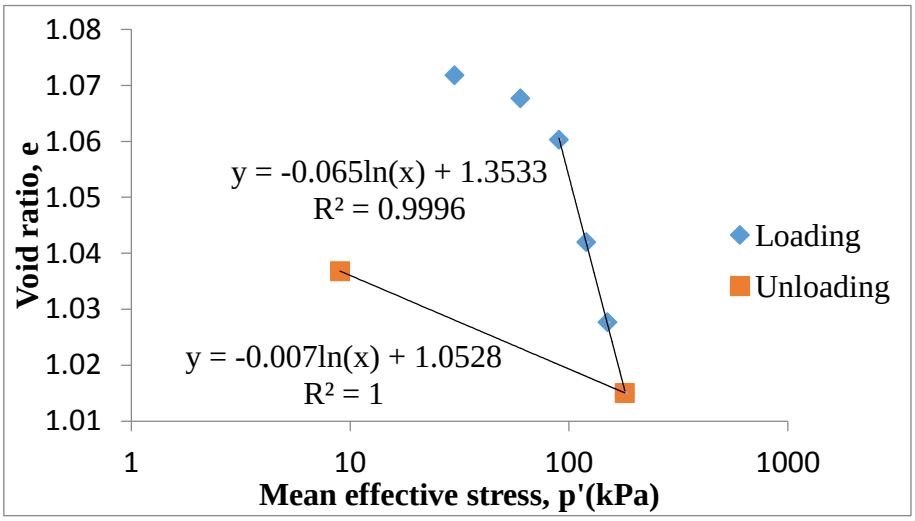

Fig. 3-9 e-p curve of Edosaki sand

3.2.2.5 CU tests of Edosaki sand

Undrained triaxial compression tests with different confining pressure, 120 kpa and 200 kpa respectively, were conducted using the same dry density of Edosaki sand, 1.25 g/cm^3. After being subjected to double vacuum for 12 hours, the samples were saturated from the bottom to top gradually using two tanks with a height difference, around 2 meters, to derive the water flow by water head difference. Then, the B value, a index related to the degree of saturation of there samples, was checked higher than 97% for all of the samples. In next step, undrained triaxial compression tests were conducted with a constant axial strain rate, 0.318 mm/min. Fig. 3-10 shows the relationship between the deviator stress, q, againsts axial strain, ε_a. This figure shows that the highter confining pressure results in higher peak stress and residual stress. The effective stress path, i.e the $q-p'$correlation, in the tests is presented in Fig. 3-11. In this figure, it indicates a consistent critical ratio, 1.22, for CU tests with different confining pressure. Combiming the test results plotted in Fig. 3-9, Fig. 3-10 and Fig. 3-11, the elasto-plastic parameters of Edosaki sand were estimated and are listed in Table 3-4.

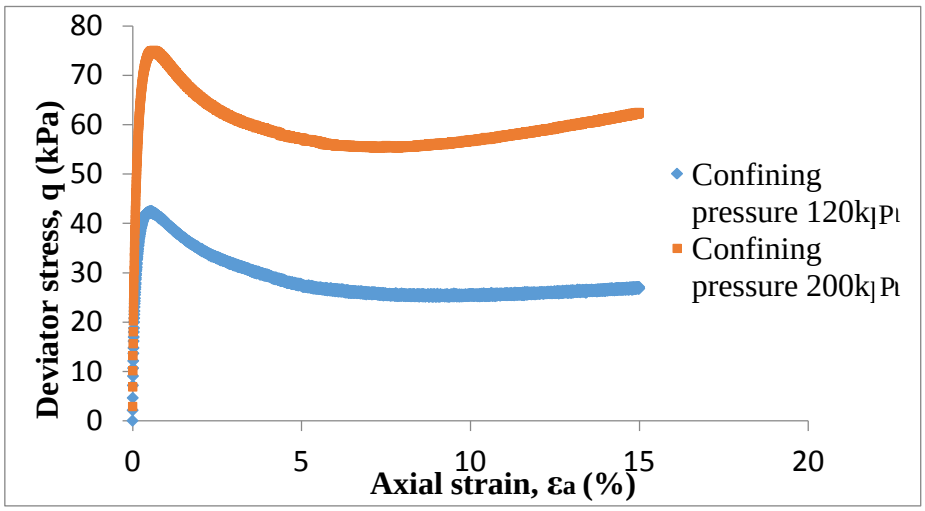

Fig. 3-10 The relationship between axial strain and deviator stress of Edosaki sand

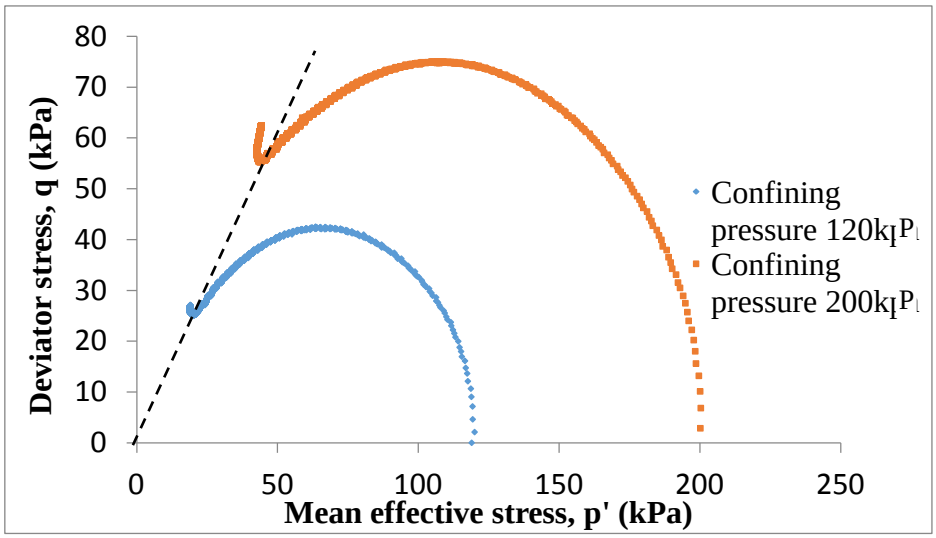

Fig. 3-11 The relationship between mean effective stress and deviator stress of Edosaki sand

Table 3-4 Elasto-plastic parameters of Edosaki sand

Elasto-plastic parameters	Value
Compression index, λ	0.065
Swelling index, κ	0.007
Critical state constant M	1.2
Void ratio at $p' = 98.1$kpa on NCL N	1.22

3.3. Apparatus setup

To investigate the tilting behaviour of slope in pre-failure stage, small-scaled model tests with different kinds of materials were conducted in laboratory. Additionally, field tests by applying rainfall were also carried out with Guangxi University, in Guangxi Province, China. In this chapter, the experimental setup involved in laboratory tests as well as in field tests is briefly decribed in following sections.

3.3.1 Apparatus exploited in small-scaled model tests

In model tests, several types of apparatus were exploited, including tilt sensors, data acquisition systems, nozzles, water content sensors and so on.

3.3.1.1 HOBO RX3000 data logger

HOBO RX3000 data logger (Fig. 3-12), manufactured by Onset Computer Corporation, is a data logging station which can record the converted digital data at a sampling rate of 1Hz. Specification of the logger is given in table 3-5. Moreover, the data recorded in the logger is transferred to a personal computer and analysed by *HOBOware* software.

Fig. 3-12 HOBO RX3000 data logger

Table 3-5 Specification of HOBO RX3000 data logger

Features of HOBO RX3000	Values
Size	186mm×181mm ×118mm
Weight	2.2kg
Channel	10
Memory	32MB, 2 million measurement
Fastest logging rate	1s
Operating temperature range	-40°C to +60°C

3.3.1.2 Tilt sensors

Tilt sensors of SCA61T-series, which are manufactured by VTI Technologies and based on Micro Electro Mechanical technology, were used to measure the rotation angles of slope models. Details about this series of tilt sensors are given in Fig. 3-13 and table 3-6.

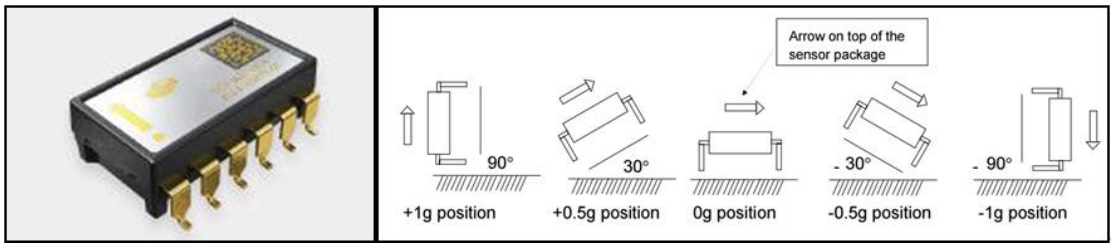

Fig. 3-13 SCA61T-Series single axis MEMS sensor and direction specification (VTI Technologies).

Table 3-6: Specification of SCA61T MEMS sensor

Features of SCA61T MEMS sensor	Values
Range	± 30°
Rated voltage	5.0V
Sensitivity	4V/g
Package	12-SMD
Number of axis	1

Weight	14.5g
Resolution	0.0025^{o}
Analogue to digital converter	12 bit
Measuring output resolution	70mV/^{o} => 14.2857^{o}/V
Measuring tilt angle range	Horizontality ± 30^{o}

3.3.1.3 Model tanks

Two types of wooden boxes as shown in Fig. 3-14 were explomed in the study to investigate the slope failure in laboratory. The box in Fig. 3-14-a, measuring 1165 mm×450 mm×380 mm, is made of four numbers of plywood sheets with a thickness of 20 mm. The waterproof pigment was painted on the surface of walls to prevent damages from water. Furthermore, silicon sealant is used at the joints to prevent water leakage. On the other hand, another model tank shown in Fig. 3-14-b is made of plywood sheets on four sides and transparent plastic sheet on one side. Same waterproof treatment was done to both of these two boxes. Geotextile is used on top of the horizontal surface to prevent soil leakages and the size of the box is 800 mm× 300 mm×400 mm. At the bottom of this box, there are several holes for water drainage during the tests by applying rainfall.

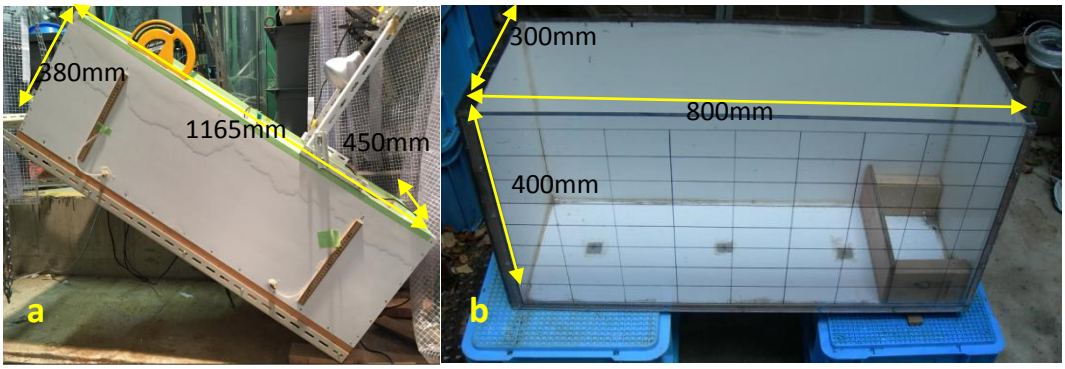

Fig. 3-14 Model tanks

3.3.1.4 Lifting mechanism

A chain block, with 5 ton lifting capacity, was used to lift one edge of the soil tank to form desired initial slope angle at the beginning of each test while the other end of the

box was allowed to rotate around a solid point on the horizontal surface of the ground as shown in Fig. 3-15. Steel chain links were used to connect soil box with the chain block.

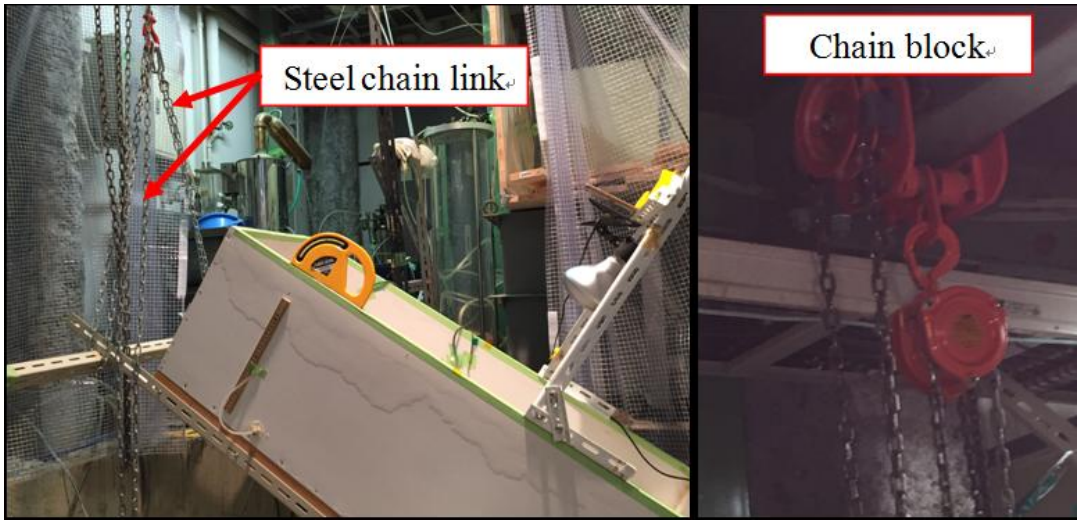

Fig. 3-15 Lifting arrangement for making slope

3.3.1.5 Artificial rainfall supply system for model tests

The artificial rainfall supply system consists of a water tank, an air pressure system and a square spray nozzle (SSXP) were used as shown in Fig.3-16. Water was compressed to the nozzle from the water tank by applying the air pressure using a air pump controled by regulator. During the rainfall tests, the water tank is with a continuing water supply from a tap directly.

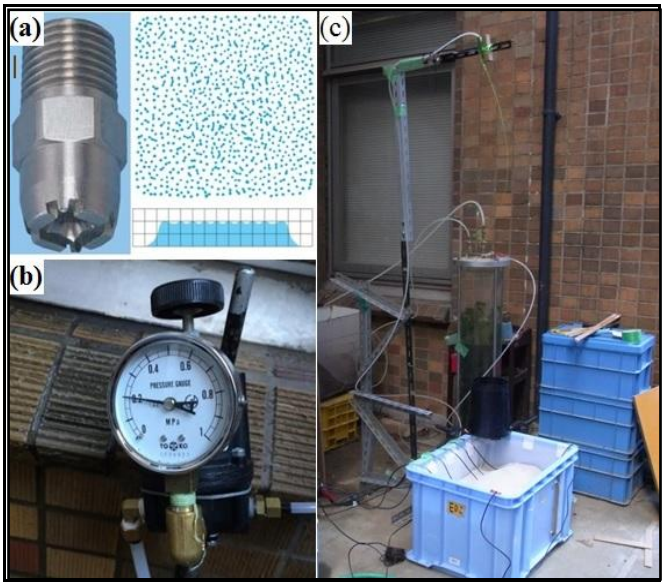

Fig 3-16 Components of artificial rainfall supply system

3.3.2 Apparatus exploited in field tests

Some other intruments exploited in field tests, such as extensometers DP-E500, are introduced in this part.

3.3.2.1 Extensometers DP-E500

The DP-E500 displacement transducer was used to measure a large amount of displacement. A stainless steel wire is drawn to measure displacement. The wire tension is constant in the same direction regardless of the amount of displacement. DP-E500 is a small, lightweight, and high-accuracy transducer, and details are shown in following.

Fig. 3-17 Extensometer DP-E500

Table 3-7 Specifications of DP-E500

TYPE	DP-500E
Capacity	500mm
Rated Output	5mV/V(10000×10^{-6} strain) ±0.3%
Sensitivity(×10^{-6} strain)/mm	20
Non-linearity	0.3%RO
Voltage resistance	Input 210Ω　Output 360Ω
Spring force	1.5N

Allowable temperature range	-10 ~ +80°C (no condensation)
Weight	210g

The calibration characteristics of extensometer sensors used in this study is presented as follows

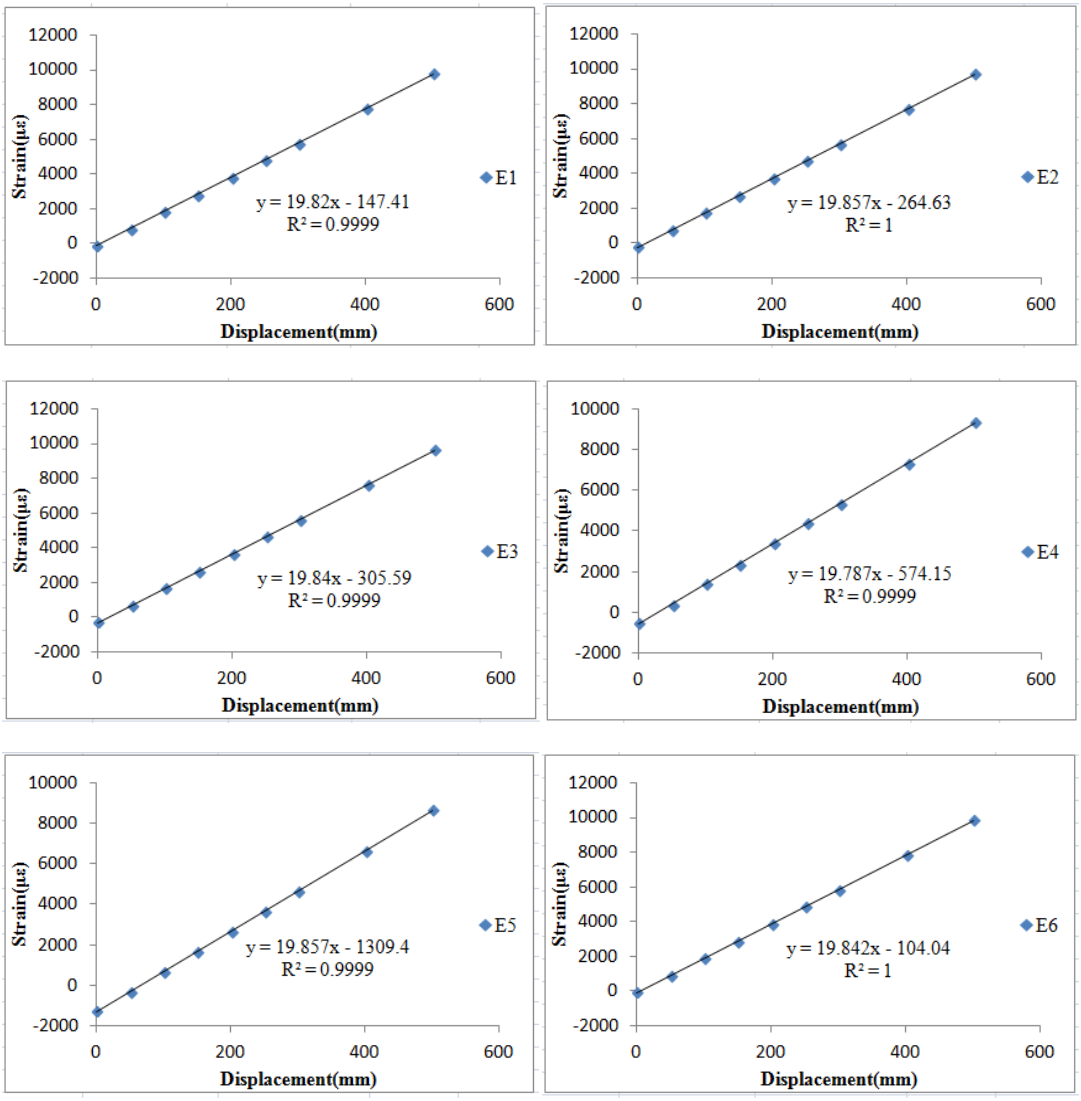

Fig 3-18 Calibration characteristics of 6 extensometers

3.3.2.2 Digital converter of tilt sensors in field tests

In field tests, the digital converter of tilt sensors consist two part, EPD-96 connector and AIO-163202FX-USB. The EPD-96 connector is a general purpose terminal fastened with screws, which relays the I/O wirings of CONTEC interface board/card or card with a 96-pin half-pitch connector. The pins in connector correspond to their

respective terminals on the terminal strips on a one-to-one basis, allowing users to easily connect the board/card to an tilt sensors installed in slope via the terminal strips. AIO-163202FX-USB is a USB2.0-compliant analog I/O unit which connects EPD-96 connector to PC. Details about these apparatus are shown below.

Fig. 3-19 EPD-96 Connections

Table 3-8 Specifications of EPD-96 Connections

Item	Specification
Rated insulative voltage	125VAC, 125VDC
Rated current	1A
Compatible wiring	$2mm^2$(Max.)
Insulative resistance	100MΩ or later
Voltage resistance	1000VAC, 60Hz, One minute
Compatible pins	Crimp-style pins, Max. diameter 7.2mm
Connector	PCR-E96MD+ (mfd. by HONDA) equivalent
Compatible rail	35mm (wide) DIN rail
Operating conditions	0 - 50°C, 10 - 90%RH (No condensation)
Weight	360g

Fig. 3-20 AIO-163202FX-USB

Table 3-9 Specifications of AIO-163202FX-USB

Item	Specification
Input/Output voltage	90-264VAC, 5.0VDC
Rated current	2.0A(Max.)
Frequency	50-60Hz
Dimention	40×105×30mm
Operating conditions	0 - 40°C, 20 - 80%RH (No condensation)
Weight	160g

On the other hand, the digital converter of extensometer DP-E500 is analogue, which is a high-performance data acquisition system and used to convert the signals from extensometers into digital data as shown in Fig. 3-21. The strain NR-500 is manufactured by Keyance Corporation Ltd., and it can convert analogue signals into digital data in 4 or 8 channels and realise continuous recording of displacement with a high sampling rate. Further, the data recorded is directly recorded and saved in a personal computer by using the *NR-HA08* software.

Fig. 3-21 Strain NR-500

Table 3-10. Specifications of EPD-96 Connections

Item	Specification
Input signal	±50mV
Channels	4
Frequency	50kHz
Memory depth	4M
Power consumption	<3W

3.4. Summary

In this chapter, the property of materials, which are used in the tests, including Silica number 7 sand as well as Edosaki sand, are presented. Furthermore, apparatus setup employed in this study are discussed.

3.5. References

Gallage, C. P. K. (2006). "Real-time prediction of rain-induced embarkment failure by minimum measurements with back-analysis for SWCC parameters." PhD Thesis, Unversity of Tokyo, Japan.

Hemakanth, S. (2017). "Use of elastic wave refraction method to observe slope conditions in pre-failure stages." Master Thesis, Unversity of Tokyo, Japan.

Irfan, M. (2014). "Elastic wave propagation through unsaturated soils concerning early warning of rain-induced landslides." PhD Thesis, Unversity of Tokyo, Japan.

Zamsyar, G. F. (2016). "1G shaking table test on liquefaction of embankment and its numerical simulation." Master Thesis, Unversity of Tokyo, Japan.

CHAPTER 4

METHODOLOGY

4.1. Introduction

The main objective of this study is to investigate the tilting behaviour of slope in pre-failure stage. A comprehensive understanding of tilting of slope is indeed necessary to use it in practical landslide early warning. As mentioned in Chapter 2, in this study, the following three problems are explored.

1) The tilting directions of tilt sensors installed on slope surface after the onset of accelertationg stage are unclear.
2) The relationship between the surface displacement and tilting angle in the pre-failure stage of slope failure is still under consideration .
3) The landslide prediction methods based on the time history of tilting of slope surface are still unclear.

In the coming sections, efforts are made to investigate these three problems based on model tests as well as field tests.

4.2. Methodologies for the tilting directions investigation

Based on the existing data from model tests and field events, some tilt sensors installed on the slope surface tilted forward, while other sensors tilted backward (Uchimuira et al., 2008; Uchimuira et al., 2010). This inconsistent tilting directions even occurred within the same landslides, as shown in the Fig. 4-1. Fig. 4-1 presents that one tilt sensor embedded near to the bottom part tilted forward, while the tilt sensor located in

the crest region of slope tilted backward. Other two tilt sensors installed in the middle area of this slope also show contrary tilting directions. Although this inconsistent tilting direction of tilt sensors has been observed in model tests and field events, there are few studies carried out to investigate this problem. In this section, small-scaled model tests with different pre-defined slip surfaces, and tilt sensors attached to various length of rods were carried out to gain an insight into the tilting behaviour of sensors installed on the slope surface. In addtion, field tests were also conducted to have a better understanding of this phenomenon.

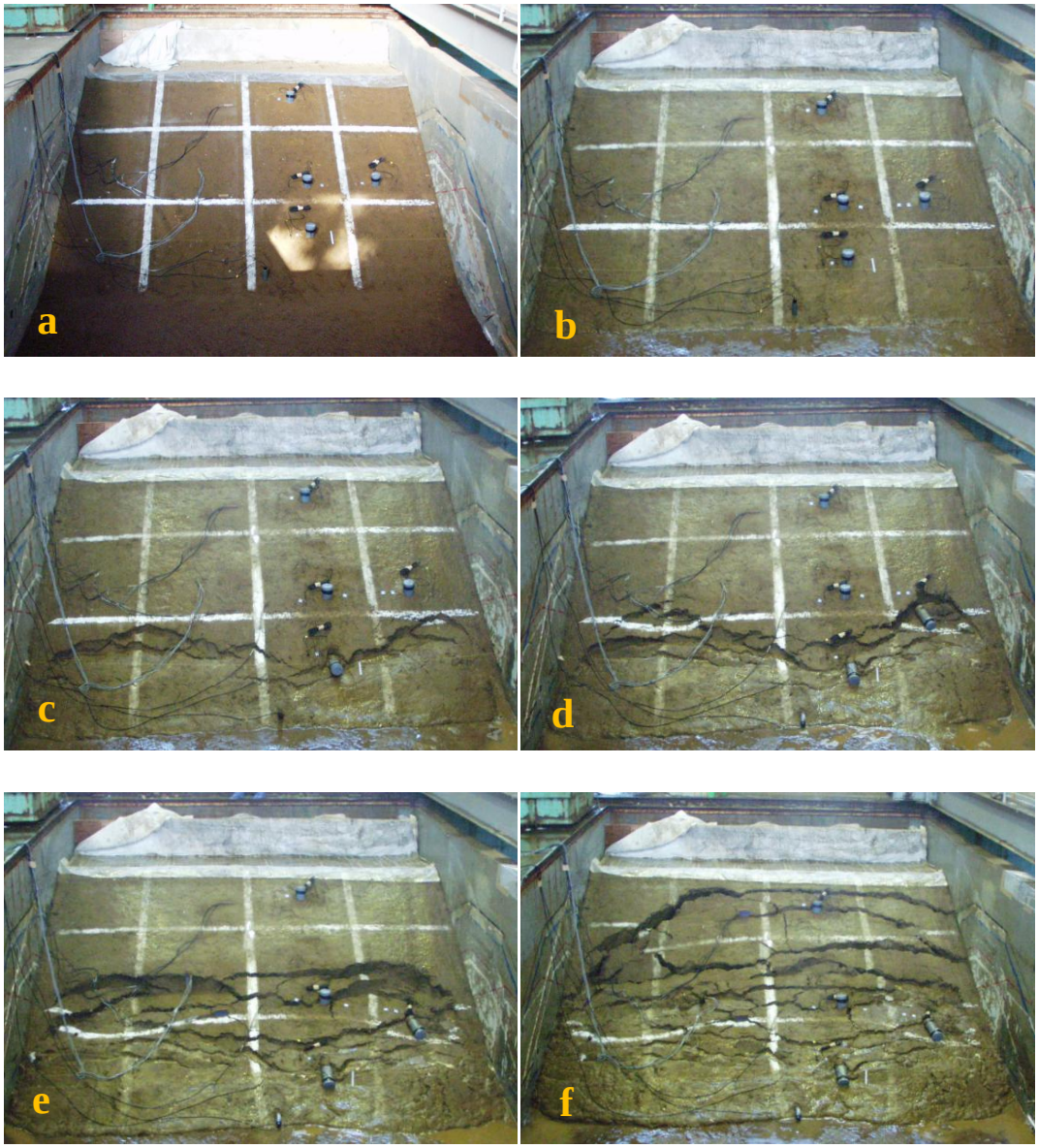

Fig. 4-1 Inconsistent tilting direction of tilt sensors (after Uchimura, 2010)

4.2.1 Small-scaled model tests for tilting direction investigation

Laboratory model tests, with different shapes of pre-defined slipe surfaces and different testing materials, were conducted using different triggering factors to induce the landslips. Tilt sensors attached to different length of rods reaching or not reaching the slip surface of slopes were installed in the slope. In these small-scaled model tests, two layers, the base layer and surface layer were built with a polythene sheet placed between these two layers to simulate a weak layer or existing slip surface.

4.2.1.1 Procedures of slope model tests induced by different triggering factors

Different triggering factors, including tilting the container tank gradually and applying periodical or continuous artificial rainfall to induce the slope failure, were performed to explore the tilting directions of tilt sensors embedded into the slope. The procedure for the model tests by tilting container tank is listed below.

1) Desired weight of oven dried sand was used and mixed with water to get the specific moisture content.
2) The moist soil was compacted to the maximum dry density to make the base layer in the container tank at horizontal as shown in Fig. 4-2-a. In order to build this layer with uniform density, it was divided into several thinner layers, and each of these layers was constructed by compaction with a certain amount of sand to obtain the specific relative density. The surface of each compacted layer was roughened before making the next layer to achieve a good bond.
3) After the base layer constructed, the slip surface was modeled by caving the base layer into a required shape (Fig. 4-2-b).
4) Then, a polythene sheet was placed on the caved slip surface before building the surface layer. The polythene sheet between the base layer and surface layer was to simulate a weak layer or existing slip surface.
5) The surface layer was constructed by compacting the soil into a desired dry density, and the procedure is similar as that in the base layer constrution. Then, sensors were carefully installed in the pre-designed locations in the surface layer of slope models (Fig. 4-2-c).

6) For the model tests induced by tilting, slope models were tilted using a lifting mechanism step by step(Fig. 4-2-d). In each step, when the monitoring data from each tilt sensor is stable, then it moves to the next step.

7) By increasing the tilting angle of the container step by step, the shear stress and resistant stress along pre-defined slip surface will be changed. Slopes begin to slip when the balance between shear stress and resistant force along the slip surface can not be sustained. The data collected by sensors installed in the surface layer was continuously recorded during the tests.

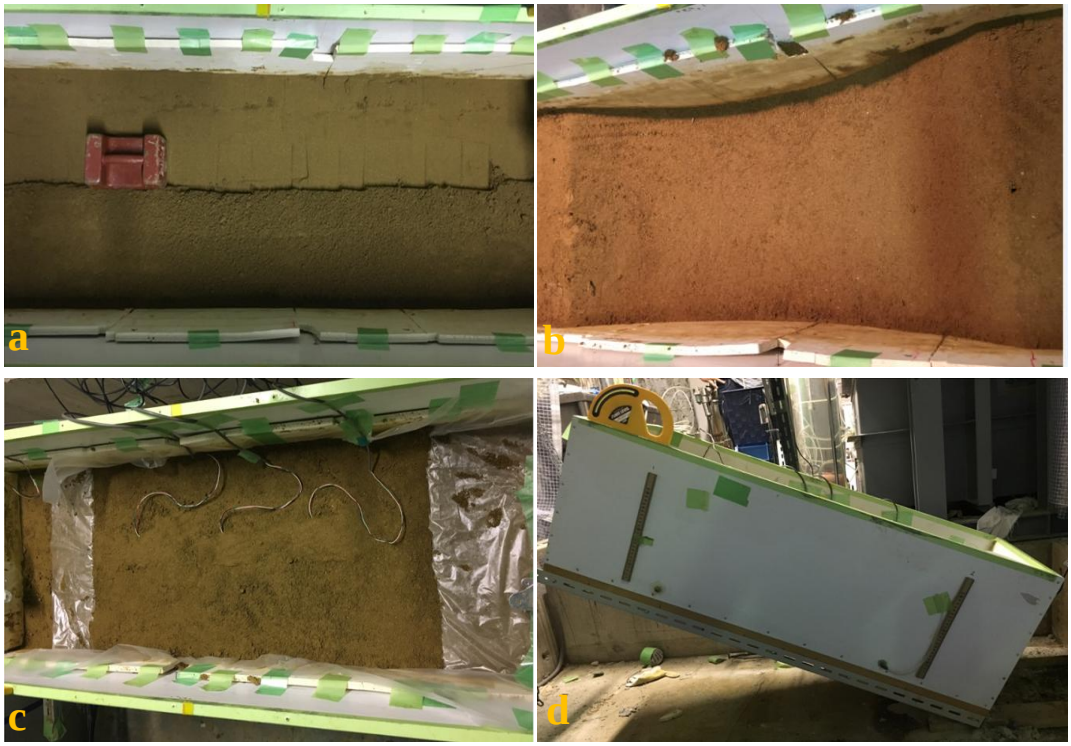

Fig. 4-2 Images of procedure for model tests induced by lifting

On the other hand, the procedure for the model tests induced by rainfall is presented as follows.

1) to 5) is similar as the procedure mentioned before.

6) For the model tests induced by rainfall, after the installation of sensors, slope models were then tilted and kept at an angle .

7) Setting up artificial rainfall simulation system.

8) Artificial rainfall was supplied periodically or continuously. With the infiltration of rainwater, the shear stress increases while resistant stress near the slip surface

decreases. Slopes begin to slide along the slip surface when shear stress exceeded the resistant force along the pre-defined slip surface (Fig. 4-3).

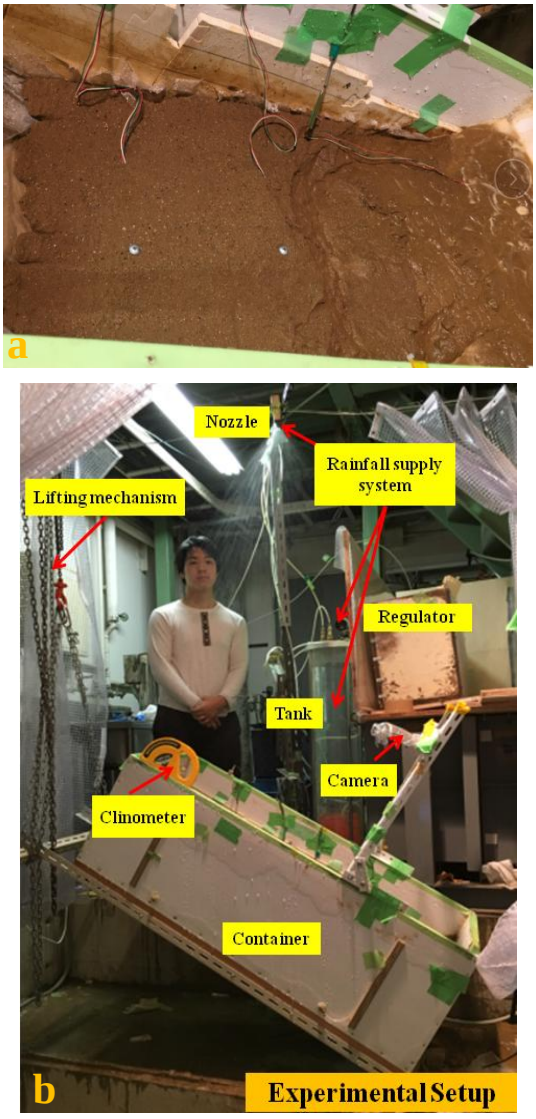

Fig. 4-3 Images for model tests induced by rainfall

4.2.1.2 Slope model tests using tilt sensors with different length of rods

In the small-scaled model tests with pre-defined slip surfaces, tilt sensors attached to different lengths of rods were used to explore the tilting behavior of tilt sensors installed in slope. The first type is the tilt sensors without rods. As shown in Fig. 4-4, tilt sensors were pressed into the surface layer at the depth around 2 cm or 3 cm, and an external tilt sensor was attached to the wooden box (container) to record the tilting angle of the box. The second type is tilt sensors with short rods, 55 mm and 70 mm, also located over the slip surface (Fig. 4-5). The final type is using long rods reaching

the slip surface, as presented in Fig. 4-6.

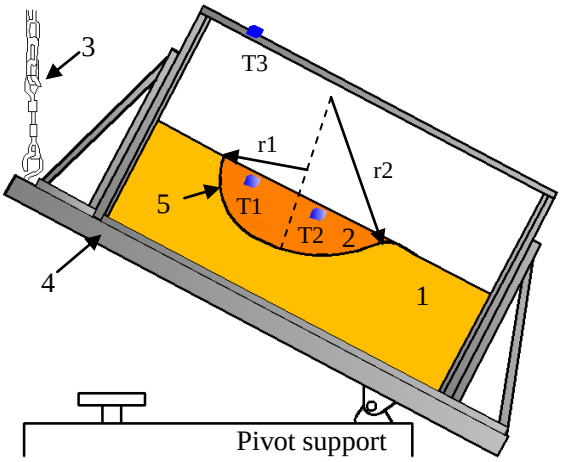

Fig. 4-4 Illustration of model tests using tilt sensors without rods

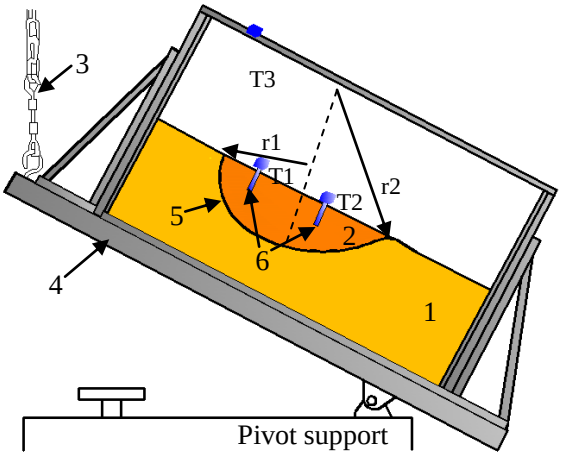

Fig.4-5 Illustration of model tests using tilt sensors with short rods

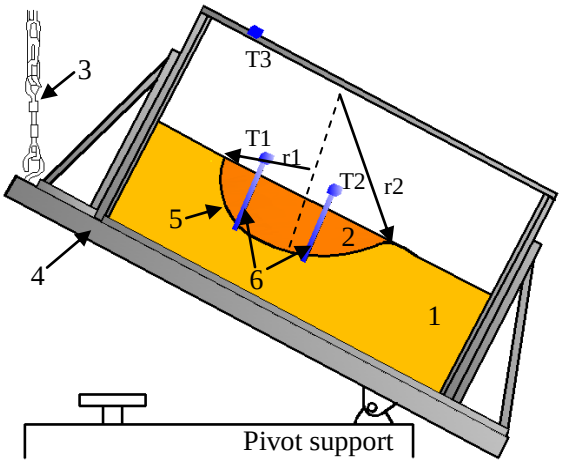

Fig. 4-6 Illustration of model tests using tilt sensors with long rods

Where 1 and 2 represent for base layer and surface layer. 3 is the lifting mechanism and 4 is the wooden box (container). 5 is the pre-defined surface, and 6 represents for

the rods attached to tilt sensors.

4.2.2 Field tests for tilting direction investigation

Field tests were also conducted together with Guangxi University in Guangxi Province, China. In field tests, tilt sensors attached to three types of rods with different lengths, as shown in Fig. 4-7. The location of slip surface could not be decided precisely, so tilt sensors with these three different lengths of rods were installed on the natural slopes. By measuring failed areas after the tests, it indicated that the depth of slope slip surfaces are less than 25 cm, and the tilt sensors with long length of rods, around 70 cm were too strong to be pushed down by the failed part. Schematic illustration for the field tests is presented in Fig. 4-8. Six tilt sensors attached to different lengths of rods were arranged in three different columns in testing areas.

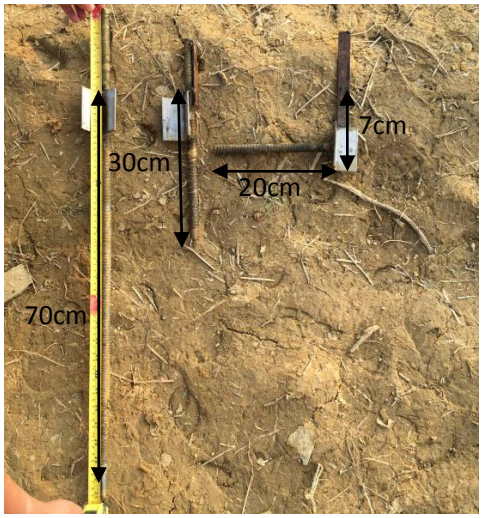

Fig. 4-7 Different types of rods attached to tilt sensors used in field tests

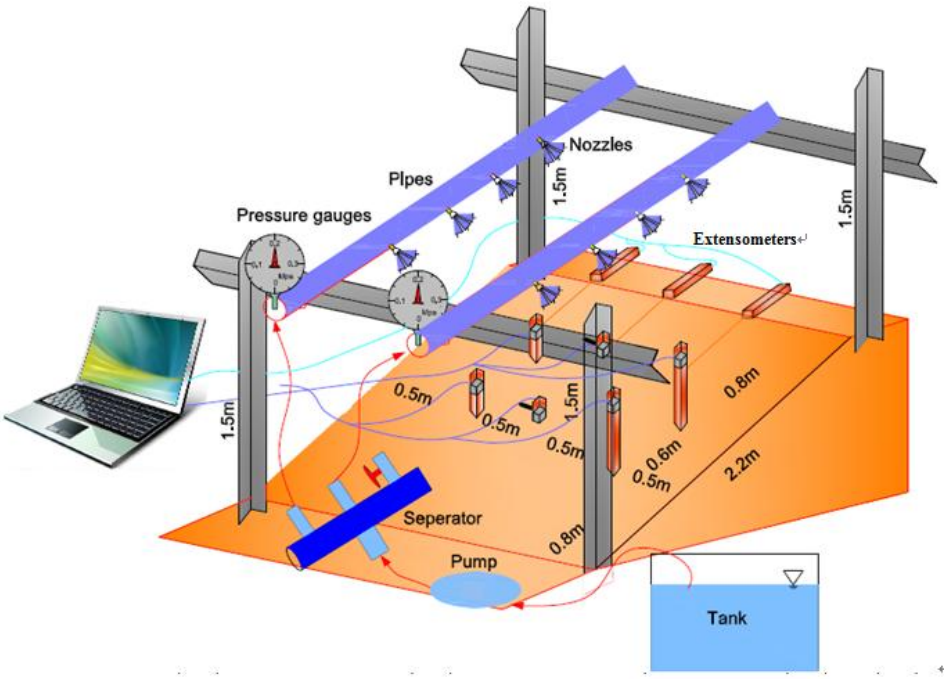

Fig. 4-8 Illustration for the arrangement of sensors and rainfall supply system in field tests

4.3 Methodologies for the exploration of the relationship between surface displacement and tilting angle of slope

Depending on the existing monitoring data of surface displacements and tilting angles against time in slope failure from field events or model tests, a similar trend has been observed (Lee, 2009; Uchimura, 2015). However, few researches have been carried out on the relationship between displacements and tilting angles of the slope surface in the pre-failure stage of landslides. In this study, the relationship between surface displacement and surface tilting angle is explored and validated by small scaled model tests with pre-defined slip surface as well as field tests on natural slopes.

4.3.1 Small-scaled model tests for the relationship between surface displacement and tilting angle of slope investigation

In laboratory tests, slope models were constructed with different shapes of pre-defined slip surfaces, and surface deformation of these slopes, including tilting angle as well as surface displacement, was measured in the tests. The tilting behavior was measured by tilt sensors while the surface displacement was approached by the application of image

analysis technique to trace the moving path of marked points on the slope surface.

4.3.1.1 Illustration of apparatus setting up

As shown in Fig.4-9 and Fig.4-10, the arrangement of sensors is presented. Fig. 4-9 shows the illustration of testing conditions in the tests using tilt sensors without rods, while Fig. 4-10 presents the details of the tests using tilt sensors with short rods located above the slip surface. In these tests, some nail marks were pressed into the surface layer near to the location of tilt sensors. By tracing these marks using image analyzing techniques introduced in the following sections, the surface displacement of slope at these points can be obtained. The testing conditions in those tests using tilt sensors with long rods reaching the pre-defined slip surface are shown in Fig. 4-11, and the marked points were setted on tilt sensors because gaps occurred between the rods and the sliding body in the tests (Fig. 4-12), so the surface displacement obtained based on the marked points on tilt sensors represent for the actual surface displacement.

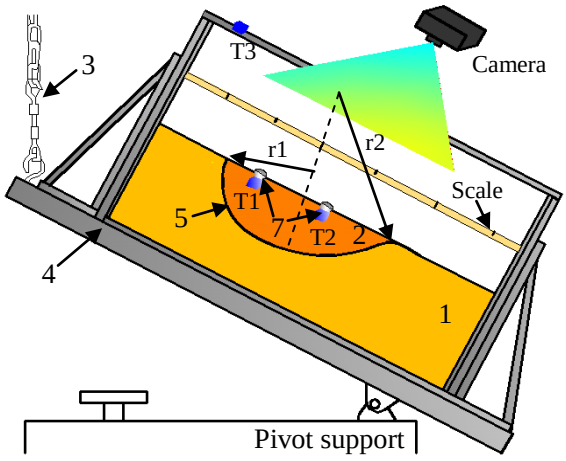

Fig. 4-9 Illustration for the arrangement of sensors without rods

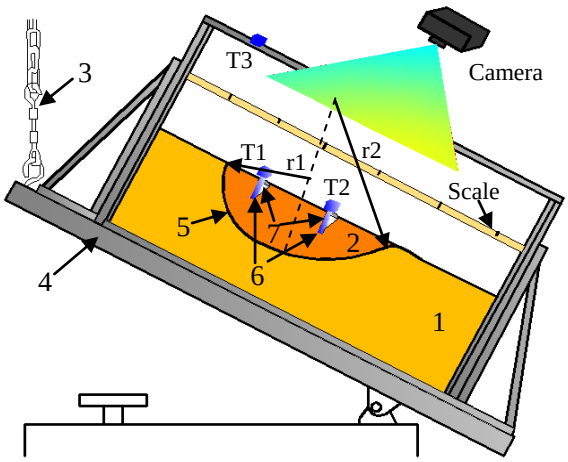

Fig. 4-10 Illustration for the arrangement of sensors with short rods

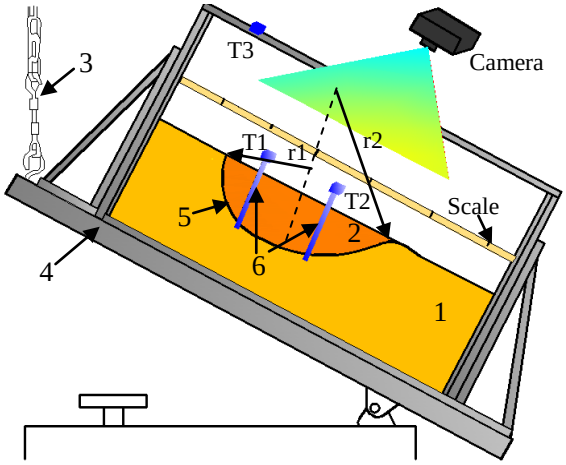

Fig.4-11 Illustration for the arrangement of sensors with long rods

Where 1 and 2 represent for base layer and surface layer. 3 is the lifting mechanism and 4 is the wooden box (container). 5 is the pre-defined surface, and 6 represents for the rods attached to tilt sensors. 7 is the mark points.

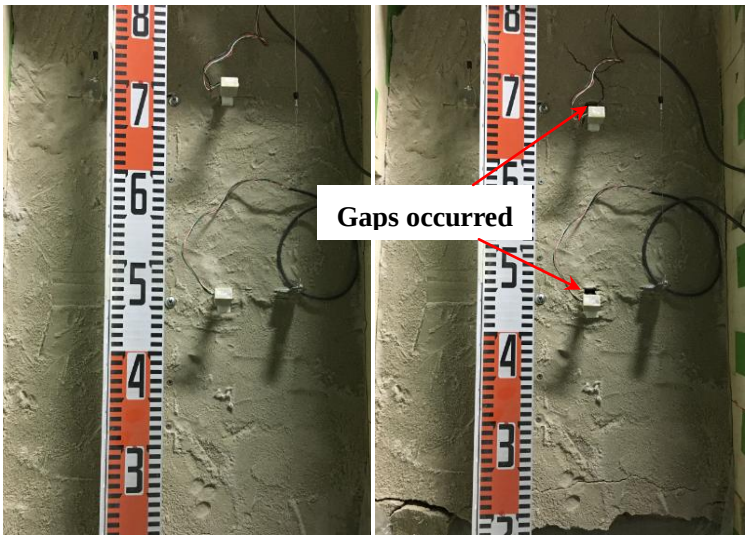

Fig. 4-12 Gaps occurred betweent the rods and the sliding block

4.3.1.2 Image analysis technique for surface displacement measurement

In the tests, the tilting behavior of slopes was recorded by tilt sensors, which were installed in the surface layer of slopes, and an extra tilt sensor attached to the wooden box was also used to measure the box tilting as shown in Fig. 4-9, Fig. 4-10 and Fig. 4-11. On the other hand, the surface displacement was obtained by tracing the moving path of points nail marks on the slope surface by image analyzing techniques. The schematic illustration for image analyzing in model tests is presented in Fig. 4-13.

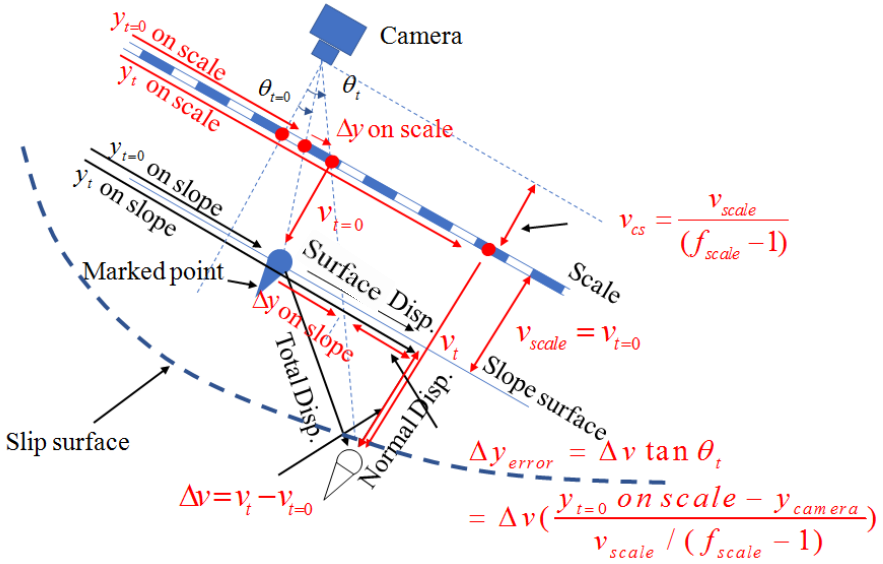

Fig. 4-13 Schematic illustration for image analyzing method in model tests

In the tests, a camera was employed to record the moving path of marked points pressed into the slope surface by photo taking during the tests and a scale fixed over the slope surface was used as a reference coodinate. The surface displacement of marked points shown in Fig. 4-13 can be approached by following equation

$$\Delta y_{actual} = f_{scale} \bullet \Delta y\, on\, scale + \Delta v \bullet (\frac{\Delta y\, on\, scale - y_{camera}}{v_{scale}/(f_{scale}-1)}) \quad (4\text{-}1)$$

Where Δy_{actual} and Δy on scale represent the actual surface displacement and the surface displacement obtained from images as shown in Fig. 4-13. f_{scale} is the ratio $f_{scale} = \Delta y_{on\,slope} / \Delta y_{on\,scale}$, and $\Delta y_{on\,slope}$ represents for the actual value on the slope surface whlie $\Delta y_{on\,scale}$ is the value approached from photos. y_{camera} means the location of camera in the coordinate of images, and it is always located at the center of the

images. v_{scale} is the height difference between the scale and initial slope surface, and Δv represents for the normal displacement variation measured by a vernier. Then, the total displacement can be obtained by equation 4-2

$$\Delta s = \sqrt{\Delta v^2 + \Delta y_{actual}{}^2} \tag{4-2}$$

Where Δs is the total displacement of marked points near to the tilt sensors, and Δv is displacement variation in normal direction of the slope surface. Δy_{actual} means the actual surface displacement on slopes.

In the model tests using long rods with marks setted on tilt sensors, the equation for total displacement calculation is the same as equation 4-2.

4.3.1.3 Data analyzing in model tests

Model tests were conducted with different triggering factors, including box tilting or artificial rainfall applying. The data analyzing method the model tests are discussed in following sections.

As for the landslides induced by box tilting, the relationship between the total displacement and tilting angle of slopes is investigated based on the total displacement approached using equation 4-2 and the corresponding tilting angle recorded by tilt sensors. In these tests, the corresponding tilting angle were selected in every tilting step at the time when the total displacement approached. As shown in Fig. 4-14-a, marked points on the green curve and red curve, were the selected data points in each step from tilt sensor 1 and tilt sensor 3 respectively. Tilt sensor 3 was attached to the wooden box, as shown in Fig. 4-9, Fig. 4-10 and Fig. 4-11, so the time history of tilting monitored by Tilt sensor 3, the blue curve, indicates the tilting angle of the wooden box in each step in the tests. On the other hand, the red curve from Tilt sensor 1 results from the box tilting and slope deformation. The large difference between the blue curve and red curve in Fig. 4-11-a was caused by the slope deformation. Fig. 4-14-b presents the tilting angle induced by deformation in each step. The plot in Fig. 4-14-c is the total displacement Δs of tilt sensor 1 against time obtained by equation 4-2.

The relationship between total displacement and tilting angle caused by the slope deformation recorded by tilt sensor 1 is presented in Fig. 4-14-d. A linear relationship is indicated in Fig. 4-14-d, and the physical meaning of this linear relationship will be introduced in following Chapters.

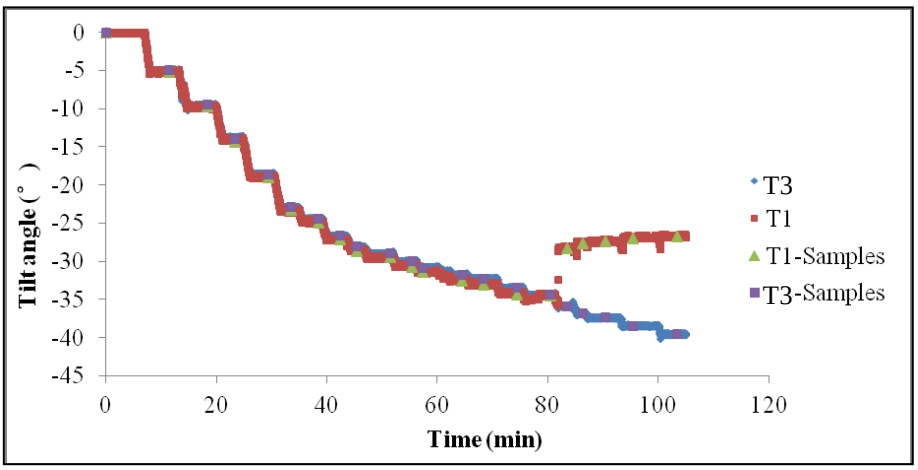

(a) Time series data of tilting angle of T1 and T3

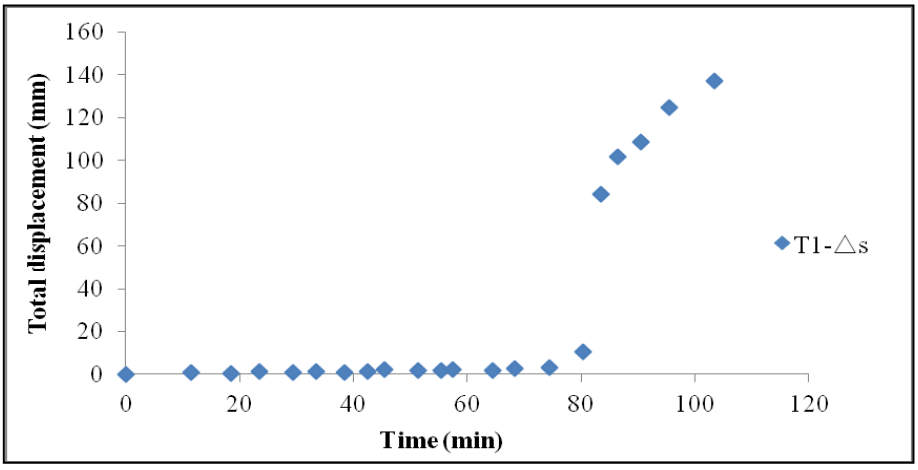

(b) Variation of surface displacement of T1 against time

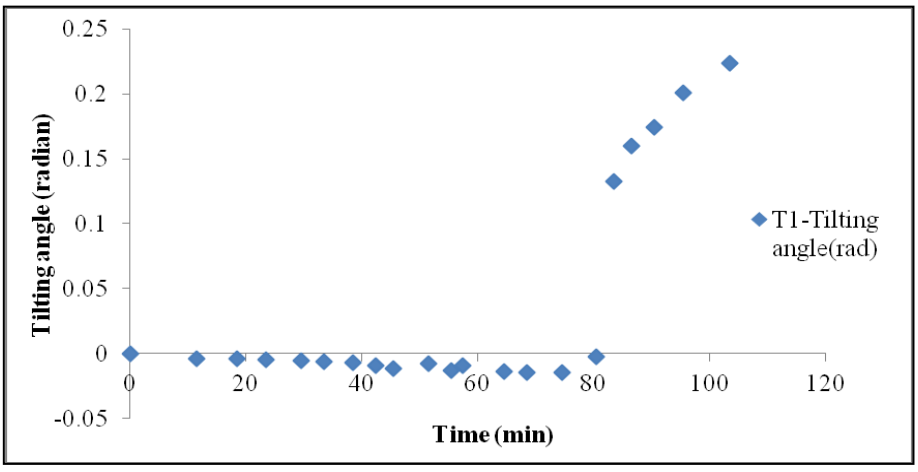

(c) Variation of tilting angle of T1 agianst time

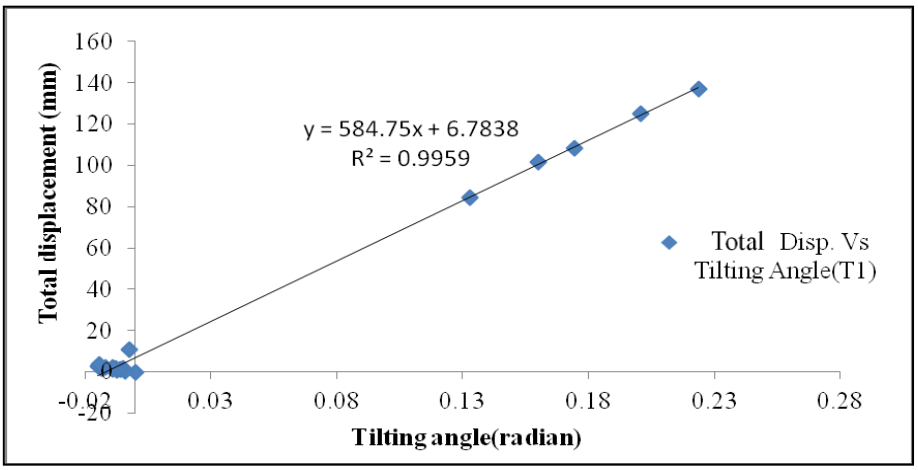

(d) The relationship between tilting angle and surface displacement

Fig.4-14 Data analyzing method of model tests induced by lifting

On the other hand, Fig. 4-15 shows the analyzing method for model tests by applying artificial rainfall. In these tests, slope models were inclined with an angle, and then periodical rainfall was applied. In every step, rainfall was supplied periodically. During the tests, photos were taken to trace the moving path of nail marks on surface layer while the tilting behaviour of surface layer was measured by tilt sensors and the selected data points for analyzing were also picked out at the time when photos were taken as shown in Fig. 4-15-a). Fig. 4-15-b shows the time history of total displacement. The tilting angle induced by rainfall is presented in Fig. 4-15-c. Similar as Fig.4-14-d, the data of total displacement is plotted against the corresponding tilting angle recorded by tilt sensor 1 in Fig. 4-15-d. Compared with the model tests, of which slope failure was induced by tilting the container, a linear relationship between the total displacement and tilting angle is also indicated in the tests that slope failure was triggered by applying rainfall.

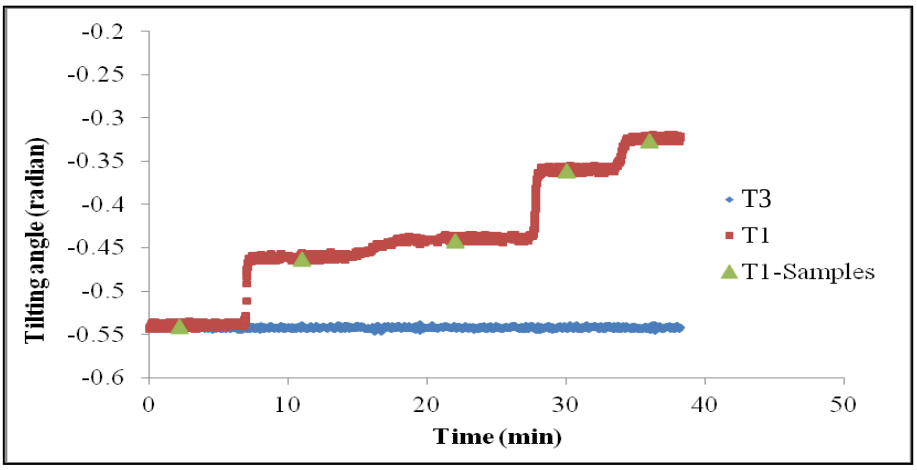

(a) Time series data of tilting angle of T1 and T3

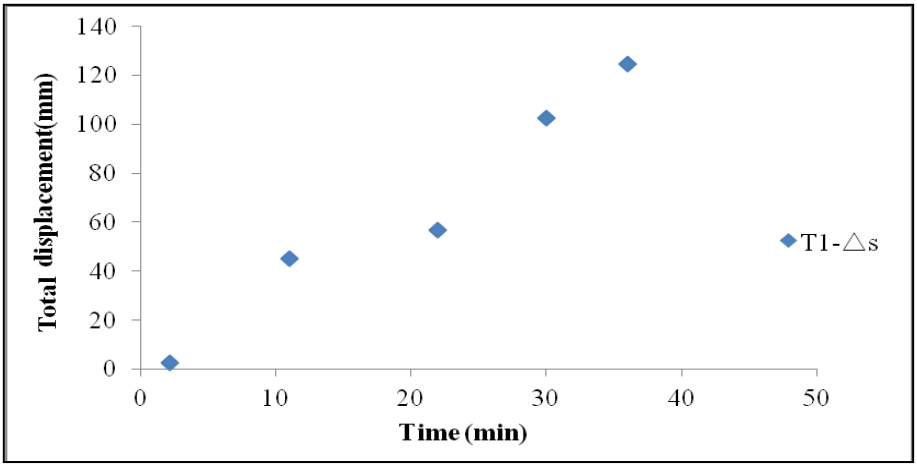

(b) Variation of surface displacement of T1 with time

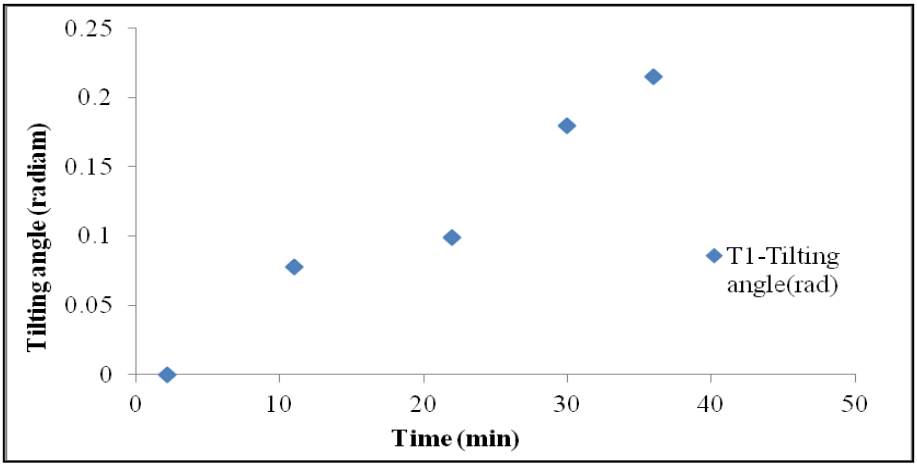

(c) Variation of tilting angle of T1 with time

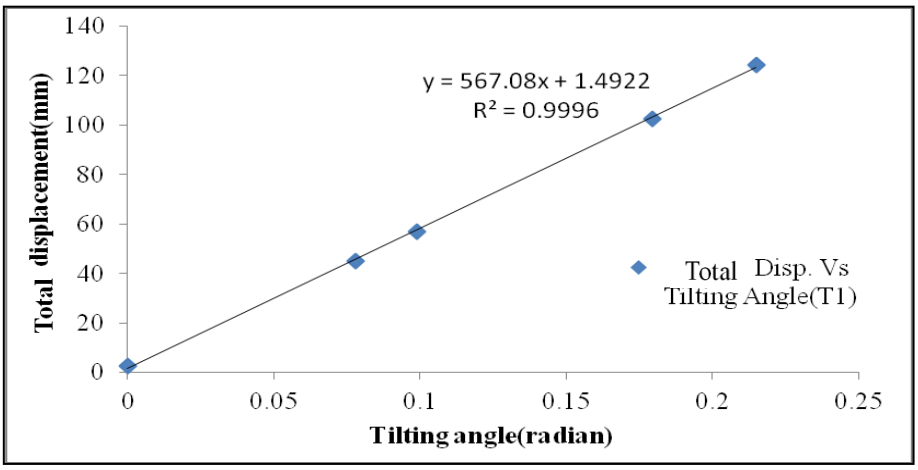

(d) The relationship between tilting angle and surface displacement

Fig.4-15 Data analyzing method of model tests induced by rainfall

4.3.2 Field tests for the relationship between surface displacement and tilting angle of slope investigation

In field tests, tilt sensors and extensometers were used to measure the tilting angel and displacement of the testing areas under artificial rainfall. The schematical illustration for the arrangement of sensors is presented in Fig. 4-8. The tilting behaviours along the slope direction was monitored by tilt sensors and the monitoring data from was converted by a Analog/Digital converter, and sent to the computer every second in the tests. The displacement measured by extensometers was recorded by a high performance data logger produced by Keyence Corporation every 500 ms.

An artificial rainfall supply system was used in field tests, comprising of a pump, a tank, water separators, pressure gauges and nozzles. The tank was to impound water, and the pump with capacity 0.75 kw per hour was to supply the water for artificial rainfall. Additionally, water separators and pressure gauges were used for controlling rainfall intensity.

Fig. 4-16 shows the data analyzing method for field tests. The tilting angle is from tilt sensor T1 and displacement is from extensometer E2 which was attached to the rod of T1 using a magnet as shown in Fig. 4-16. In the Fig. 4-16-a shows the testing area before slope failure while Fig. 4-16-b is the image after the slope failure. The time

history of slope displacement from E2 is indicated in Fig. 4-16-c, and the time history of tilting angle monitored by T1 is presented in Fig. 4-16-d. The relationship between displacement and tilting angle is shown in Fig. 4-16-e, and a linear relationship between displacement and tilting angle is also indicated.

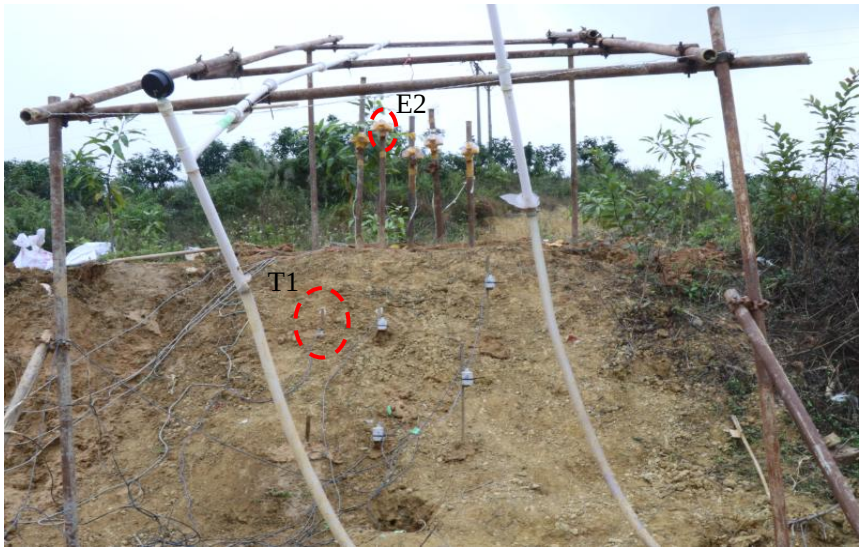

(a) The image for the testing site before slope failure

(b) The image for the testing site after slope failure

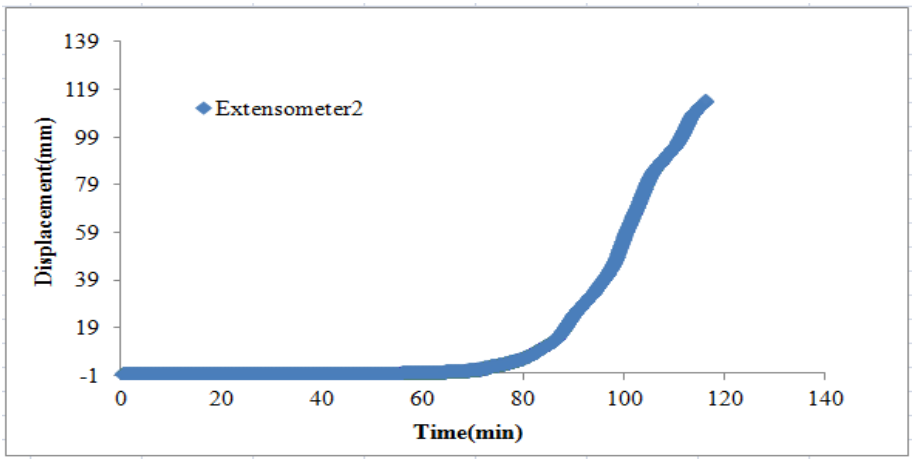

(c) Variation of surface displacement of E2 with time

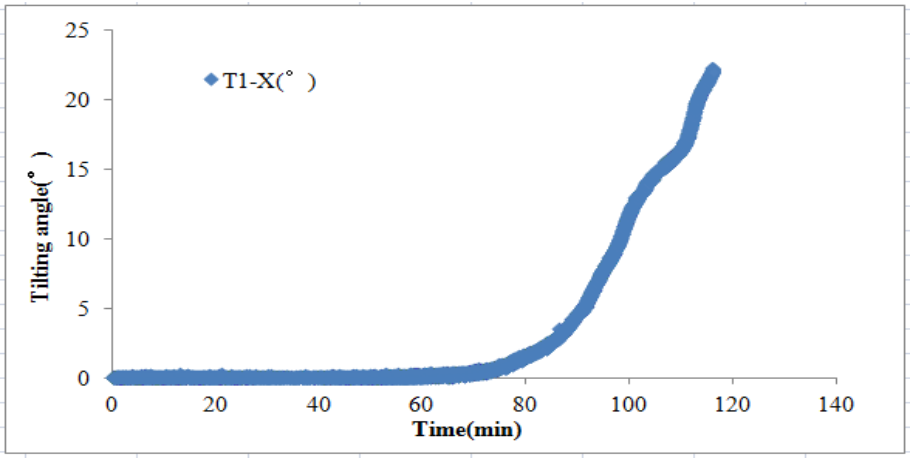

(d) Variation of tilting angle of T1 in X direction with time

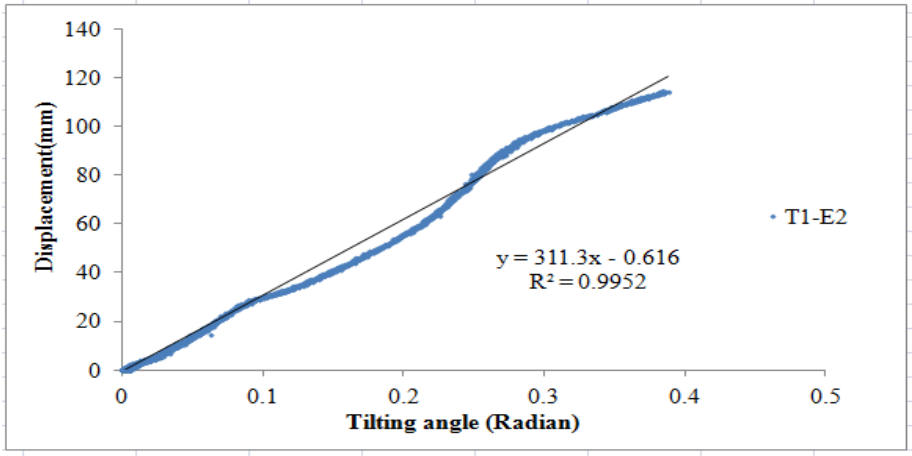

(e) The relationship between tilting angle and surface displacement

Fig. 4-16 Data analyzing method of field tests induced by rainfall

4.4 Methodologies for the exploration of the predicting methods based on the time history of tilting angle of slope

4.3.1 Types of tests for landslide prediction methods investigation using tilting angle

In this study, different types of small-scaled slope model tests as well as the field tests using artificial rainfall were carried out. The first type of model tests was with pre-defined slip surface as shown in Fig. 4-17. In these tests, artificial rainfall was applied to induce the slope failure.

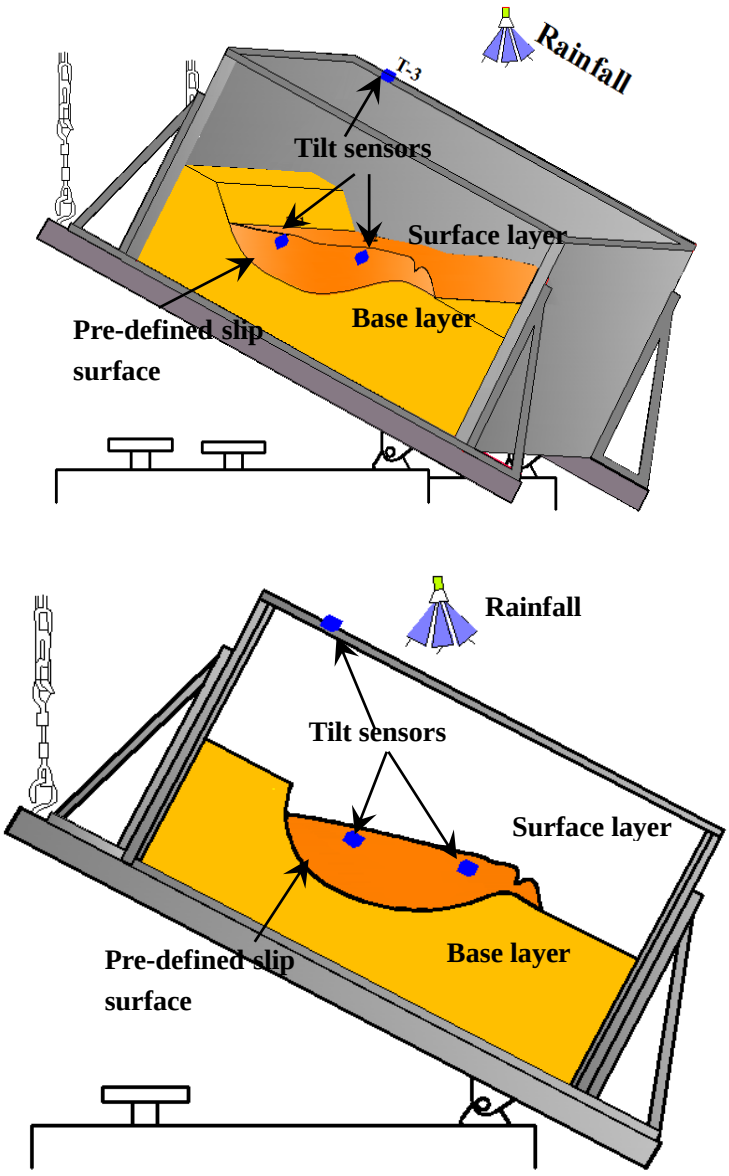

Fig. 4-17 Illustration of model tests with pre-defined slip surface by applying rainfall

The schematic illustration of the second type of model tests was presented in Fig. 4-18. In these model tests, two layers, base layer and surface layer, were constructed in a wooden tank, measuring 800 mm×300 mm×400 mm(Fig. 3-17-b), with different dry density. The procedure of slope model construction is presented in Fig. 4-19-a, Fig. 4-19-b, and Fig. 4-19-c, Fig. 4-19-d, respectively. Similar as the testing condition mentioned before, artificial rainfall was applied to trigger the landslips. Several tests considering various conditions, such as changing the dry density or thickness of the surface layer and changing the slope angle, were performed listed in Table 4-1. Most of these tests showed progressive failure process and the tilt sensor with long rods installed in the bottom part of the models indicate abnormal tilting behaviour before the slope failure.

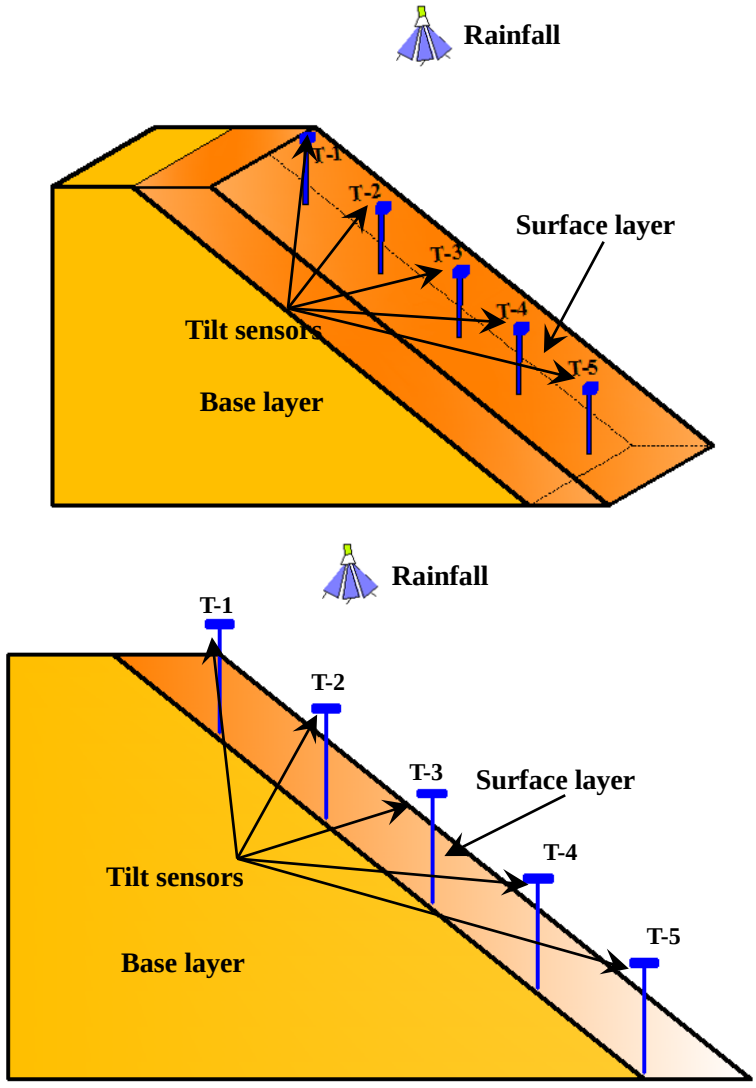

Fig. 4-18 Illustration of the second type fo model tests

Fig. 4-19 The procedures for slope model construction

Table 4-1 Details about the model tests

Test No.	Materials	Thickness(cm)	Slope angle(°)	Dry density (g/cm3)
1	Edosaki sand	15	38.5	1.22
2	Edosaki sand	10	38.5	1.22
3	Edosaki sand	15	38.5	1.35
4	Edosaki sand	15	38.5	1.35
5	Edosaki sand	15	45	1.22
6	Edosaki sand	20	38.5	1.22

Field tests were also conducted together with Guangxi university in Baise city of Guangxi Province. The sites consist of weak expansive soil and the slope angle is around 43°. The image about one of the testing sites is shown in Fig. 4-20. In the tests,

the slope failure was also induced by applying artificial rainfall using an artificial rainfall supply system, which comprises of a pump, an artificial pond, two pressure gauges, some water separators and spray nozzles. The spray pattern and rainfall distribution of the nozzles (1/8MJJXP005PVDF) are designed by H.IKEUCHI & Co.,Ltd. In order to achieve an uniform distribution rainfall intensity, parameters for the rainfall supply system, such as interval distance between each spray nozzle, driving pressure for water spray, and the location of nozzles were carefully designed. In this system, the pump with a capacity 0.75 kw per hour is used to supply the water for rainfall, while an artificial pond is employed to impound water. In the field tests, rainfall intensity was controlled by a water separator which was used to adjust the driving pressure for rainfall supply. Furthermore, tilt sensors with different lengths of rods were implemented on the natural slopes in these tests to measure the surface tilting of slopes, and extensometers attached to the rods of tilt sensors were used to measure the displacement of slopes.

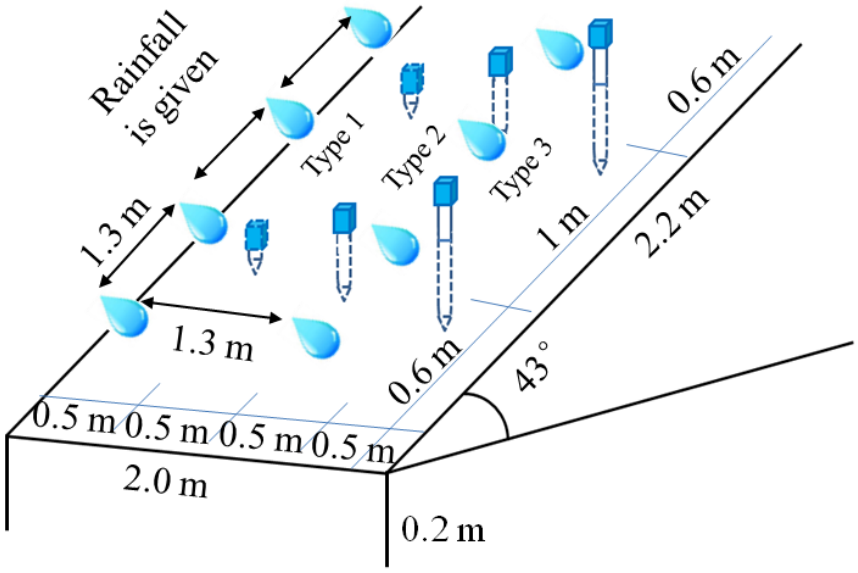

Fig. 4-20 Image about the field test in Guangxi

4.4.2 Landslide prediction based on the time history of tilting angel of slopes

The time history of tilting angle of slope surface recorded by tilt sensors is presented in Fig. 4-21. In the accelerating stage as shown in this figure, data of tilting angle is

selected every 1° , as shown in Fig. 4-21 using red squares. The inverse of tilting angle rate can be calculated by $\frac{dt}{d\theta}$, where $d\theta$=1° and dt represents for the interval time of every 1° , as shown in Fig. 4-22. The plot of the inverse of tilting angle rate against time is presented in Fig. 4-23, and the failure time of landslide can be predicted based on the fit line, and the predicted failure time is the intersection of the fit line and the time axis, as shown in Fig. 23.

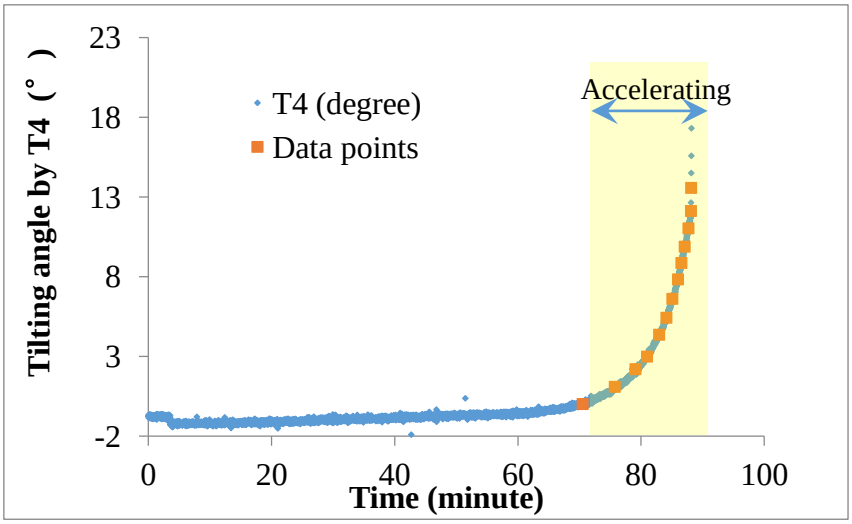

Fig. 4-21 Time history of tilting angle

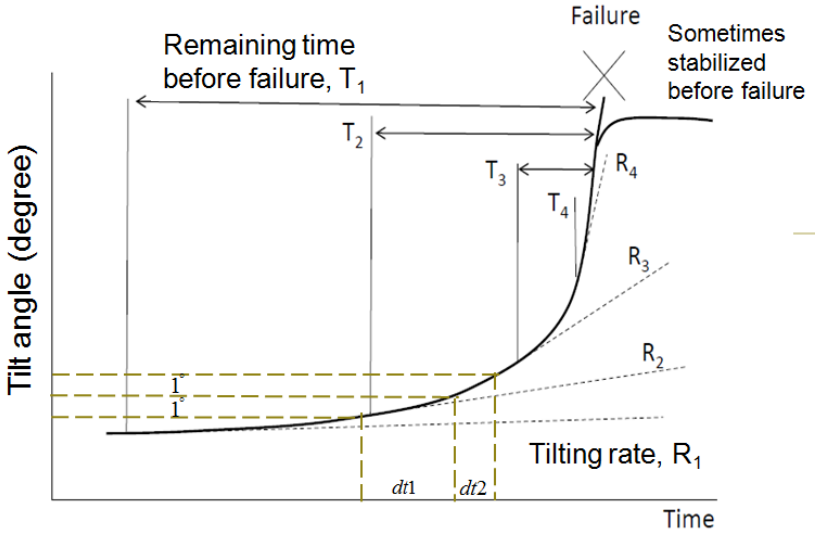

Fig. 4-22 Data analyzing

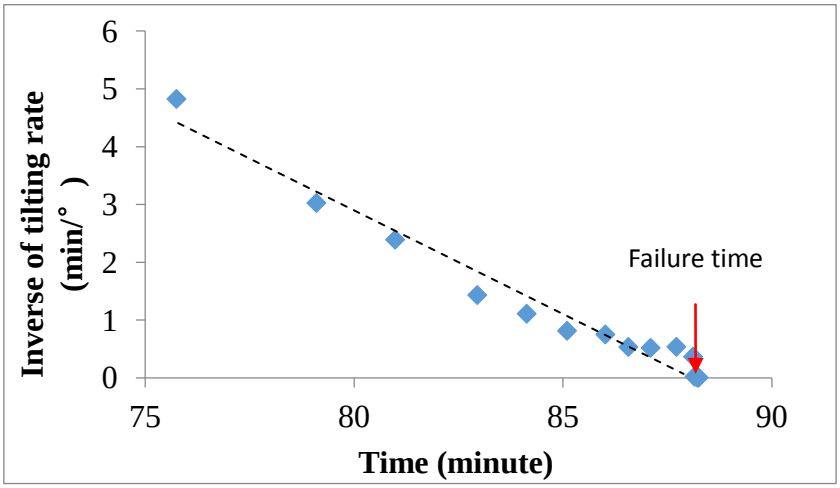

Fig. 4-23 The inverse of tilting angle rate against time

4.5. Summary

In this section, the methodology to investigate the tilting directions of tilt sensors installed on slope surface, the relationship between the surface displacement and tilting angle, and landslide prediction methods based on time history of tilting of slope surface is introduced. The test conditions of different types of model tests as well as field tests are presented in this chapter.

4.6. References

Lee, J. M. S. (2009). "Real-time monitoring of landslides using wireless network." Doctor dissertation, The Ohio State University.

Uchimura T., Towhata I., Wang L., Seko I. (2008). "Simple and low-cost wireless monitoring units for slope failure." Proc. of the First World Landslide Forum, International Consortium on Landslides (ICL), Tokyo, 611–614.

Uchimura, T., Towhata, I., Trinh, T. L., Fukuda, J., Carlos, J. B. B., Lin, W., Seko, I., Uchida, T., Matsuoka, A., Yosuke I., Onda, Y., Iwagami, S., Min-Seok, K., Sakai, N. (2010). "Simple monitoring method for precaution of landslides watching tilting and water contents on slopes surface." Landslides, 7, 351-357.

Uchimura T., Towhata I., Wang L., Nishie S., Yamaguchi H., Seko I. and Qiao J. (2015). "Precaution and early warning of surface failure of slopes by using tilt sensors." Soil and Foundation, 55(5), 1086-1099.

CHAPTER 5

TEST RESULTS FOR THE TILTING DIRECTIONS

5.1. Introduction

Although inconsistant tilting direction of tilt sensors has been detected even in the same landslide, limited researches for the exploration of this problem can be found in literatures. In this chapter, small-scaled model tests and field tests are conducted to understand the inconsistent tilting behaviour of tilt sensors observed in previous studies(see Fig. 4-1). In small-scaled model tests, tilt sensors with different lengths of rods were used, and slope failure was induced by different triggering factors under diverse testing conditions introduced in Chapter 4. Additionally, field tests were also carried out by applying artificial rainfall. The results from these tests are presented and discussed in this chapter.

5.2. Test results from small-scaled model tests

Laboratory model tests, with pre-defined slipe surfaces using tilt sensors attached to different lengths of rods, including no rods, short rods and long rods reaching to the slip surface, were conducted under various testing conditions. In the following sections, test results from these tests were discussed in details.

5.2.1 Small-scaled model tests using tilt sensors without rods

Details about the slope model construction and arrangement of sensors in laborotory tests using tilt sensors without rods was discussed in Chapter 4. In this section, the speicific testing conditions, including the shape of the pre-defined slip surface in each

test as shown in Table 5-1, time history of container tilting and so on, are presented. Together with the introduction of testing conditions, the test results were also discussed in this part.

Table 5-1: Small-scaled tests using tilt sensors without rods

Test No.	Materials	Radius of the slip surface(mm)	Relative desity,Dr(%)	Triggering factor
1	Silica sand #7	R600	30	Lifting
2	Silica sand #7	R1000	50	Lifting
3	Silica sand #7	R600	50	Lifting
4	Edosaki sand	R600	40	Lifting
5	Silica sand #7	R600+R400	50	Lifting
6	Edosaki sand	R600+R400	40	Lifting
7	Silica sand #7	R300+R800	50	Lifting
8	Silica sand #7	R300+R800	50	Rainfall
9	Edosaki sand	R600	40	Rainfall
10	Silica sand #7	Infinite(planar)	50	Lifting

1) Test 1 using tilt sensors with no rods

The model was constructed in the wooden container (Fig. 3-17-a) following the procedure introduced in Chapter 4. Silica sand number 7 was performed in this test with a dry density around 1.25 g/cm^3 for the surface layer and 1.60 g/cm^3 for the base layer. The initial moist content is 10%. Fig. 5-1 shows the details about the shape of pre-defined slip surface, arrangement of instruments and so on. The landslip in this test was caused by inclining the wooden container step by step, and the tilting angle of the container was recorded by tilt sensor T3 attached to the edge of the container as shown in Fig. 5-1. The time history of the tilting angle of the container is presented in Fig. 5-2. The angle change of tilt sensor T1 and T2 installed in the surface layer, was caused by the container lifting and slope deformation. The difference between T1 and T3, or between T2 and T3 as shown in Fig. 5-3 is induced by slope deformation.

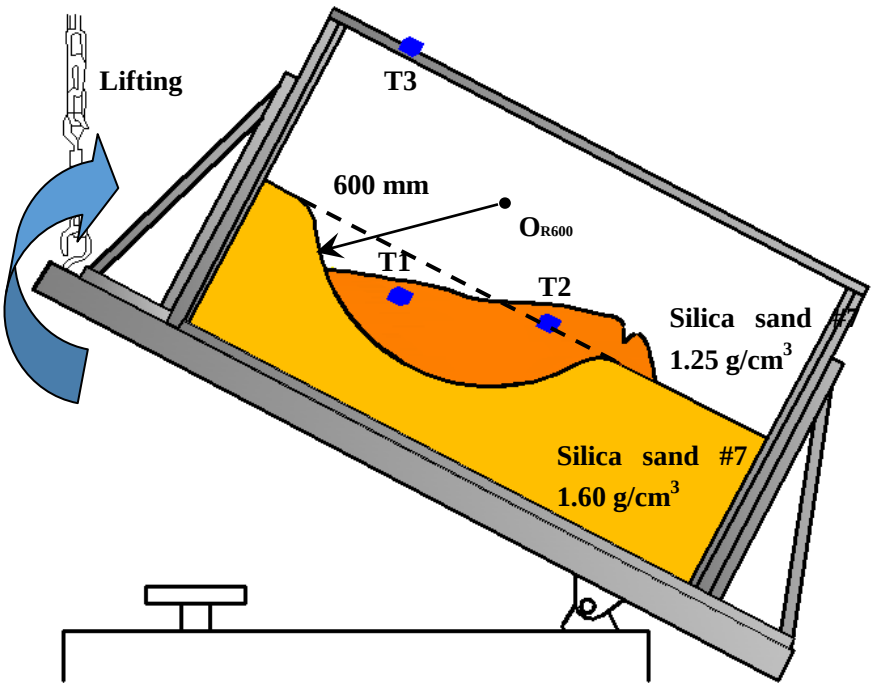

Fig. 5-1 Illustration of Test 1

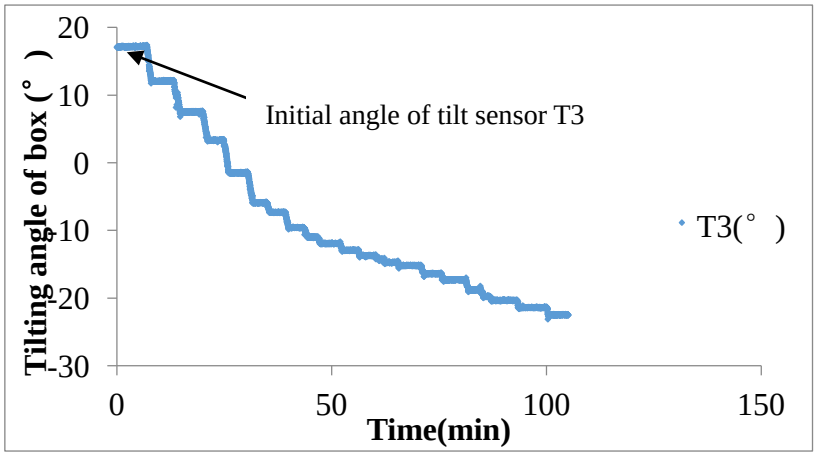

Fig. 5-2 Time history of wooden container lifting recorded by T3 in Test 1

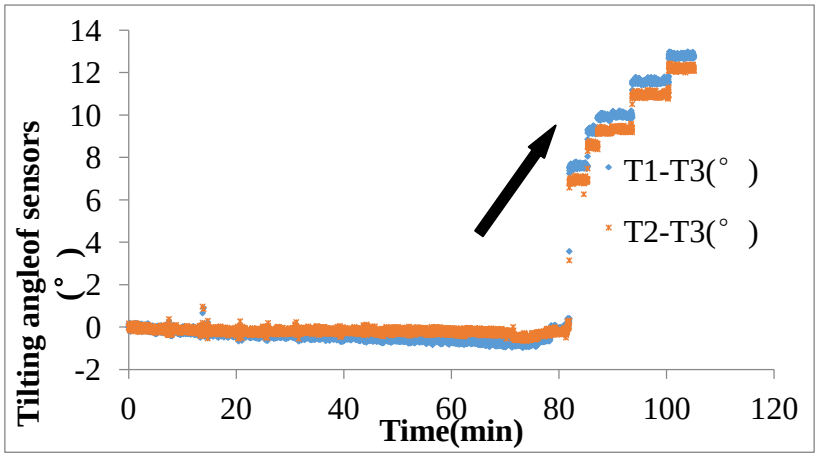

Fig.5-3 Time history of slope tilting recorded by T1 and T2 in Test 1

2) Test 2 using tilt sensors with no rods

The details about Test 2 is illustrated in Fig. 5-4. Compared with the testing condition in Test 1, in this test, the radius of slip surface and the dry density for surface layer were different, as shown in the following Fig. 5-4. Similar as that shown in Test 1, Fig. 5-5 and Fig. 5-6 shows the inclinating angle of the container and the tilting angle of the sliding block caused by slope deformation against time, respectively. In test 2, the tilt sensors also tilted backward even though the shape of slip surface and dry density of the surface layer are changed.

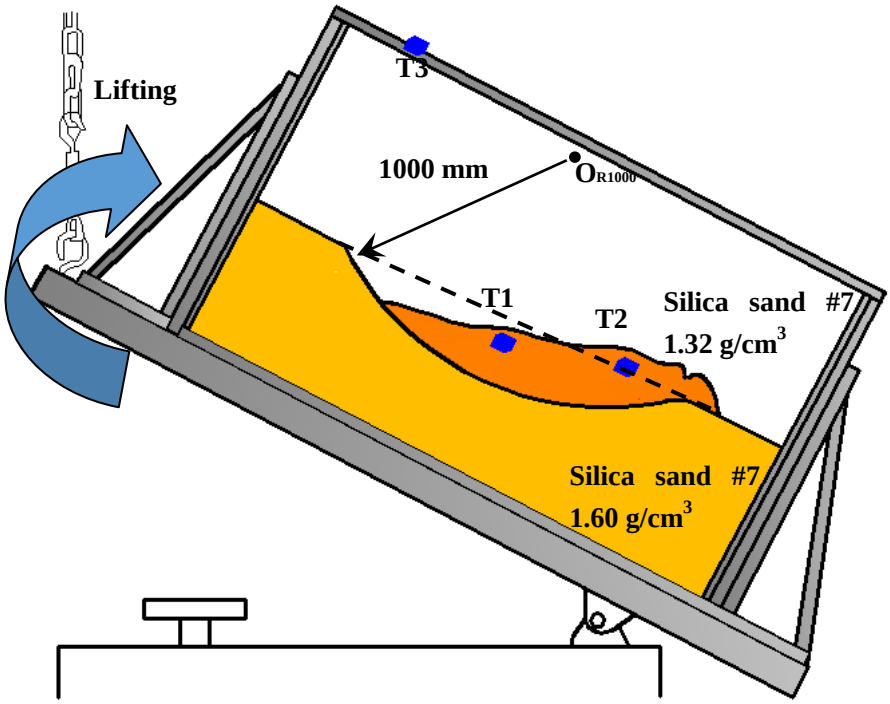

Fig. 5-4 Illustration of Test 2

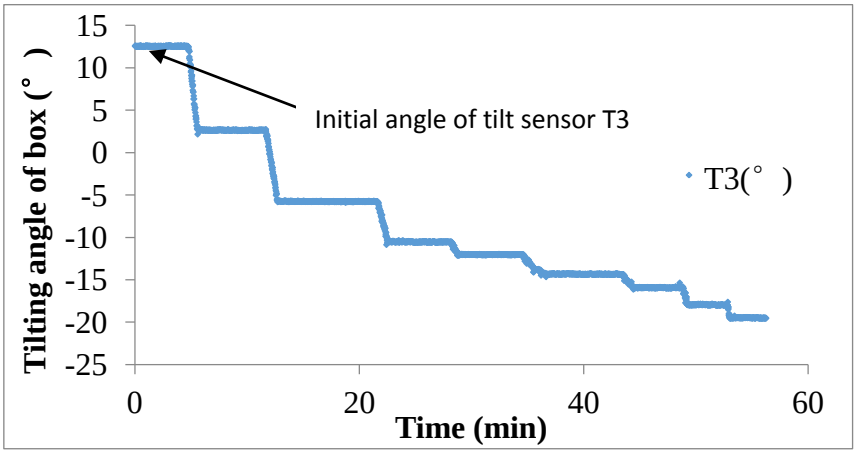

Fig. 5-5 Time history of wooden container lifting recorded by T3 in Test 2

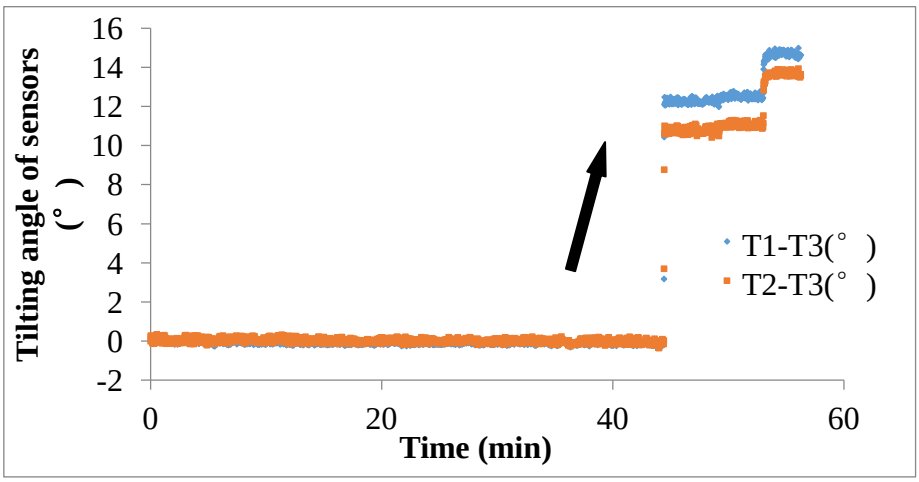

Fig. 5-6 Time history of slope tilting recorded by T1 and T2 in Test 2

3) Test 3

In this test, silica sand #7 with an dry density 1.32g/cm^3, was used for the surface layer, and three tilt sensors T1, T2 and T3 were installed in the surface layer of this slope with an external tilt sensor T4 attached to the top of the wooden container to record the tilting angle of this wooden container as shown in Fig. 5-7. The slope sliding in this test was also triggered by container tilting step by step. Fig. 5-8 shows the T1, T2 and T3 tilted backward, and the slope rupture at the bottom part of slope model caused the data of tilt sensor T3 dropped suddenly, as shown in Fig.5-8.

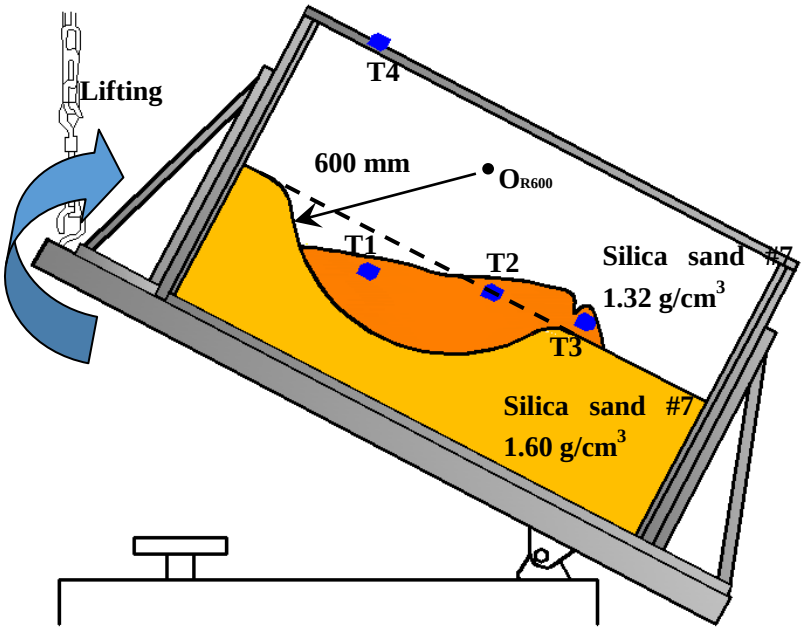

Fig. 5-7 Illustration of Test 3

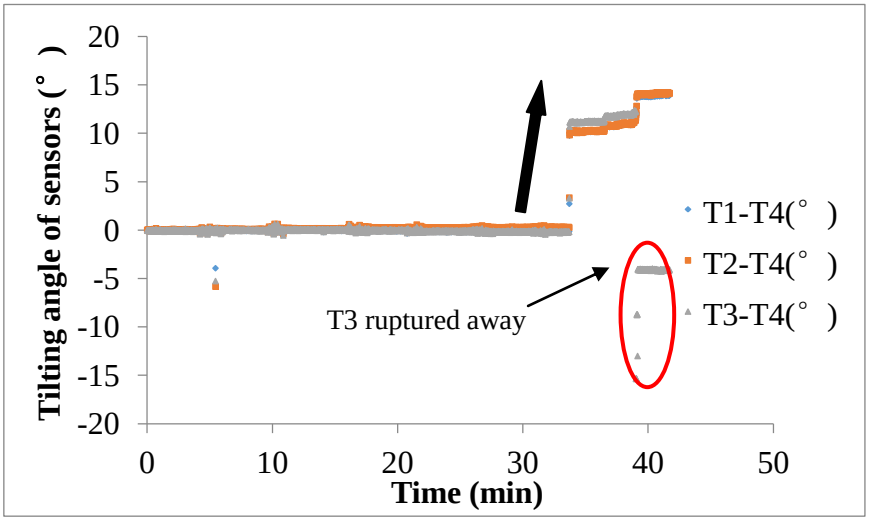

Fig. 5-8 Time history of slope tilting recorded by T1, T2 and T3 in Test 3

4) Test 4 using tilt sensors with no rods

Compared with the condition in Test 3, the only difference is that the material used in this test is Edosaki sand with a dry density around 1.25 g/cm^3 for the surface layer and 1.70 g/cm^3 for the base layer. The slope sliding in this test was also caused by container lifting, and Fig. 5-9 indicates the illustration of the apparatus arrangement while the test results is presented in Fig. 5-10. All of the tilt sensors in this test tilted backward.

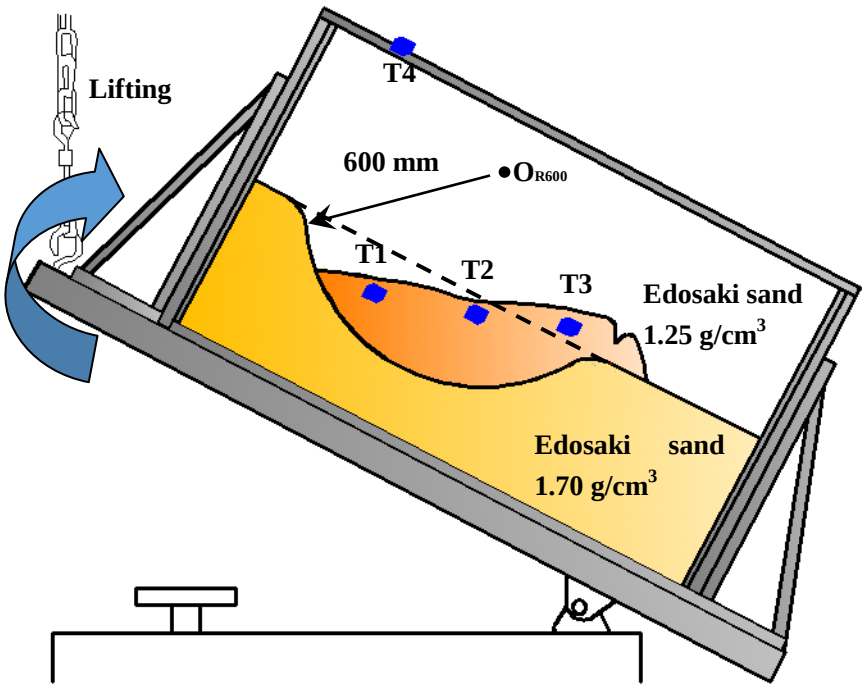

Fig. 5-9 Illustration of Test 4

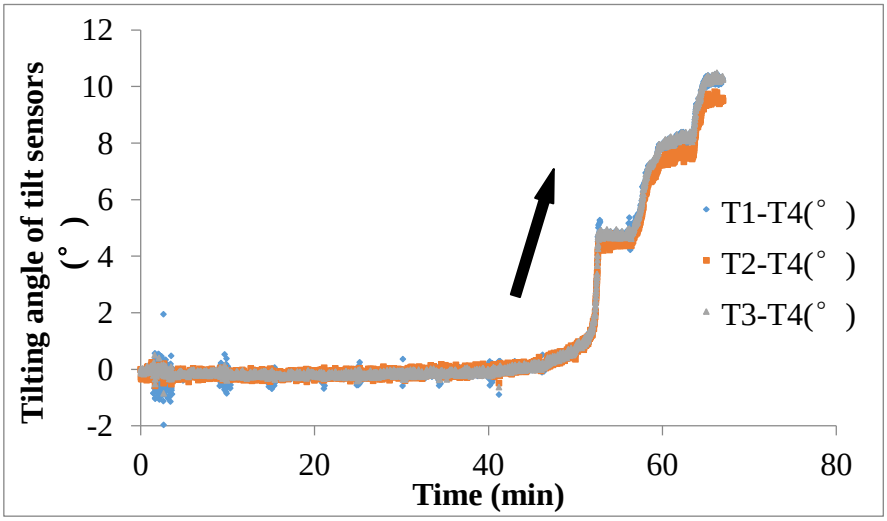

Fig. 5-10 Time history of slope tilting recorded by tilt sensors in Test 4

5) Test 5 using tilt sensors with no rods

In Test 5, the radius of slip surface in the upper part where T1 was installed is 600 mm, while that in the bottom part where T2 was installed is 400 mm. The material used in this test is Silica sand number 7 with a dry density around 1.32 g/cm^3 for the surface layer and 1.60 g/cm^3 for the base layer, and the slope sliding was also caused by lifting. Results in Fig. 5-12 indicate that the sensors in the slope tilted backward.

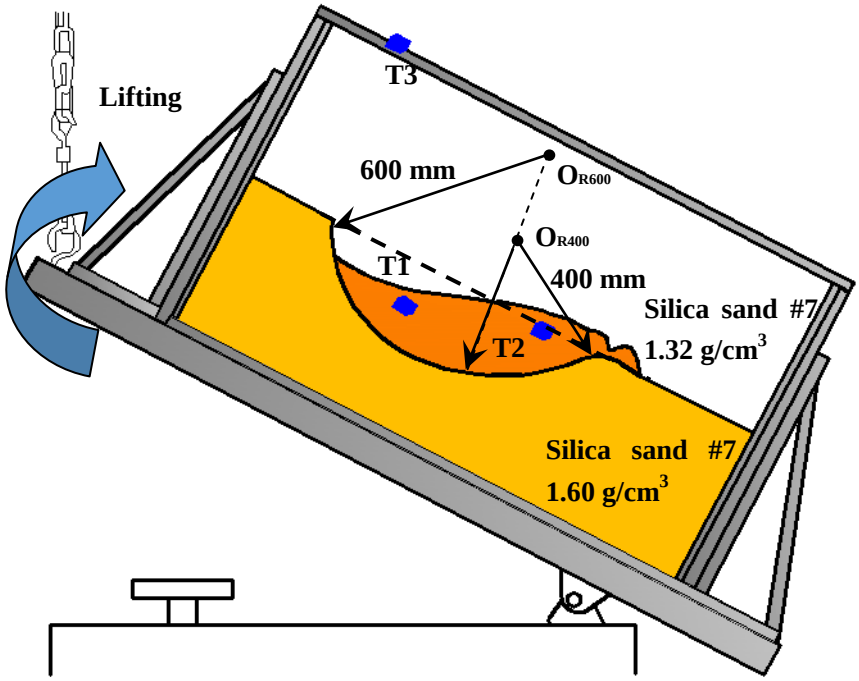

Fig. 5-11 Illustration of Test 5

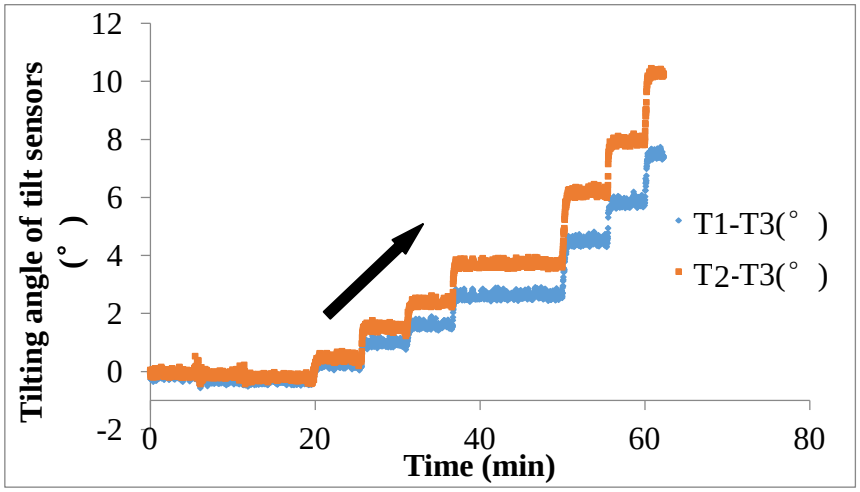

Fig. 5-12 Time history of slope tilting recorded by tilt sensors in Test 5

6) Test 6 using tilt sensors with no rods

Compared with the testing condition in Test 5, Edosaki sand was used in Test 6, as shown in Fig. 5-13. Similar as the results in Test 5, tilt sensors also tilted backward in Test 6 regardless of different testing materials (Fig. 5-14).

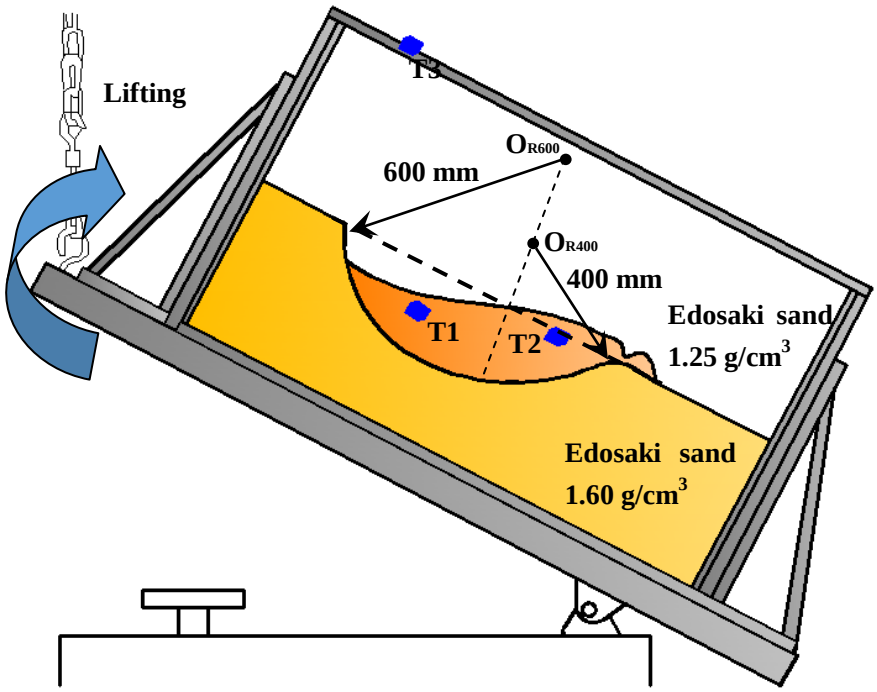

Fig. 5-13 Illustration of Test 6

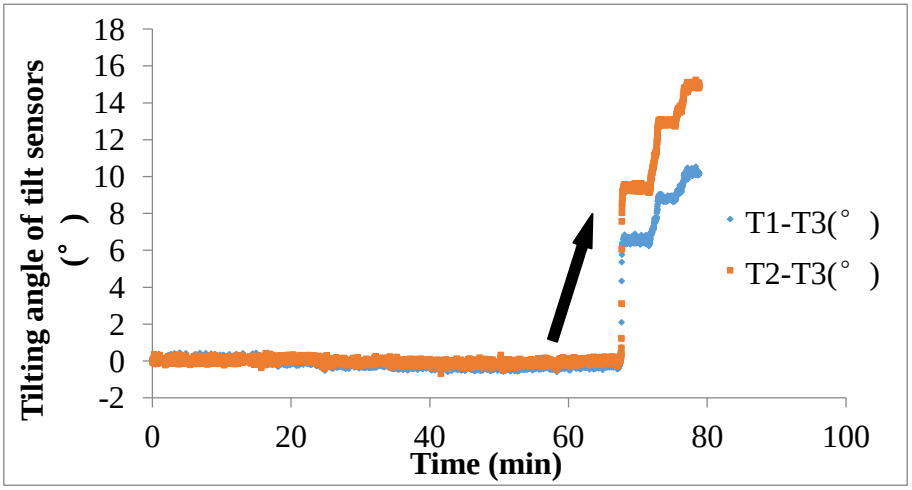

Fig. 5-14 Time history of slope tilting recorded by tilt sensors in Test 6

7) Test 7 using tilt sensors with no rods

In Test 7, the radius of slip surface in the upper part where T1 was installed is 300mm, while that in the bottom part where T2 was installed is 800mm. Details about this test are presented in Fig. 5-15. Fig. 5-16 shows that T1 and T2 in the slope tilted backward.

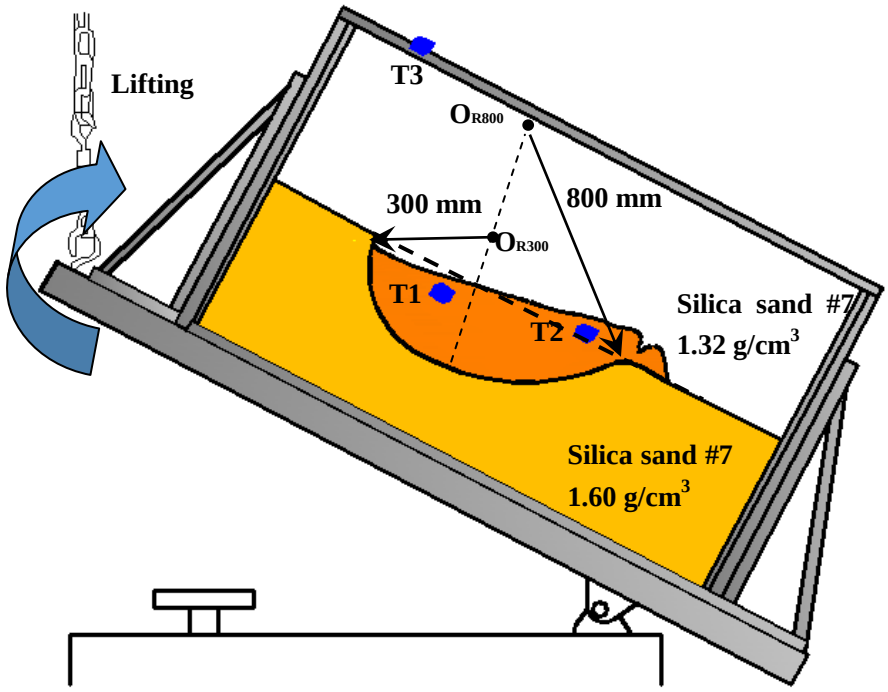

Fig. 5-15 Illustration of Test 7

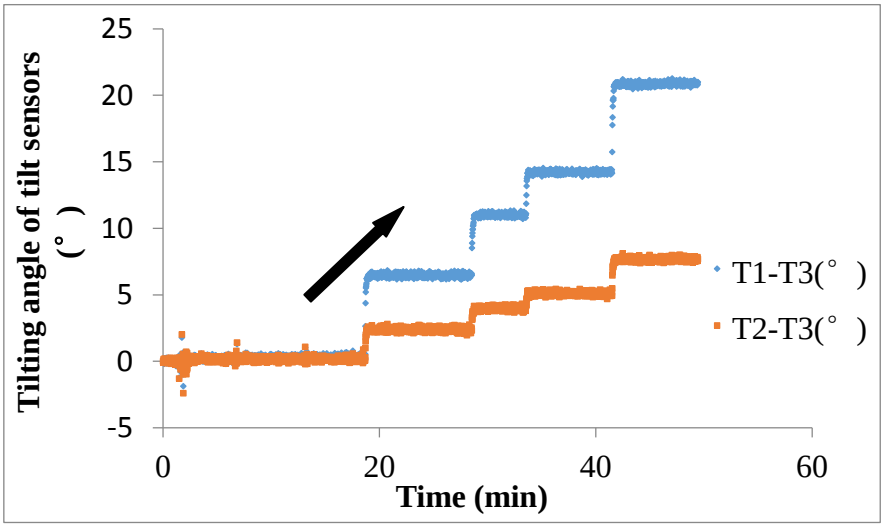

Fig. 5-16 Time history of slope tilting recorded by tilt sensors in Test 7

8) Test 8 using tilt sensors with no rods by applying artificial rainfall

The slope sliding in this test was caused by artificial rainfall supplied periodically. Similar as the testing conditions in Test 7, the radius of slip surface in the upper part is 300mm, and 800mm in the bottom part (Fig. 5-17). Fig. 5-18 shows the time history of wooden container tilting, and Fig. 5-19 indicates that both T1 and T2 tilted backward.

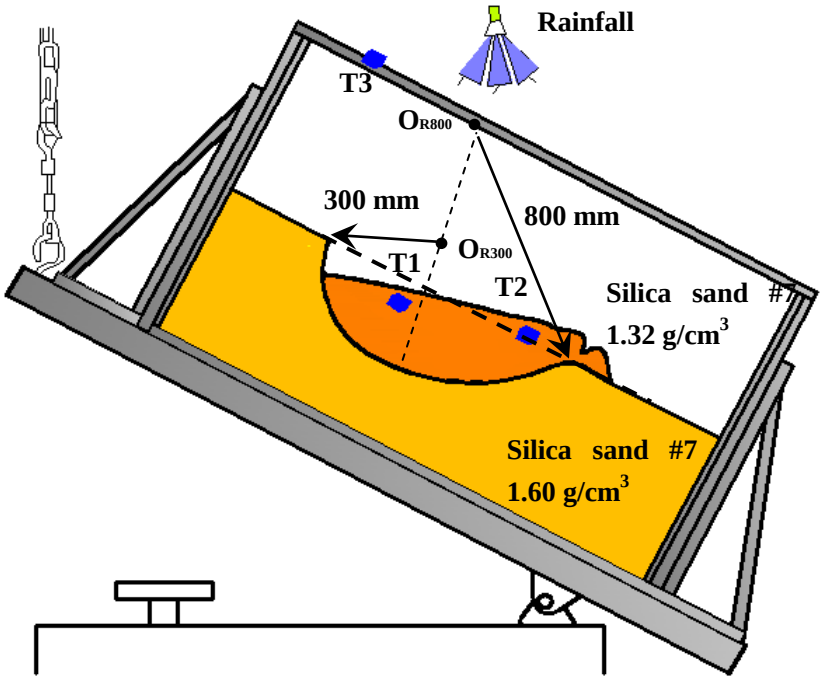

Fig. 5-17 Illustration of Test 8

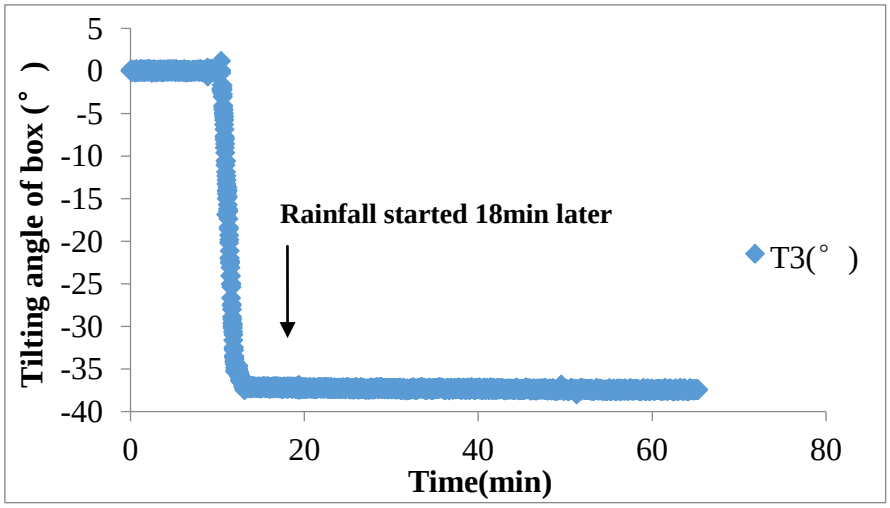

Fig. 5-18 Time history of tilting of wooden container recorded by T3 in Test 8

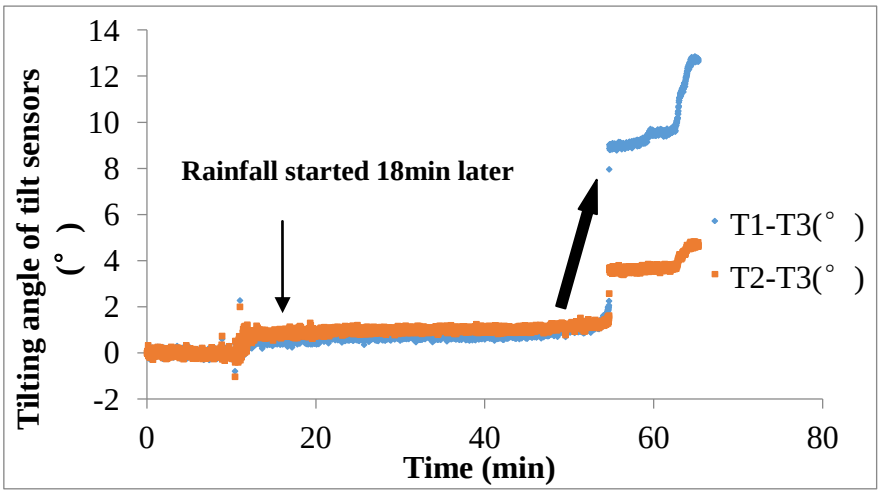

Fig. 5-19 Time history of slope tilting recorded by tilt sensors in Test 8

9) Test 9 using tilt sensors with no rods by applying artificial rainfall

In Test 9, the slope sliding was induced by continous artificial rainfall, and radius of slip surface is 600 mm. Details about the testing condition of Test 9 is illustrated in Fig. 5-20, and all of those three tilt sensors located in surface layer of slope tilted backward based on the test results presented in Fig. 5-21.

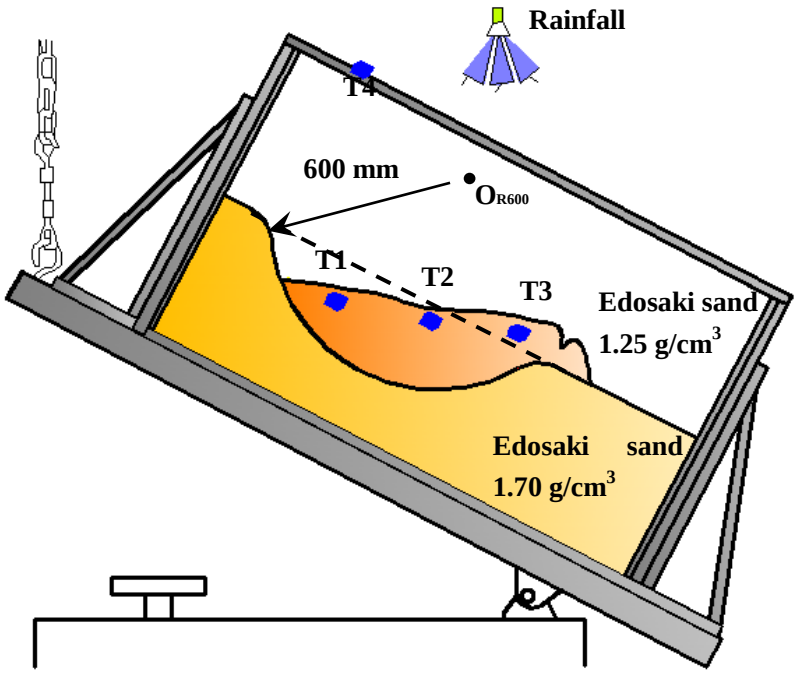

Fig. 5-20 Illustration of Test 9

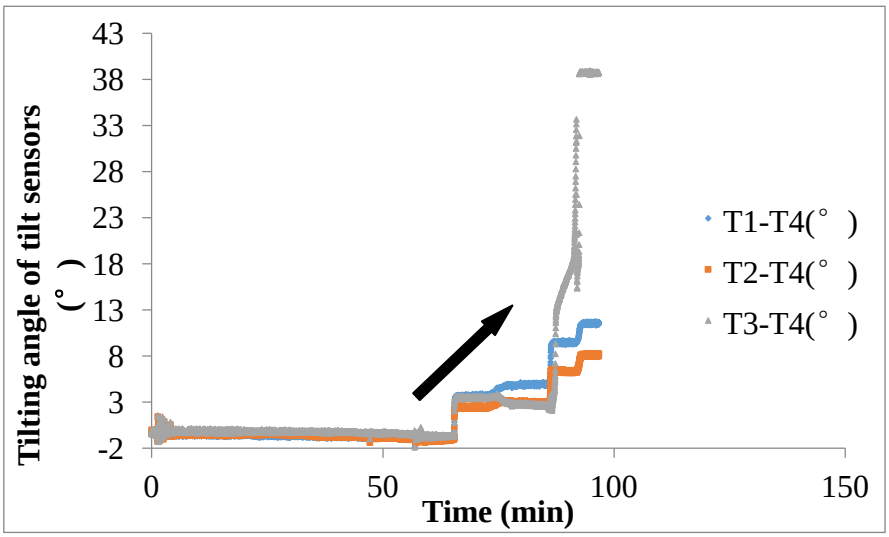

Fig. 5-21 Time history of slope tilting recorded by tilt sensors in Test 9

10) Test 10 using tilt sensors with no rods with planar slip surface

A planar slip surface was setted to investigate the tilting behaviour of translational landslide in this test. As shown in Fig. 5-22, three tilt sensors, T1, T2 and T3 were installed in the surface layer of the slope, and an external tilt sensor T4 was attached to the container. The slope sliding was induced by lifting one end of the container. Fig. 5-23 shows that neglectable tilting angle was observed when slope moved with a large

displacement (Fig. 5-24).

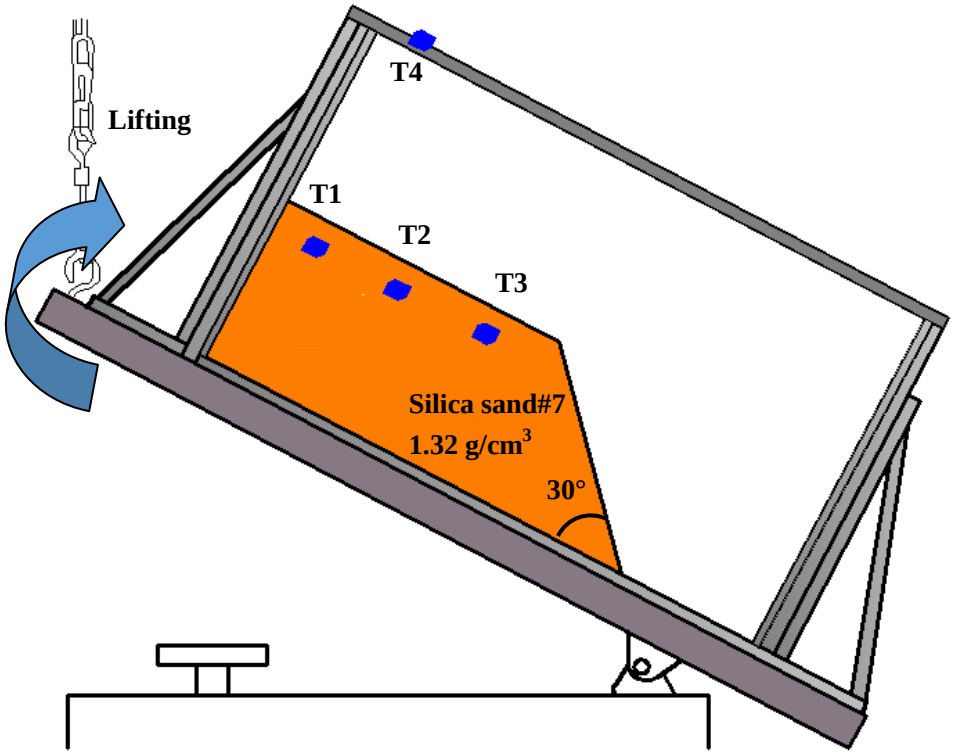

Fig. 5-22 Illustration of Test 10

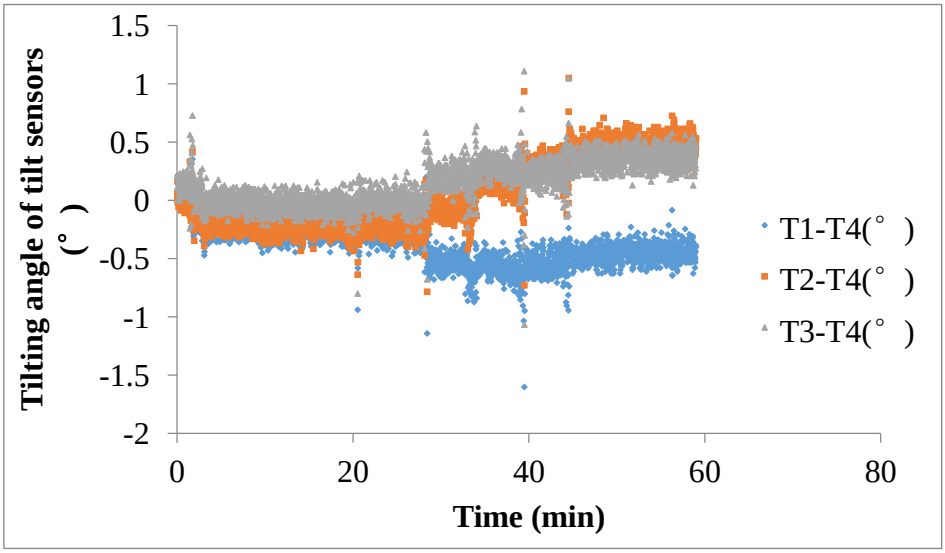

Fig. 5-23 Time history of slope tilting recorded by tilt sensors in Test 10

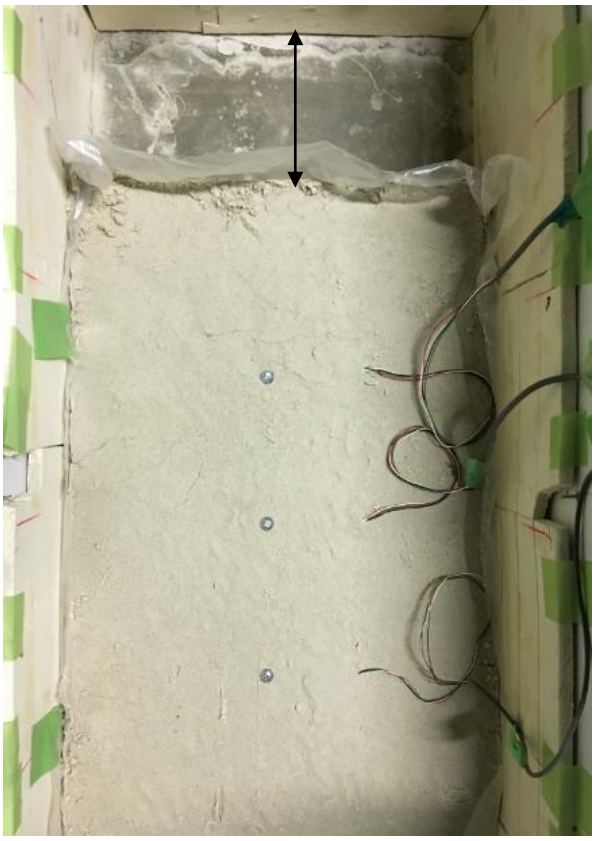

Fig. 5-24 The image of slope failure in Test 10

5.2.2 Small-scaled model tests using tilt sensors with short rods

In this section, model tests using tilt sensors with short rods installed above the pre-defined slip surface were conducted to investigate the tilting direction of tilt sensors installed in slopes and the details about the tests are listed in table 5-2.

Table 5-2: Small-scaled tests using tilt sensors with short rods above the slip surface

Test No.	Materials	Radius of the slip surface(mm)	Length of rods (mm)	Relative desity,Dr(%)	Triggering factor
1	Edosaki sand	R600	70	40	Lifting
2	Silica sand#7	R300+R800	70	50	Lifting
3	Silica sand#7	R300+R800	55	50	Lifting
4	Silica sand#7	R300+R800	70	50	Rainfall
5	Silica sand#7	R300+R800	70 and 0	50	Lifting

1) Test 1 using tilt sensors with short rods

In this test, the radius of pre-defined slip surface is 600 mm, and the slope failure was induced by lifting the container step by step. Two tilt sensors, T1 and T2 attached to a rod with the length 70mm were installed in the surface layer, and tilt sensor T3 was fixed on the wooden container to measure the tilting angle of the container. Test results shown in Fig. 5-26 indicate that both T1 and T2 tilted backward.

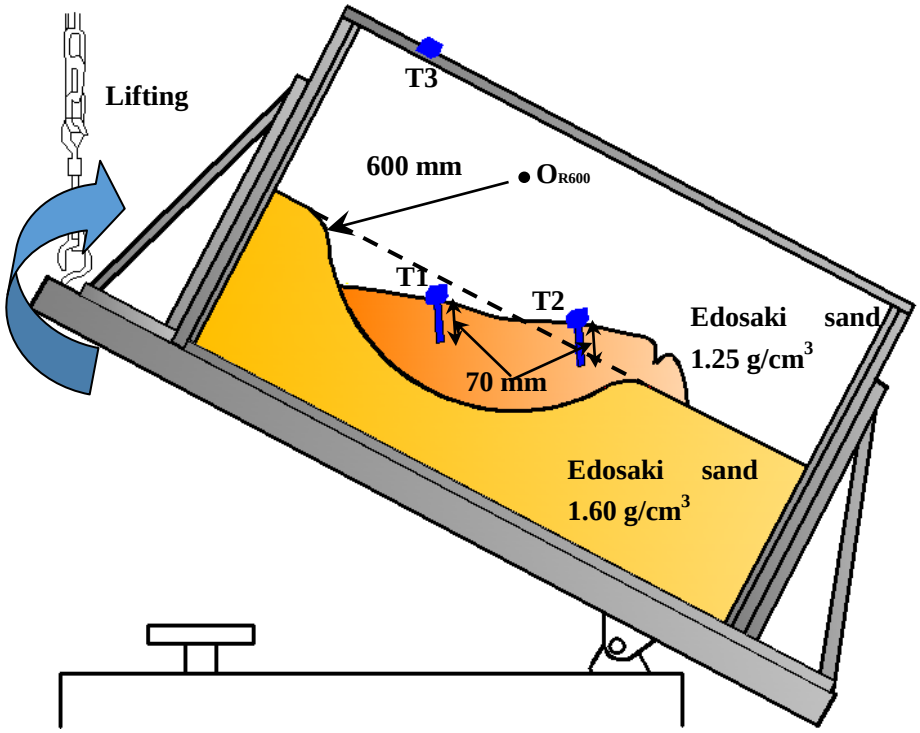

Fig. 5-25 Illustration of Test 1 using the tilt sensors with short rods

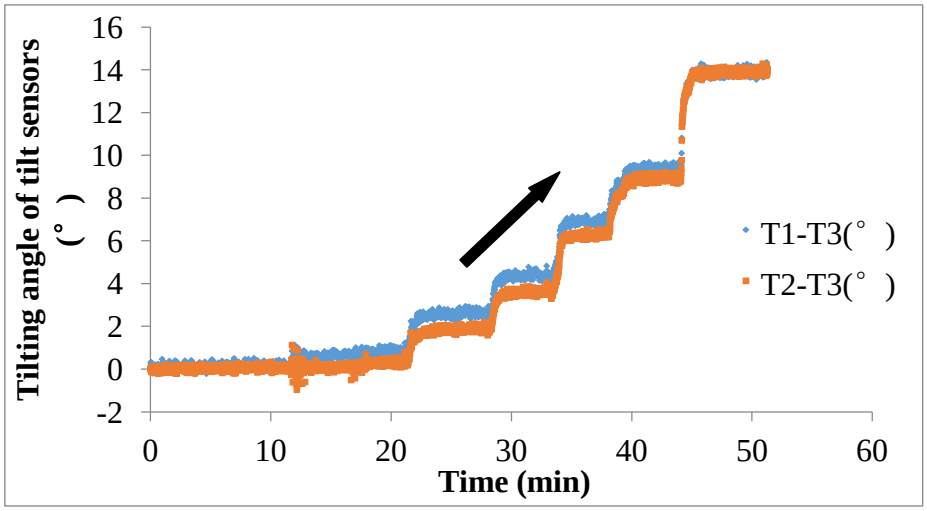

Fig. 5-26 Time history of slope tilting recorded by tilt sensors in Test 1 with short rods

2) Test 2 using tilt sensors with short rods

In this test, the radius of slip surface in the upper part is 300 mm, while that in the bottom part is 800 mm. Details about this test are presented in Fig. 5-27 and Fig. 5-28 shows that T1 and T2 with the rod, 70mm, also tilted backward regardless of the different shapes of pre-defined slip surface, and materials compared with Test 1 using tilt sensors with short rods.

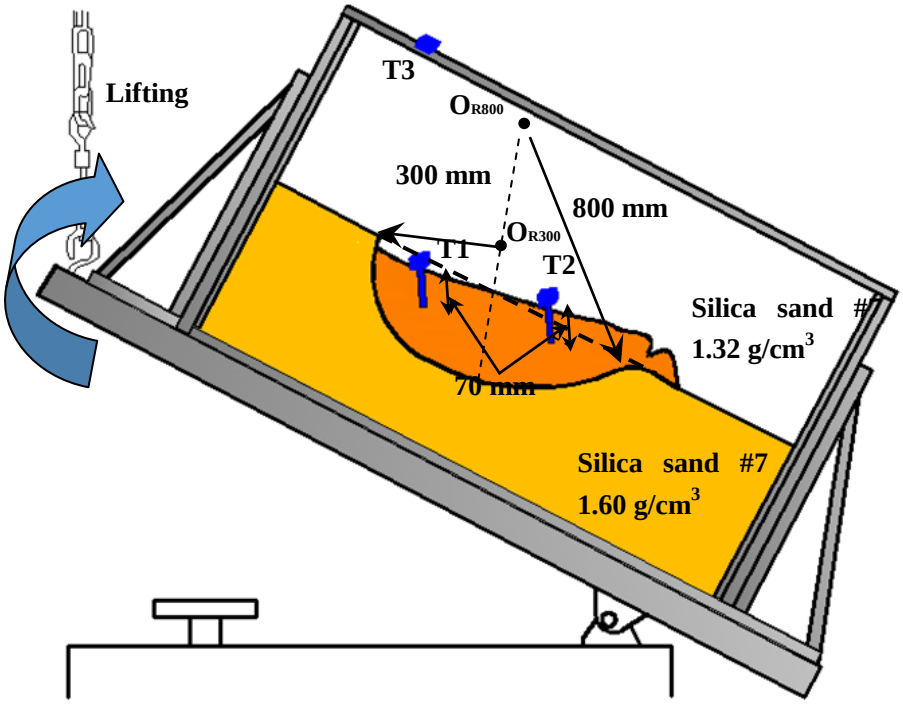

Fig. 5-27 Illustration of Test 2 using the tilt sensors with short rods

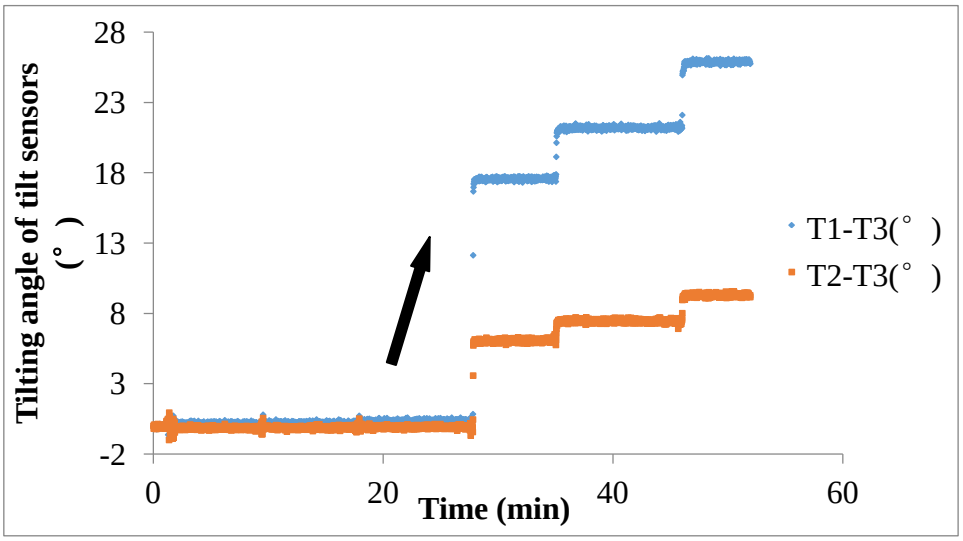

Fig. 5-28 Time history of slope tilting recorded by tilt sensors in Test 2 with short rods

3) Test 3 using tilt sensors with short rods

Compared with the testing condition in Test 2 using tilt sensors with short rods, the length of rods attached to the tilt sensors is 55 mm in this test (Fig. 5-29). Even though the length of rods is different, T1 and T2 installed in the surface layer of the slope model also tilted backward as shown in Fig. 5-30.

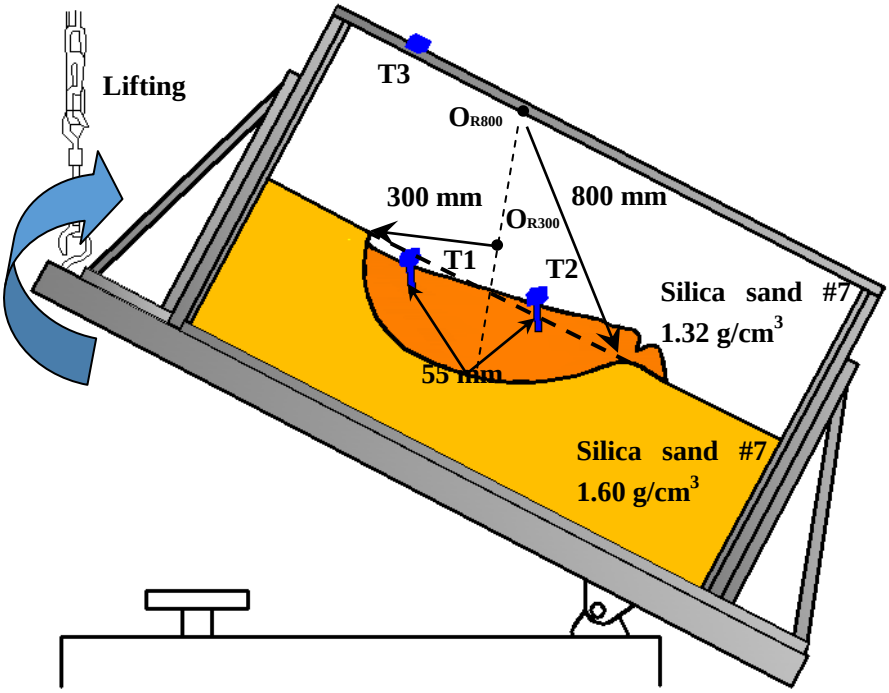

Fig. 5-29 Illustration of Test 3 using the tilt sensors with short rods

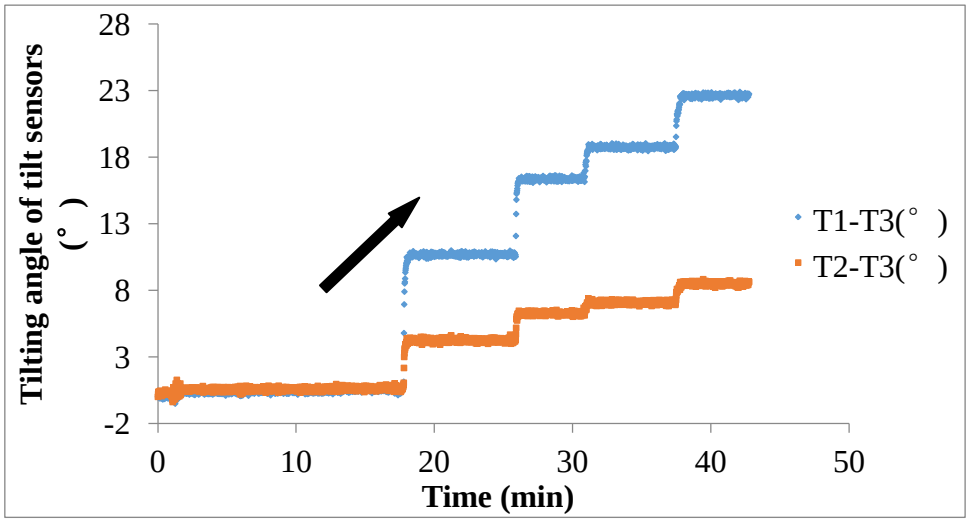

Fig. 5-30 Time history of slope tilting recorded by tilt sensors in Test 2 with short rods

4) Test 4 using tilt sensors with short rods by applying artificial rainfall

The slope failure in this test was induced by artificial rainfall supplied periodically, and Fig. 5-31 illustrates the testing condition of this test. The results shown in Fig. 5-32 indicate that T1 and T2 tilted backward, and the flat part of T2 marked in the Fig. 5-32 was caused by errosion occured in the bottom area of this test.

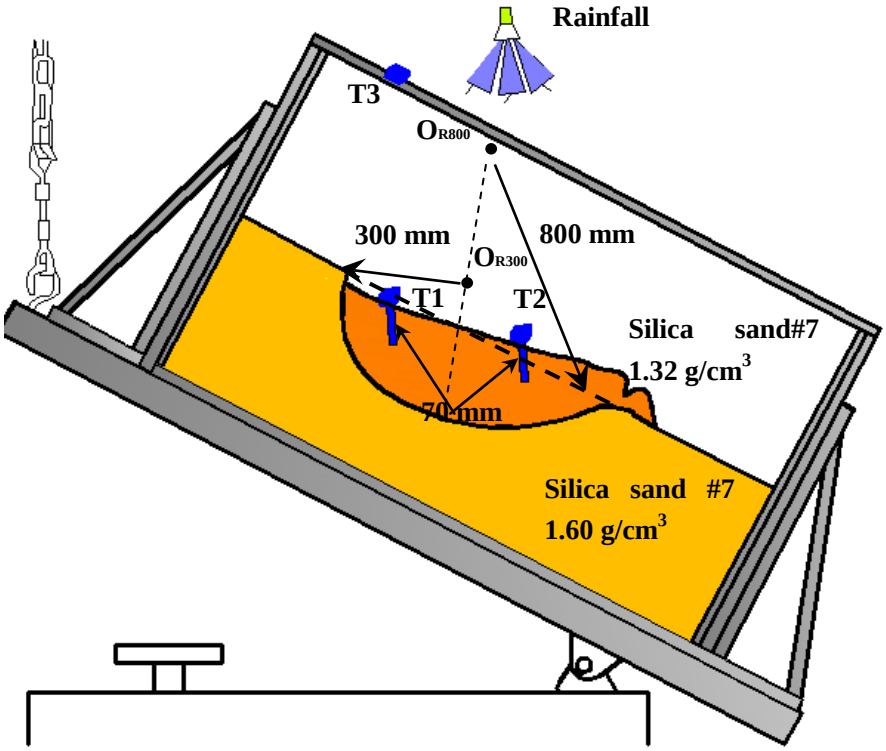

Fig.5-31 Illustration of Test 4 using the tilt sensors with short rods

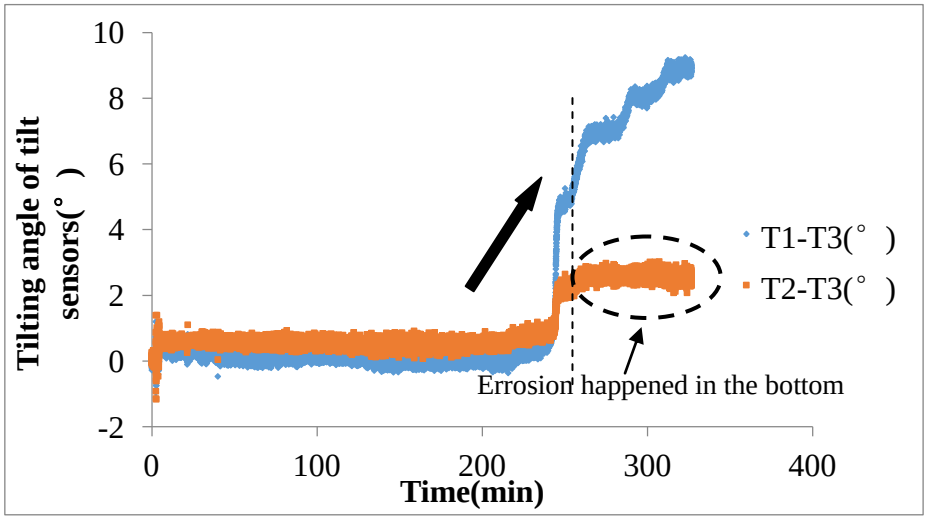

Fig.5-32 Time history of slope tilting recorded by tilt sensors in Test 4 with short rods

5) Test 5

In this test, five tilt sensors were used. T5 was attached to the wooden container to measure the tilting angle of the wooden container. T1 and T2 with short rods, 70 mm, were installed in the upper part and bottom part of the slope. Additionally, T3 and T4 without rods were installed close to the location of T3 and T4 respectively, as illustrated in Fig. 5-33 and Fig. 5-34. The relationship between the tilt angle measured by the tilt sensors with short rods, T1 and T2, and that measured tilt sensors without rods, T3 and T4 are plotted in Fig. 5-35. The plots in Fig. 5-35 indicates that tilt sensors with no rods or with short rods installed above the slip surface show a similar tilting behaviour when slope sliding.

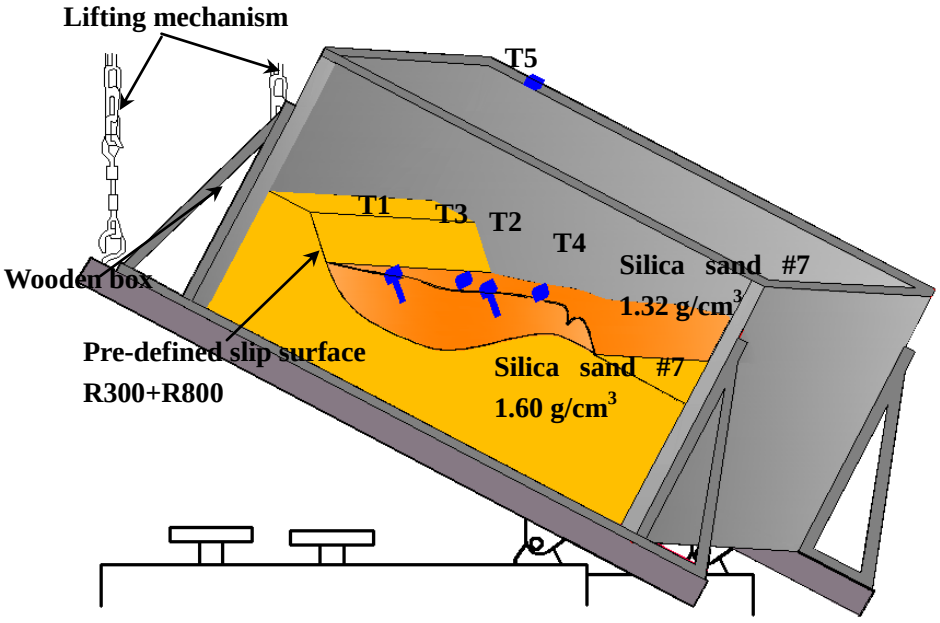

Fig. 5-33 Illustration of Test 5 using different types of the tilt sensors in 3 dimention

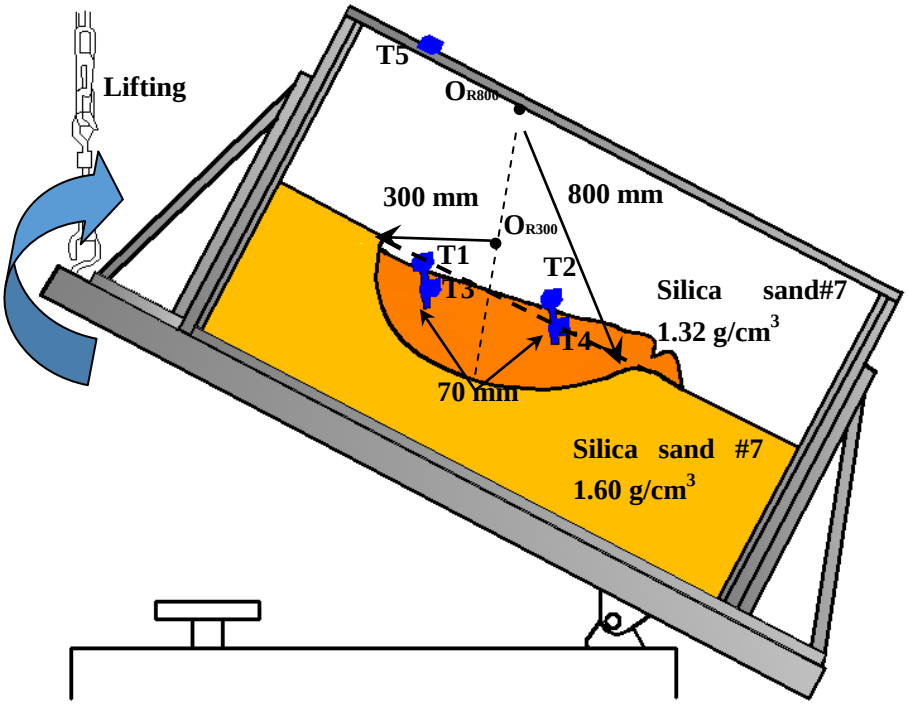

Fig. 5-34 Illustration of Test 5 using different types of the tilt sensors in 2 dimention

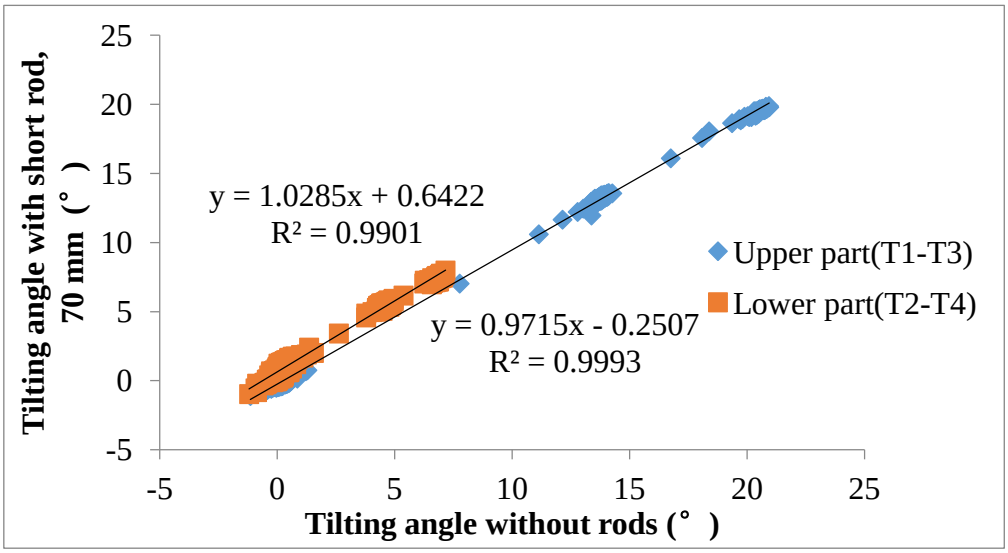

Fig. 5-35 The relationship between tilt angle measured without rods and with short rods

5.2.3 Small-scaled model tests using tilt sensors with long rods reaching the slip surface

1) Test 1 with long rods reaching the slip surface

In this model test, the tilt sensors T1 and T2 were attached to a long rod reaching the slip surface. Details about this test is illustrated in Fig. 5-36. The test results plotted in

Fig. 5-37 show that T1 and T2 tilted forward, which is contrary to the test results discussed before. The main reason for this unconsistent tilting behaviour is that, tilt sensors without rods or with short rods installed above the slip surface are moving together with the unstable slope and rotating around the centers of slip surfaces when slope sliding, while the tilt sensors with long rods reaching the slip surface are rotating against the tip point of rods reaching the slip surface.

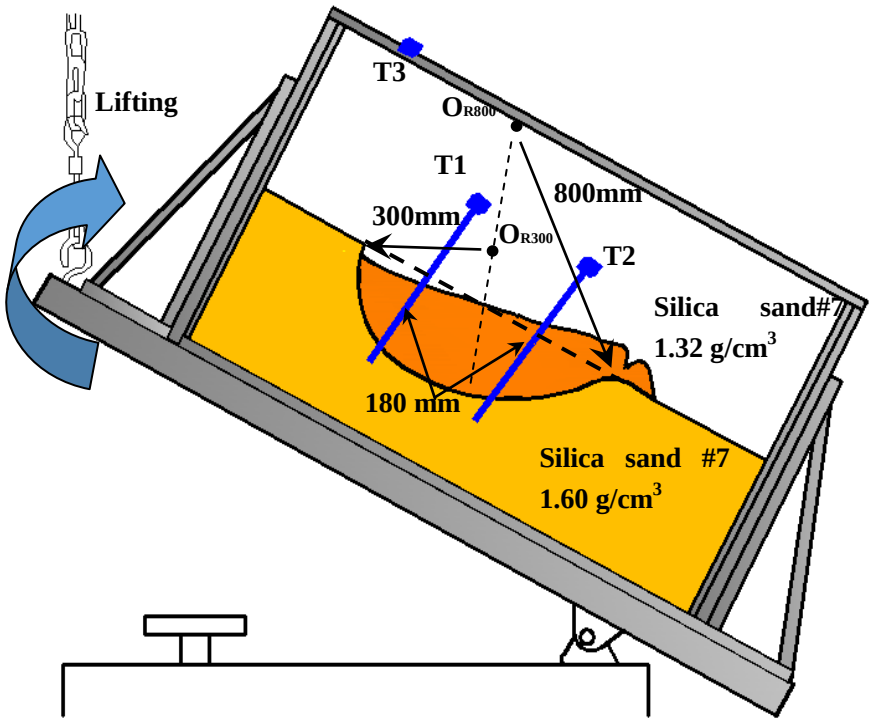

Fig. 5-36 Illustration of Test 1 using tilt sensors with long rods reaching the slip surface

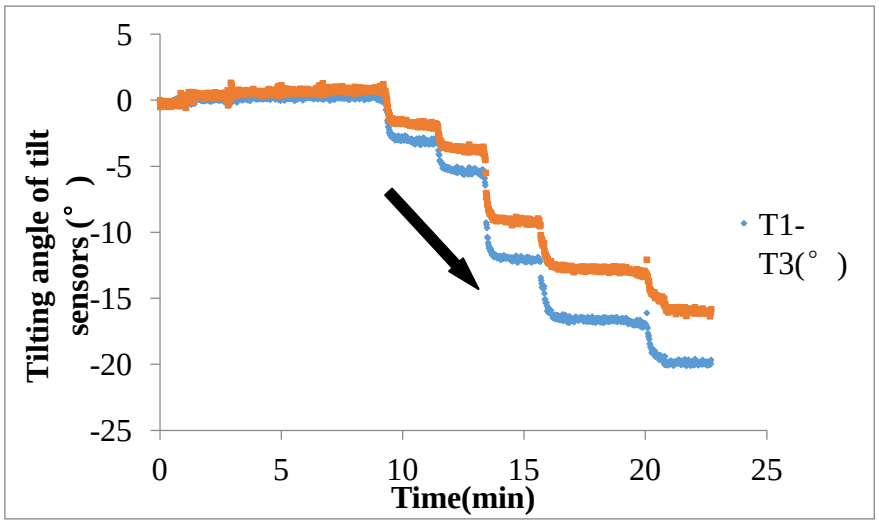

Fig. 5-37 Time history of slope tilting recorded by tilt sensors in Test 1 using tilt sensors with long rods reaching the slip surface

2) Test 2 with long rods reaching the slip surface

The difference between Test 1 and Test 2 is that the triggering factor for slope sliding in this test was caused by rainfall, while the slope failure in Test 1 was induced by tilting the container. Details about this test is presented in Fig. 5-38. Fig. 5-39 presents that the tilt sensors with long rods tilted forward when slope failed, which is consistent with the results in Test 1 using tilt sensors with long rods regardless of different triggering factors.

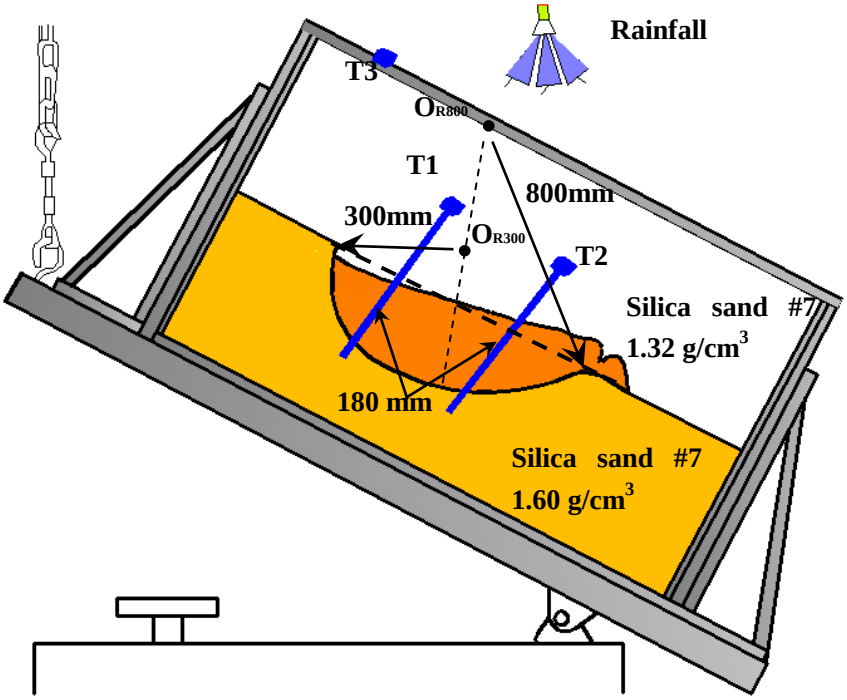

Fig. 5-38 Illustration of Test 2 using tilt sensors with long rods reaching the slip surface

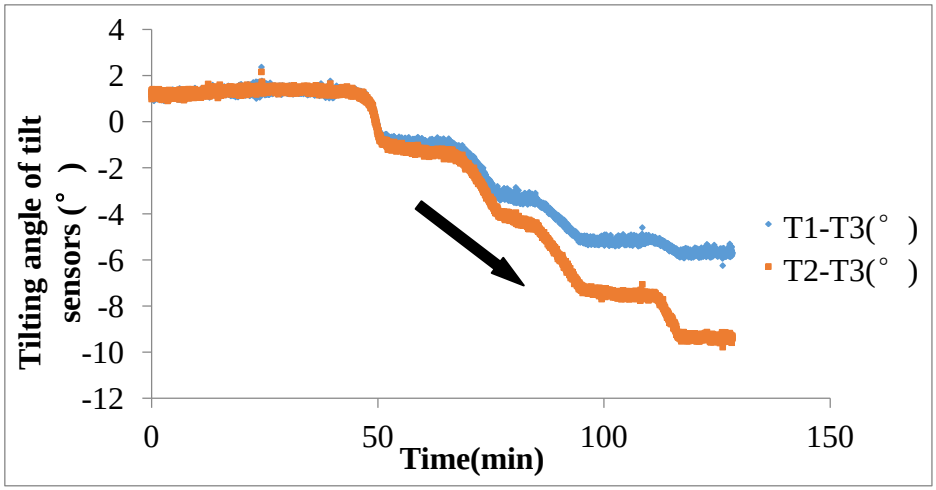

Fig. 5-39 Time history of slope tilting recorded by tilt sensors in Test 2 using tilt sensors with long rods reaching the slip surface

3) Test 3 with long rods reaching the planar slip surface

Compared with Test 10 using tilt sensors with no rods with planar slip surface, tilt sensors with long rods reaching the slip surface was used. When the slope failed, the surface layer pushed the tilt sensors with long rods tilted forwand , and the test results are presented in Fig. 5-41. The huge gap between T1 and T2 in Fig. 5-41 is because of that the bottom part where T2 installed ruptured away. In this test, the test results show that tilt sensors with long rods reaching the slip surface can detect the translational landslides.

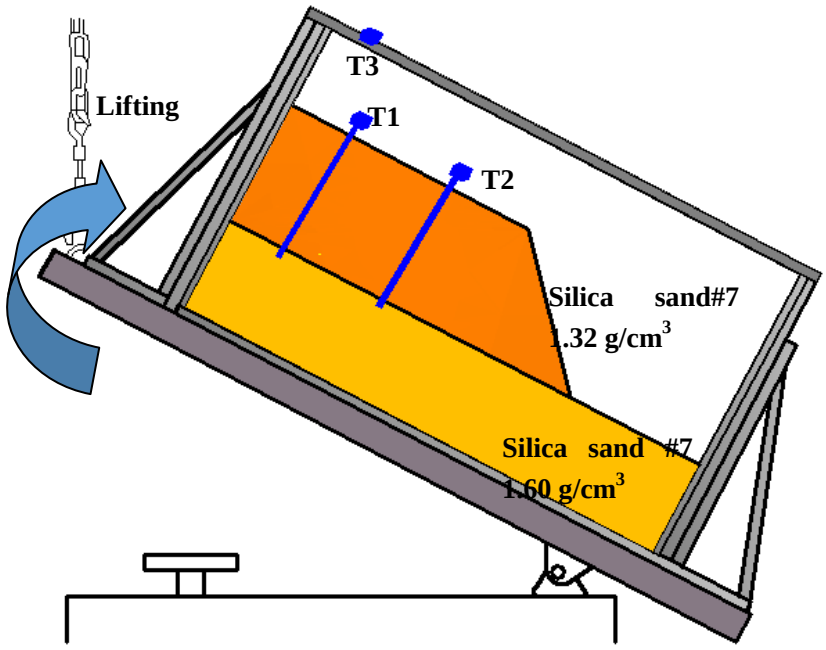

Fig. 5-40 Illustration of Test 3 using tilt sensors with long rods reaching the slip surface

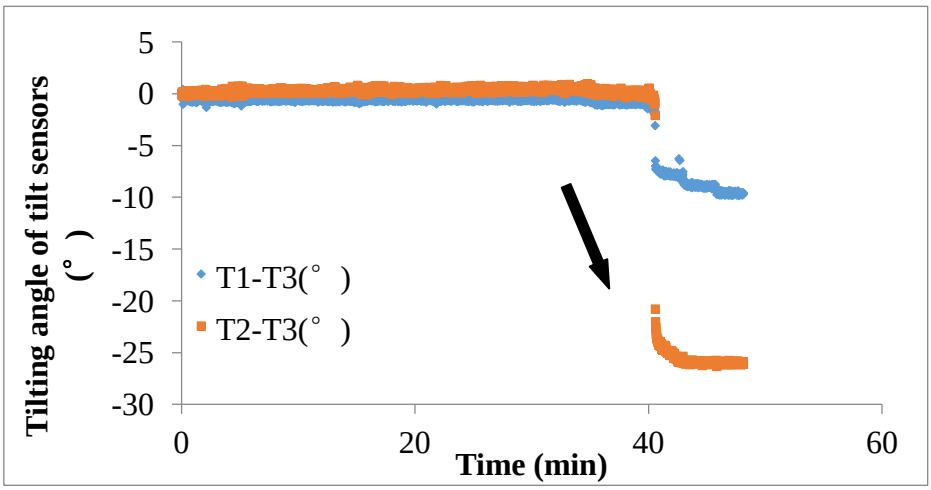

Fig. 5-41 Time history of slope tilting recorded by tilt sensors in Test 3 using tilt sensors with long rods reaching the slip surface

5.3. Test results from field tests

To study the tilting behaviour of tilt sensors, field tests by applying artificial rainfall were carried out on nature slopes of weak expansive soil. In filed tests, tilt sensors with different length of rods were installed in testing areas, and monitoring data from tilt sensors was converted by a Analog/Digital converter, and sent to the computer every second during the tests. The soil properties of this region is listed in Table 5-3

Table 5-3: Soil properties

Gs	**ρd**	**w**	**ρ**	**Ip**	**Iw**
2.72	1.89 g/cm^3	11.99%	2.12 g/cm^3	25.8%	46.6%

1) Field test 1

This site is located in Guangxi Province, China. The slope angle is 43 degrees. Trenches were excavated both at the toe and the crest of this slope with a depth 0.4 m .The slope consists of weak expansive soil and some plant roots. In this test, tilt sensors with different length of rods, 50 mm, 300 mm and 700 mm were installed in the slope, as shown in Fig. 5-42 and Fig. 5-43.

Fig. 5-42 The image for the field test 1

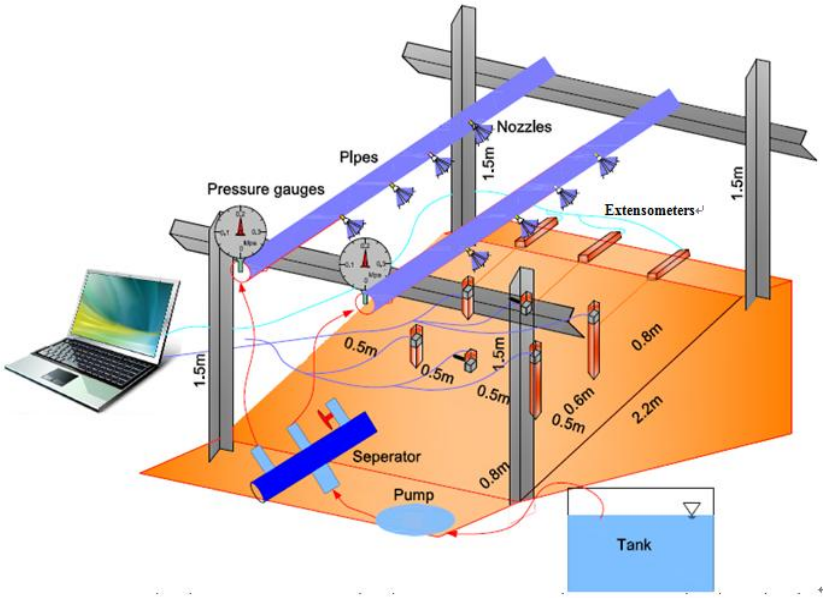

Fig. 5-43 Illustration for the arrangement of sensors in Field test 1

Rainfall was supplied at 11 :20 in the morning with an intensity 21 mm per minute by an artificial rainfall supply system consisting of pump, artificial pond, water separator and nozzles.

Major deformation occured in the top part of the slope around 15:00 in the afternoon. The tilting behaviours of slope surface was recorded by the tilt sensor attached to a rod 50 mm long, which was installed in the upper part of the slope marked in Fig. 5-43. The time histories of the tilting angel from the failed tilt sensor is presented in Fig. 5-44. The depth of slip surface of this slope is around 250 mm, which is deeper than the length of the rod attached to the tilt sensors. Fig. 5-44 and Fig. 5-45 show that the tilt sensor located in the failed area tilted backward, and this result is consistent with the result of model tests.

Fig. 5-44 Images of the testing area before and after the slope failure

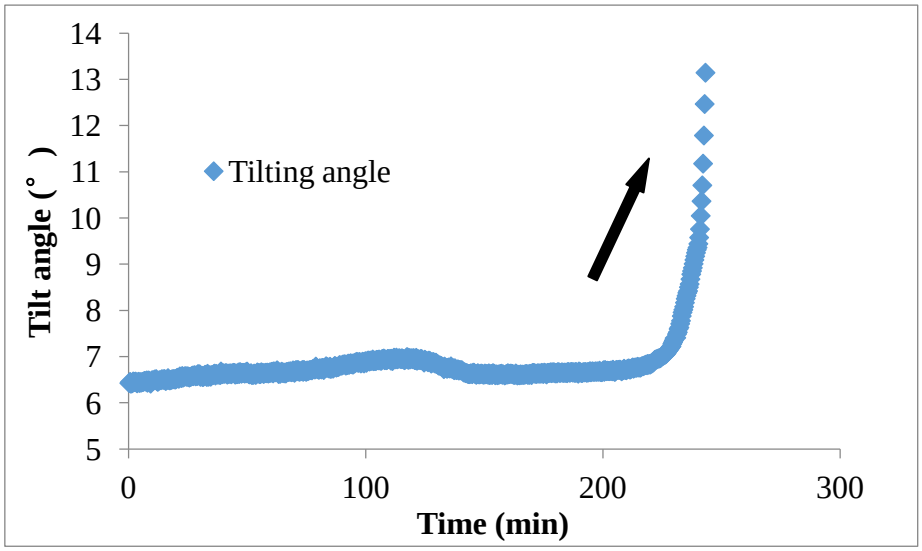

Fig. 5-45 Time history of slope tilting recorded by tilt sensor with a rod 50mm long located in failed area in Field test 1

2) Field test 2

The site for field test 2 is next to the site where Field test 1 was conducted. Compared with the Field test 1, the rainfall intensity in this test was 27 mm per hour. The arrangement of sensors and geometry of the slope is shown in Fig. 5-46 and Fig. 5-47.

Fig. 5-46 The image for the field test 2

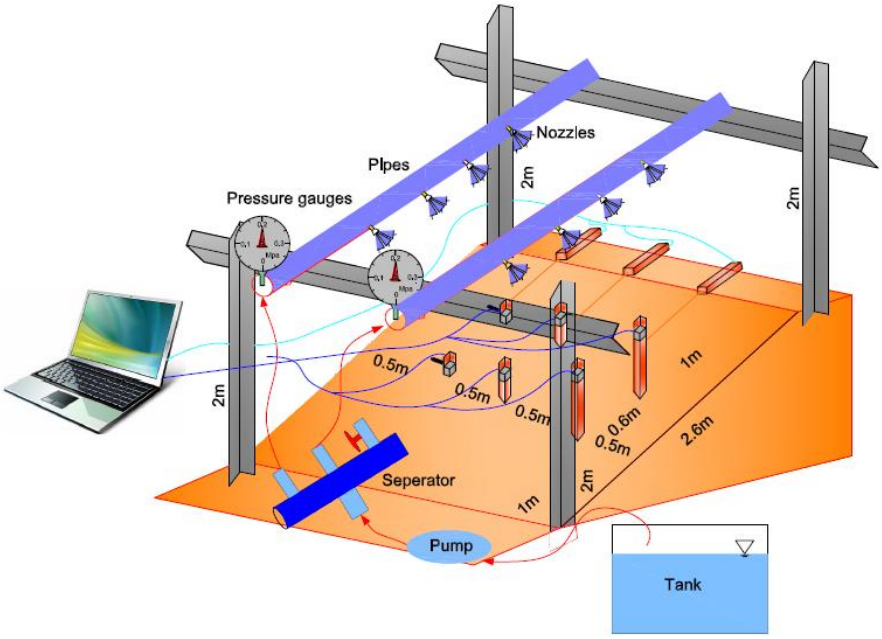

Fig. 5-47 Illustration for the arrangement of sensors in Field test 2

In this field test, the failure of tilt sensors with different length of rods, 50 mm and 300 mm, installed in the lower part of the slope were caused by erossion (Fig. 5-48).

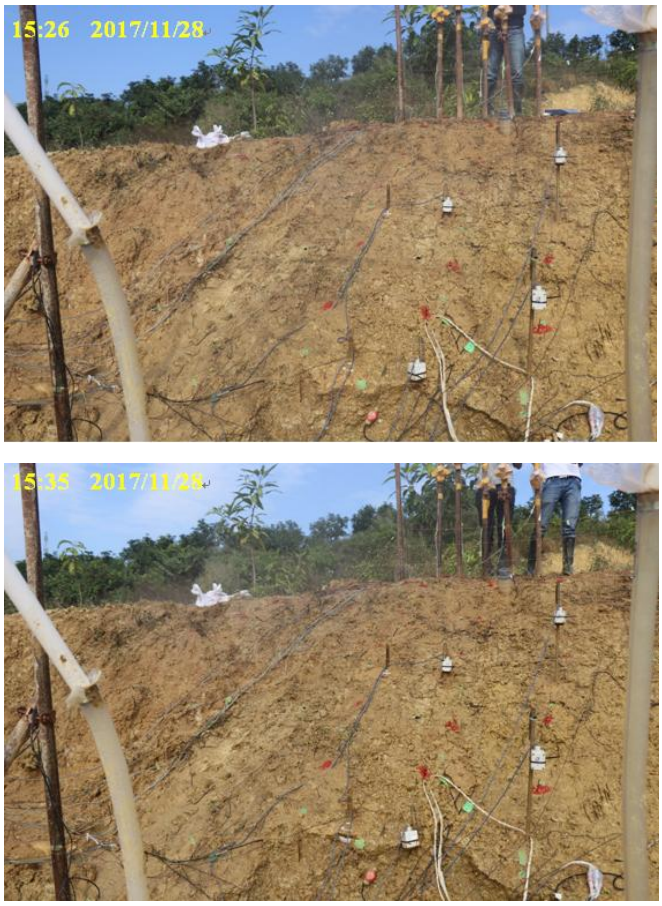

Fig. 5-48 Erossion occurred in lower part and caused the tilt sensors failed

Major deformation occured in the top part of the slope as shown in Fig. 5-49, and the depth of slip surface is also around 250 mm. As a result, the tilt sensor attached to a short rod, 50 mm, installed in the this part tilted backward(Fig. 5-50), while the tilt sensor attached to a longer rod, around 300 mm, tilted forward (Fig. 5-51).The other two tilt sensors with long rods (800 mm), did not fail in this test.

Fig. 5-49 Images of the testing area before and after the slope failure

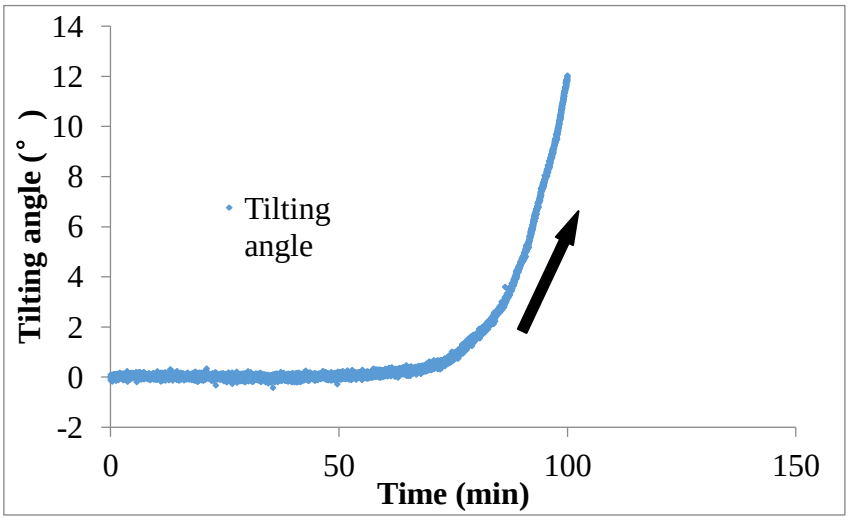

Fig. 5-50 Time history of slope tilting recorded by tilt sensor with a rod 50mm long located in failed area of the slope in Field test 2

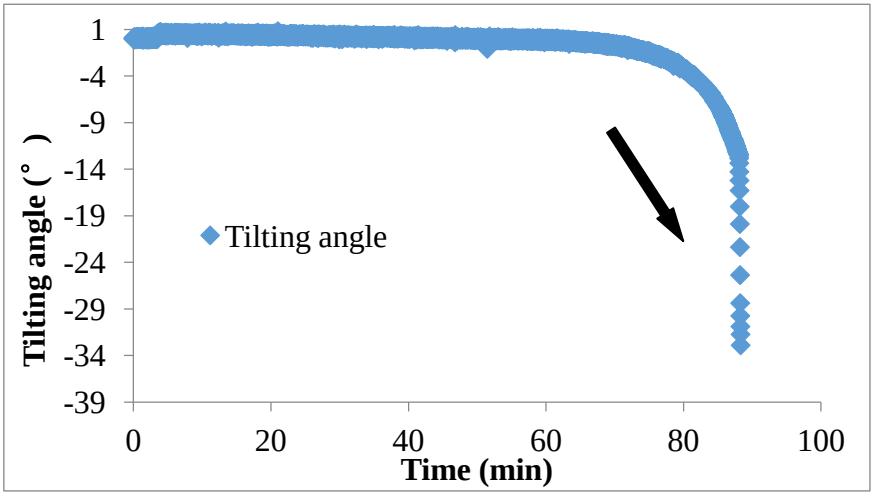

Fig. 5-51 Time history of slope tilting recorded by tilt sensor with a rod 300mm long located in failed area of the slope in Field test 2

5.4. Summary

In this chapter, the tilting direction of tilt sensors installed in slope is investigated by conducting various types of laboratory tests and field tests. The test results show that tilt sensors located above the slip surface move together with the slope and rotate backward. On the other hand, the tilt sensors with long rods reaching the slip surface rotate forward. The test results also indicate that the tilt sensors installed above the slip surface is similar to the pendulum, while the tilt sensors with long rods reaching the slip surface of slope is more like the inclinometer.

CHAPTER 6

TEST RESULTS FOR THE RELATIONSHIP BETWEEN SURFACE DISPLACEMENT AND TILTING ANGLE

6.1. Introduction

In 1985, Carter and Bentley developed a method to predict the slip surface of landslides based on the moving path of the particles on the slope surface after the initiation of slope sliding (Carter et al. 1985).

In their research, model tests were conducted in a 1.0 m×0.75 m×0.2 m glass-sided tank, as it is shown in Fig. 6-1.

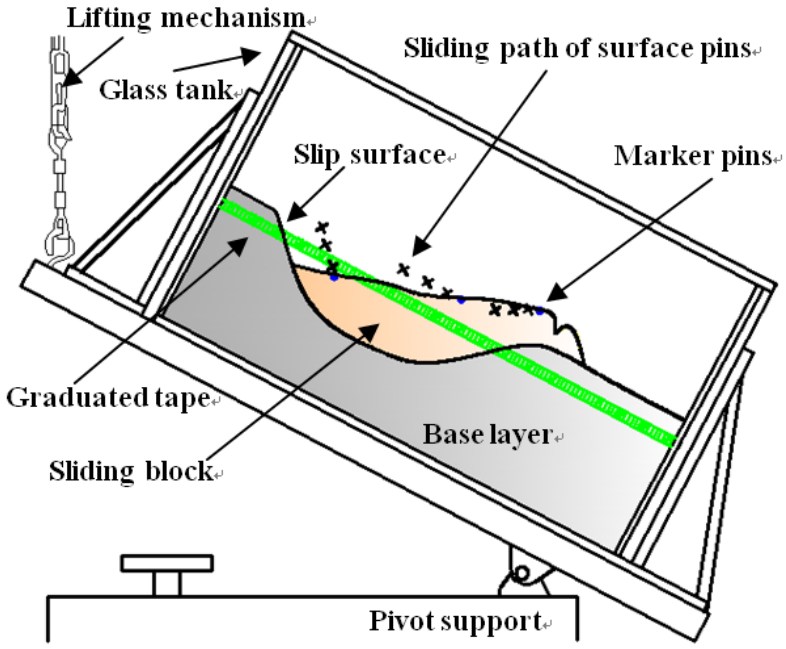

Fig. 6-1 Schematic diagram of model tests (Carter et al., 1985)

Polythene sheets with petroleum jelly or liquid detergent between them were placed below the sliding body and modelled by shape of underlying layer. Models were constructed at horizontal place in the beginning, and then slope sliding along those polythene sheets was induced by raising one end of the tank. Several short steel dowels, which were pressed into the model surface and with their ends on the glass sides, were used to measure the surface displacement when slope failure happened. These model tests were carried out with different shapes of slip surface and different types of landslip materials. The results shows that the slip surface can be predicted by tracing the movement of marked points on the slope surface, and the method also has been validated against several events from real sites by different research groups independently. However, further studies, such as the investigations for this phenomenon or the moving process of slope slideing, were not carried out in their researches.

In addition, a similar trend between surface displacements and tilting angles of slopes against time has been observed in the slope failures based on the existed monitoring data of surface displacements and tilting angles from field events as well as the results of model tests. However, poor studies have been carried out to explore the relationship of displacements and tilting angles.

In this chapter, the relationship between surface displacement and tilting angle was investigated by conducting small-scaled model tests with pre-defined slip surface. In these model tests, slope models were constructed using different shapes of pre-defined slip surfaces and landslip materials. In the tests, tilting behavior and surface movement, was recorded. The tilting behavior was measured by tilt sensors embedded into the subsurface of slopes, while the surface displacement was approached by the application of image analysis technique to trace the moving path of marked points on the slope surface. The relationship between slip surface and surface deformation and the moving process of the sliding block in these tests was then studied. Additionally, field tests were also carried out to verify the relationship between the displacement and tilting angle.

6.2. Test results of small-scaled model tests

Similar as the methodology used for the investigation of tilting directions of tilt sensors, small-scaled model tests with pre-defined slipe surfaces using tilt sensors attached to different length of rods, were conducted under different testing conditions, and field tests were also carried out to check the results concluded in the model tests in the following sections. In part, results from model tests for the exploration of the relationship between surface displacement and tilting angle were discussed. Futhermore, the moving process of the sliding block was also presented in this part.

6.2.1 Small-scaled model tests using tilt sensors without rods

In this section, the method for surface deformation measurement, consisting of surface movement as well as tilting behaviour, are discussed in details. In addition, the results of the tests are presented in this part. Table 6-1 shows the testing conditions of each test using tilt sensors without rods.

Table 6-1: Small-scaled tests using tilt sensors without rods above the slip surface

Test No.	Materials	Radius of the slip surface(mm)	Relative desity,Dr(%)	Triggering factor
1	Silica sand #7	R1000	50	Lifting
2	Silica sand #7	R600	30	Lifting
3	Silica sand #7	R600	50	Lifting
4	Edosaki sand	R600	40	Lifting
5	Silica sand #7	R600+R400	50	Lifting
6	Edosaki sand	R600+R400	40	Lifting
7	Silica sand #7	R300+R800	50	Lifting
8	Silica sand #7	R300+R800	50	Rainfall
9	Edosaki sand	R600	40	Rainfall

1) Test 1 using tilt sensors without rods

In this test, the slope sliding was induced by tilting the container step by step, and details about the testing conditions are presented in Fig. 6-2. The surface displacement,

Δh, obtained based on the image analyzing technology introduced in Chapter 4 is plotted against time in Fig. 6-3. The time history of normal displacement(Δv) of the marked points on the slope surface measured by vernier is shown in Fig. 6-4. Fig. 6-4 indicates that the marked point on the upper part settled down, while the point on the lower part of the slope model rose up. Fig. 6-5 shows the calculated distance of each tilt sensor to the center of corresponding slip surface in the tests, and the distance between tilt sensors and centers of the corresponding slip surfaces is approached by following equation

$$D = \sqrt{(h_{sensors} - h_{center})^2 + (v_{sensors} - v_{center})^2} \tag{6-1}$$

Where $h_{sensors}$ and $v_{sensors}$ are the position of tilt sensors in the direction parallel and normal to the initial slope surface repectively. h_{center} and v_{center} are the position of of the slip surface center, which is constant during the test.

Fig. 6-5 indicates that in this test the sliding slope rotated around the center of the slip surface.

In Fig. 6-6, the relationship between calculated tilting angle and the tilting angle measured by tilt sensors is presented. The calculated tilting angle can be obtained by equation 6-2

$$\theta_{cal} = \arccos\left(\frac{\sqrt{\Delta h_{sensors}{}^2 + \Delta v_{sensors}{}^2}}{v_{center}}\right) \tag{6-2}$$

Where $\Delta h_{sensors}$ and $\Delta v_{sensors}$ are the surface displacement and normal displacement of tilt sensors. v_{center} is normal distance between the initial slope surface and the slip surface center.

Fig. 6-6 shows that the measured tilting angle using tilt sensors is close to the calculated tilting angle, and also indicates that the tilt sensors installed in the slope

above the slip surface are possible to trace the path of the slope movement.

Fig. 6-7 presents the relationship between tilting angle and total displacement of sensors. The tilting angle was measured by sensors, while the total displacement was obtained by the following equation

$$\Delta s_{sensors} = \sqrt{\Delta h_{sensors}{}^2 + \Delta v_{sensors}{}^2} \tag{6-3}$$

In Fig. 6-7, the rate of the fit lines for tilting angle and total displacement is close to the actual distance between the locations of tilt sensors and the corresponding centers of slip surface. As shown in Fig. 6-7, the rate of fit line for T1 and for T2, are 1004.5 and 999.87, which are close to the actual distance 952 mm and 956 mm respectively.

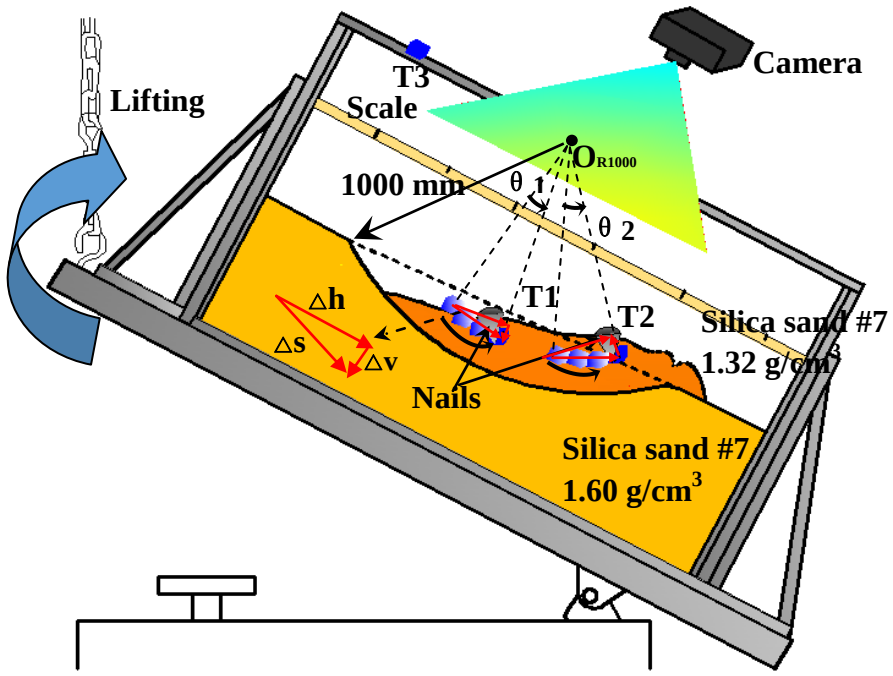

Fig. 6-2 Illustration of Test 1 using tilt sensors without rods

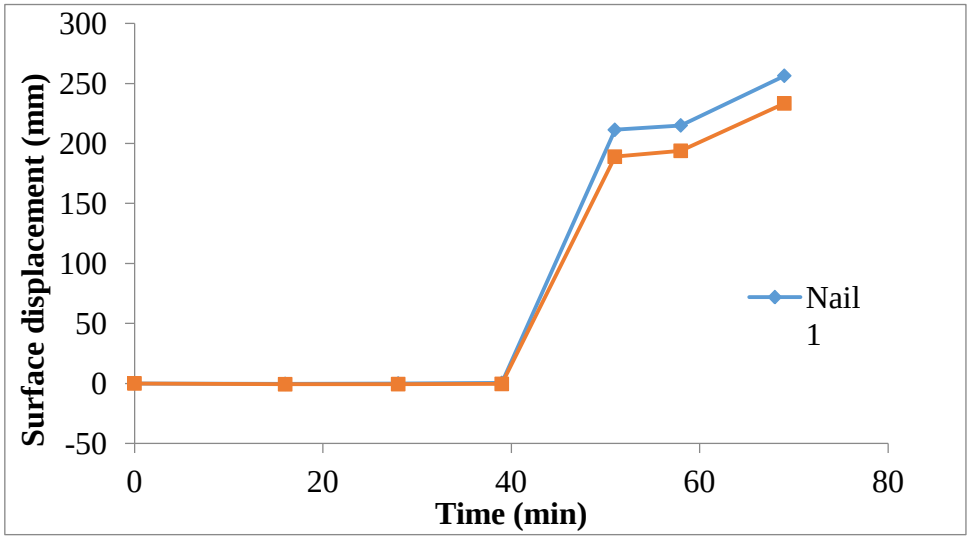

Fig. 6-3 Time history of surface displacement of Test 1 using tilt sensors without rods

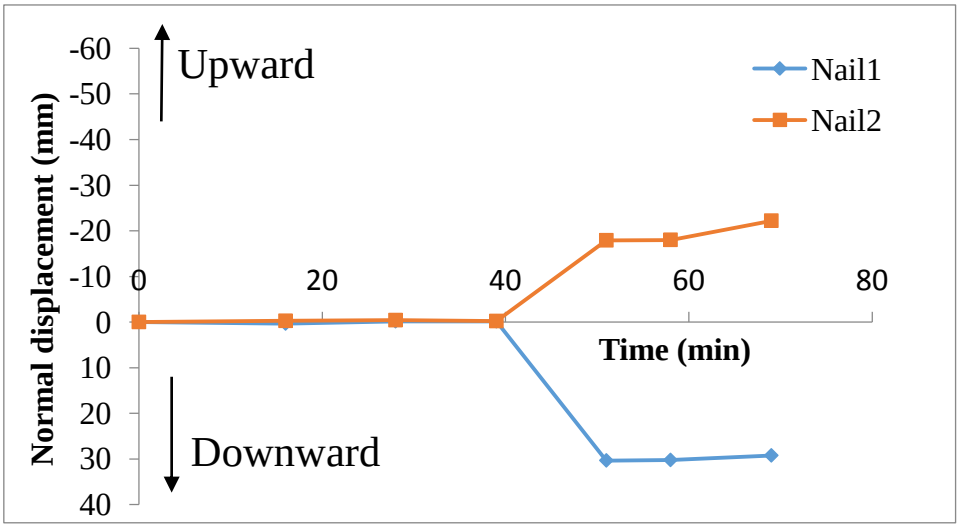

Fig. 6-4 Time history of normal displacement of Test 1 using tilt sensors without rods

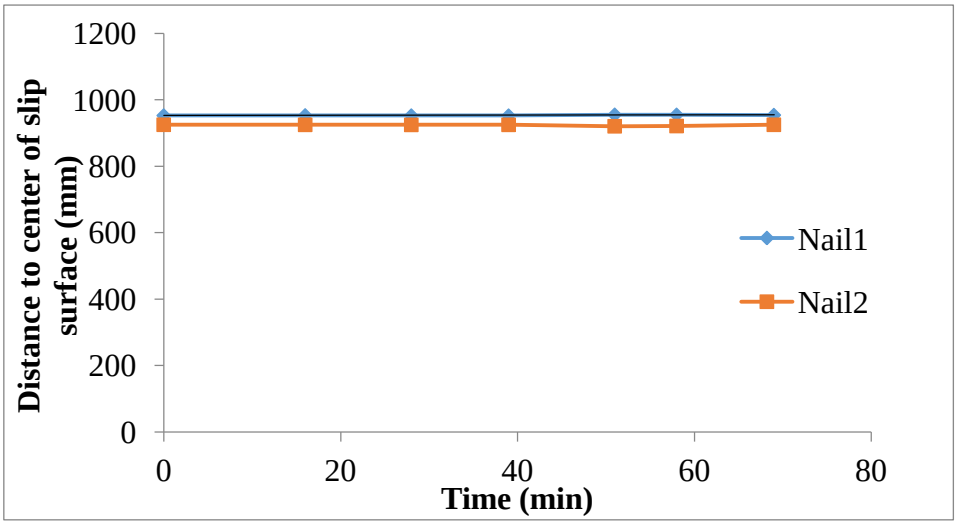

Fig. 6-5 Variation of distance between the tilt sensors and the center of slip surface

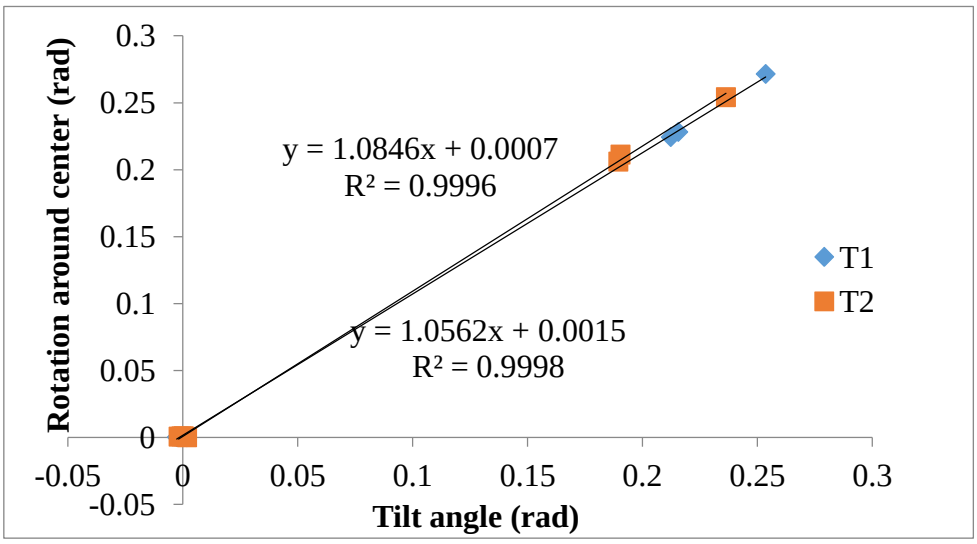

Fig. 6-6 The relationship between the calculated tilting angle and tilting angle measured by tilt sensors in Test 1

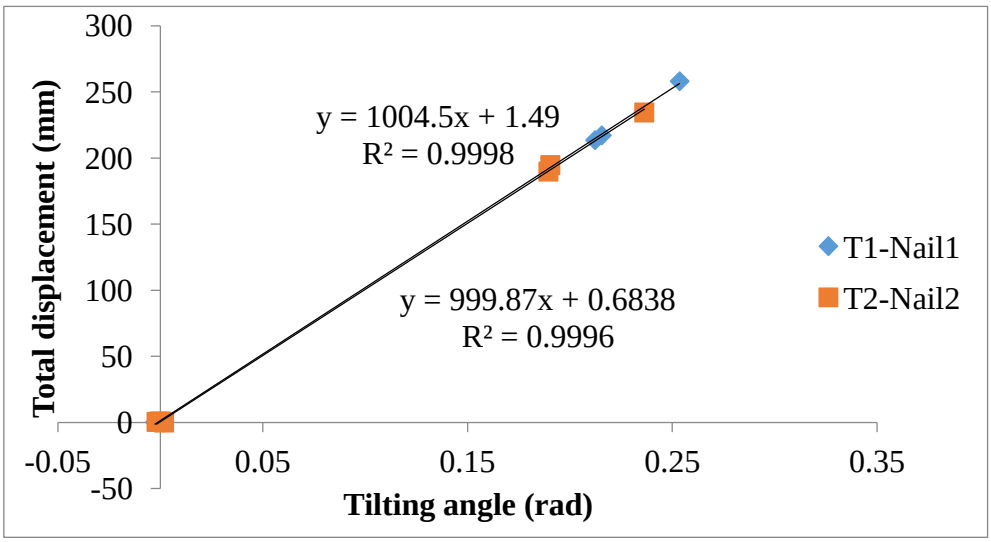

Fig. 6-7 The relationship between tilting angle measured by tilt sensors and total displacement of marked points on the slope surface in Test 1

2) Test 2 using tilt sensors without rod

Compared with Test 1, the radius of slip surface in Test 2 is 600 mm and the relative density of Silica sand number 7 of the surface layer is 30%. Fig. 6-8 shows the illustration of testing condition for this test, and time history of surface displacement and normal displacement are provided in Fig. 6-9 and Fig. 6-10. Fig. 6-11 shows the time history of calculated distance of each tilt sensor to the center of corresponding slip surface, while Fig. 6-12 presents the relationship between calculated tilting angle and the tilting angle measured by tilt sensors. Similar results are indicated in Fig. 6-11

and Fig. 6-12 compared with the results shown in Test 1. Fig. 6-13 shows the rate of fit line for T1 and T2, 582.64 and 565.52, corresponding to the actual distance 552 mm and 508 mm for T1 and T2 respectively.

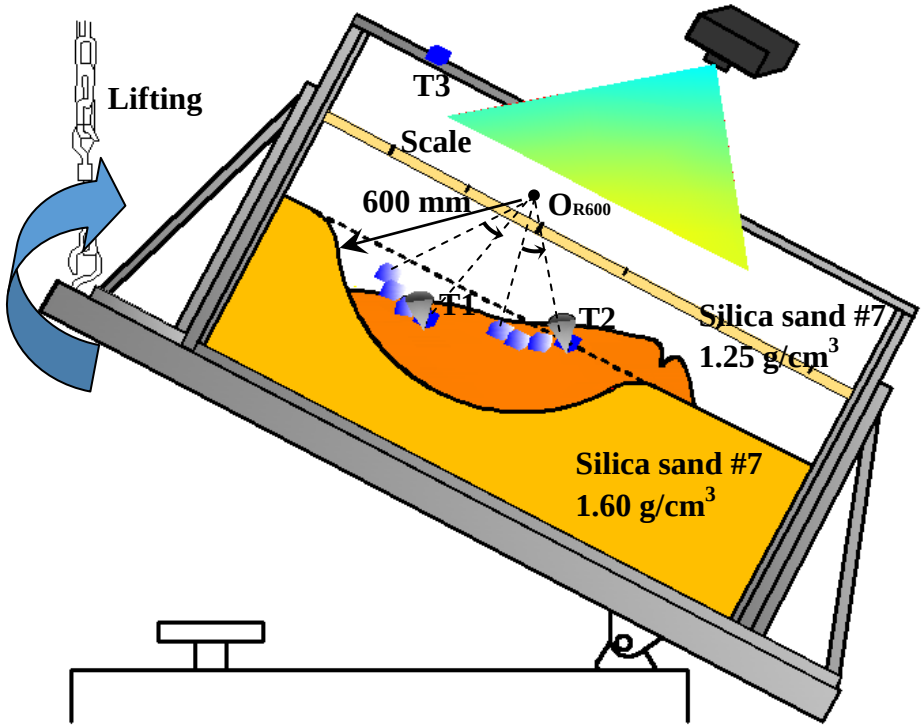

Fig. 6-8 Illustration of Test 2 using tilt sensors without rods

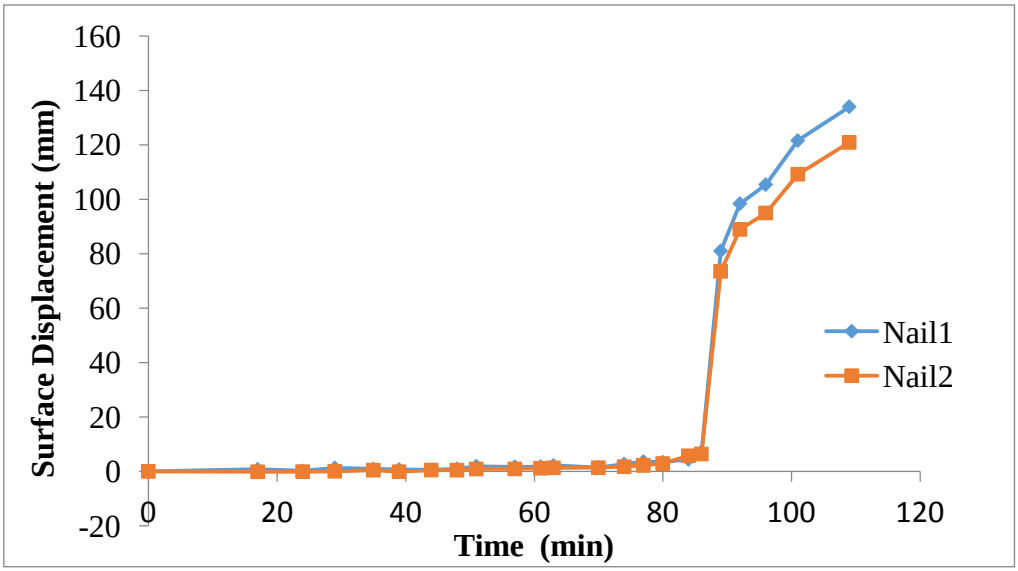

Fig. 6-9 Time history of surface displacement of Test 2 using tilt sensors without rods

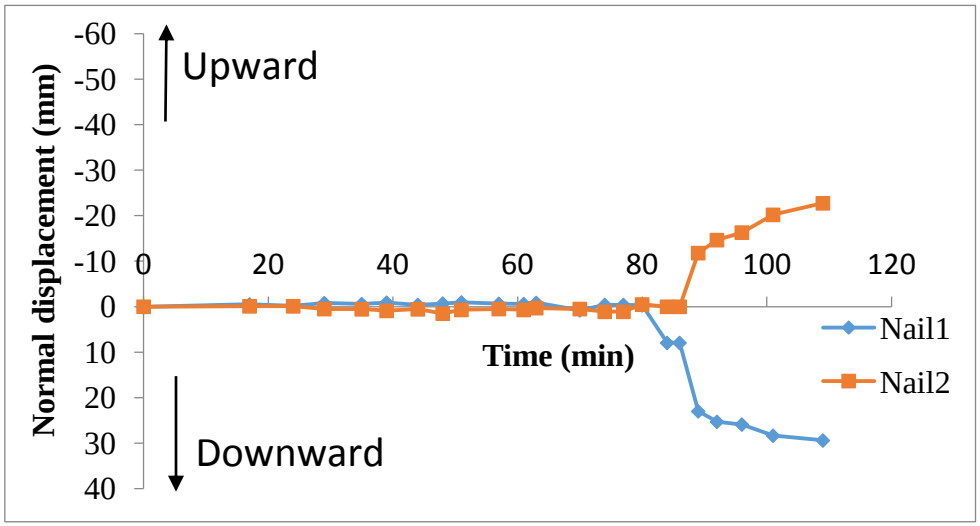

Fig. 6-10 Time history of normal displacement of Test 2 using tilt sensors without rods

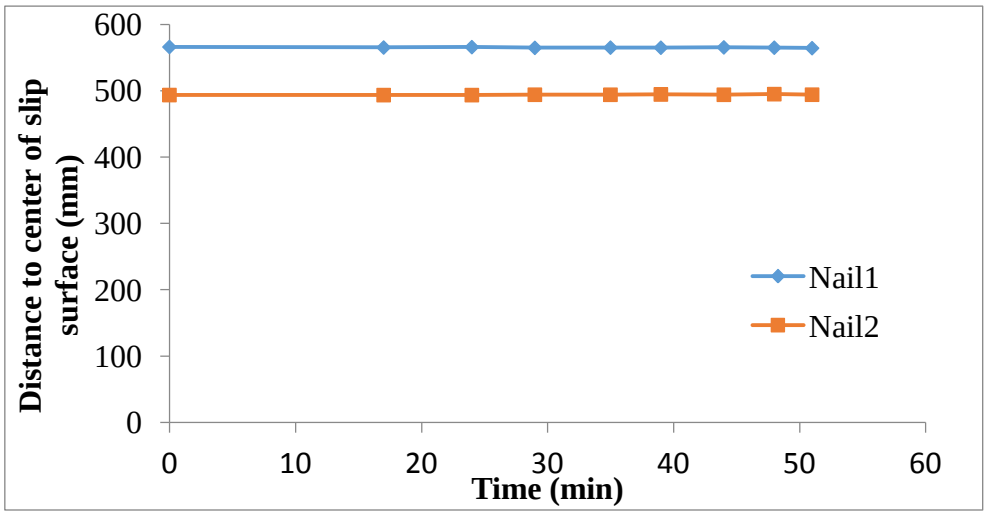

Fig.6-11 Variation of distance between the tilt sensors and the center of slip surface

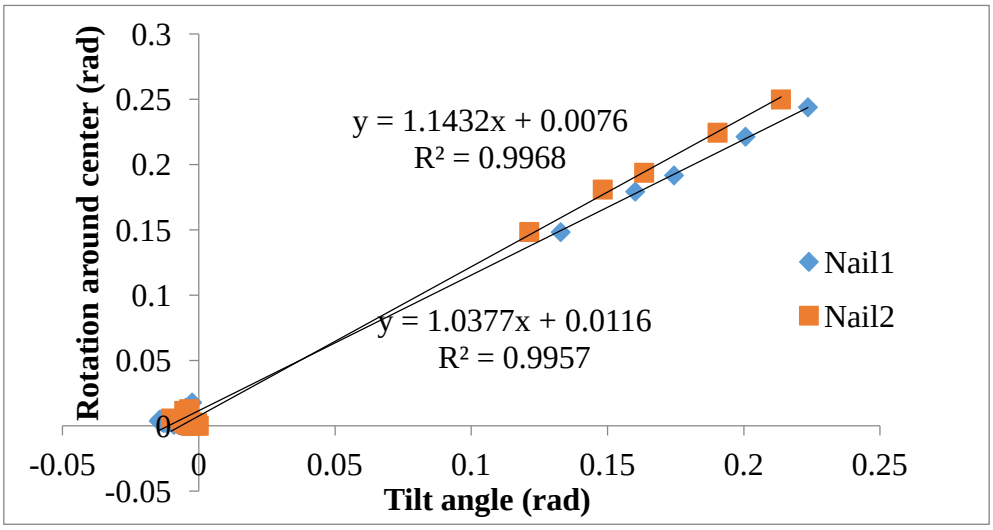

Fig. 6-12 The relationship between the calculated tilting angle and tilting angle measured by tilt sensors in Test 2

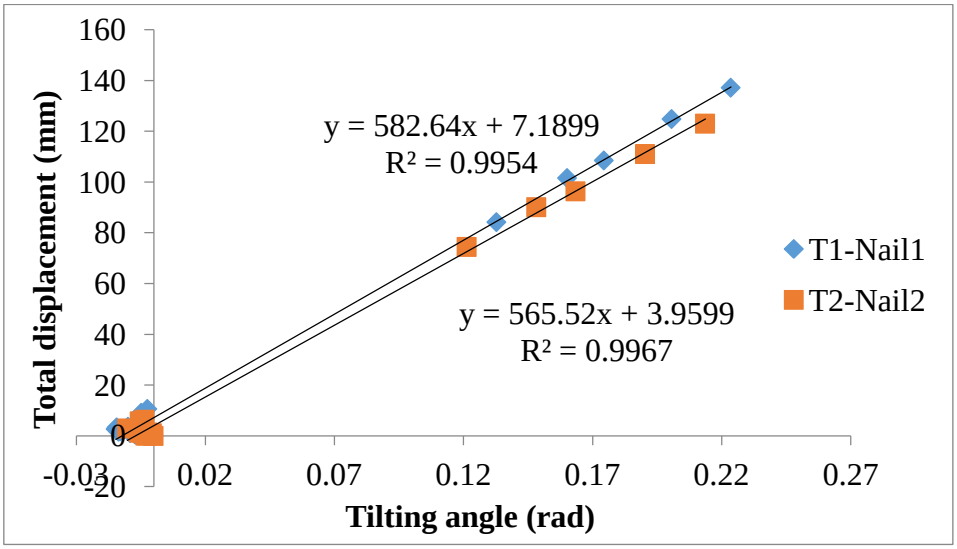

Fig. 6-13 The relationship between tilting angle measured by tilt sensors and total displacement of marked points on the slope surface in Test 2

3) Test 3 using tilt sensors without rods

The only difference between Test 2 and this test is that the relative density of Silica sand number 7 of the surface layer in Test 2 is 30%, while it is 50% in this test. In Test 3, three tilt sensors were embedded in the upper part, middel part and bottom part of the slope respectively. Details about this test is presented in Fig. 6-14. The change of surface displacement, normal displacement, and calculated distance of each tilt sensor are provided in Fig. 6-15, Fig. 6-16 and Fig. 6-17. Fig. 6-18 shows that the calculated tilting angle is close to the measured tilting angle. The actual distance for the three tilt sensors to the center of slip surface are 532 mm, 478 mm and 495 mm corresponding to the rate of fit lines around 555, 505 and 516 respectively (Fig. 6-19).

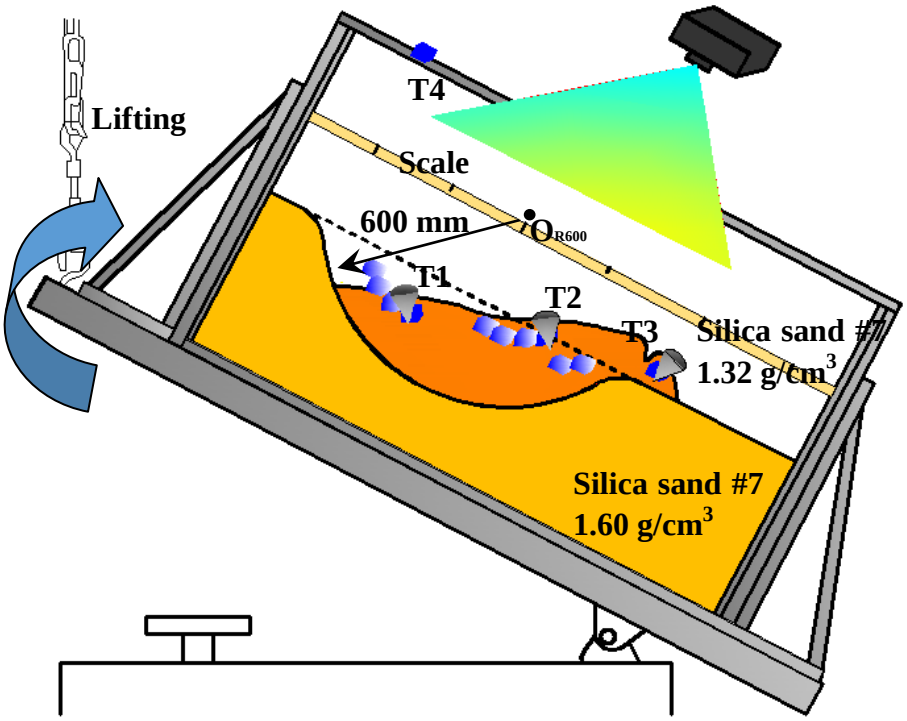

Fig. 6-14 Illustration of Test 3 using tilt sensors without rods

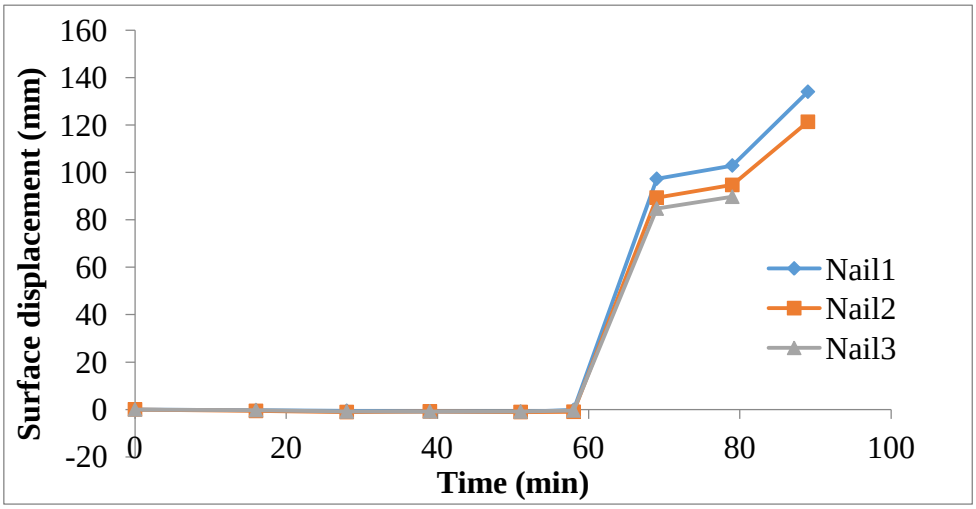

Fig. 6-15 Time history of surface displacement of Test 3 using tilt sensors without rods

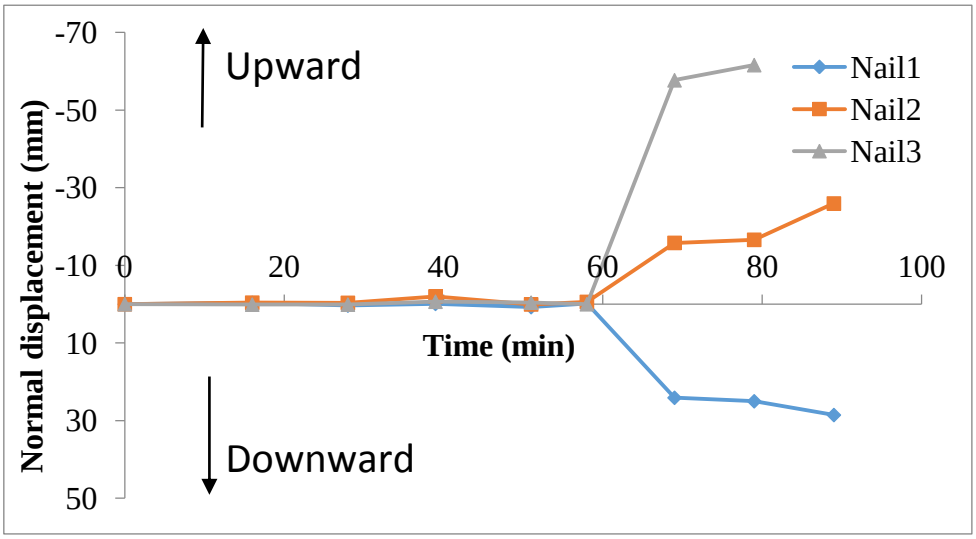

Fig. 6-16 Time history of normal displacement of Test 3 using tilt sensors without rods

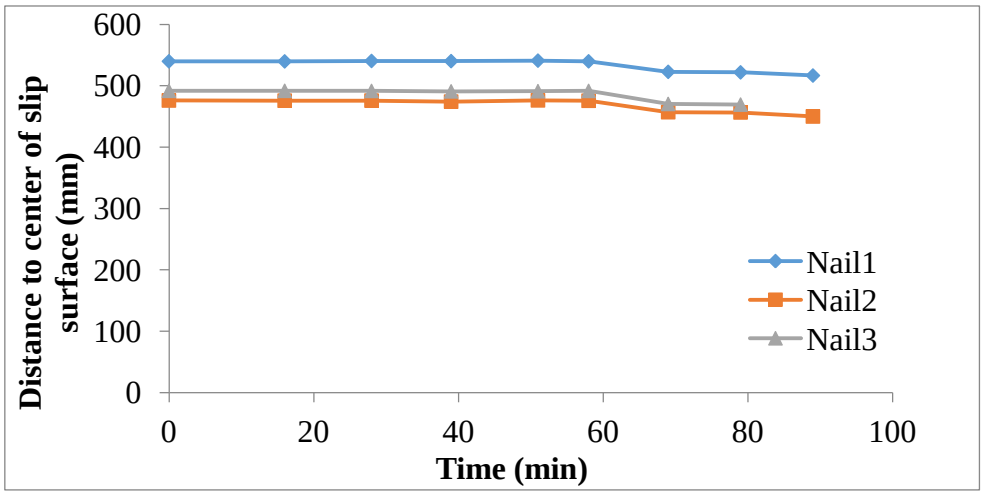

Fig. 6-17 Variation of distance between the tilt sensors and the center of slip surface

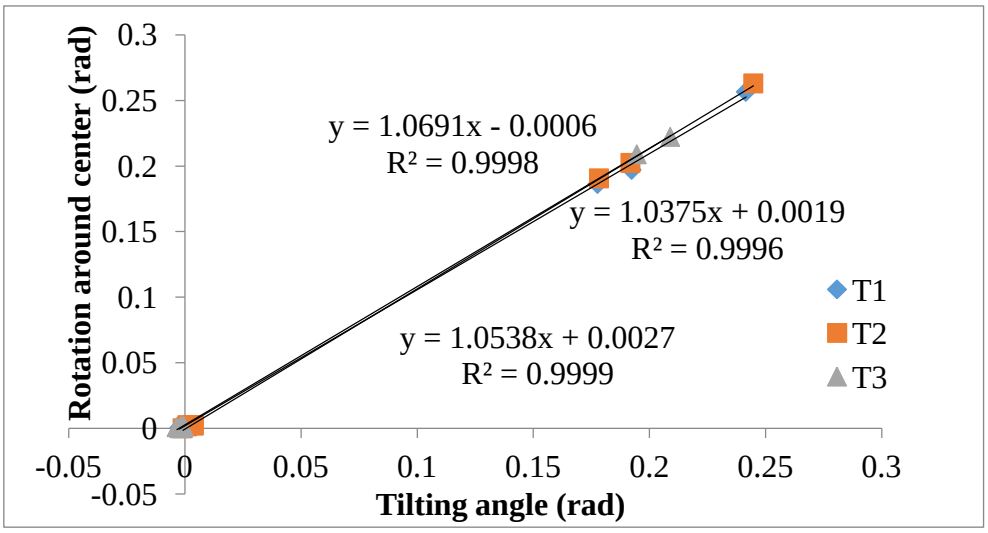

Fig. 6-18 The relationship between the calculated tilting angle and tilting angle measured by tilt sensors in Test 3

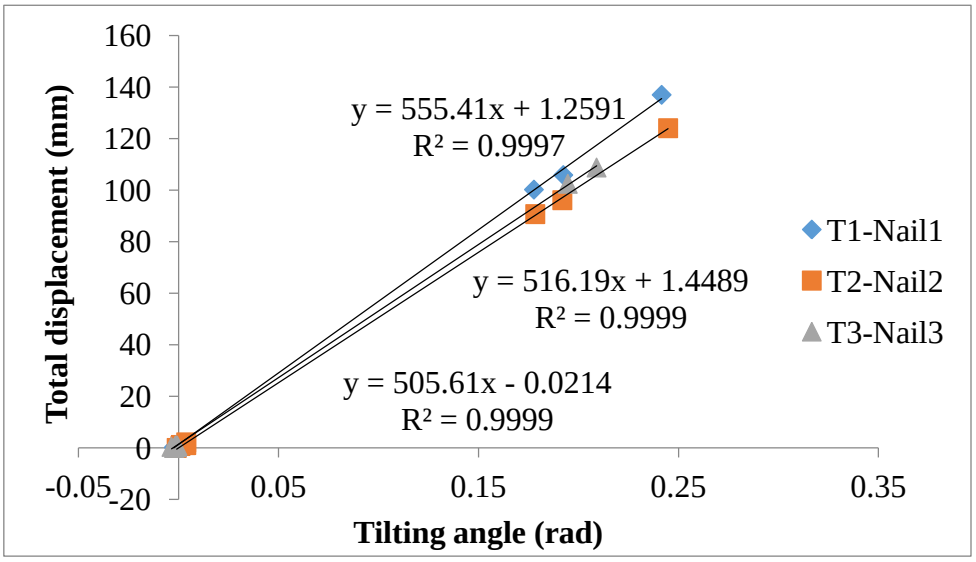

Fig. 6-19 The relationship between tilting angle measured by tilt sensors and total displacement of marked points on the slope surface in Test 3

4) Test 4 using tilt sensors without rods

In model test 4, Edosaki sand was used, and the testing conditons of this test is presented in Fig. 6-20. Compared with the test results discussed before, consistent results are achieved in this test and shown in Fig. 6-21, Fig. 6-22, Fig. 6-23 as well as in Fig. 6-24. The actual distance for the three tilt sensors to the center of slip surface are 541 mm, 483 mm and 517 mm corresponding to the rate of fit lines around 553, 533 and 536 respectively.

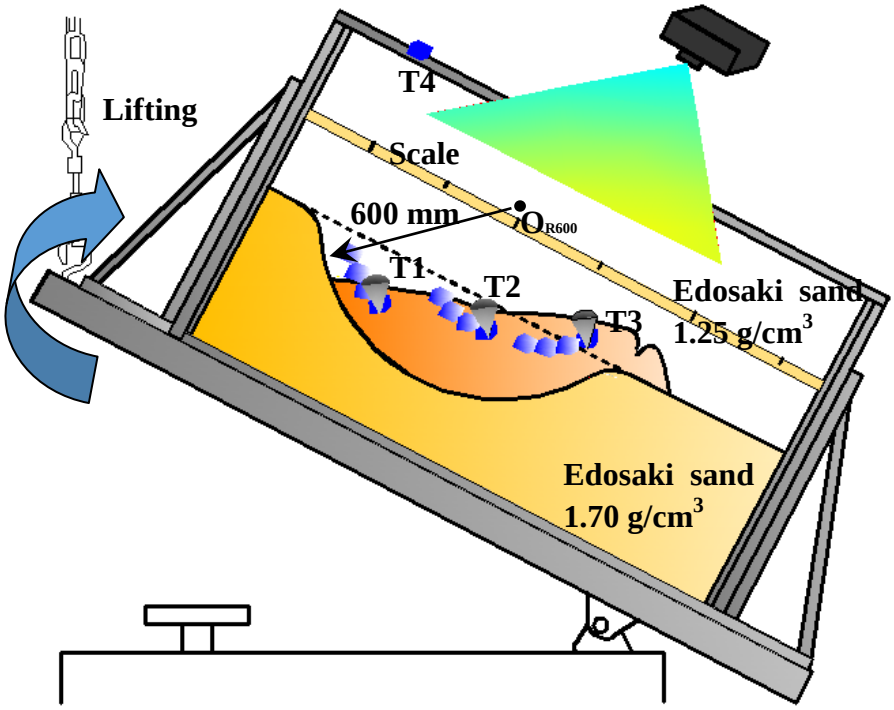

Fig.6-20 Illustration of Test 4 using tilt sensors without rods

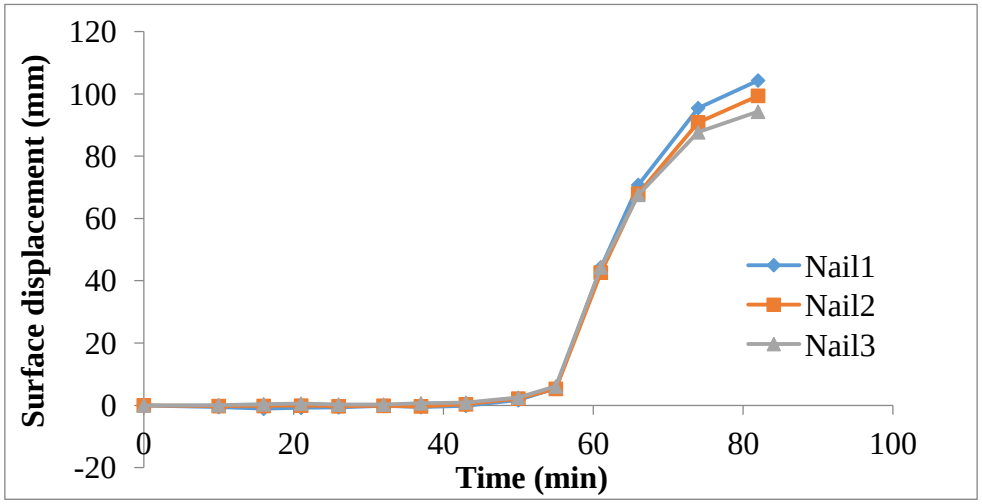

Fig. 6-21 Time history of surface displacement of Test 4 using tilt sensors without rods

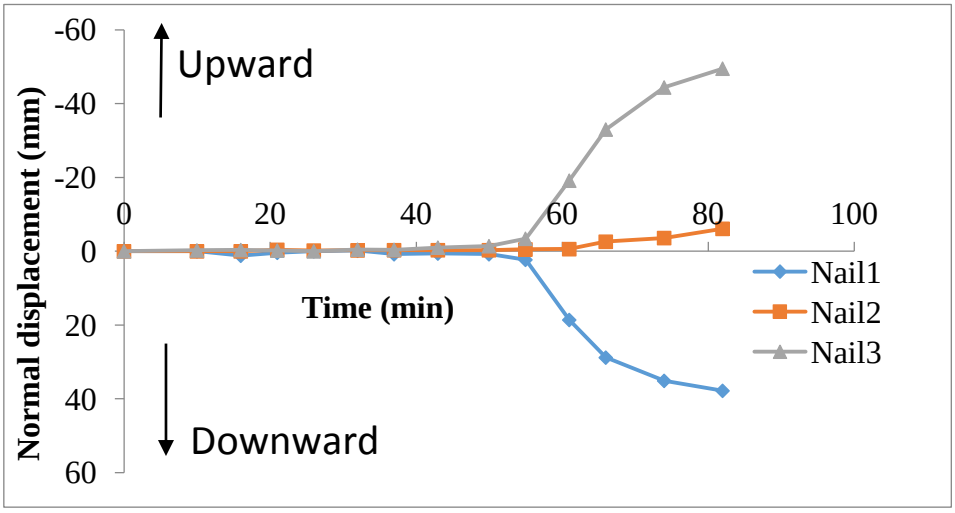

Fig. 6-22 Time history of normal displacement of Test 4 using tilt sensors without rods

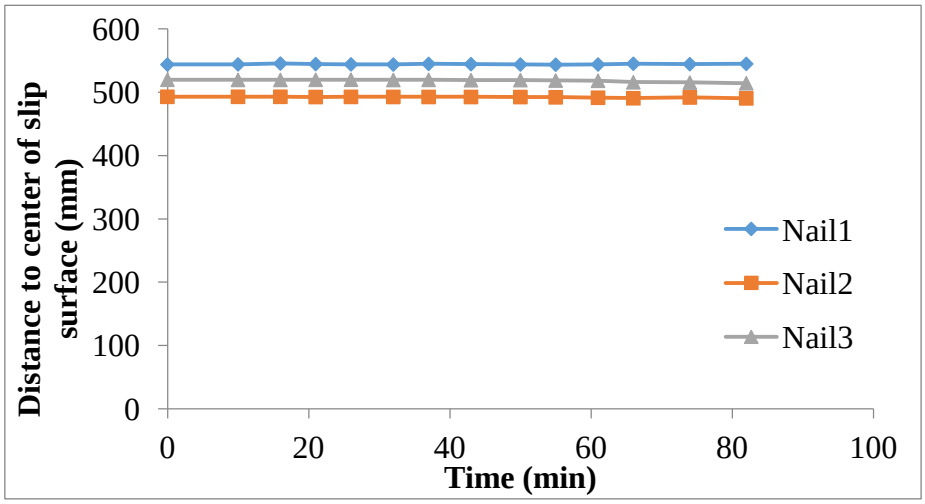

Fig. 6-23 Variation of distance between the tilt sensors and the center of slip surface

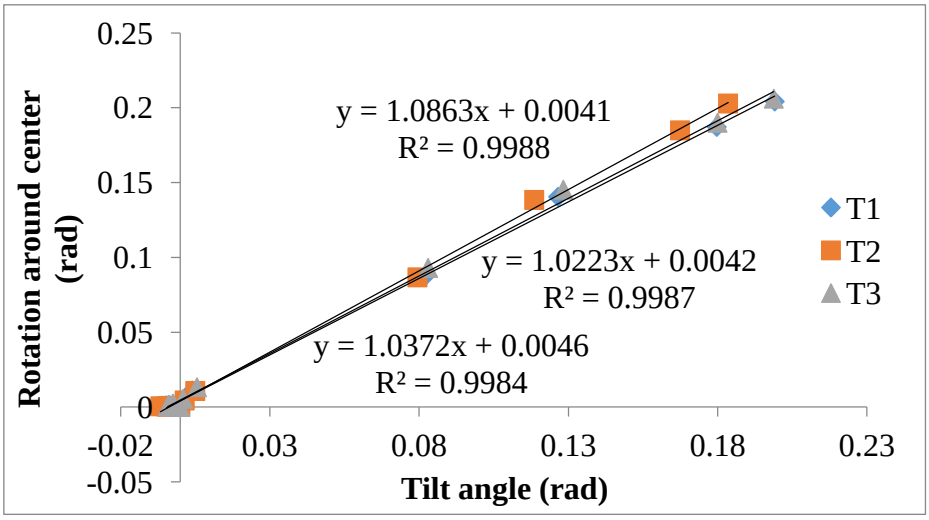

Fig. 6-24 The relationship between the calculated tilting angle and tilting angle measured by tilt sensors in Test 4

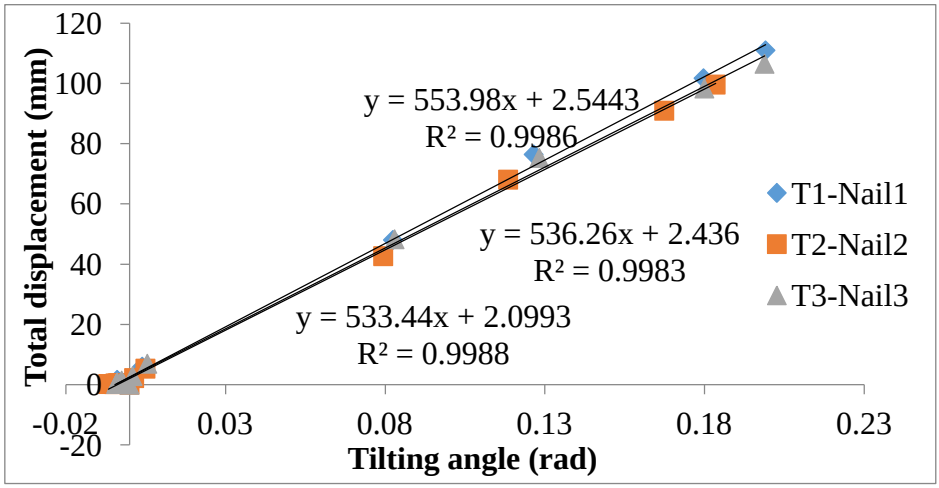

Fig. 6-25 The relationship between tilting angle measured by tilt sensors and total displacement of marked points on the slope surface in Test 4

5) Test 5 using tilt sensors without rods

In this test, the radius of slip surface for the upper part of the slope is 400 mm, and that for the lower part is 600 mm as shown in Fig. 6-26. Test results are presented in Fig. 6-27 to Fig. 6-31. The surface layer of slope slided along the pre-defined slip surface with neglectable internal deformation. The actual distance between the tilt sensors and the center of correponding slip surfaces are 537 mm and 311 mm.

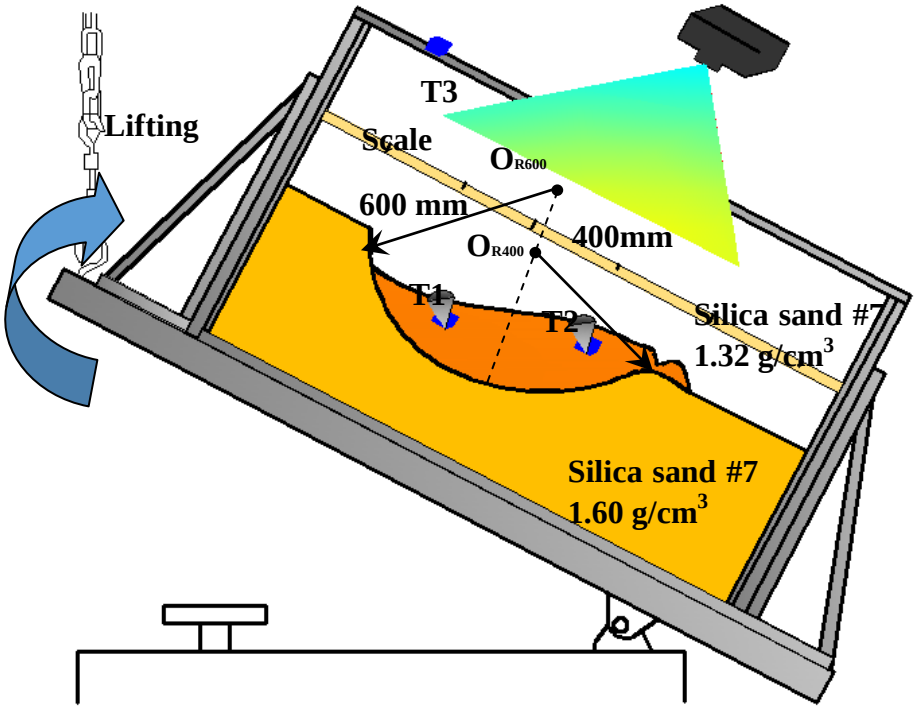

Fig. 6-26 Illustration of Test 5 using tilt sensors without rods

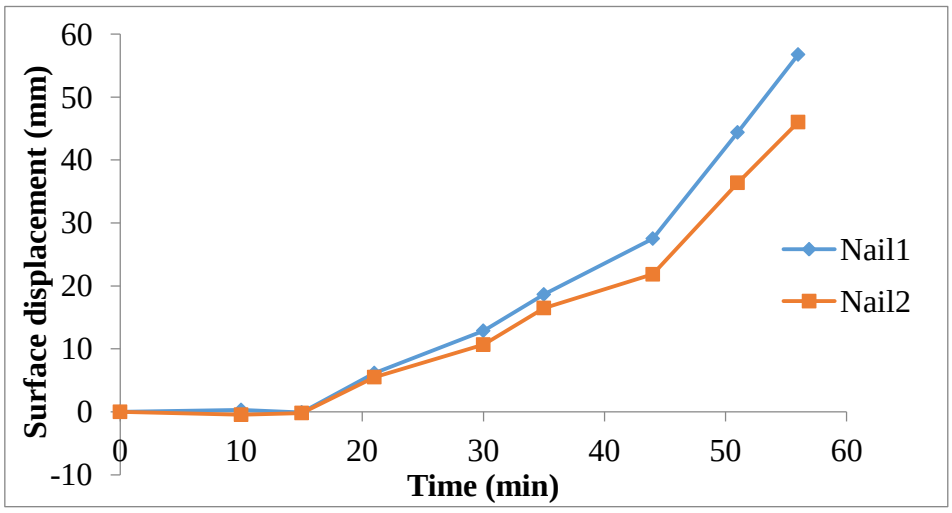

Fig. 6-27 Time history of surface displacement of Test 5 using tilt sensors without rods

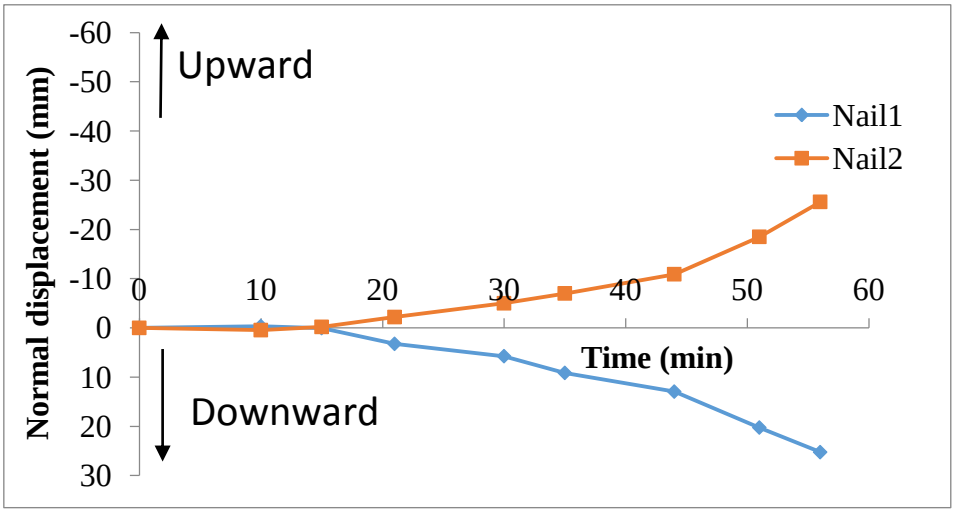

Fig. 6-28 Time history of normal displacement of Test 5 using tilt sensors without rods

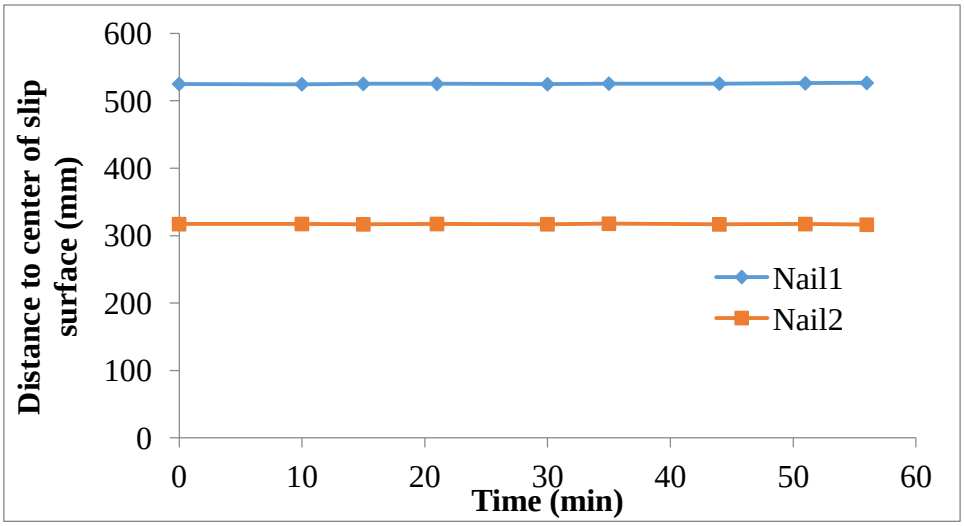

Fig. 6-29 Variation of distance between the tilt sensors and the center of slip surface

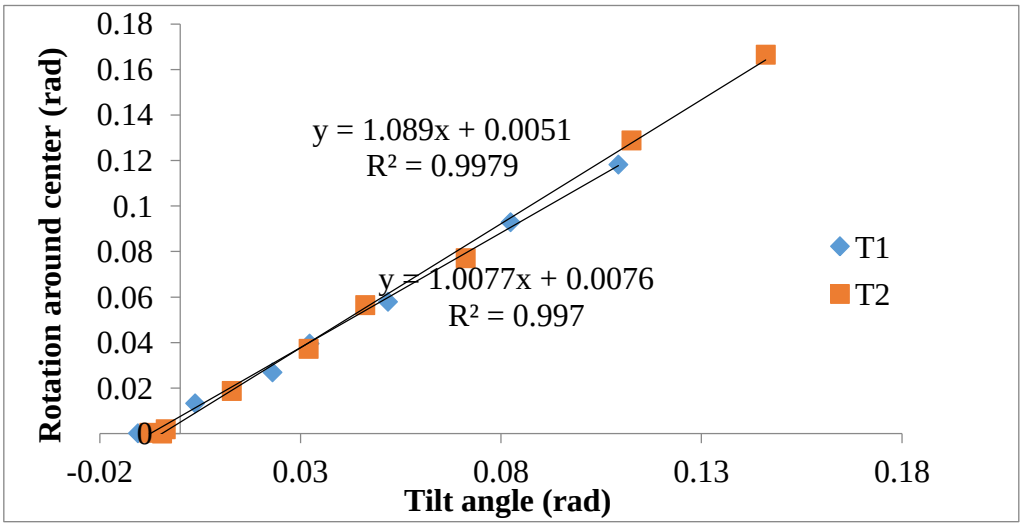

Fig. 6-30 The relationship between the calculated tilting angle and tilting angle measured by tilt sensors in Test 5

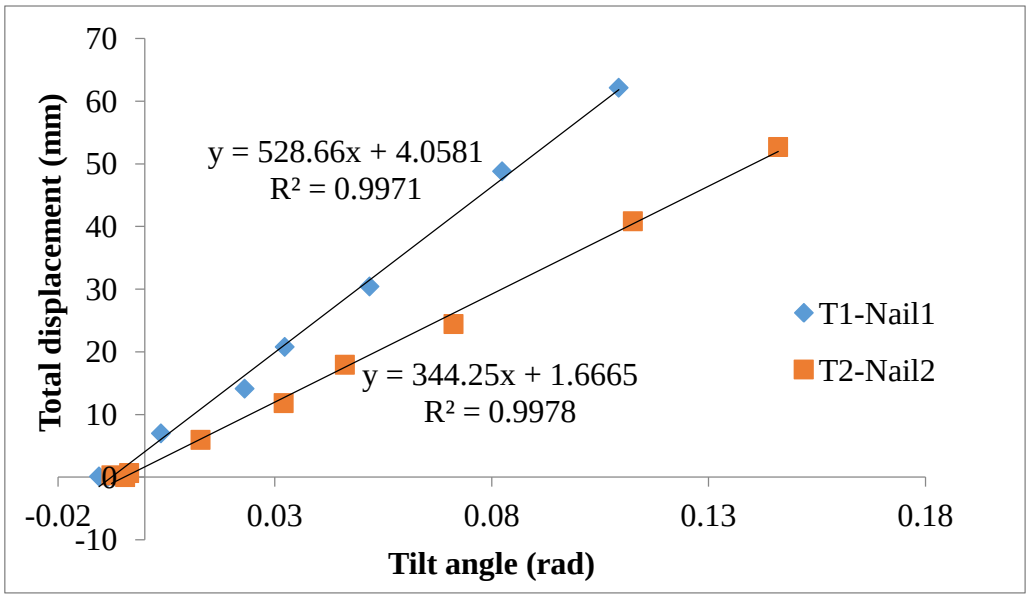

Fig. 6-31 The relationship between tilting angle measured by tilt sensors and total displacement of marked points on the slope surface in Test 5

6) Test 6 using tilt sensors without rods

Compared with Test 5, Edosaki sand was used in this test (Fig. 6-32). Consistent results are achieved in this test and shown from Fig. 6-33 to Fig. 6-37. The actual distance for T1 and T2 are 541 mm and 320 mm corresponding to the rate of fit lines around 562, and 363 respectively.

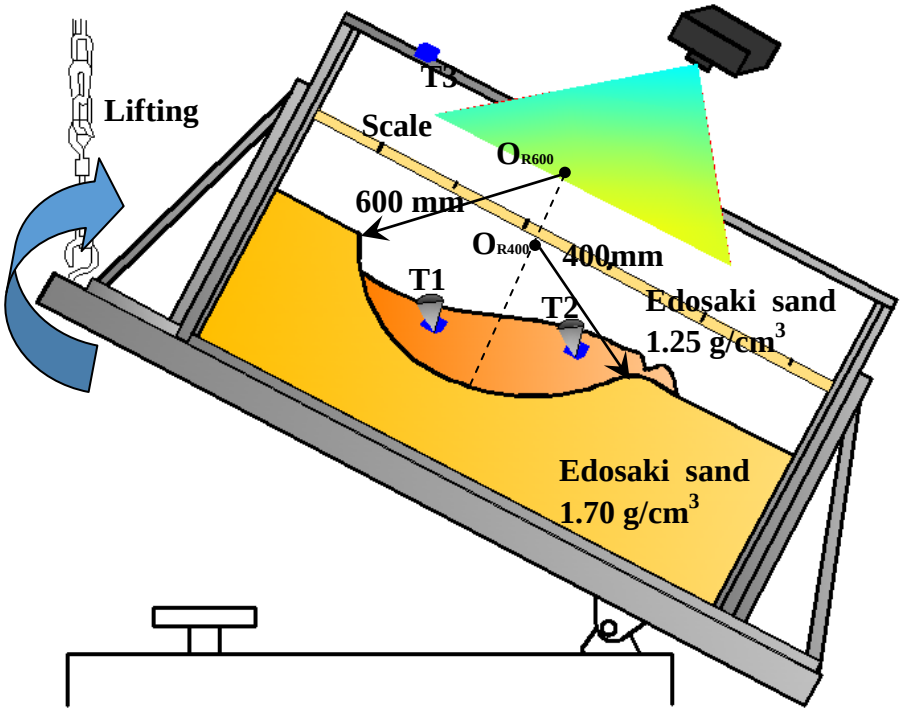

Fig. 6-32 Illustration of Test 6 using tilt sensors without rods

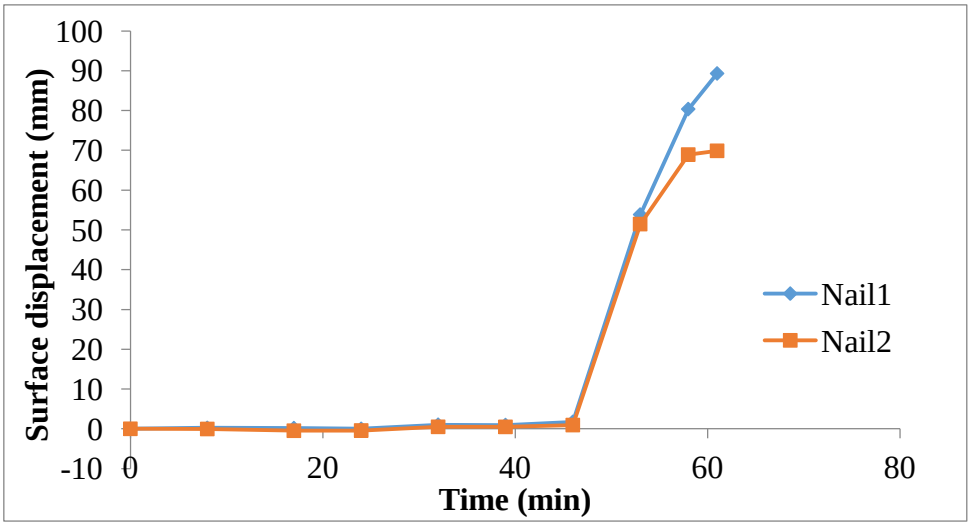

Fig. 6-33 Time history of surface displacement of Test 6 using tilt sensors without rods

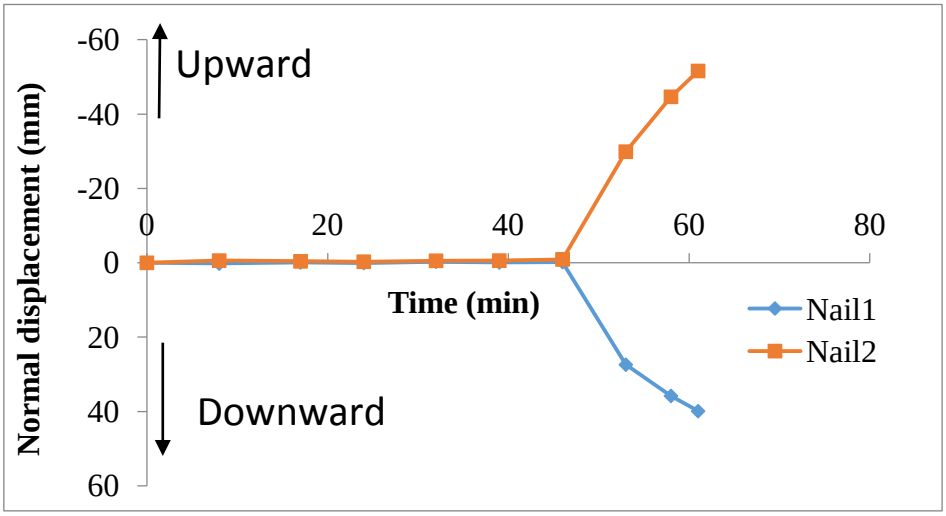

Fig. 6-34 Time history of normal displacement of Test 6 using tilt sensors without rods

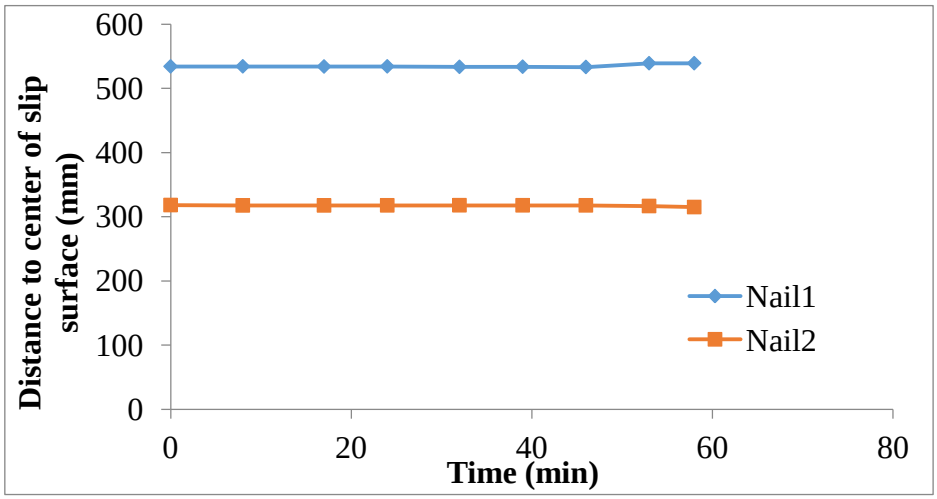

Fig. 6-35 Variation of distance between the tilt sensors and the center of slip surface

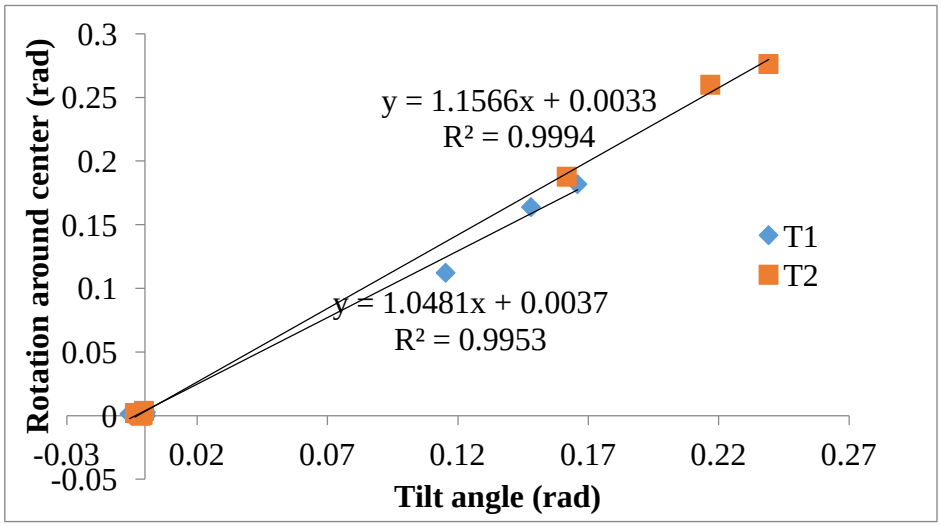

Fig. 6-36 The relationship between the calculated tilting angle and tilting angle measured by tilt sensors in Test 6

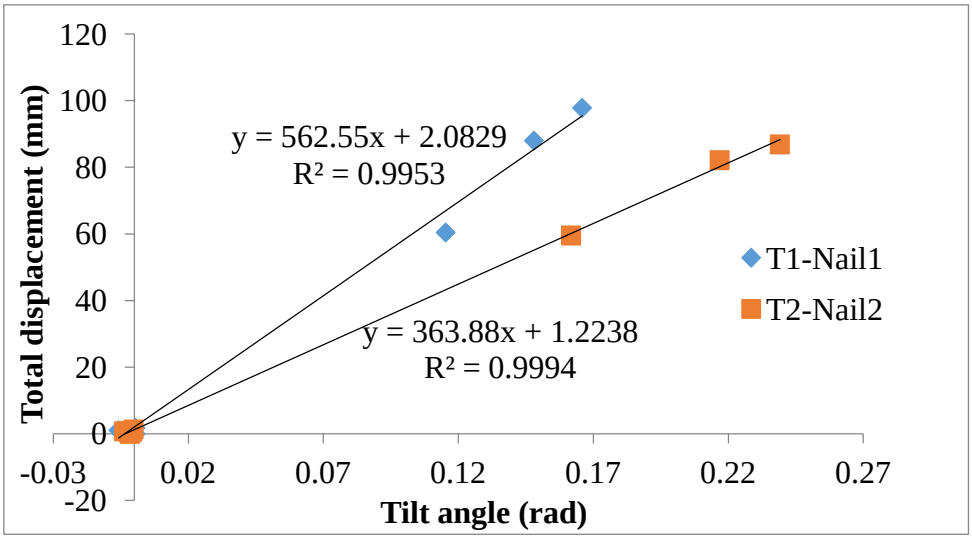

Fig. 6-37 The relationship between tilting angle measured by tilt sensors and total displacement of marked points on the slope surface in Test 6

7) Test 7 using tilt sensors without rods

In this test, the radius of slip surface for the upper part of this slope is 300 mm, and that for the lower part is 800 mm as shown in Fig. 6-38. Test results are presented in Fig. 6-39 to Fig. 6-43. Similar to the results in Test 5, during the slope sliding, the upper part of slope rotated around the center of slip surface in the upper part (O_{R300}), while the bottom part rotated around O_{R600}. Fig. 6-43 shows the rate of fit lines for T1 and T2 are 229 and 658 corresponding to the actual distance of these two tilt sensors 211 mm and 670 mm.

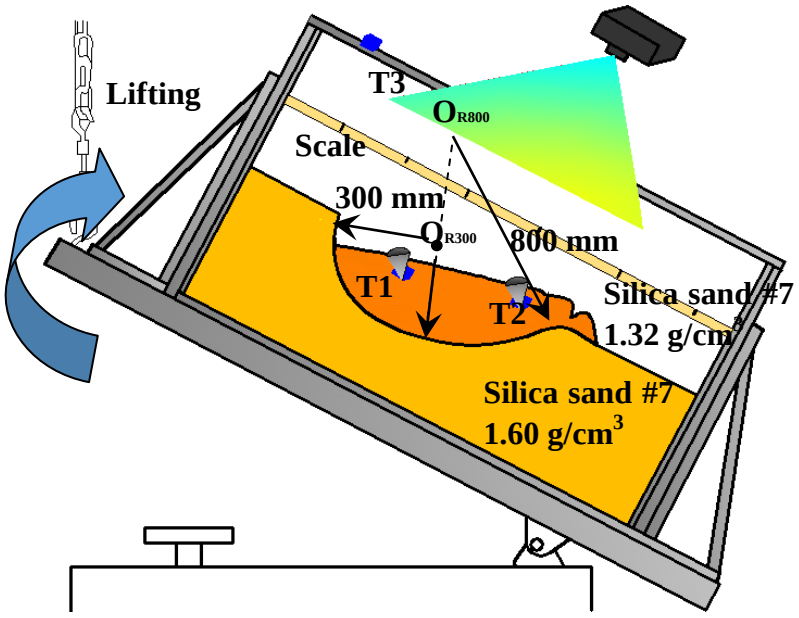

Fig. 6-38 Illustration of Test 7 using tilt sensors without rods

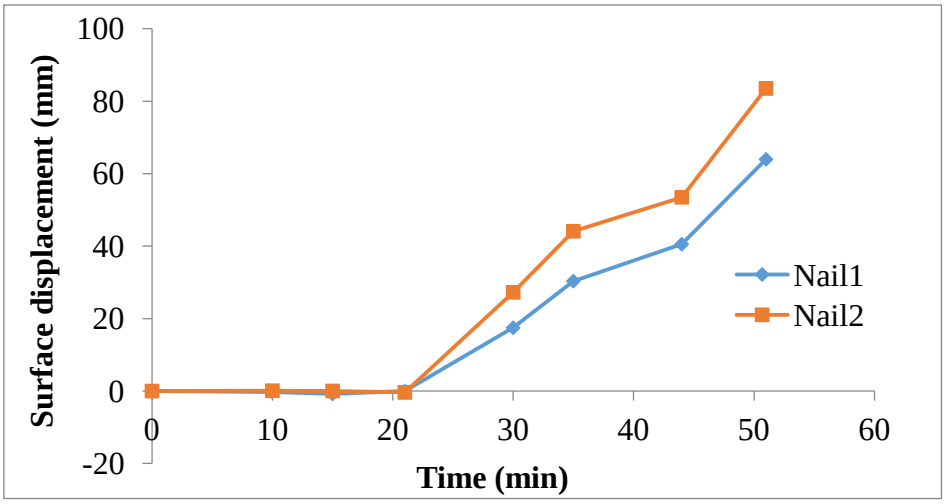

Fig. 6-39 Time history of surface displacement of Test 7 using tilt sensors without rods

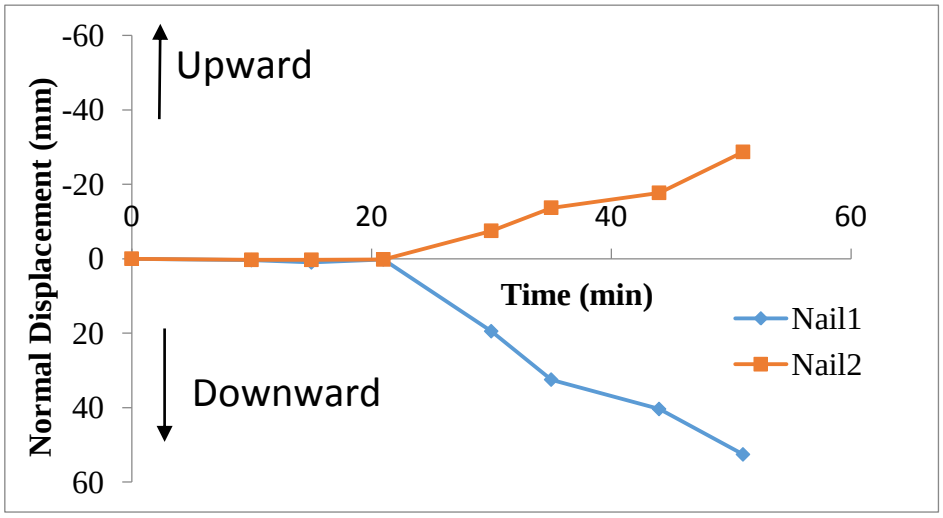

Fig. 6-40 Time history of normal displacement of Test 7 using tilt sensors without rods

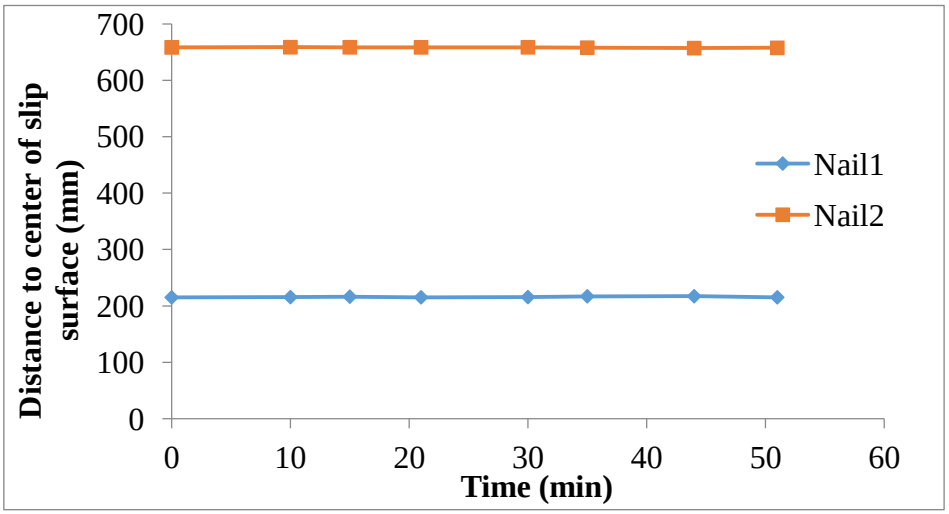

Fig. 6-41 Variation of distance between the tilt sensors and the center of slip surface

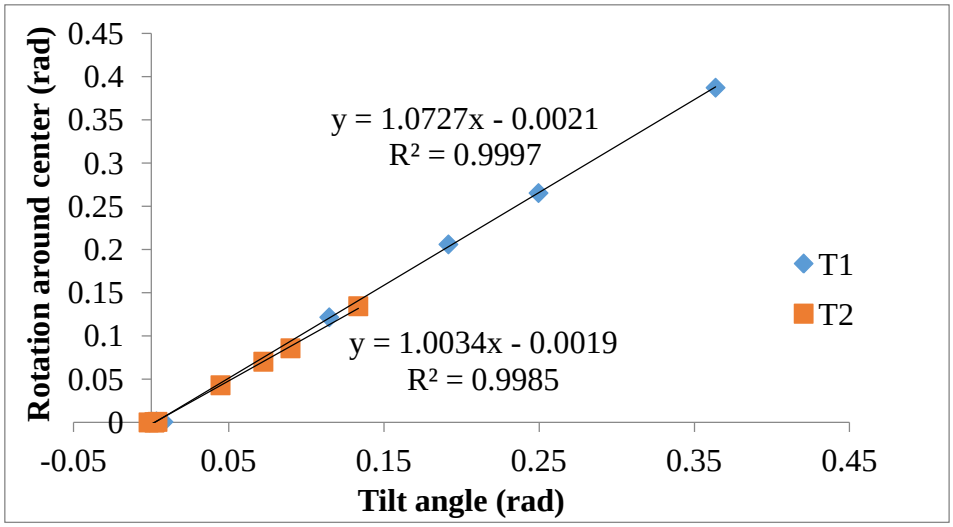

Fig. 6-42 The relationship between the calculated tilting angle and tilting angle measured by tilt sensors in Test 7

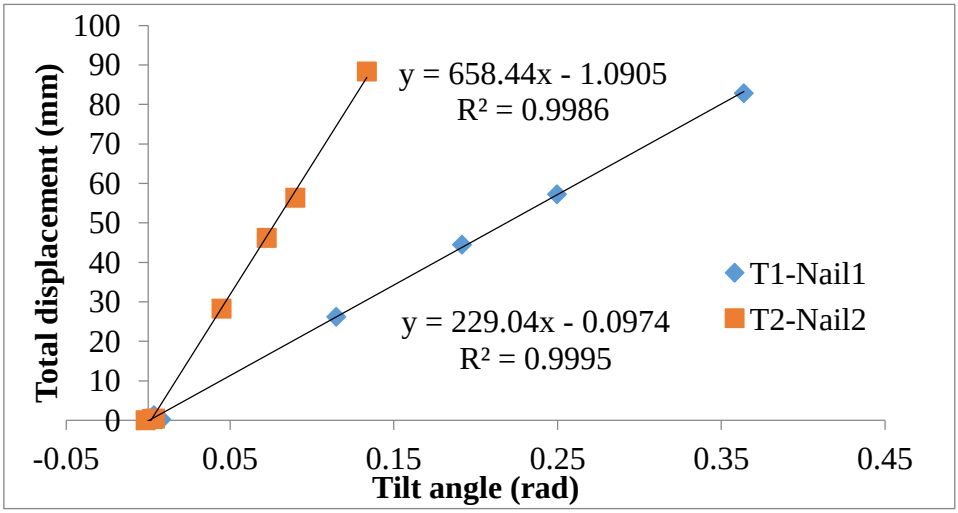

Fig. 6-43 The relationship between tilting angle measured by tilt sensors and total displacement of marked points on the slope surface in Test 7

8) Test 8 using tilt sensors without rods

Compared with Test 7, the slope sliding in this test was caused by periodical rainfall, and details about this test is illustratd in Fig. 6-44. Test results presented in Fig. 6-45 to Fig. 6-49 indicate that even though the triggering factors of slope failure are different, similar results can be approached. During the slope sliding, the upper part as well as bottom part of the slope rotated around the corresponding center of slip surfaces. Fig. 6-49 shows the rate of fit lines for T1 and T2 are 233 and 696 corresponding to the actual distance of these two tilt sensors 215 mm and 679 mm.

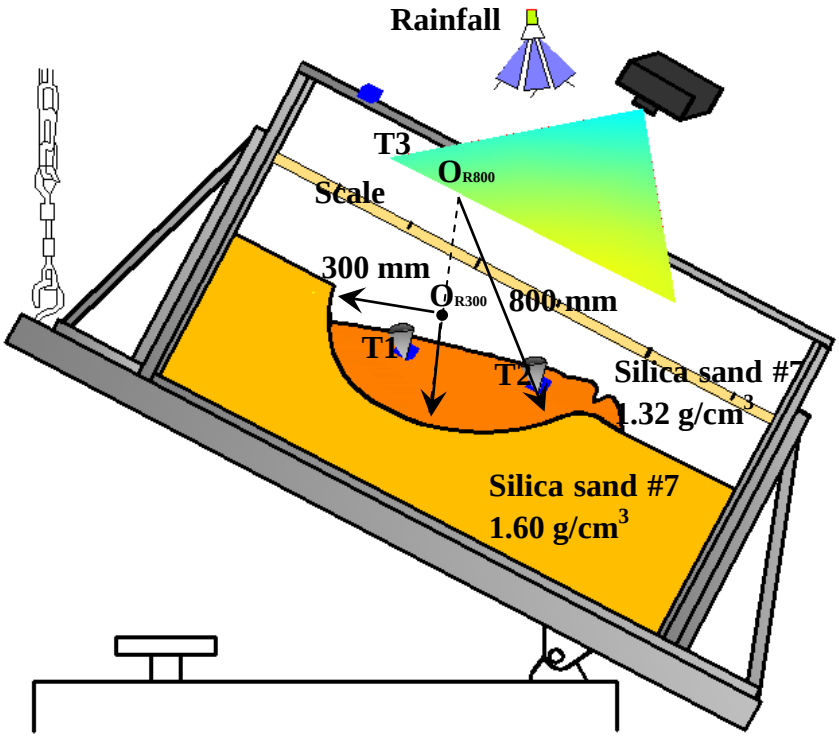

Fig. 6-44 Illustration of Test 8 using tilt sensors without rods

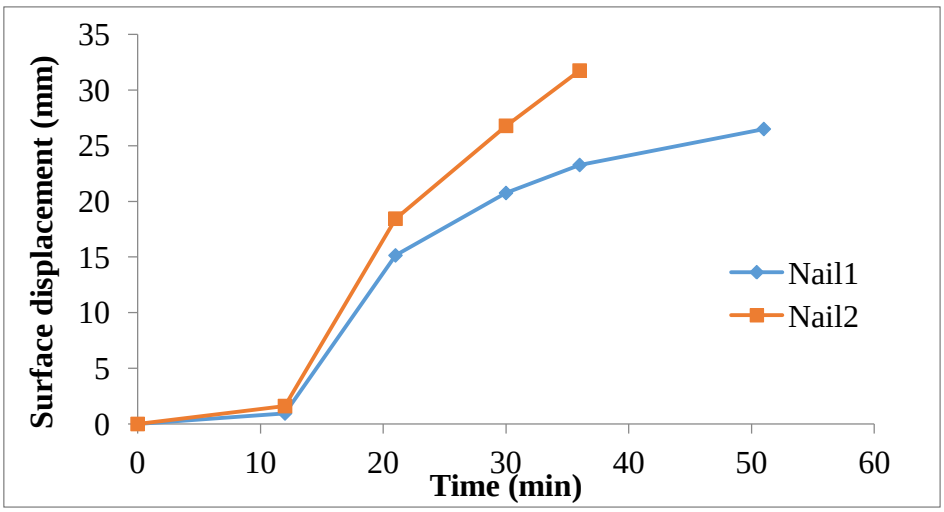

Fig. 6-45 Time history of surface displacement of Test 8 using tilt sensors without rods

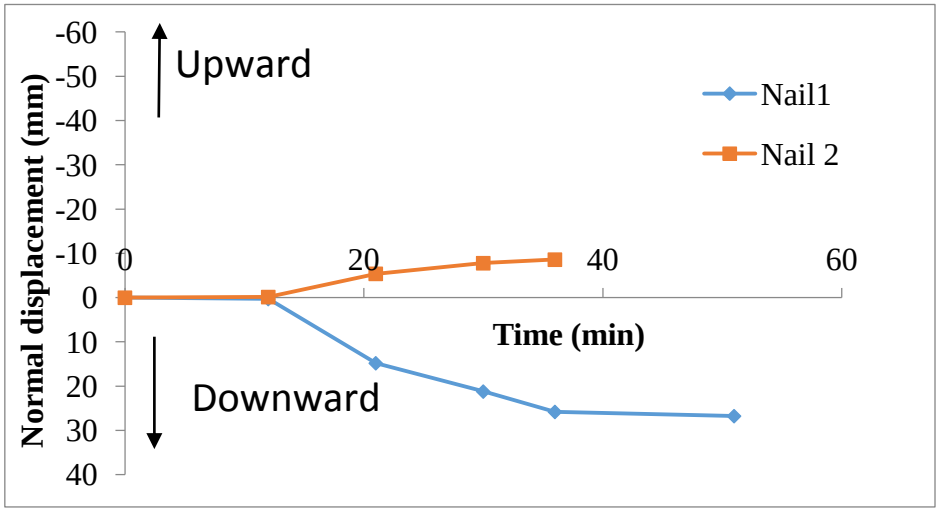

Fig. 6-46 Time history of normal displacement of Test 2 using tilt sensors without rods

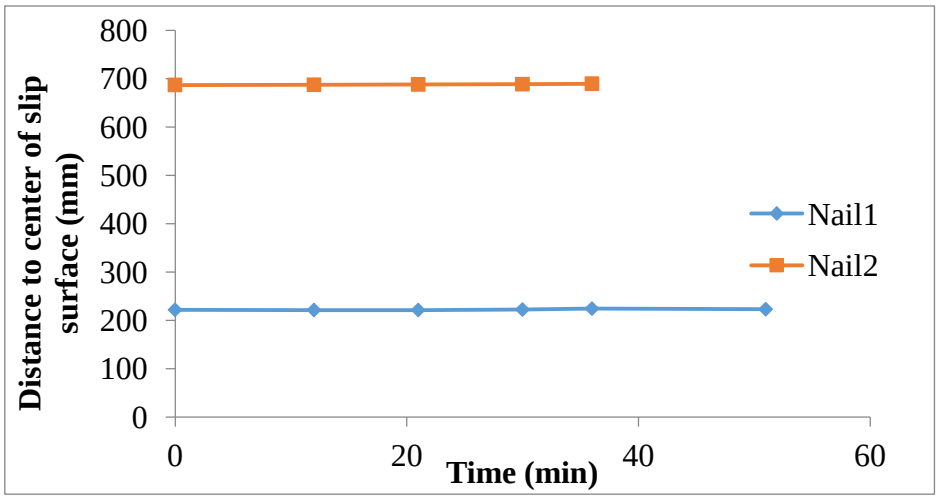

Fig.6-47 Variation of distance between the tilt sensors and the center of slip surface

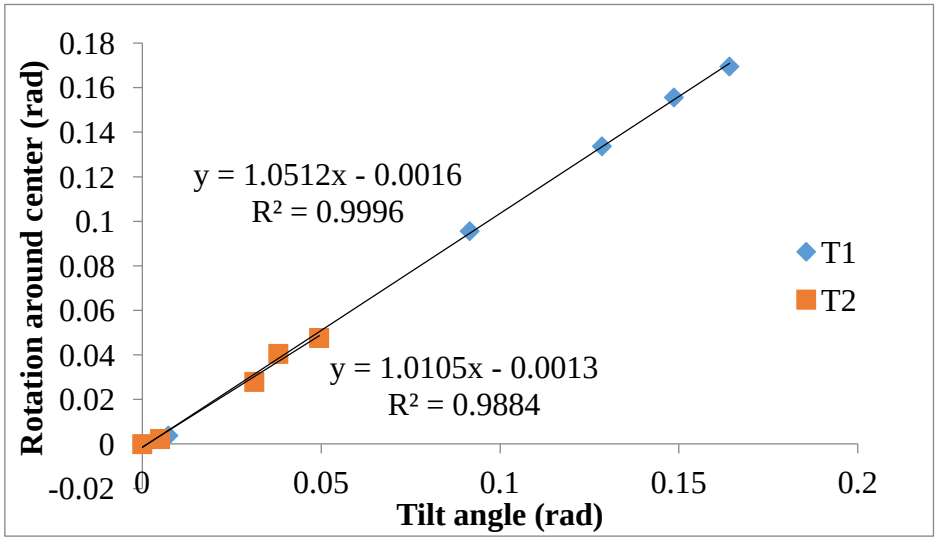

Fig. 6-48 The relationship between the calculated tilting angle and tilting angle measured by tilt sensors in Test 8

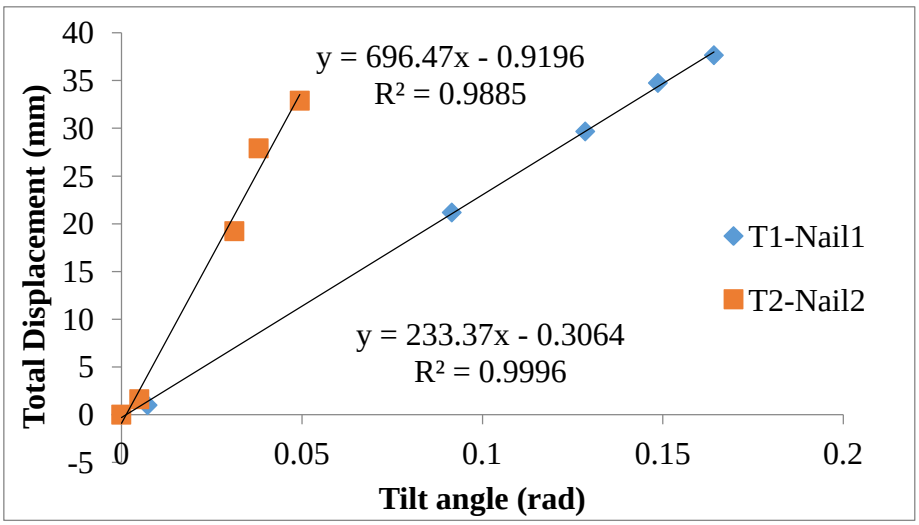

Fig. 6-49 The relationship between tilting angle measured by tilt sensors and total displacement of marked points on the slope surface in Test 8

9) Test 9 using tilt sensors without rods

In Test 9, continuous rainfall was supplied, and the displacement was measured by two extensometers introduced in Chapter 3. The time history of displacement and tilting angle are presented in Fig. 6-51 and Fig. 6-52. The relationship between tilting angle and displacement is shown in Fig. 6-52. The actual distance between the centers of the slip surface and tilt sensors are 212 mm and 685 mm corresponding to the fitting rate 179 and 749 respectively. The error between actual distance and fitting rate is a little bit larger compared with the results discussed before, and it may be caused by measurement error of slope displacement using extensometers.

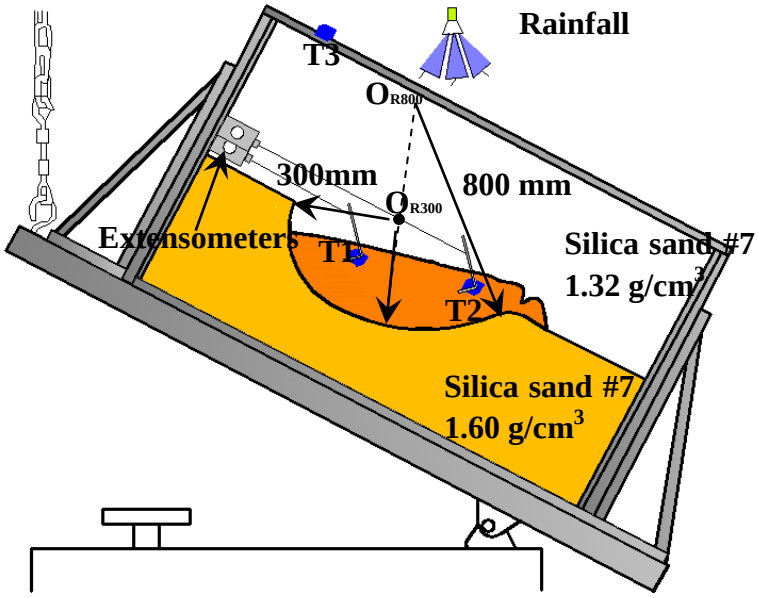

Fig. 6-50 Illustration of Test 9 using tilt sensors without rods

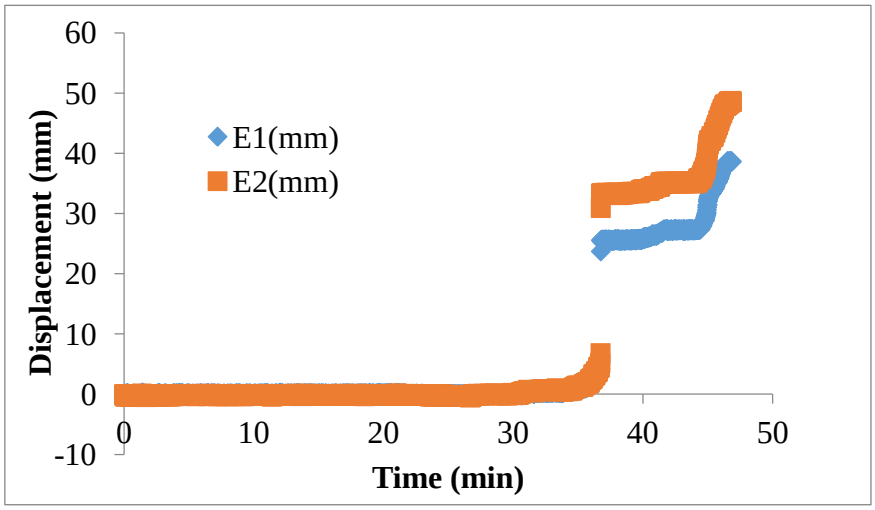

Fig. 6-51 Time history of displacement of Test 9 using extensometers without rods

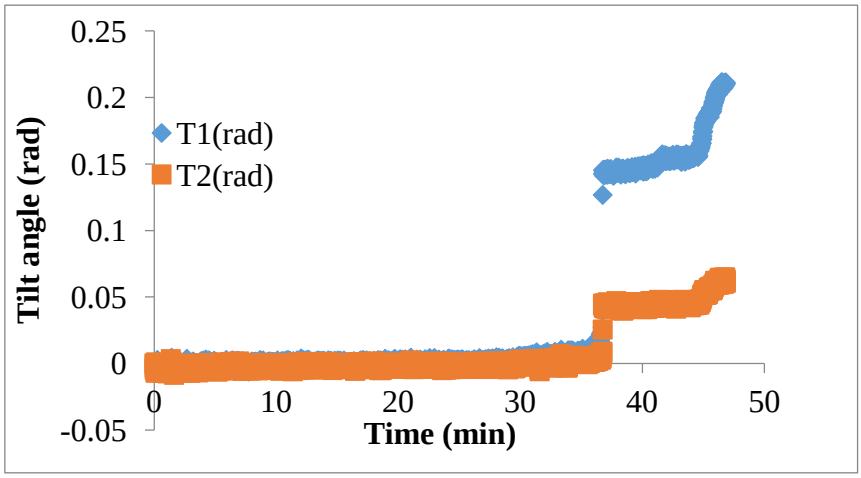

Fig. 6-52 Time history of tilting angle in Test 9 using tilt sensors without rods

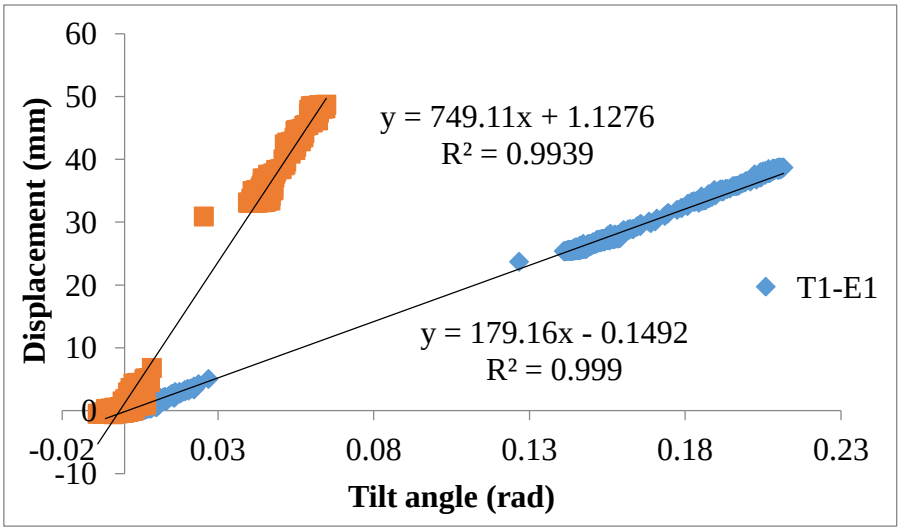

Fig. 6-53 The relationship between tilting angle measured by tilt sensors and displacement recorded by extensometers on the slope surface in Test 9

10) Test 10 using tilt sensors without rods

In this test, the Edosaki sand was used and the slope sliding was induced by periodical rainfall. Fig. 6-54 shows the illustration of testing conditions, and the test results are presented in the figures from Fig. 6-55 to Fig. 6-59. The actual distance between tilt sensors and the center of slip surface are 552 mm, 472 mm, and 508 mm. There is a big difference between the fitting rate and actual distance of T2, and Fig. 6-58 also shows the big difference between the measured tilting angle and calcuated tilting anlge for T2. The difference between the real value and calculated value for T2 may caused by that slip surface in the middle part corresponding to T2 was not well construted, and the radius of the slip surface of this part was not exact 600 mm. Results for T1 and T3 are consistent with the test results mentioned before.

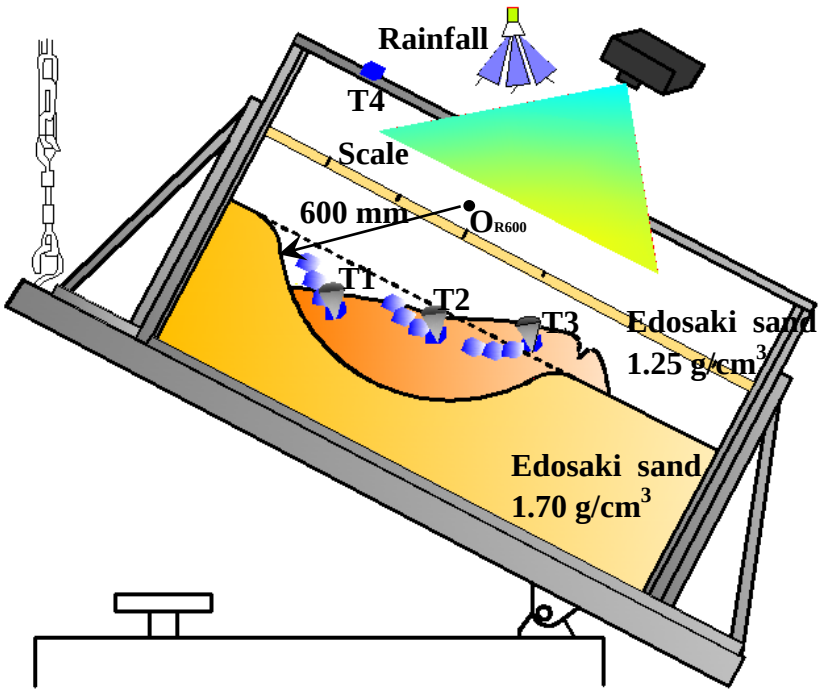

Fig. 6-54 Illustration of Test 10 using tilt sensors without rods

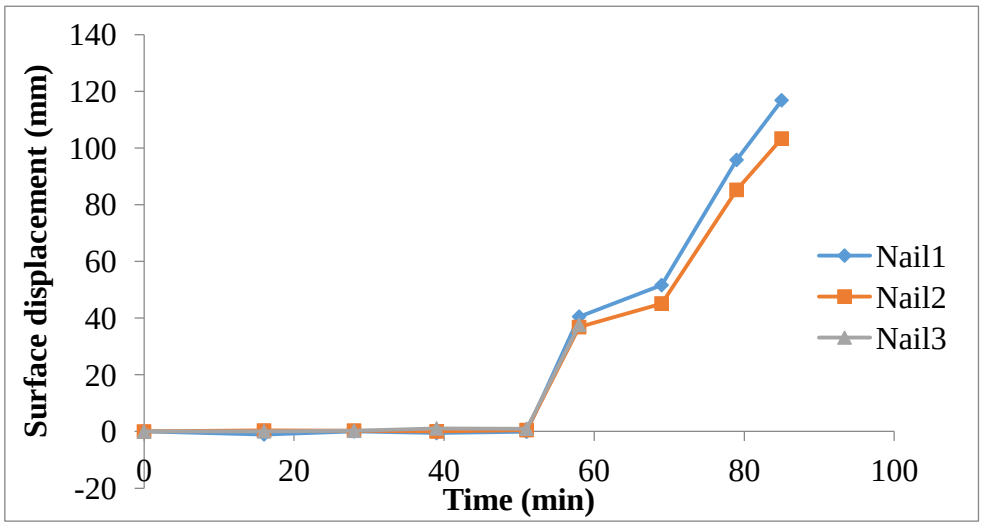

Fig. 6-55 Time history of surface displacement of Test 10 using tilt sensors without rods

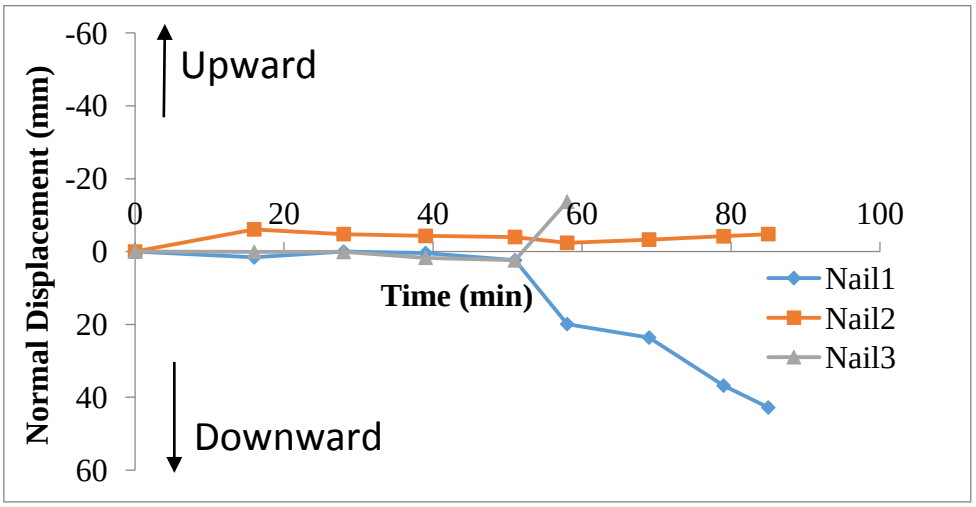

Fig. 6-56 Time history of normal displacement of Test 10 using tilt sensors without rods

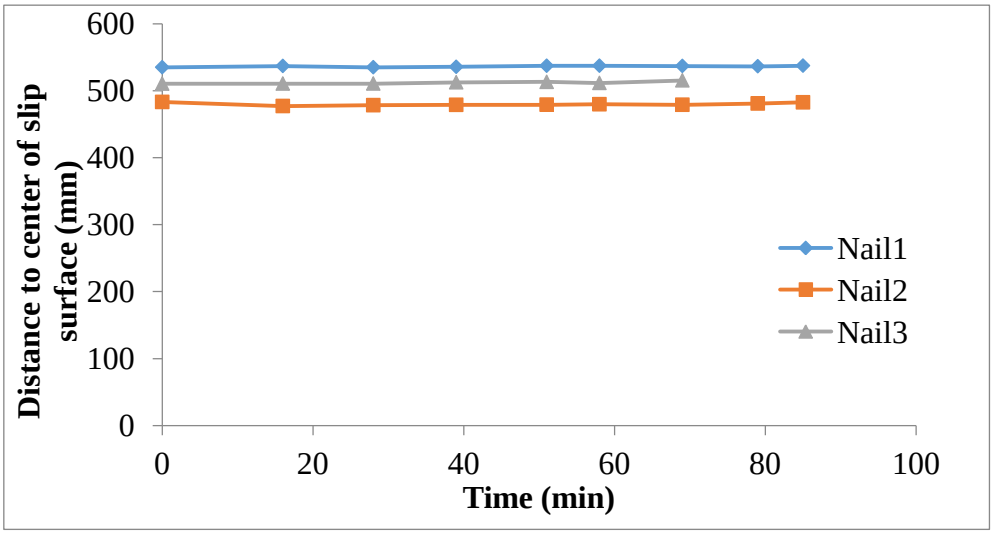

Fig.6-57 Variation of distance between the tilt sensors and the center of slip surface

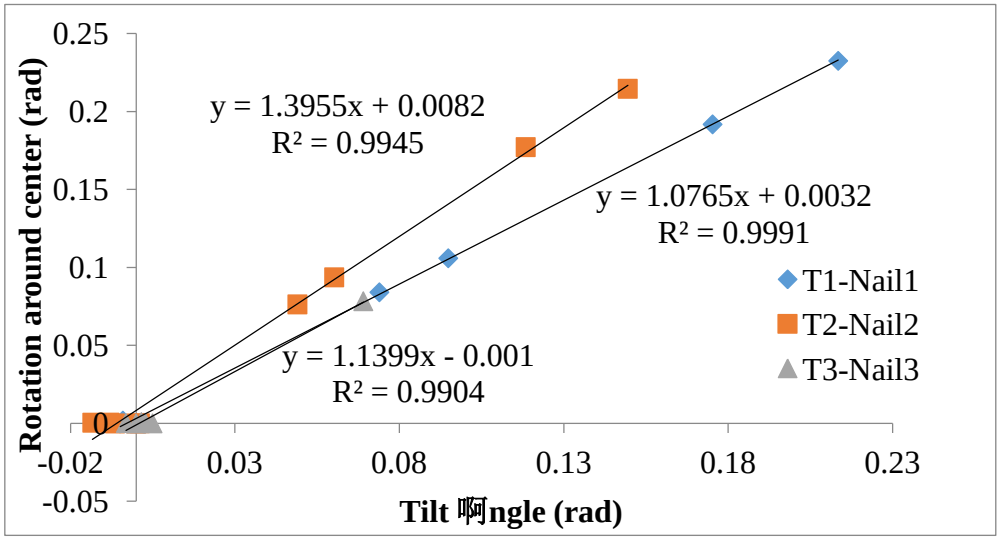

Fig. 6-58 The relationship between the calculated tilting angle and tilting angle measured by tilt sensors in Test 10

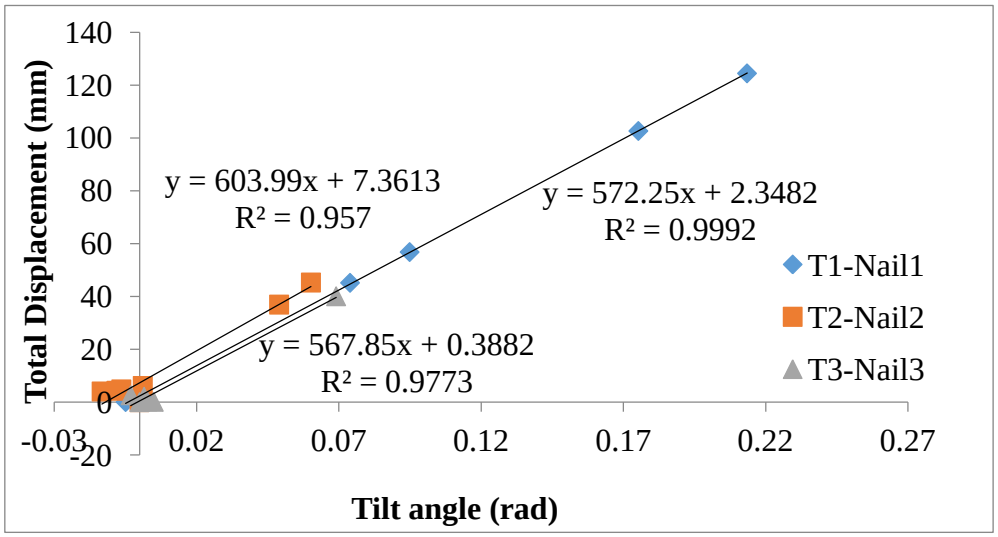

Fig. 6-59 The relationship between tilting angle measured by tilt sensors and total displacement of marked points on the slope surface in Test 10

6.2.2 Small-scaled model tests using tilt sensors with short rods

In this section, model tests using tilt sensors with short rods installed above the pre-defined slip surface were conducted to investigate the relationship between displacement and tilting angle of tilt sensors installed in slopes and the details about these tests are listed in table 6-2.

Table 6-2 Small-scaled tests using tilt sensors with short rods above the slip surface

Test No.	Materials	Radius of the slip surface(mm)	Length of rods (mm)	Relative desity,Dr(%)	Triggering factor
1	Edosaki sand	R600	70	40	Lifting
2	Silica sand#7	R300+R800	70	50	Lifting
3	Silica sand#7	R300+R800	55	50	Lifting
4	Silica sand#7	R300+R800	70	50	Rainfall

1) Test 1 using tilt sensors with short rods

In this test, the radius of pre-defined slip surface is 600mm, and the slope failure was induced by lifting the container step by step. Two tilt sensors, T1 and T2 attached to a rod with the length 70 mm were installed in the surface layer, and an extra tilt sensor T3 was fixed on side of the wooden container to measure the tilting angle of this container. Details about the testing conditions is illustrated in Fig. 6-60. The change

of surface displacement and normal displacement of tilt sensors are shown in Fig. 6-61 and Fig. 6-62, while the calculated distance of each tilt sensor to the center of corresponding slip surface against time is presented in Fig. 6-63. Additionally, the relationship between the calculated tilting angle and measured tilting angle is indicated in Fig. 6-64, and Fig. 6-65 shows the relationship between the total displacement and tilting angle of each sensors. Compared with the test results of Test 4 using tilt sensors without rods, consistent results are obtained in this tests. The actual distance between tilt sensors and the center of slip surface is 554 mm and 536 mm corresponding to the fitting rate 578 and 508 shown in Fig. 6-65.

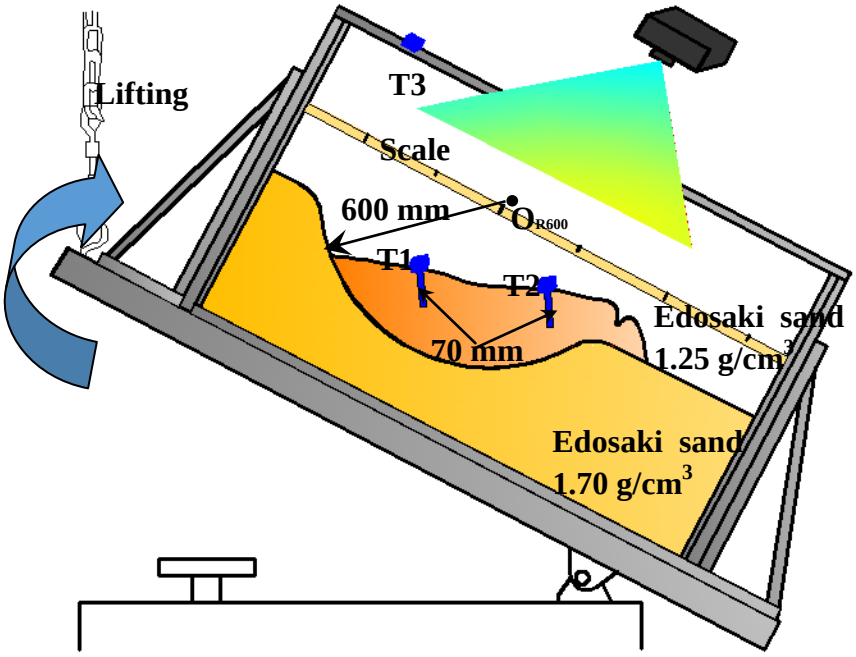

Fig. 6-60 Illustration of Test 1 using tilt sensors with short rods above the slip surface

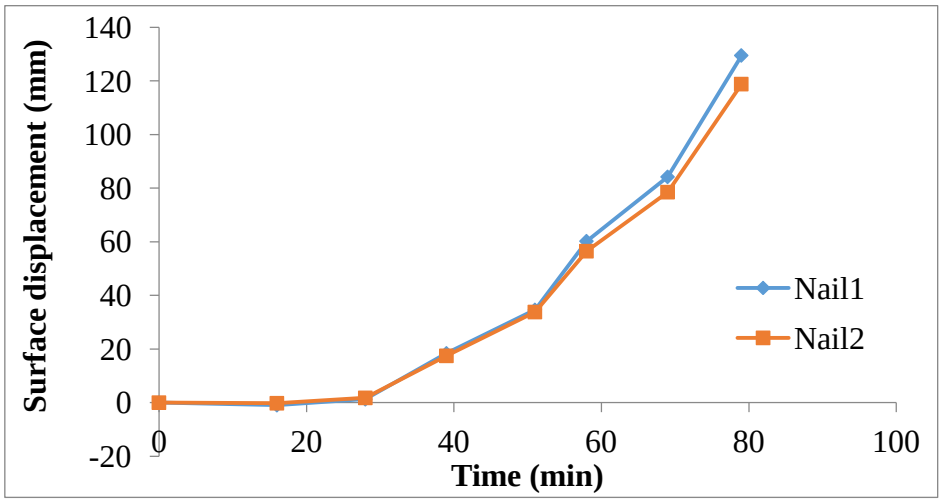

Fig. 6-61 Time history of surface displacement of Test 1 using tilt sensors with short rods above the slip surface

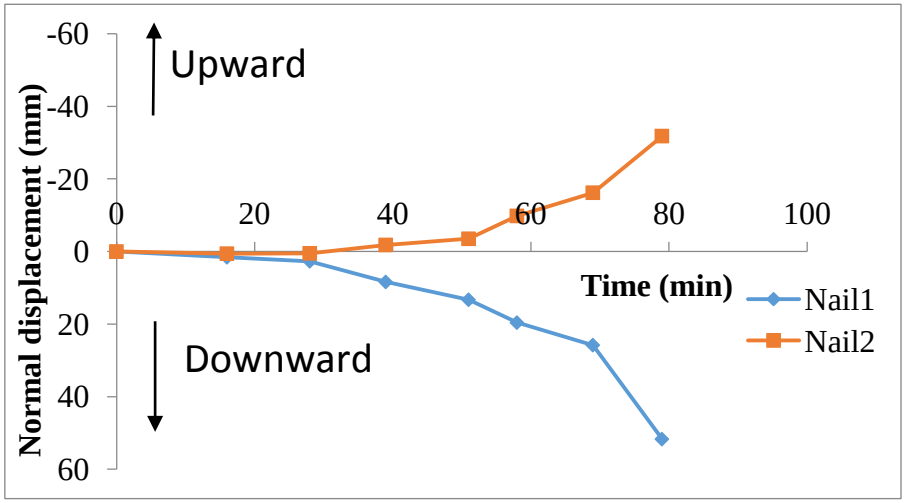

Fig. 6-62 Time history of normal displacement of Test 1 using tilt sensors with short rods above the slip surface

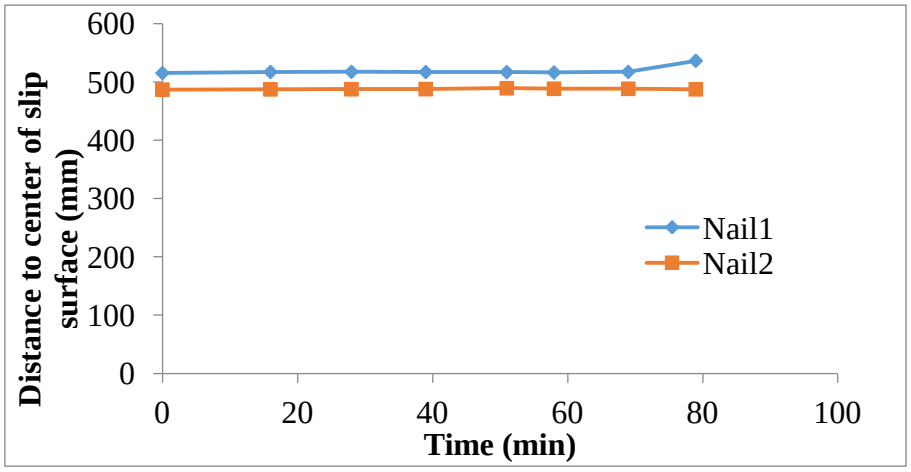

Fig. 6-63 Variation of distance between the tilt sensors and the center of slip surface

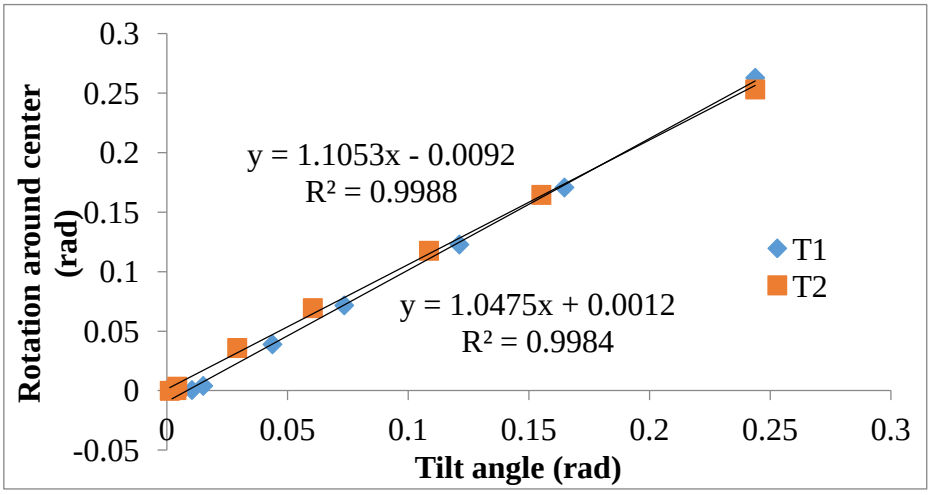

Fig. 6-64 The relationship between the calculated tilting angle and tilting angle measured by tilt sensors in Test 1

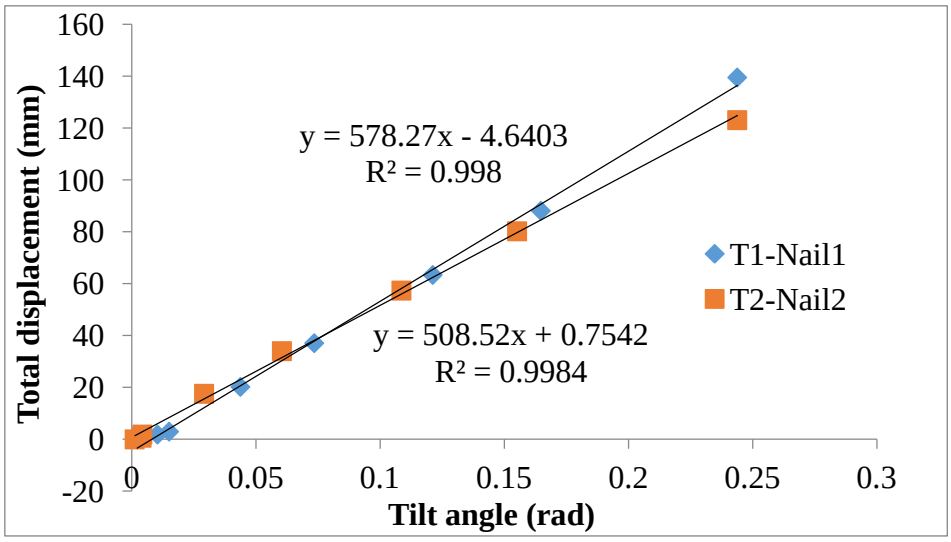

Fig. 6-65 The relationship between tilting angle measured by tilt sensors and total displacement of marked points on the slope surface in Test 1

2) Test 2 using tilt sensors with short rods

The testing conditions of this test is presented in Fig. 6-66. Compared with Test 7 using tilt sensors without rods, consistent results are obtained shown in Fig. 6-67 to Fig. 6-71. The actual distance of tilt sensors to the centers of slip surfaces are 260 mm and 726 mm corresponding to the value of fitting rate 230 and 687.

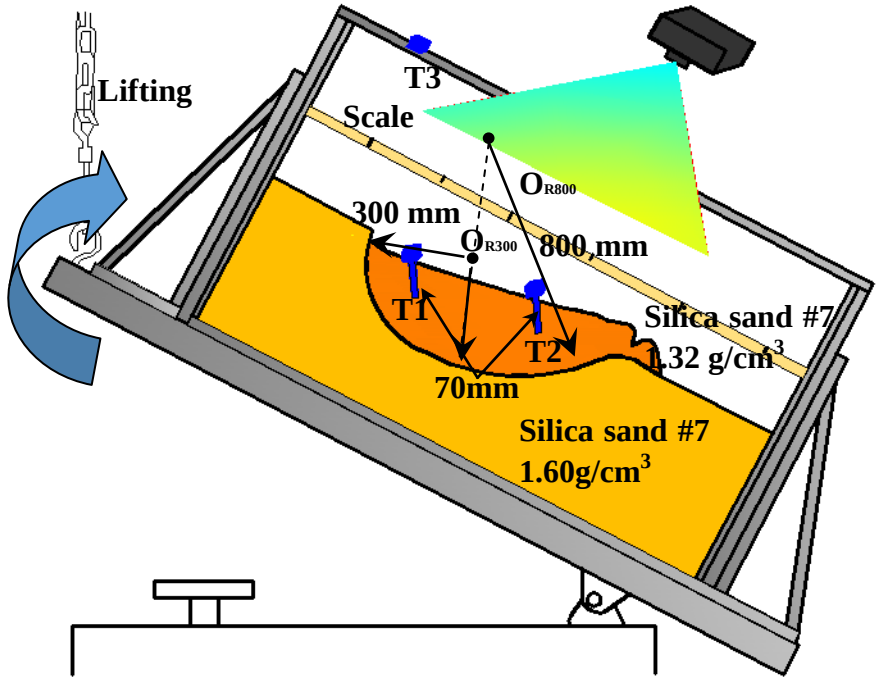

Fig. 6-66 Illustration of Test 2 using tilt sensors with short rods above the slip surface

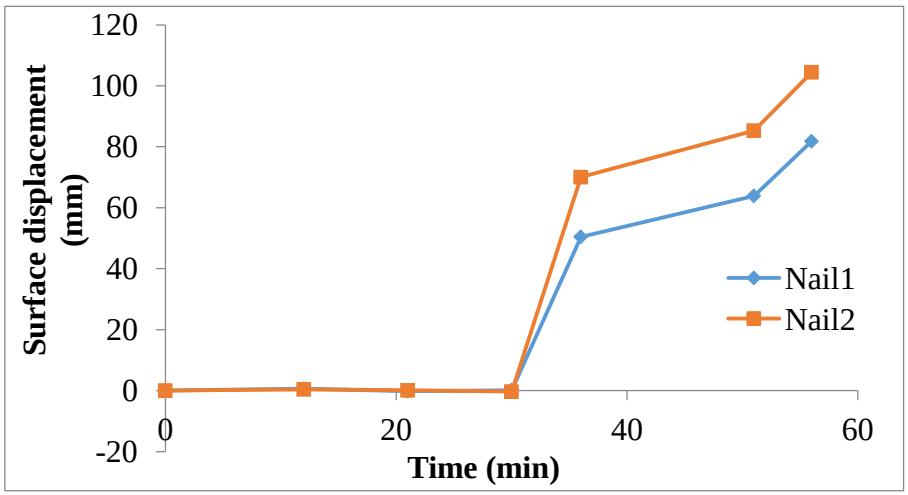

Fig. 6-67 Time history of surface displacement of Test 2 using tilt sensors with short rods above the slip surface

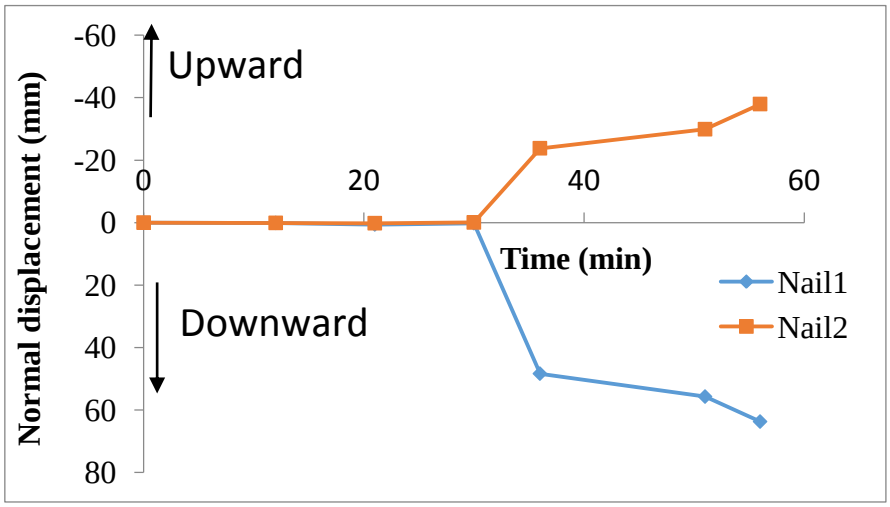

Fig. 6-68 Time history of normal displacement of Test 2 using tilt sensors with short rods above the slip surface

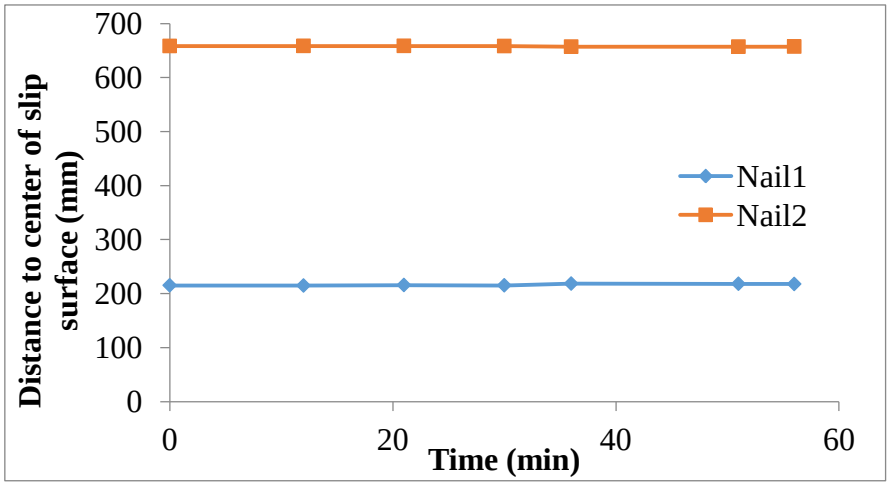

Fig. 6-69 Variation of distance between the tilt sensors and the center of slip surface

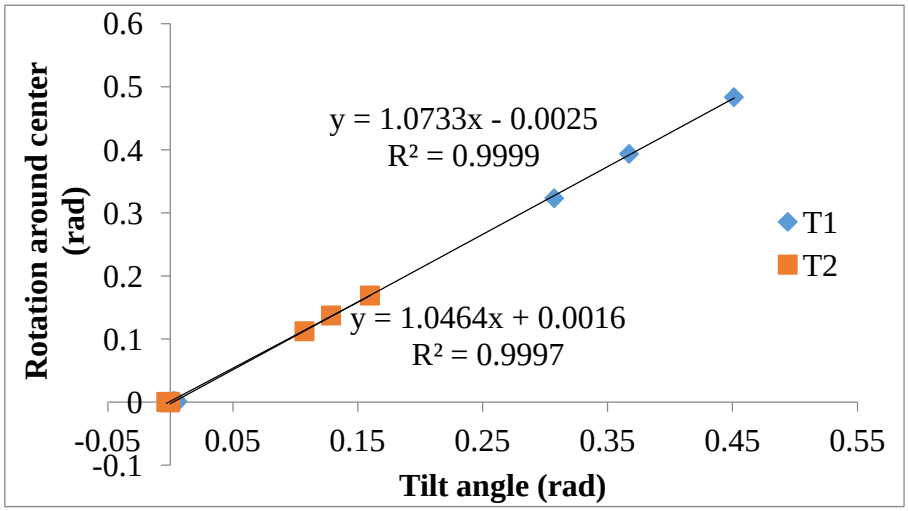

Fig. 6-70 The relationship between the calculated tilting angle and tilting angle measured by tilt sensors in Test 2

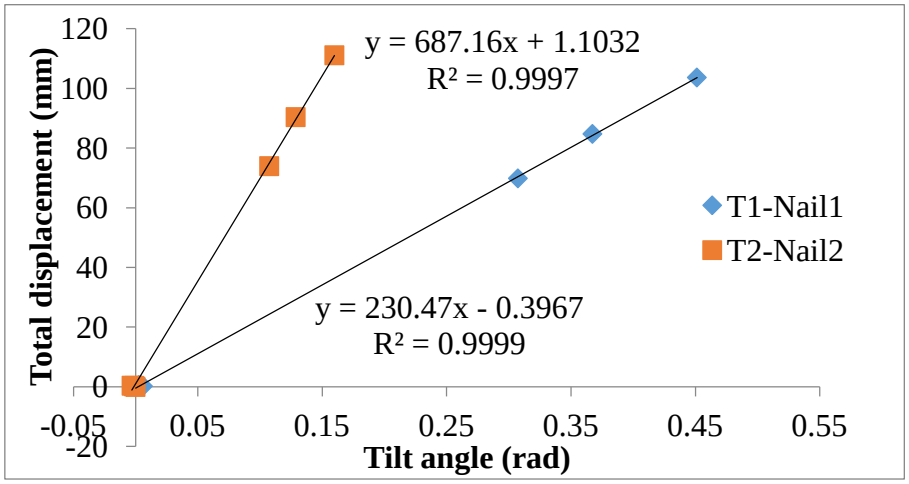

Fig. 6-71 The relationship between tilting angle measured by tilt sensors and total displacement of marked points on the slope surface in Test 2

3) Test 3 using tilt sensors with short rods

Compared with Test 2 using tilt sensors with short rods, in this test the length of rods is 55 mm as shown in Fig. 6-72. Test results are shown in Fig.6-73 to Fig.6-77. Similar results are obtained, and the value of distance of T1 and T2 to the corresponding slip surface centers are 247 mm and 714 mm corresponding to the fitting rate 225 and 670.

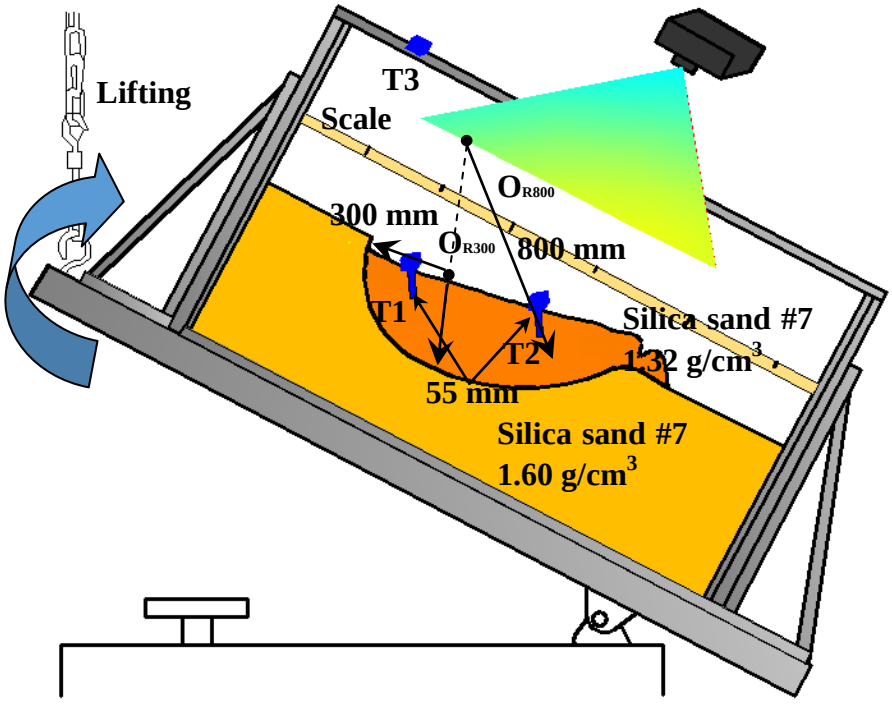

Fig. 6-72 Illustration of Test 3 using tilt sensors with short rods above the slip surface

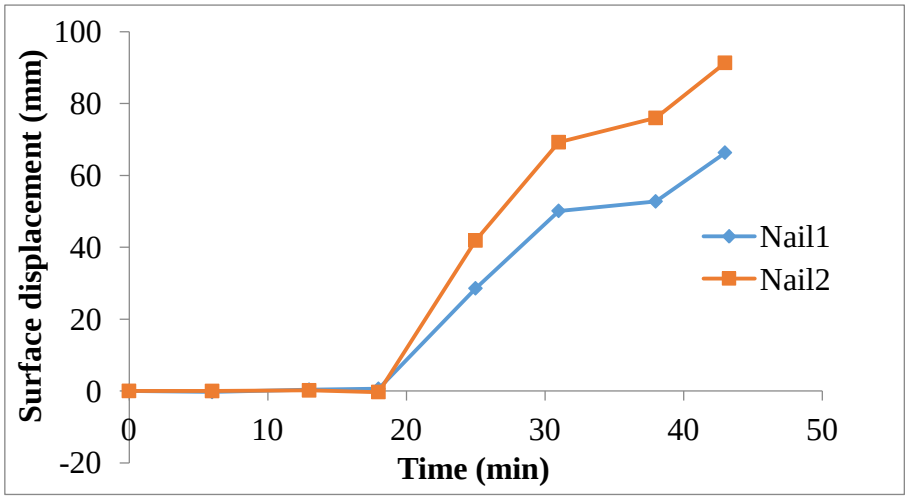

Fig. 6-73 Time history of surface displacement of Test 3 using tilt sensors with short rods above the slip surface

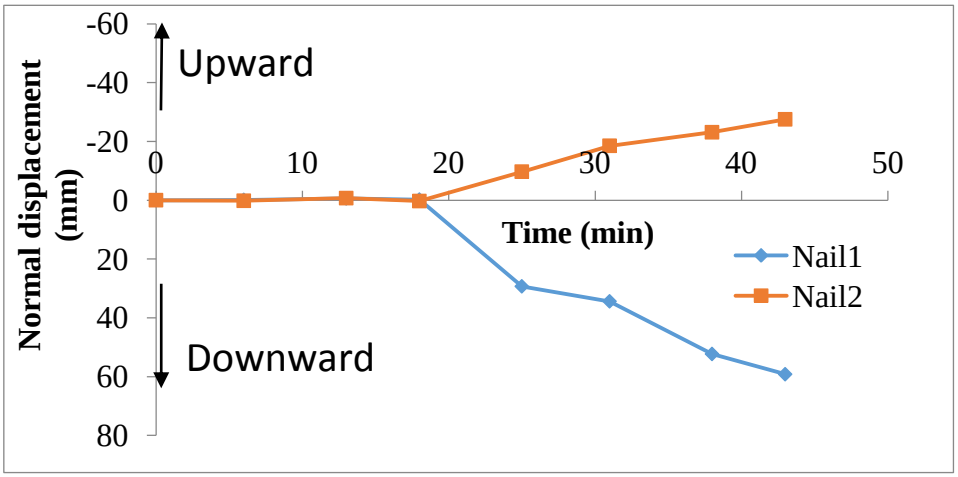

Fig. 6-74 Time history of normal displacement of Test 3 using tilt sensors with short rods above the slip surface

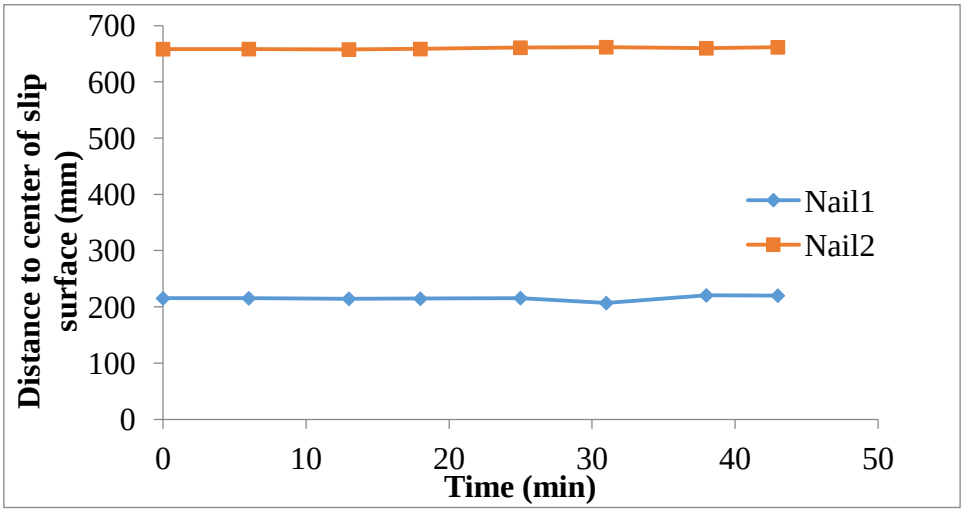

Fig. 6-75 Variation of distance between the tilt sensors and the center of slip surface

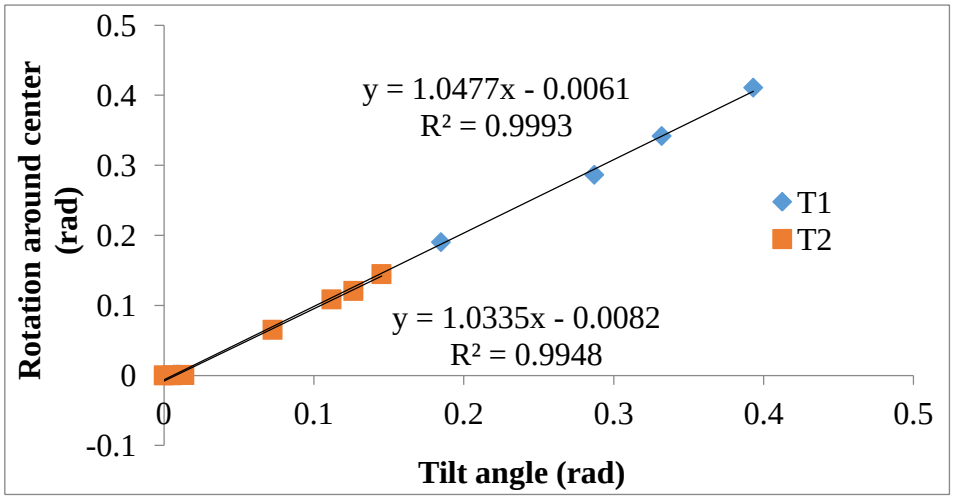

Fig. 6-76 The relationship between the calculated tilting angle and tilting angle measured by tilt sensors in Test 3

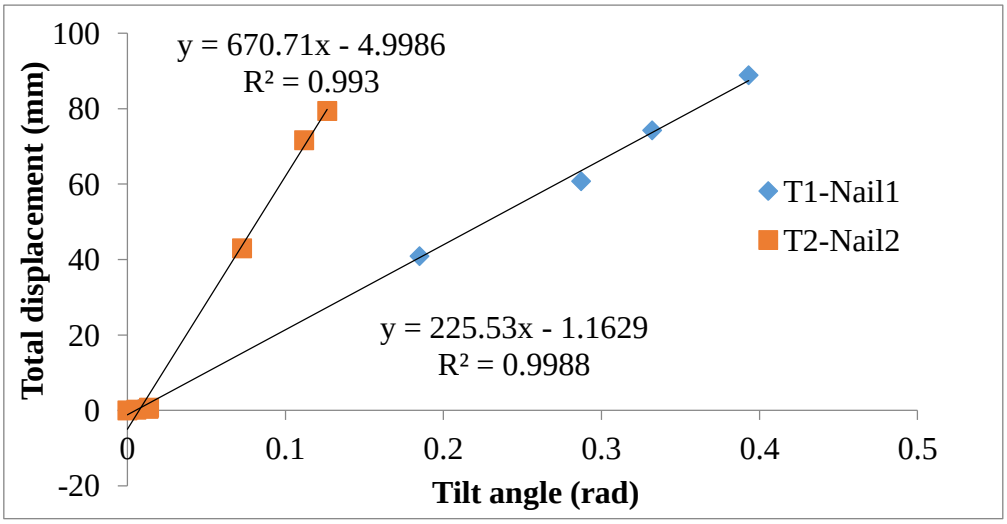

Fig. 6-77 The relationship between tilting angle measured by tilt sensors and total displacement of marked points on the slope surface in Test 3

4) Test 4 using tilt sensors with short rods

In model test 4 using tilt sensors attached to short rods, the slope slippage is triggered by periodical rainfall supply. The arrangment of sensors as well as the testing conditions are presented in Fig. 6-78. In this test, even though the triggering factor is different from that in Test 2 in this section, similar results are obtained and presented in Fig. 6-79 to Fig. 6-83. The distance to the center of slip surface of T1 and T2 is 258 mm and 732 mm close to the fitting rate 249 and 708 respectively.

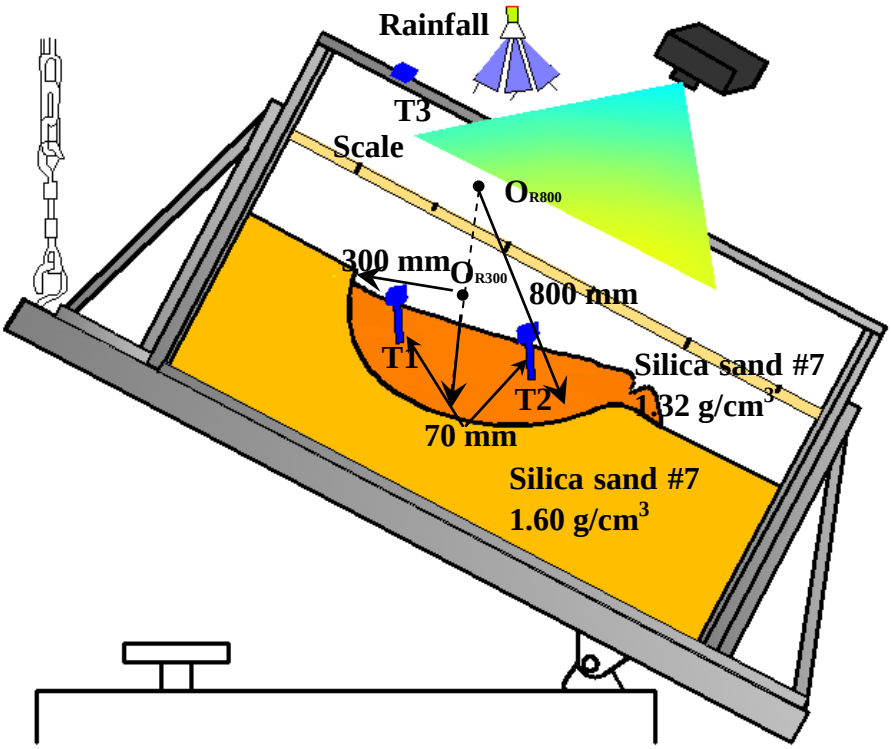

Fig. 6-78 Illustration of Test 4 using tilt sensors with short rods above the slip surface

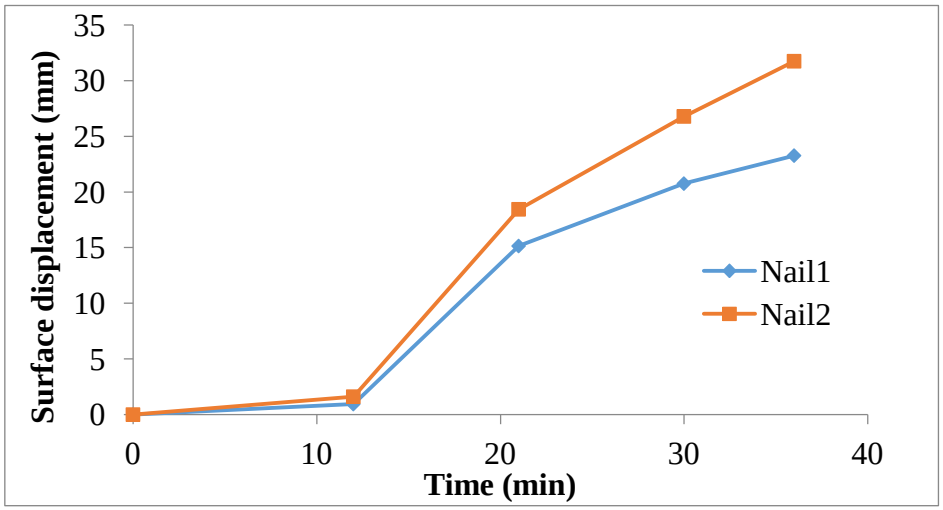

Fig. 6-79 Time history of surface displacement of Test 4 using tilt sensors with short rods above the slip surface

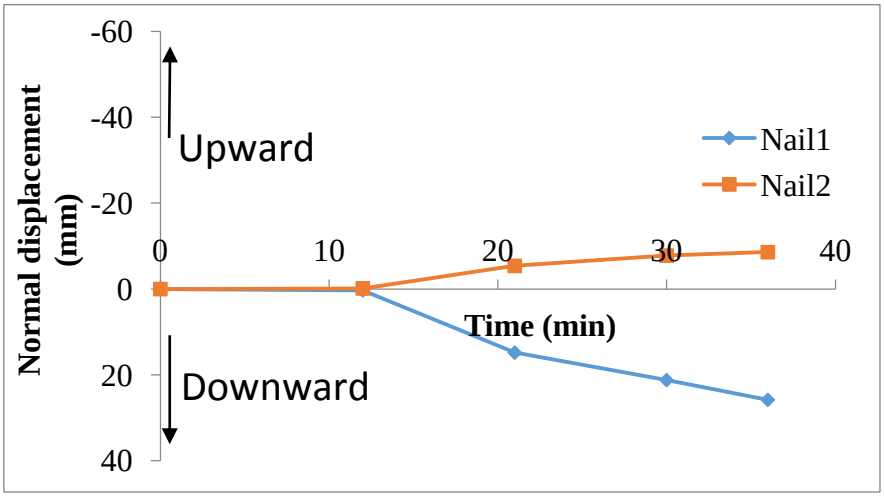

Fig.6-80 Time history of normal displacement of Test 4 using tilt sensors with short rods above the slip surface

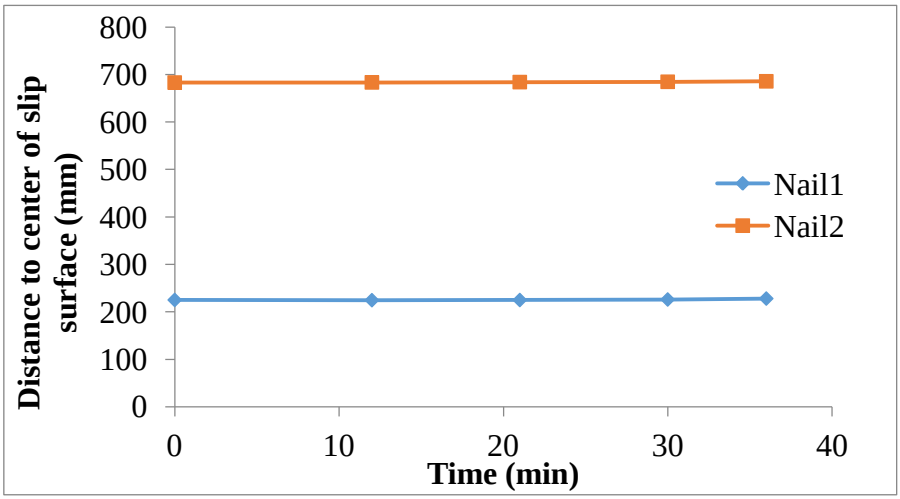

Fig. 6-81 Variation of distance between the tilt sensors and the center of slip surface

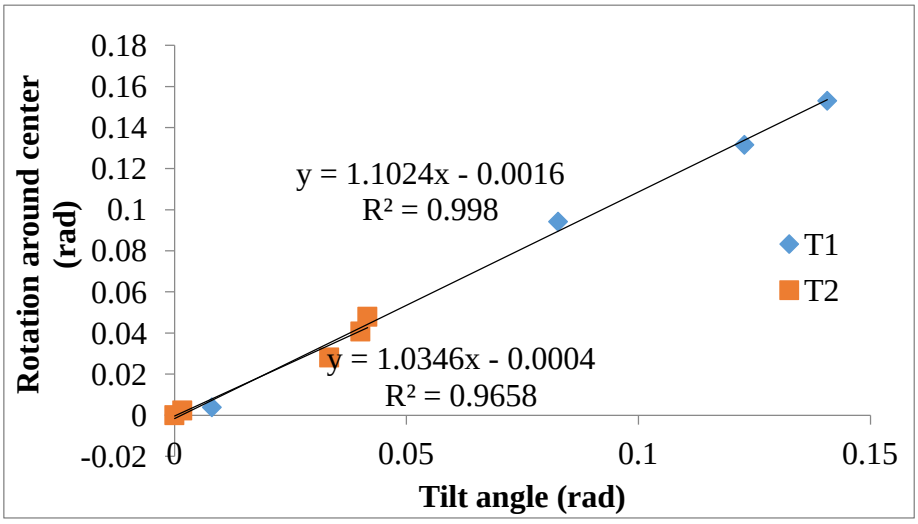

Fig. 6-82 The relationship between the calculated tilting angle and tilting angle measured by tilt sensors in Test 4

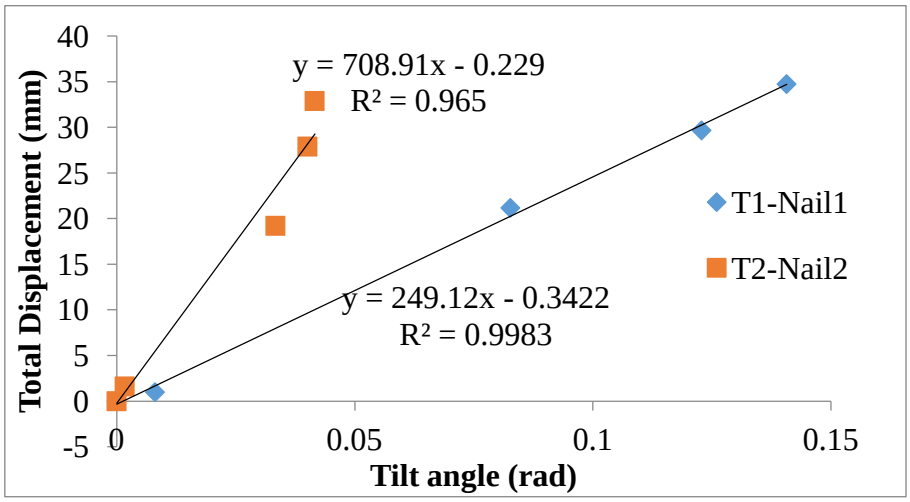

Fig. 6-83 The relationship between tilting angle measured by tilt sensors and total displacement of marked points on the slope surface in Test 4

6.2.3 Small-scaled model tests using tilt sensors with long rods reaching the slip surface of slopes

1) Test 1 using tilt sensors with long rods

In this test, the slope sliding triggered by tilting the container. Two tilt sensors with long rods, were installed in the slope with the tips pressed into the base layer, and an extra tilt sensor attached to the wooden box was employed to measure the inclination angle of the wooden box. The schematic illustration of the testing conditions is shown in Fig. 6-84. The change of displacement and tilting angle are presented in Fig. 6-85 and Fig. 6-86. Fig. 6-87 shows the linear relationship between tilting angles and surface displacements, and the rate of fitting lines is close to the distance between tilt sensors to the tip of rods, around 205 mm.

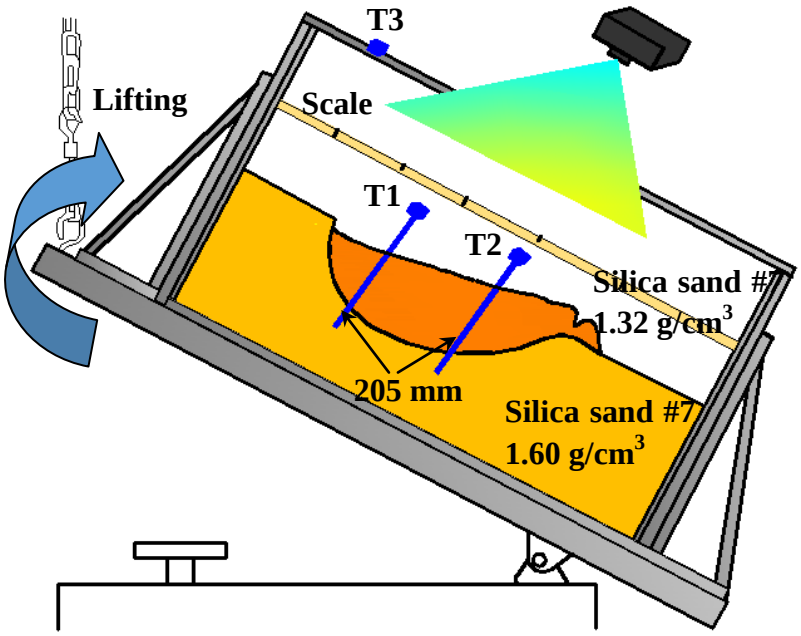

Fig. 6-84 Illustration of Test 1 using tilt sensors with long rods reaching the slip surface

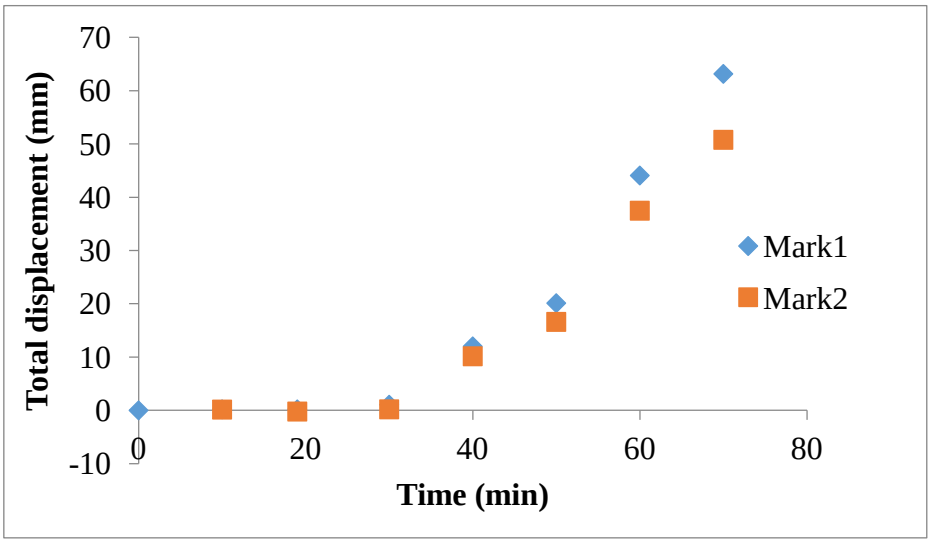

Fig. 6-85 Time history of total displacement of Test 1 using tilt sensors with long rods reaching the slip surface

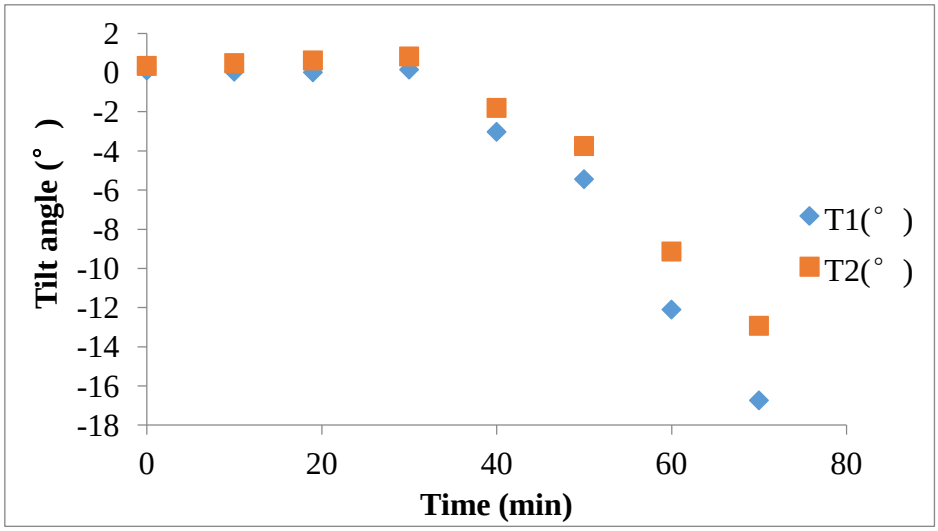

Fig. 6-86 Time history of tilting angle of Test 1 using tilt sensors with long rods reaching the slip surface

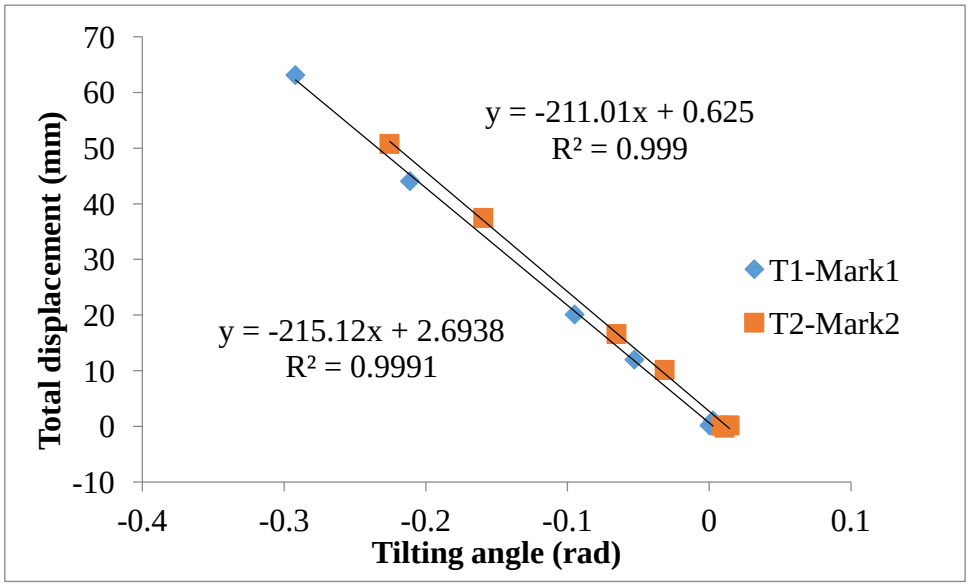

Fig. 6-87 The relationship between tilting angle measured by tilt sensors and total displacement of marked points

2) Test 2 using tilt sensors with long rods

The slope sliding in this test was triggered by artificial rainfall (Fig. 6-88), which is different from the case in Test 1 in this section. The test results of this test are presented in Fig. 6-89, Fig. 6-90 and Fig. 6-91. Although the triggering factor of slope sliding in this test is different from that in Test 1 using tilt sensors with long rods, similar results are also approached. The coefficients of fitting line for T1 in the upper part and T2 in the lower part, are 231.39 and 219.26, corresponding to the actual

distance, 205 mm respectively. During the test, a small crack occurred near the location of T1, which caused the slight variation between the ratio of T1 and that of T2.

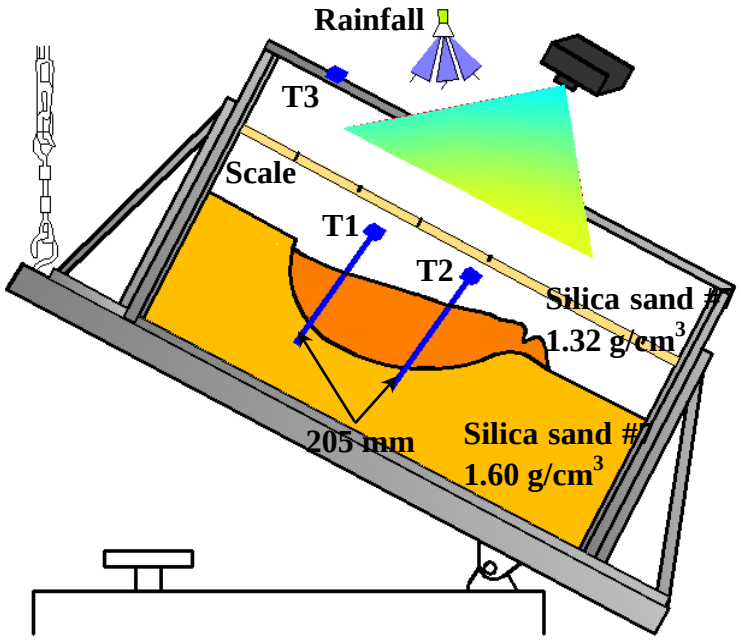

Fig. 6-88 Illustration of Test 2 using tilt sensors with long rods reaching the slip surface

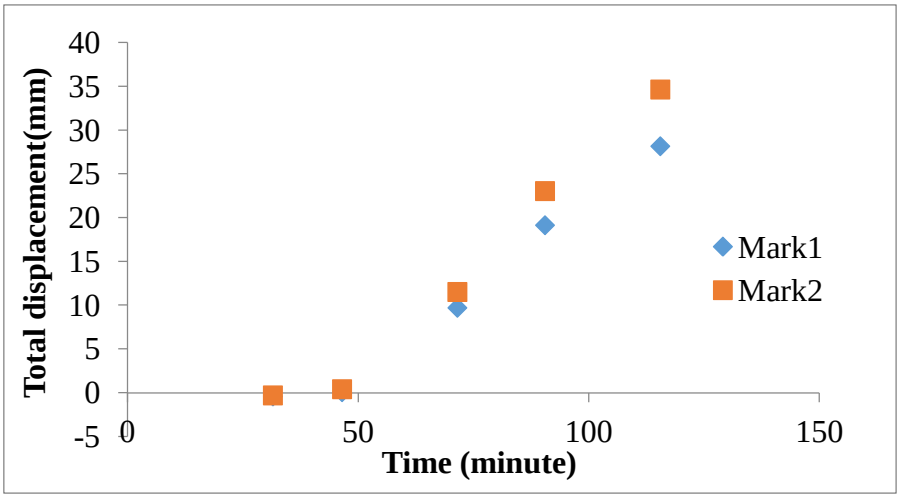

Fig. 6-89 Time history of total displacement of Test 2 using tilt sensors with long rods reaching the slip surface

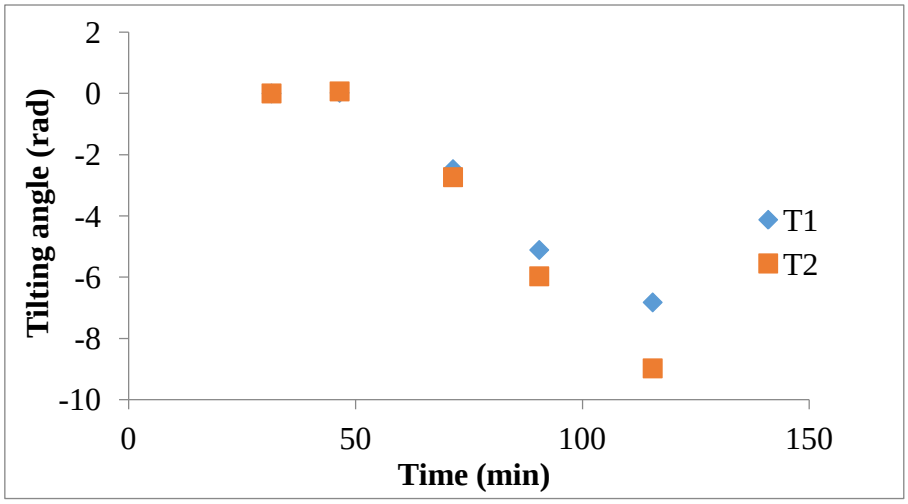

Fig. 6-90 Time history of tilting angle of Test 2 using tilt sensors with long rods reaching the slip surface

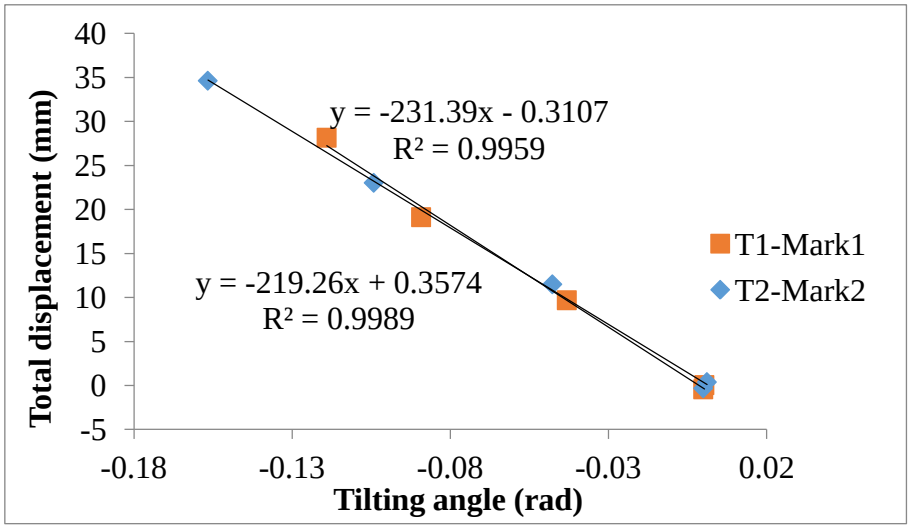

Fig. 6-91 The relationship between tilting angle measured by tilt sensors and total displacement of marked points

6.3. Test results of field tests

Field tests were also conducted to investigate the relationship between the diplacement and tilting angle in natural slopes. In field tests, tilt sensors with different length of rods were installed in testing areas to measure the tilting of slopes, and extensometers were employed to monitor the displacement of these natural slopes. The slope failure of these tests was induced by artificial rainfall.

1) Field test 1

The site is located in Guangxi Province, China, and the slope angle is 43 degrees.

Details about the testing conditions were introduced in Chapter 5. Fig. 6-92 shows the images before the test and after the slope failure, and Fig. 6-92 shows the cross section of the slope after failure.

Fig. 6-92 Images of the testing area before and after the slope failure

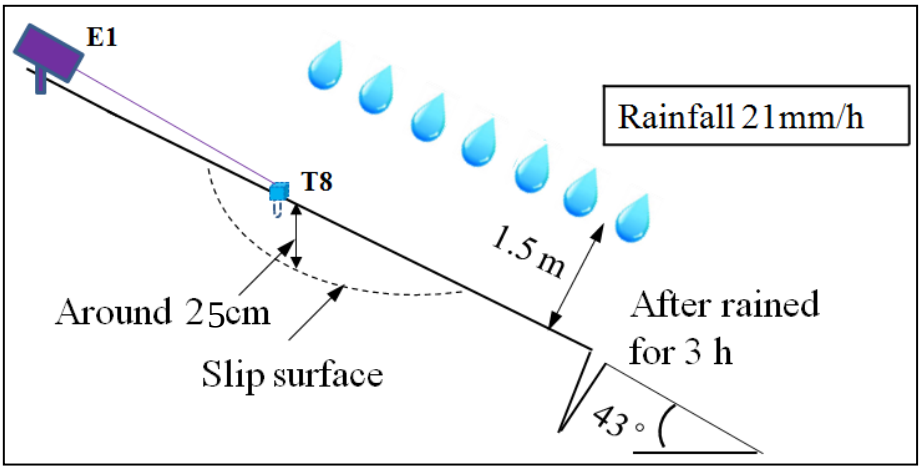

Fig. 6-93 The cross section of the slope after failure

In this test, slope failure occurred in the upper part where tilt sensor T8 installed with one end attached to the extensometer E1. The time history of displacement as well as tilting angle of slope monitored by E1 and T8 are presented in Fig. 6-94 and Fig. 6-95 respectively. Fig. 6-96 shows the relationship between displacement and tilting angle. A linear relationship is indicated and the deviation between the fit line and monitored data in the final part in Fig. 6-96 was caused by the inclination of the tilt sensor T8 in the direction which is normal to the direction of slope sliding.

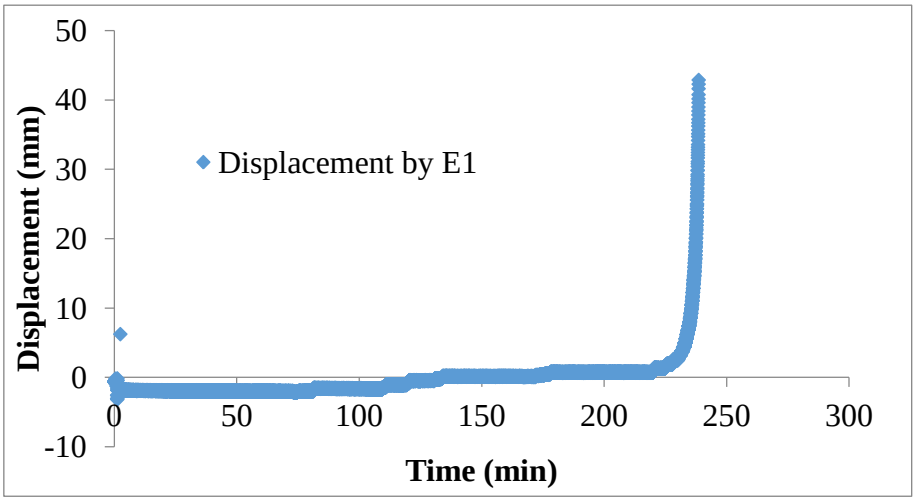

Fig. 6-94 Time history of displacement of slope recorded by E1 in Field test 1

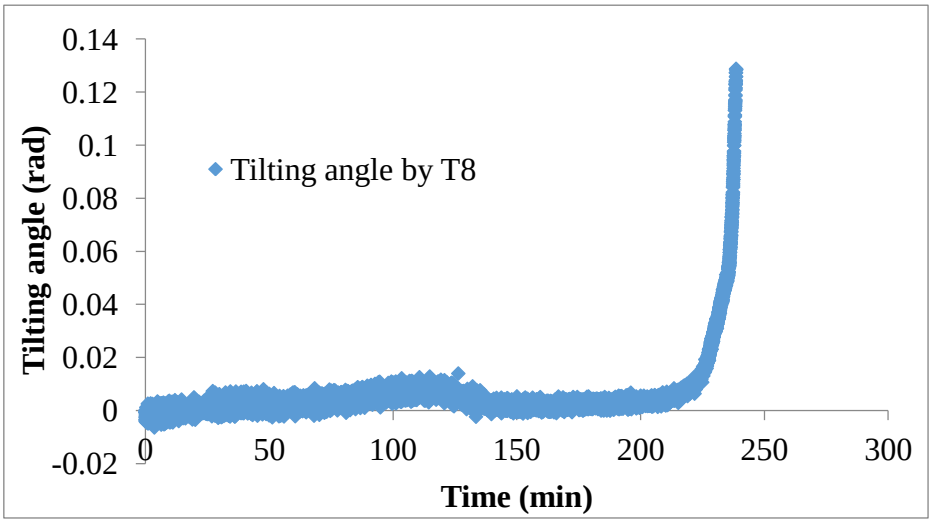

Fig. 6-95 Time history of slope tilting recorded by T8 in Field test 1

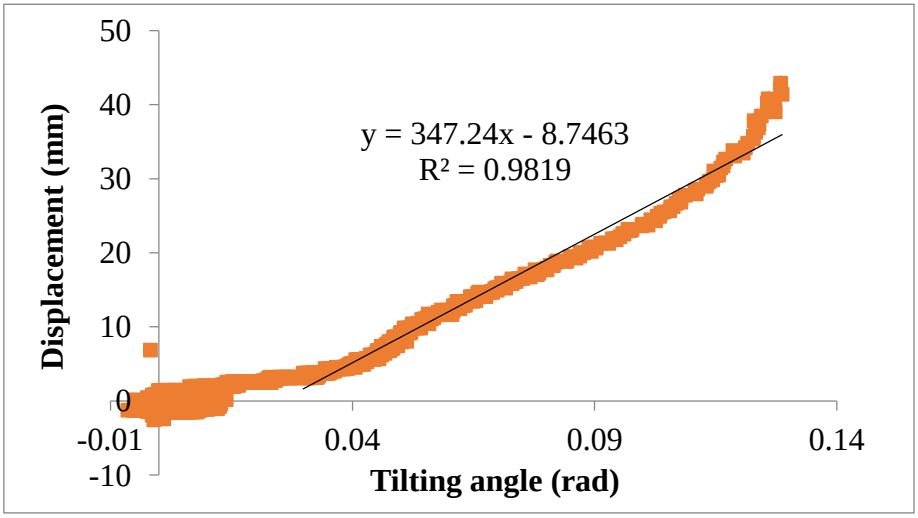

Fig. 6-96 The relationship between tilting angle displacement in Field test 1

2) Field test 2

Testing conditions of this test is introduced in Chapter 5. In this field test, the failure of tilt sensors with different length of rods, 50 mm and 300 mm, installed in the lower part of the slope were caused by erossion (Fig. 5-48). Major deformation occured in the top part of the slope as shown in Fig.6-97,where T2 and T4 were installed connecting with extensometer E1 and E4 respectively, and Fig. 6-98 shows the cross section of the slope after failed.

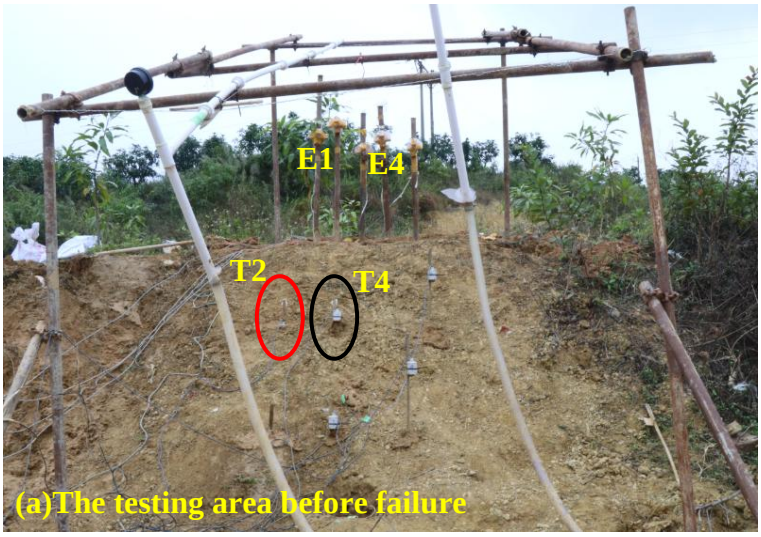

Fig. 6-97 Images of the testing area before and after the slope failure

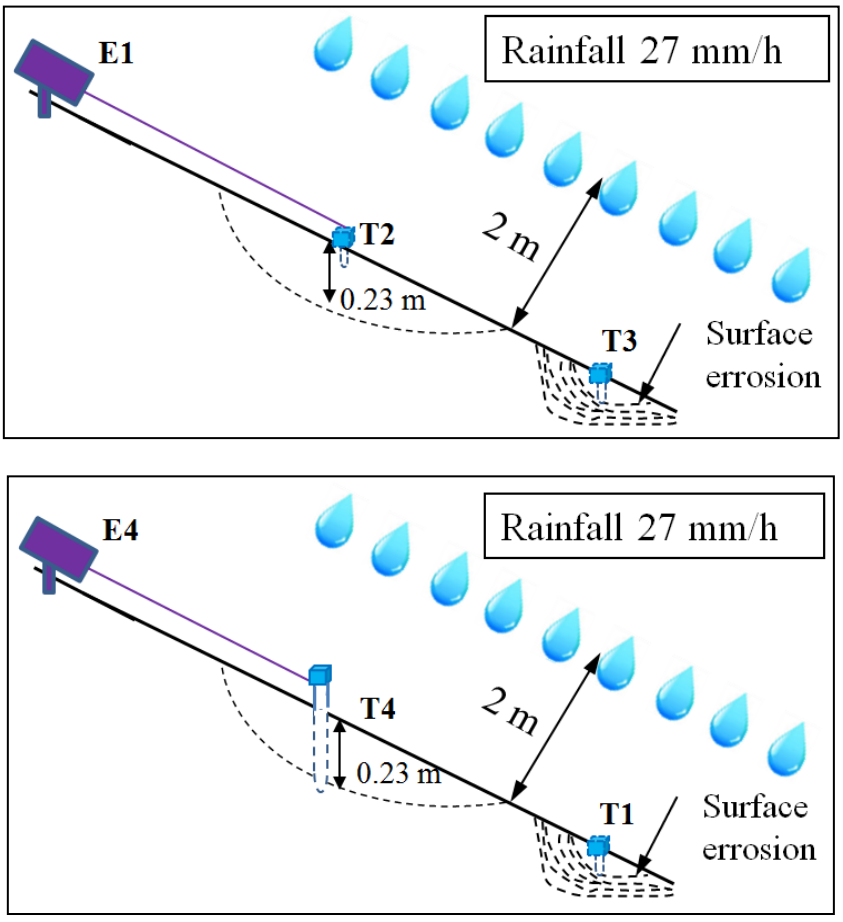

Fig. 6-98 The cross section of the slope after failure

The results monitored by E1 and T2 are presented in Fig. 6-99 and Fig. 6-100 respectively. Fig. 6-101 indicates a linear relationship between displacement and tilting anglee which is consistent with the test results metioned before .

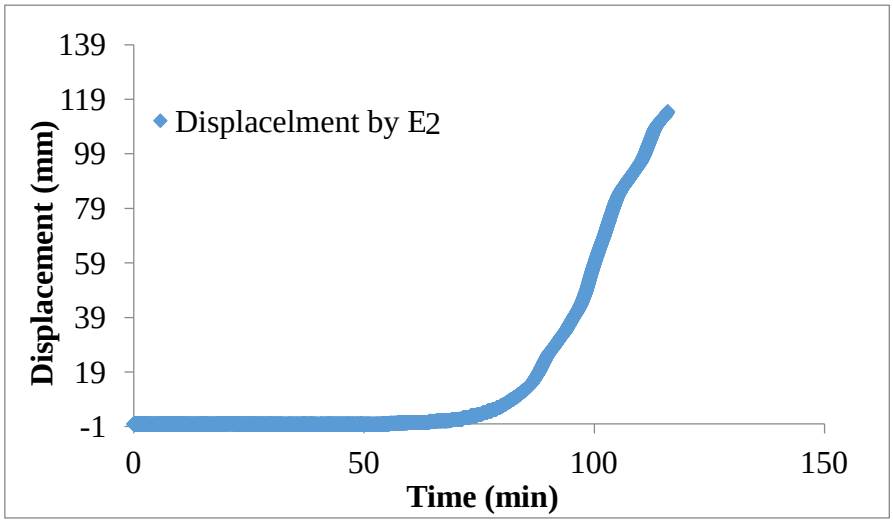

Fig. 6-99 Time history of displacement of slope recorded by E1 in Field test 2

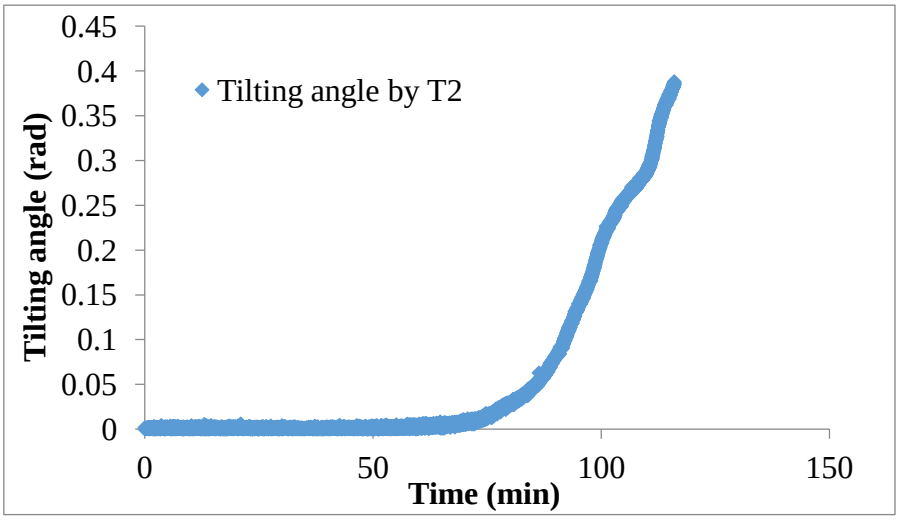

Fig. 6-100 Time history of slope tilting recorded by T2 in Field test 2

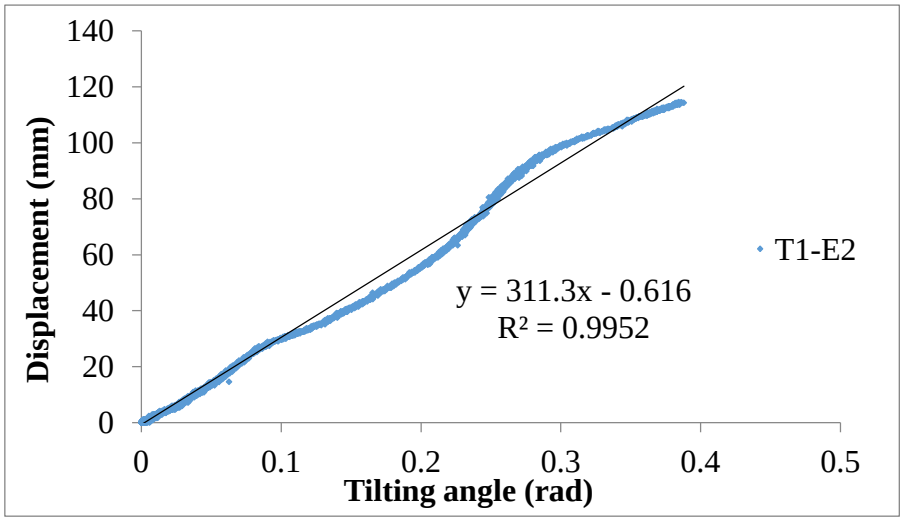

Fig. 6-101 The relationship between tilting angle displacement of T2-E1 in Field test 2

On the other hand, the results for E4 and T4 with a longer rods, around 300 mm, are presented in Fig. 6-102, Fig. 6-103 and Fig. 6-104 respectively. Even though the tilting direction is different, a linear relationship between displacement and tilting angle is also obtained as shown Fig. 6-105, and the rate of fit line is 273 mm close to depth of slip surface around 230 mm and length of the rod.

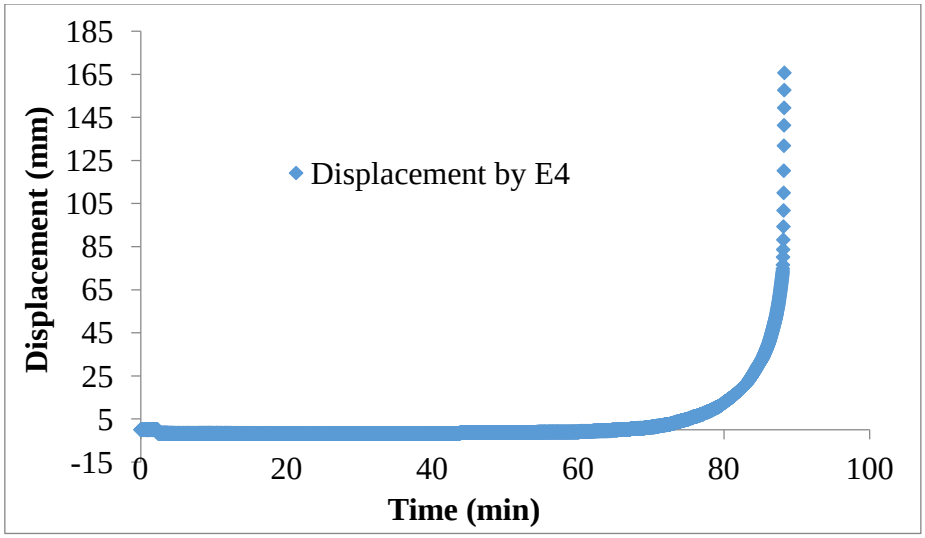

Fig. 6-102 Time history of displacement of slope recorded by E4 in Field test 2

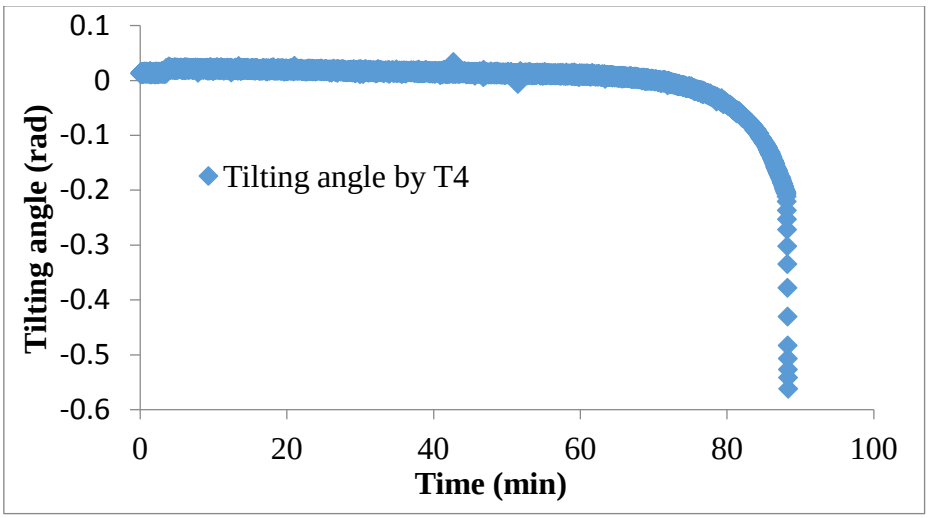

Fig. 6-103 Time history of slope tilting recorded by T4 in Field test 2

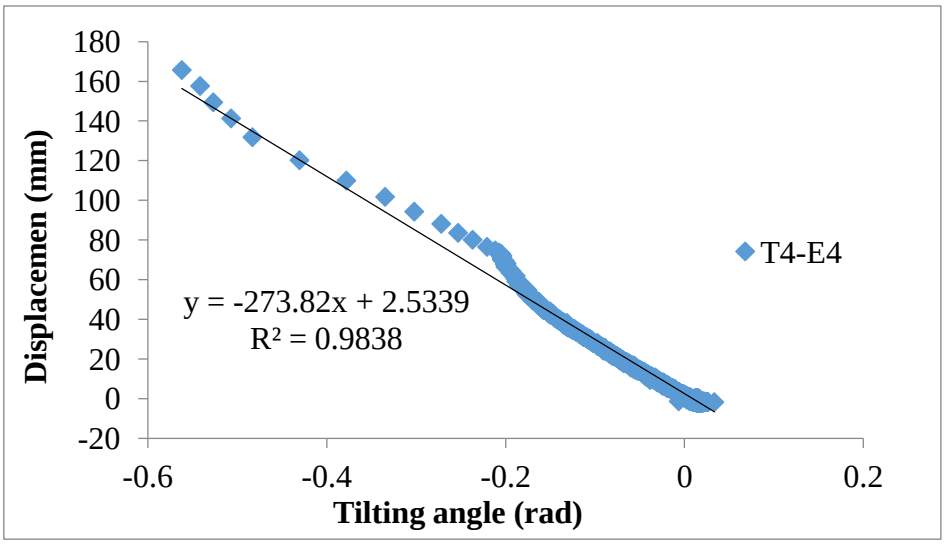

Fig. 6-104 The relationship between tilting angle displacement of T4-E4 in Field test 2

3) Field test 3

This test was carried out on a natural slope, Taziping landslide slope, in Sichuan Province in 2006 (Uchimura et al., 2015). The illustration is presented in Fig. 6-105.

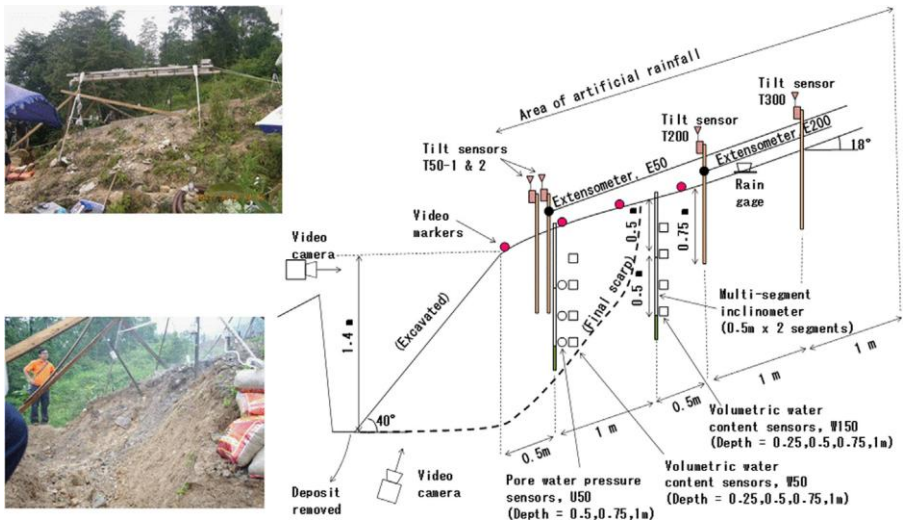

Fig. 6-105 Illustration of Field test 3 (after Uchimura, 2015)

In this test, extensometer E50 was fixed on tilt sensor T50-2 which was attached to rod with the length 950 mm. The slope failed progressively, and multiple slip surfaces occurred during the process of slope failure. Although the final slip surface is deeper then the length of rod attached to tilt sensor T50-2, the initial slip surface is shallower than 950 mm (Yang et al., 2017). The test results are shown in Fig. 6-106, Fig. 6-107

and Fig. 6-108. A linear trend between the displacements and tilting angle is also indicated in this field test (Fig. 6-108), and the fitting rate, 903.22, is close to the length of the rod, 950 mm.

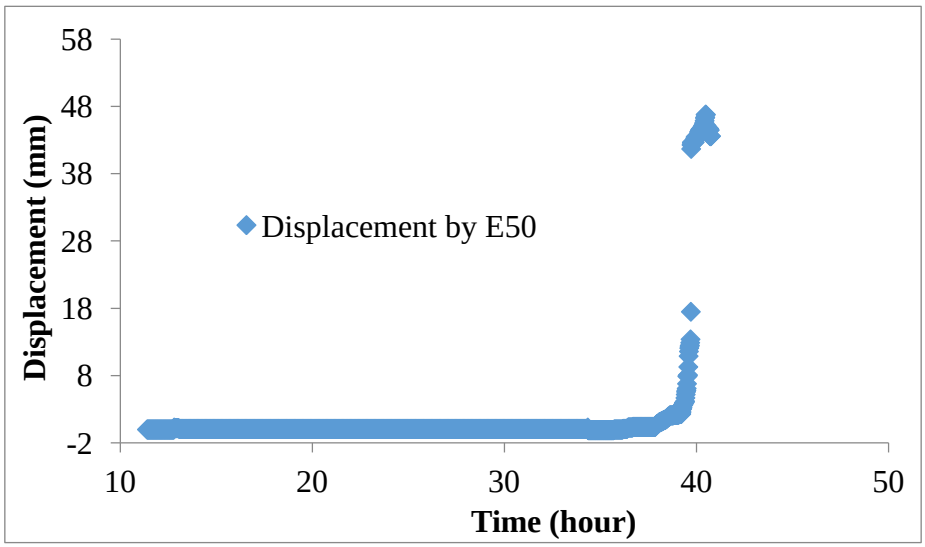

Fig. 6-106 Time history of displacement of slope recorded by E50 in Field test 3

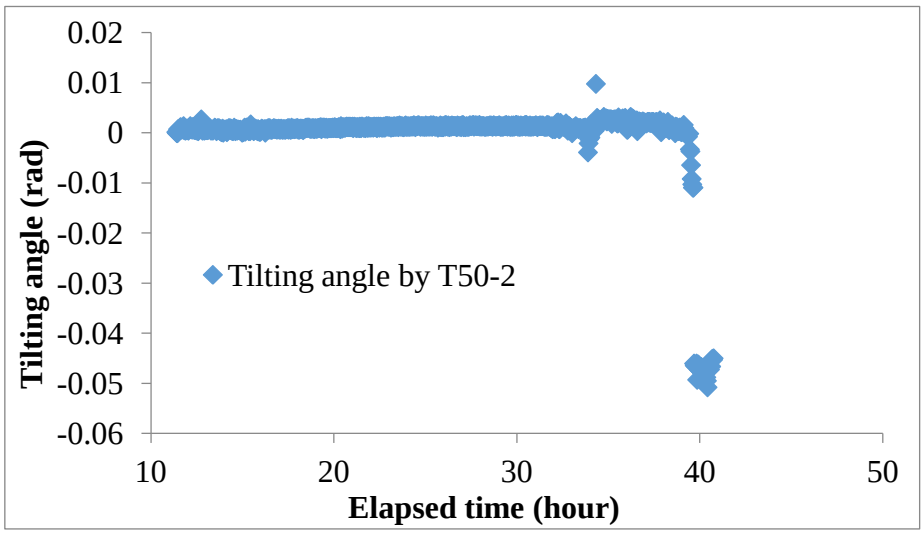

Fig. 6-107 Time history of slope tilting recorded by T50-2 in Field test 3

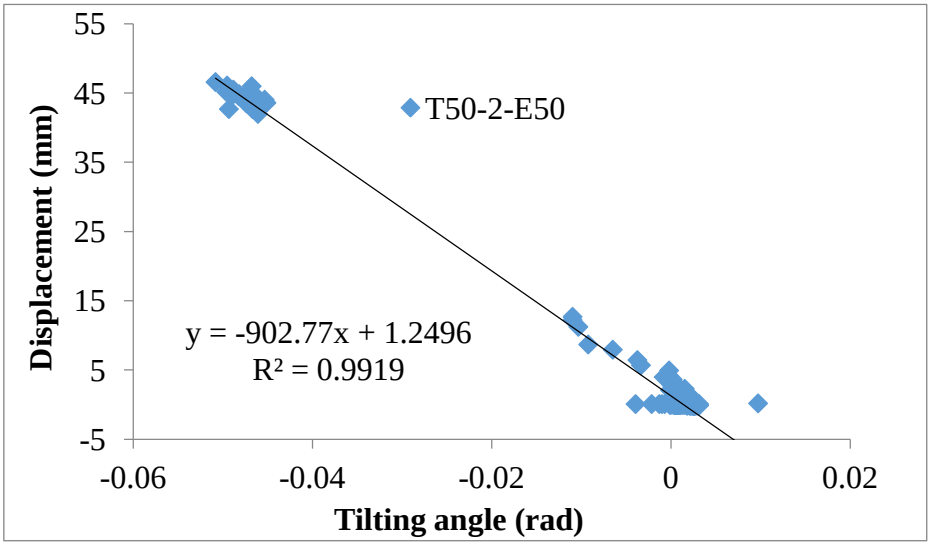

Fig. 6-108 The relationship of T50-2-E50 in Field test 3

6.4. Summary

In this chapter, the relationship between displacement and tilting angle of slopes is investigated by conducting various types of laboratory tests and field tests. Rates of fitting lines for the displacement and tilting angle from model tests as well as field tests are plotted against the actual distance between the location of tilt sensors and corresponding rotational centers, and all of the results are shown in Fig. 6-109.

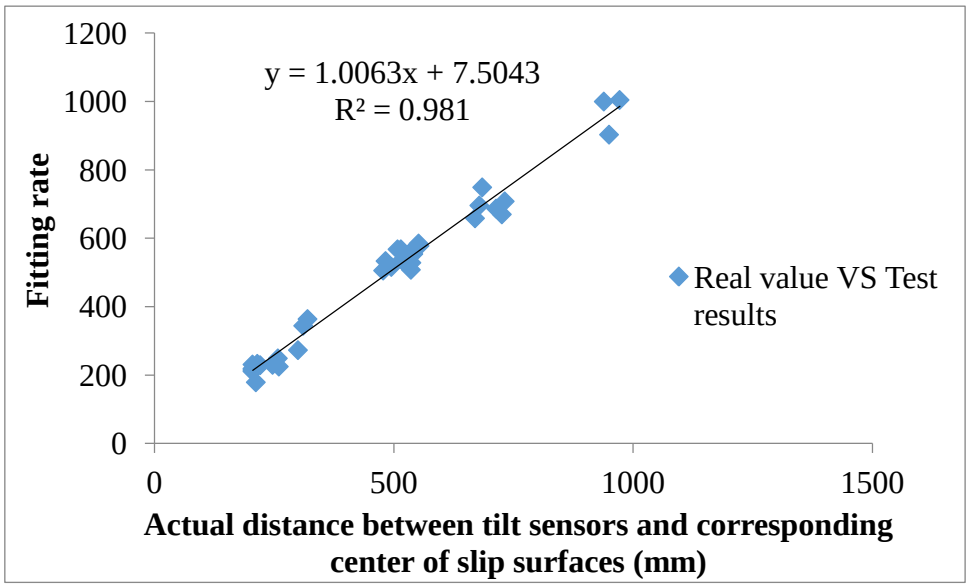

Fig. 6-109 The actual distance between tilt sensors and corresponding center of slip surfaces against the fitting rate

The test results in Fig. 6-109 indicates that the rate of fitting lines close to the actual distance between the location of sensors and corresponding rotational centers. Furthermore, Fig. 6-109 also indicates that the following equation (6-4) can be used to describe the relationship between displacement and tilting angle of slopes for all types of tilt sensors as shown in Fig. 6-110 and Fig. 6-111 when slope sliding.

$$\Delta s_i = r_i \cdot \left|\Delta\theta_i\right| \tag{6-4}$$

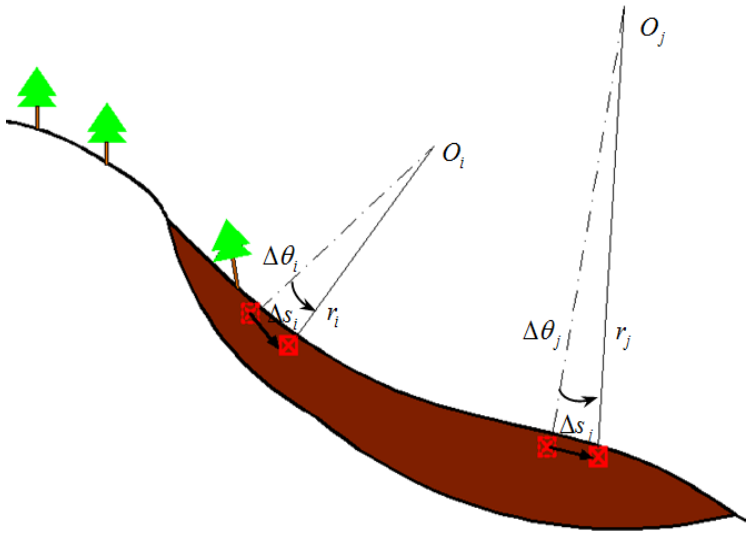

Fig. 6-110 The tilt sensors are located above the slip surface

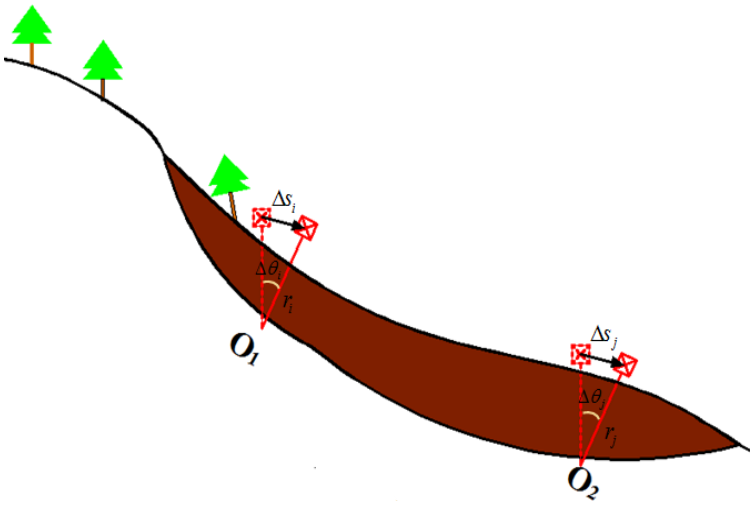

Fig. 6-111 The tilt sensors with long rods reaching the slip surface

6.5. References

Carter, M., Bentley, S., P. (1985). "The geometry of slip surfaces beneath landslides:

predictiom surface measurements." Can.Geotech.J., 22, 234-238.

Uchimura T., Towhata I., Wang L., Nishie S., Yamaguchi H., Seko I. and Qiao J. (2015). "Precaution and early warning of surface failure of slopes by using tilt sensors." Soil and Foundation, 55(5), 1086-1099.

Zong, J. Y., Jian,P.Q., Dong, H., Uchimura, T., Lin, W. (2017). "Experimental Identification on Thresholds for early warning of Rainfall-induced Failure on Fractured Slopes after Giant Earthquake." Engineering Geology, 46(11), 2022-2034.

CHAPTER 7

NEW METHOD FOR LANDSLIDES PREDICTION USING TIME HISTORY OF TILTING OF SLOPES

7.1. Introduction

Forecasting the timming of landslides is an essential goal of landslide disaster risk mitigation. A reasonably accurate prediction of failure time would reduce the quantity of fatalities as well as the cost of property damaged by slope failure. Even though adequate countermeasures can prevent the landslides, it is practically impossible to be performed for the large number of slopes with a potential risk of failure(Federico et al., 2015).

In recent decades, an approach of the landslide prediction based on the rheological behaviour of geomaterials has been developed by Saito in 1965 and modified by many researchers later. This approach is an empirical proposition deduced from creep tests and has been substantiated by the time history of surface displacement of slopes in the accelerating stage of slope failure (Saito 1965, Fukuzono 1985, Voight 1988,Petley et al. 2002). The formular of this method is expressed as

$$\frac{d\Omega}{dt} = \left[A \cdot (\alpha - 1)\right]^{\frac{-1}{\alpha-1}} (t_r - t)^{\frac{-1}{\alpha-1}} \tag{7-1}$$

Where Ω is the surface displacement of slopes, $\frac{d\Omega}{dt}$ represents the first derivatives of Ω. A and α are constant parameters, while t and t_r represent for the current time and failure time respectively. α is the parameter which is approached by data

fitting, and it is widely reported that the value of α is in the vicinity of 2. When α=2, the equation (7-1) can be rewritten as

$$\frac{d\Omega}{dt}\cdot(t_r - t) = A \tag{7-2}$$

Although this method has been validated against field events as well as laboratory tests, there are still some limitations for this method which are listed below.

1) This method is not suitable for the slope failure without a very clear accelerating stage.

2) This predicting method is associated with the slope surface displacements monitoring generally using extensometers, which will cause the following problems. Firstly, skilled workers are required for the installation of these extensometer sensors, which results in the increase of costs. Additionally, the stable areas of slopes for the installation of extensometer sensors can not be decided precisely, and this may make the monitoring data invalid if the extensometers are implemented in the unstable regions. Considering these problems, a new landslide predicting method based on the slope surface tilting angle monitoring using low-cost and simple-installation tilt sensors, is more suitable.

3) The fundamental physics underpinning of this method has not yet been fully elucidated. Furthermore, the influence of many factors on the method, such as rainfall intensity, data noise, and so on, has not been discussed. In this respect, more studies should be carried out.

In this Chapter, a new method for slope failure prediction based on the time history of tilting of slope surface is presented. Validation of this new method is also carried out against the laboratory tests and field tests under constant rainfall intensity as well as the rainfall intensity changed. The influence of data noise and fluctuation of the trend for the monitored data is also studied. Finally, some suggestions for field application based on this method and the limitation of this method are discussed.

7.2. A new predicting method for landslide with tilting

The relationship between displacement and tilting angle on slope surface was

discussed in Chapter 6, and the results from model tests as well as field tests indicate that a linear relationship exists between displacement and tilting angle. Furthemore, the rate of the fit lines for the relationship between displacement and tilting angle of each sensor is close to actual distance between the location of each sensor and the rotational center of tilt sensors as shown in Fig. 7-1.

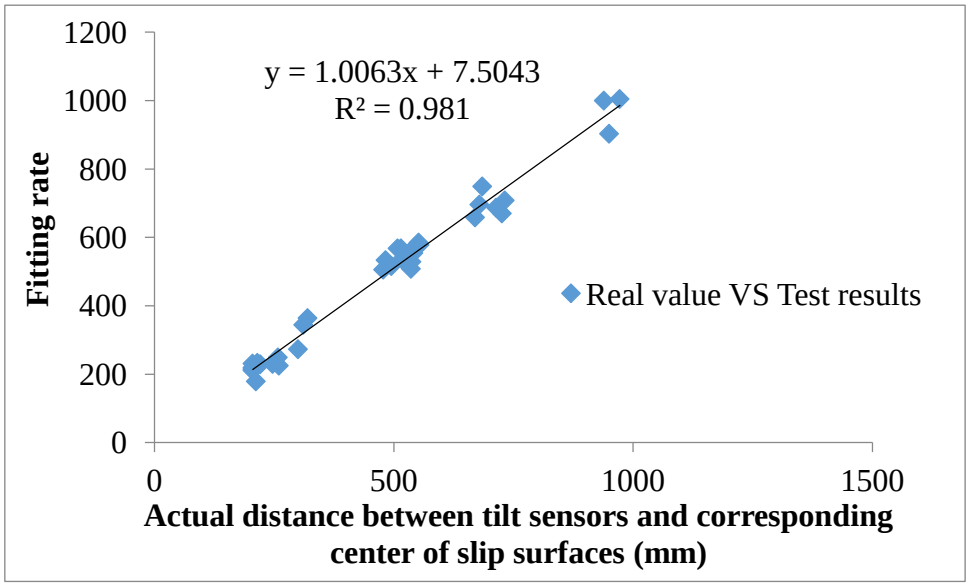

Fig. 7-1 The actual distance between tilt sensors and corresponding center of slip surfaces against the fitting rate

Consequently, the relationship between displacement and tilting angle can be expressed as

$$ds = |d\theta| \cdot r \tag{7-3}$$

Where ds is the displacement on slope surface, and $|d\theta|$ is the absolute value of tilting angle. r represents the distance between the location of sensors and the center of corresponding slip surface.

The equation 7-2 can be rewritten as

$$\frac{|d\theta|}{dt} = B \cdot (t_r - t)^{\frac{-1}{\alpha-1}} \tag{7-4}$$

Where $B = \frac{1}{r}\left[A \cdot (\alpha - 1)\right]^{\frac{-1}{\alpha-1}}$, and $\frac{|d\theta|}{dt}$ is the tilting angle rate. t and t_r are the current time and failure time respectively.

α is close to 2 (Saito, 1969; Voight, 1989), so the equation (7-4) can be simplified as

$$\frac{|d\theta|}{dt} = B \cdot (t_r - t)^{-1} \tag{7-5}$$

The equation (7-5) also can be expressed as

$$\frac{dt}{|d\theta|} = -\frac{t}{B} + \frac{t_r}{B} \tag{7-6}$$

7.3. Validation of the new predicting method

The proposed method is deduced from the equation (7-2) which was obtained under the nearly constant stress condition in the accelerating stage of material failure. Considering this situation, to validate the new method for slope failure prediction using the time history of tilting angle of slopes, labotary tests and field tests under constant rainfall intensity were carried out, and the data for analyzing was selected in the accelerating stage of slope failure. Furthermore, the influence of rainfall intensity change and data selection on this method is also discussed in this part.

7.3.1 Tests conducted under constant rainfall

1） Test 1 with constant rainfall

In this model test, the pre-defined slip surface consists of two parts. The upper part as shown in Fig. 7-2 is with the radius of 400 mm, while the radius for the lower part is 600mm. The landslip in this test was induced by constant artifical rainfall, 46.6 mm/h, and the time history of tilting of tilt sensor T1 and T2 is presented in Fig. 7-3. Additionally, Fig. 7-3 also shows the data of T1 and T2 selected every 1° in the accelerating stage as marked in the figure. The tilting angle rate of T1 and T2, $\frac{d\theta}{dt}$, can be obtained using the marked points in Fig. 7-3. Then, the reciprocal of tilting rate, $\frac{dt}{d\theta}$ is approached and plotted againt time shown in Fig. 7-4. Depending on the equation (7-6), it indicates that the failure time t_r can be predicted when $\frac{dt}{d\theta}$=0, which means equation (7-6) can be rewritten as

$$-\frac{t}{B}+\frac{t_r}{B}=0 \tag{7-7}$$

Then,

$$t_r=t \tag{7-8}$$

When $\frac{dt}{d\theta}=0$.

In Test 1, the linear trend between the reciprocal tilting rate and time is indicated in Fig. 7-4. The predicted failure time approached by equation (7-7) is 47.4 minutes corresponding to the actual failure time 47.2 minutes. Fig. 7-5 shows the images before and after the slope failure.

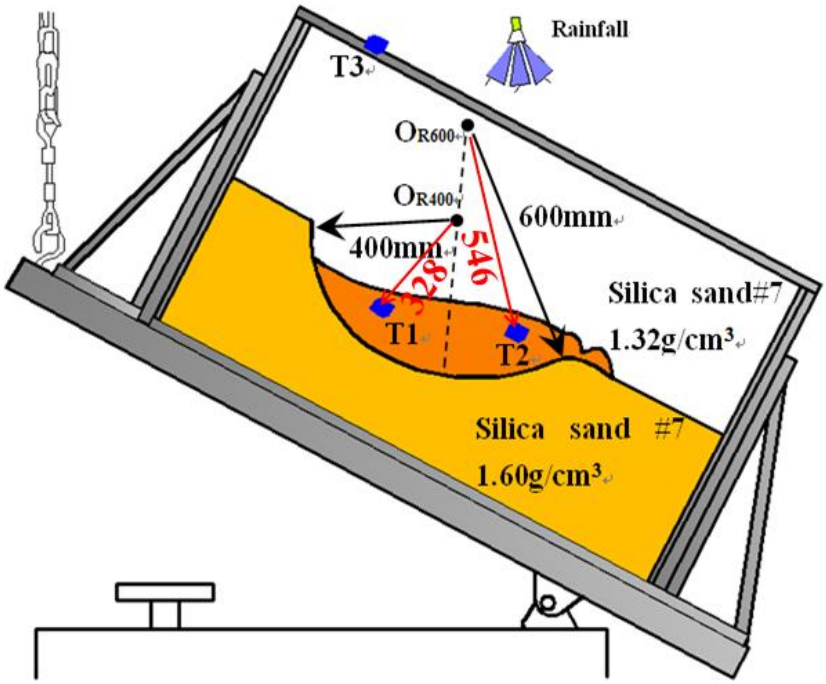

Fig. 7-2 The illustration of Test 1

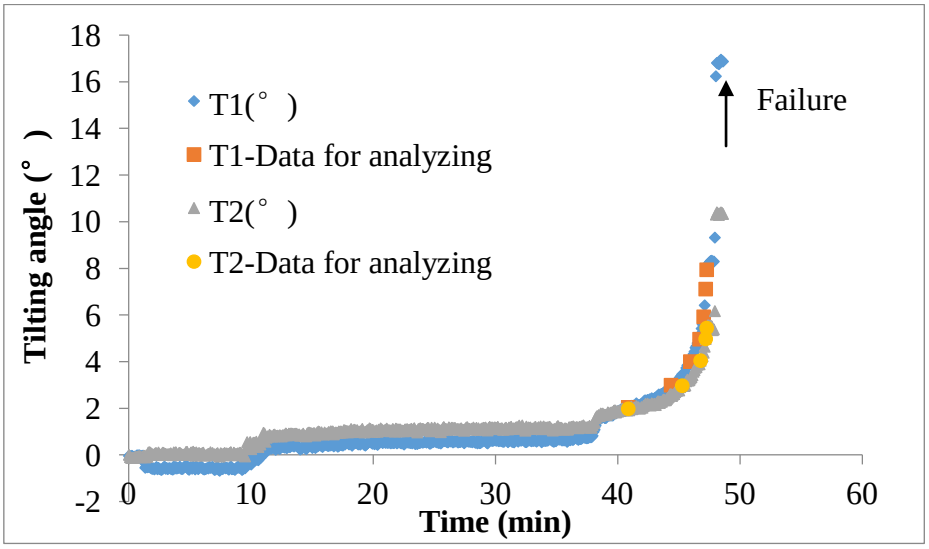

Fig. 7-3 The time history of tilting and the data for analyzing for T1 and T2

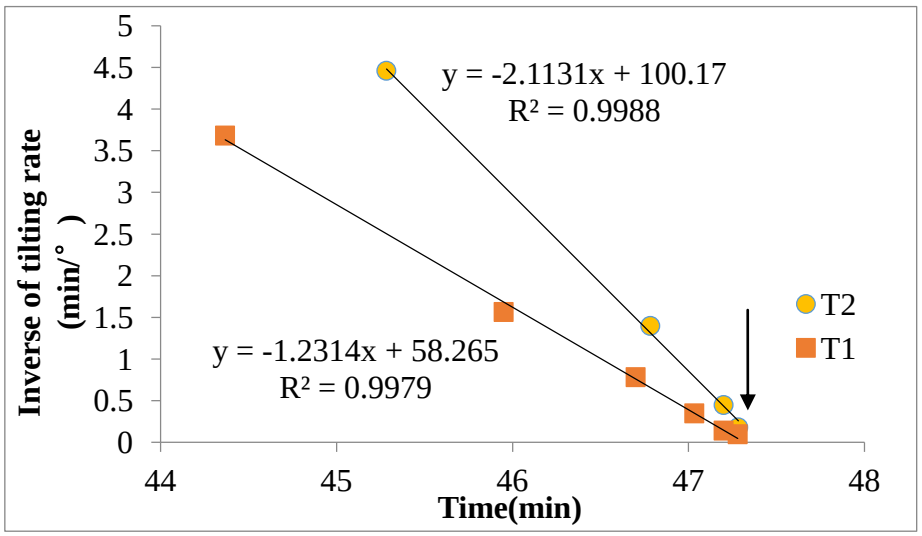

Fig. 7-4 The reciprocal of tilting rate against time in Test 1

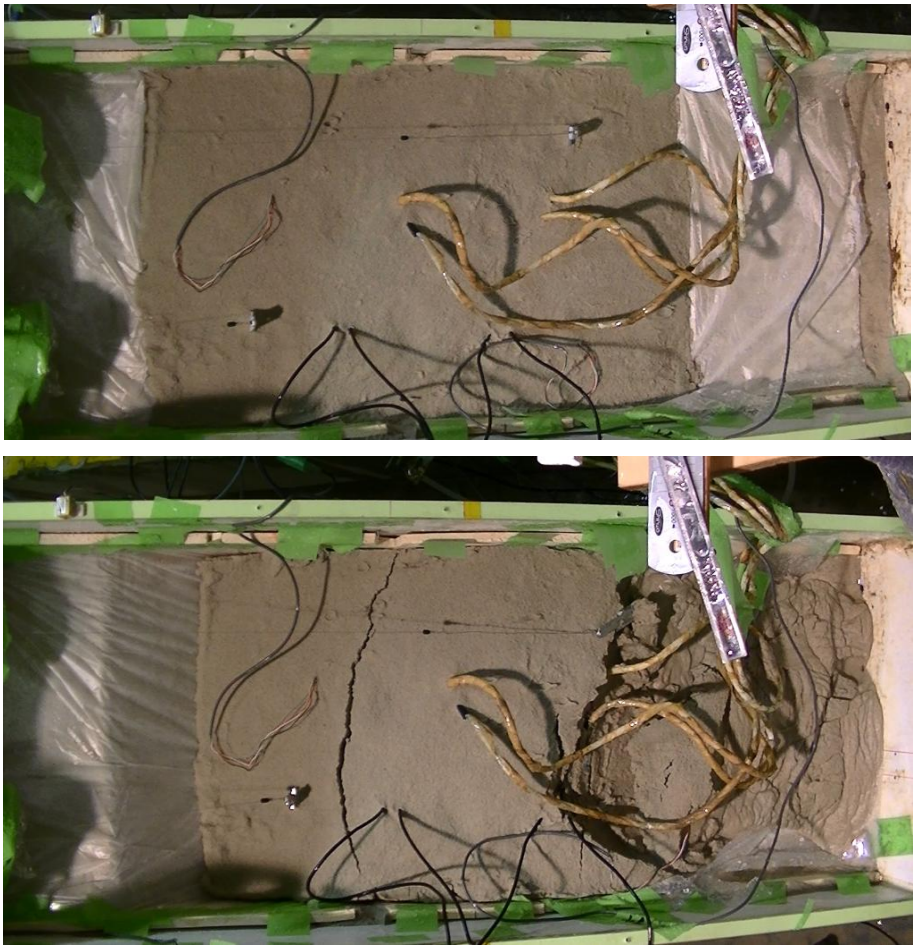

Fig. 7-5 The image before and after the slope failure in Test 1

2） Test 2 with constant rainfall

The slope model in this test was constructed in a wooden tank, measuring 800 mm× 300 mm×400 mm (Fig. 3-17-b), and two layers with different dry density using Edosaki sand were built. The dry density is 1.25 g/cm^3 for the surface layer with the water content 10% while the dry density for the base layer is around 1.7 g/cm^3 as shown in Fig. 7-6. The slope failure was induced by constant aritifial rainfall and began in the bottom part of the slope model where tilt sensor T5 located. After T5 failed, the remaining part slided away subsequently. The pre-failure behaviour of the slope was recorded by T5 presented in Fig. 7-7, and the predicted failure time using the new proposed method is 46.4 minutes corresponding to the actual failure time 46.6 minutes (Fig. 7-8).

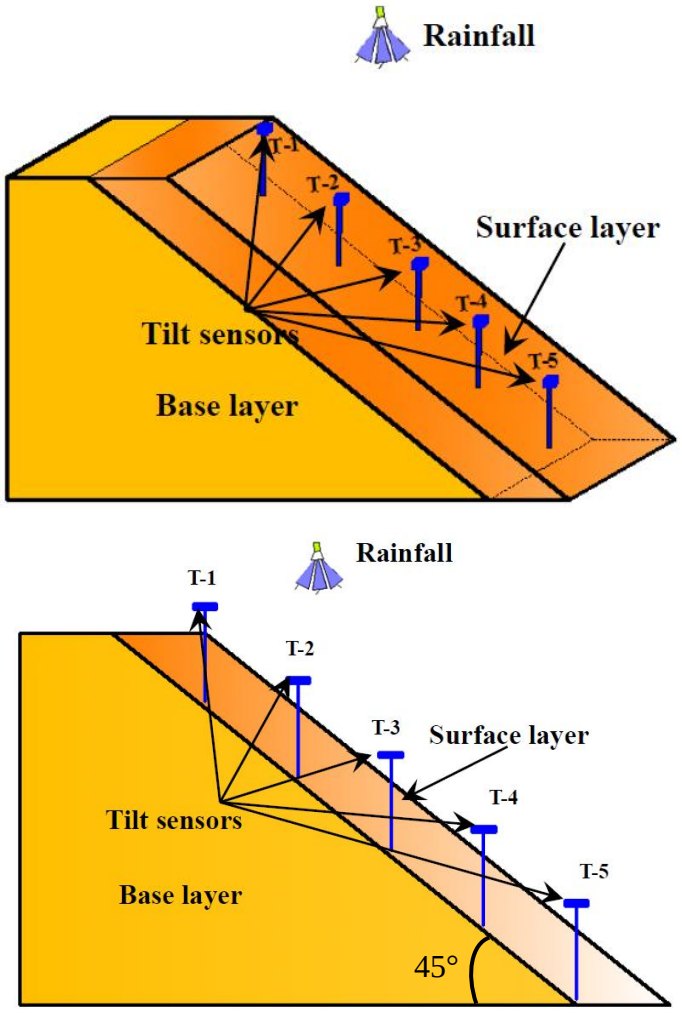

Fig. 7-6 The illustration of slope model and apparatus setup in Test 5

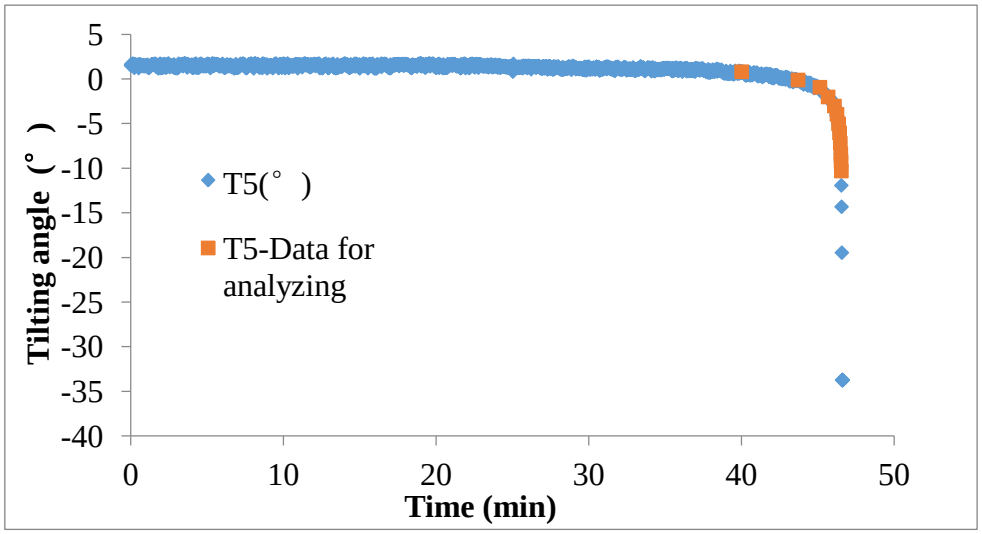

Fig. 7-7 The time history of tilting and the data for analyzing for T5 in Test 5

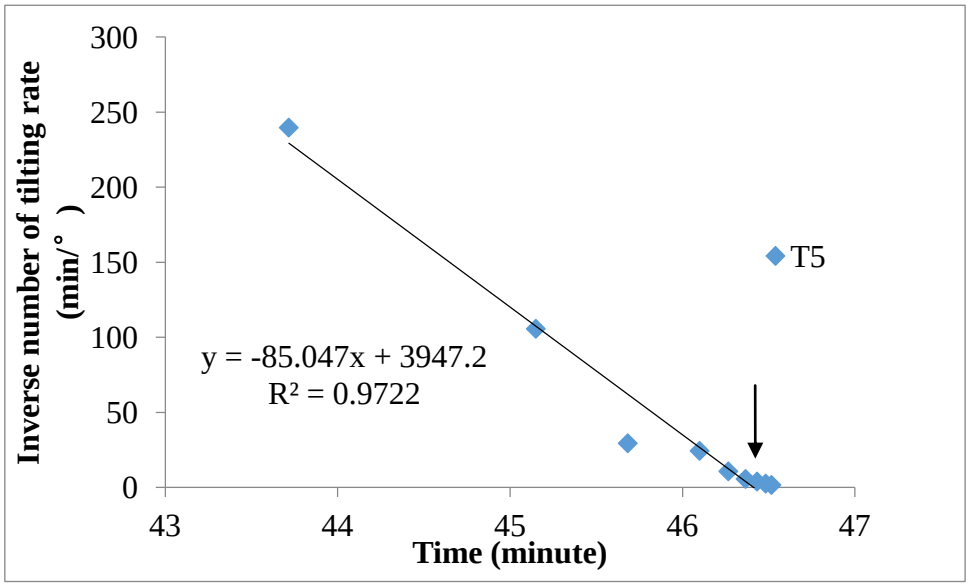

Fig.7-8 The reciprocal of tilting rate against time for T5 in Test 5

3） Test 3 (Field test 1) with constant rainfall

The testing conditions of this test (Field test 1) and the arrangement of sensors are introduced in previous chapters. The photos, which were taken before and after the test are presented in Fig. 7-9. The slope began to fail in the upper part after rained for around 5 h. The time history of tilting and data for analyzing are presented in Fig. 7-10, and the reciprocal of tilting rate is plotted againt time presented in Fig. 7-11. In the accelerating stage of slop failure, a linear trend is indicated and the predicted failure time is 243.5 minutes close to the actual failure time 243.3 minutes.

Fig. 7-9 The image before and after the slope failure in Test 3

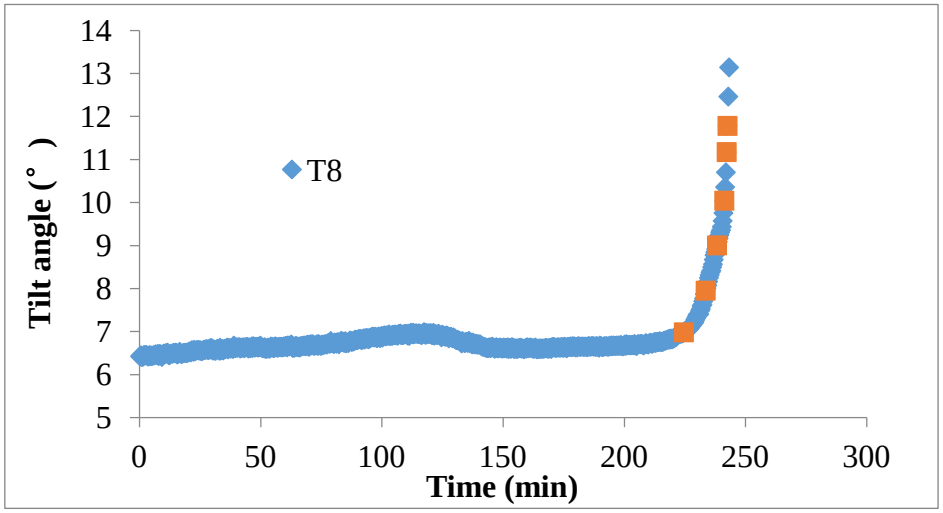

Fig. 7-10 The time history of tilting and the data for analyzing for T8

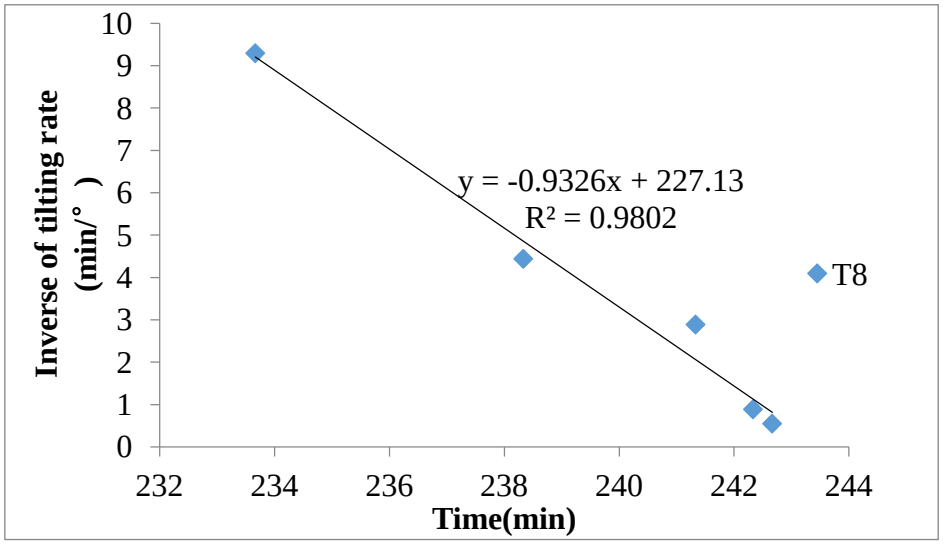

Fig.7-11 The reciprocal of tilting rate against time in Test 3

4） Test 4 (Field tests 2) with constant rainfall

In this test, errosion took place at the bottom of the slope and caused two tilt sensors (T1 and T3) located in bottom area failed in the first day. The main deformation occurred at the top part of the slope in the second day, and the failure process was recorded by two tilt sensors (T2 and T4) with different length of rods (Fig. 7-12). The time history of T2 with a short rods, 50 mm, shallower than the depth of slip surface is presented in Fig. 7-12. In the final stage of failure as marked in Fig. 7-13, the slope slipped at a constant velocity, which can be considered as slope failure. Before the slope sliding at a high speed, a linear relationship between the reciprocal of tilting rate

of T2 and the time occurred (Fig. 7-14), and the predicted failure time based on this linear trend is 89.5 minutes.

The time history of T4 with a long rods reaching the slip surface is presented in Fig.7-15, and the inverse number of tilting rate against time is shown in Fig. 7-16. The predicted failure time is 88.2 minutes close to the actual failure time 88.2 minutes. Furthermore, the failure time of T4 is close to the predicted failure time of T2, and the consistent results also prove that the new prediction method based on the time history of tilting of slope surface is applicable to predict the slope failure induced by constant rainfall.

Fig. 7-12 The image before and after the slope failure in Test 4

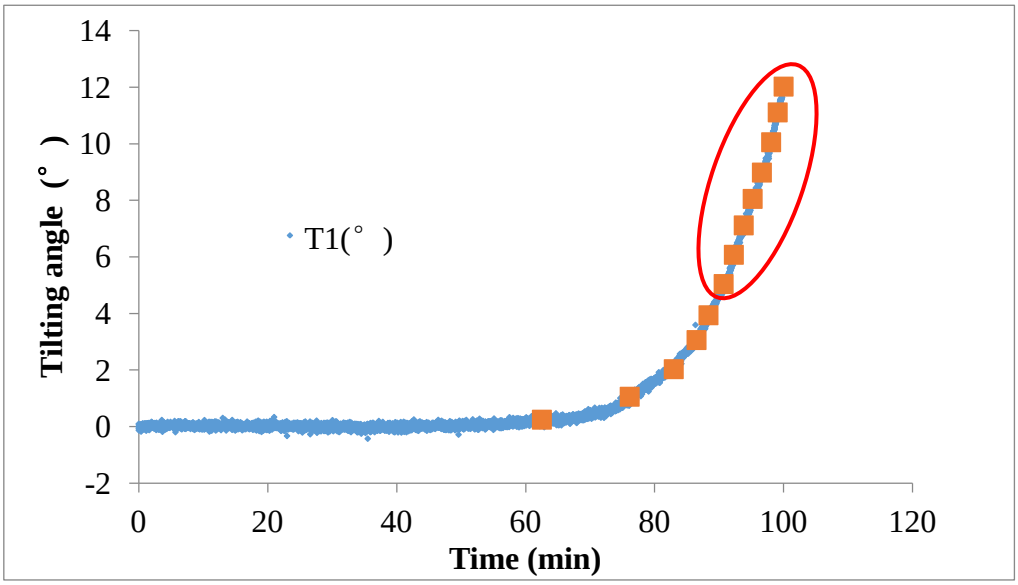

Fig. 7-13 The time history of tilting and the data for analyzing for T1 in Test 4

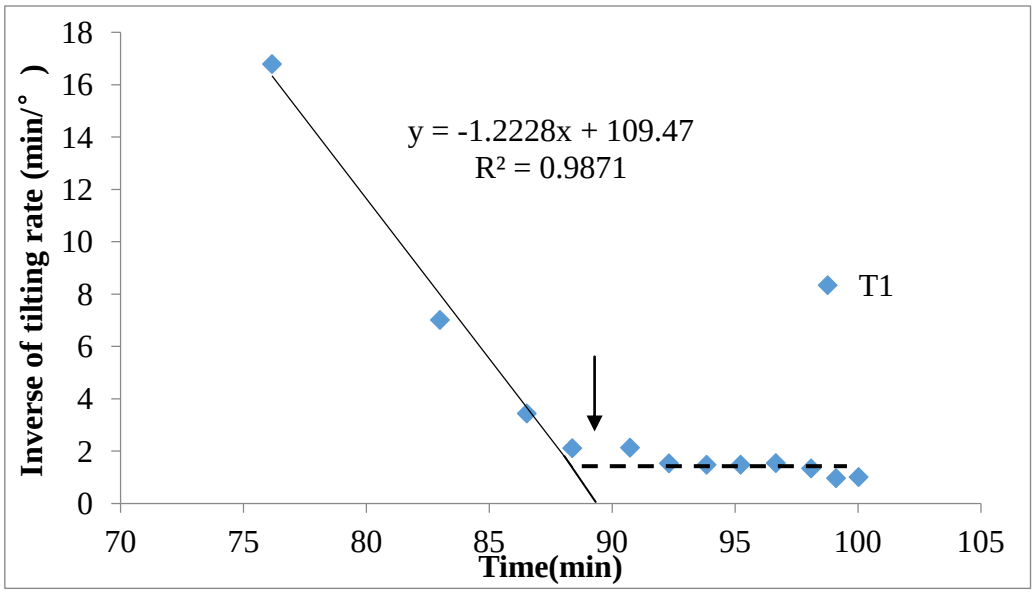

Fig. 7-14 The reciprocal of tilting rate against time for T1 in Test 4

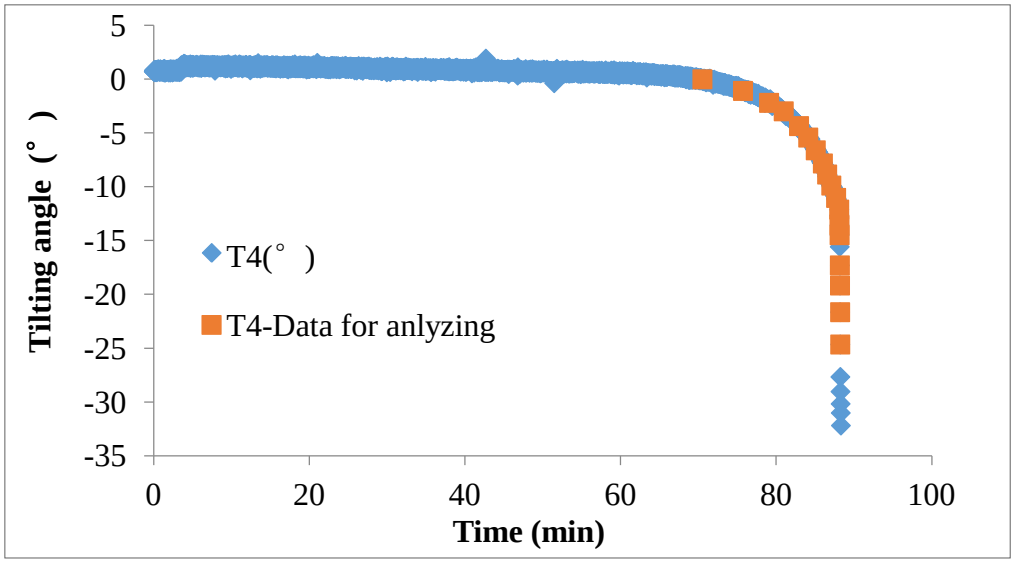

Fig. 7-15 The time history of tilting and the data for analyzing for T4 in Test 4

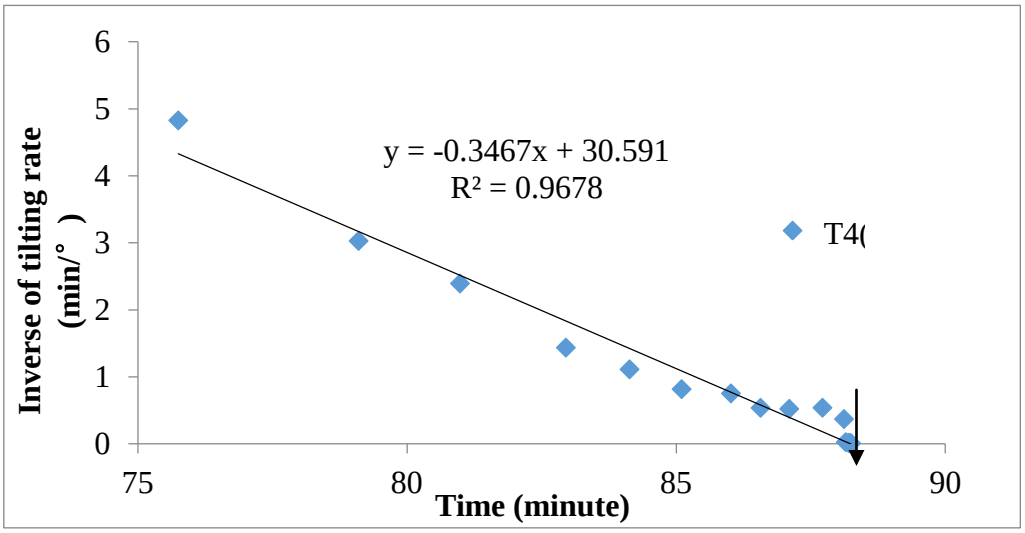

Fig. 7-16 The reciprocal of tilting rate against time for T4 in Test 4

In this section, laboratory model tests as well as field tests were conducted by applying constant rainfall, and the test results indicate that the proposed predicting method for slope failure based on the time history of tilting angle of slopes, are applicable for landslides induced by constant rainfall.

7.3.2 Tests and field event under inconstant rainfall

To investigate the influence of rainfall intensity change on the new proposed method , two model tests were carried out using inconstant rainfall. Furthermore, a field landslide event with a variable rainfall history is also studied in this part.

1) Test 1 with inconstant rainfall

In this test, the rainfall intensity, which is controlled by air pressure, was changed in the test as shown in Fig. 7-18. Fig. 7-17 indicates the testing conditions of this test. The model was first constructed at horrizontal place. After the model construction, the slope model was lifted to an angle around 40° and test began. Rainfall started with the intensity 39.8 mm/h at 230 minute, and increased to 46.6 mm/h after 28 minutes. Then, the rainfall intensity increased to 51.8 mm/h at 268 minute. After that, the rainfall intensity dropped back to 30.3 mm/h at 274 minutes and was kept constant. In this test, the failure of T2 located in the bottom part of the slope model was caused by errosion. The time history of tilting of T1 is presented in Fig. 7-18 and the selected data for analyzing is indicated in Fig. 7-19. Additionally, the reciprocal of tilting rate is plotted againt time presented in Fig. 7-20. Fig. 7-20 shows that a time delay is caused by the rainfal intensity change on the deformation of this slope, and the linear trend between the reciprocal tilting rate and time is also indicated under constant rainfall in this figure. The images before and after the slope failure are shown in Fig. 7-21.

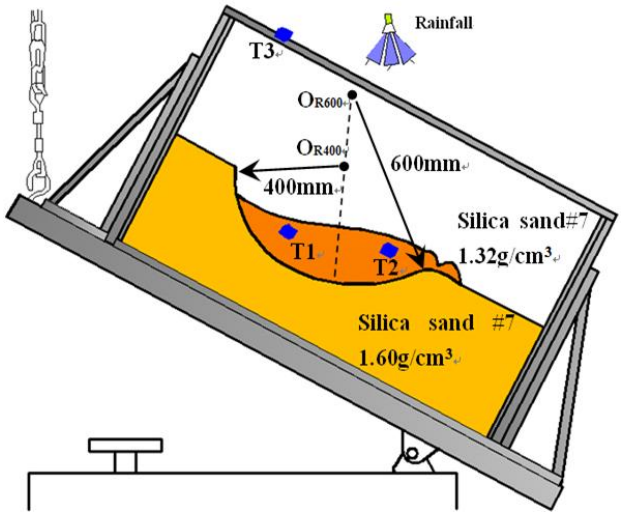

Fig. 7-17 The illustration of Test 2

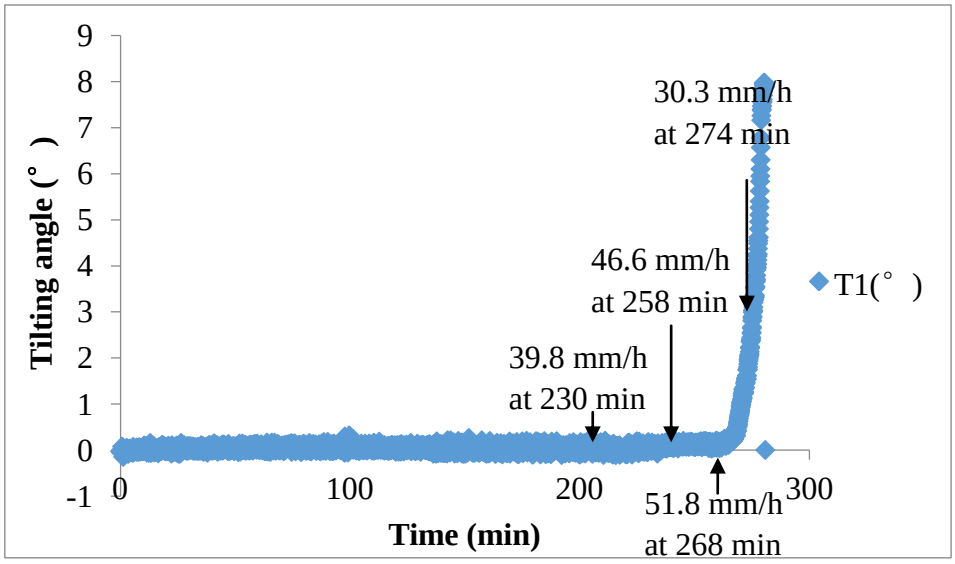

Fig. 7-18 The time history of tilting and rainfall supply

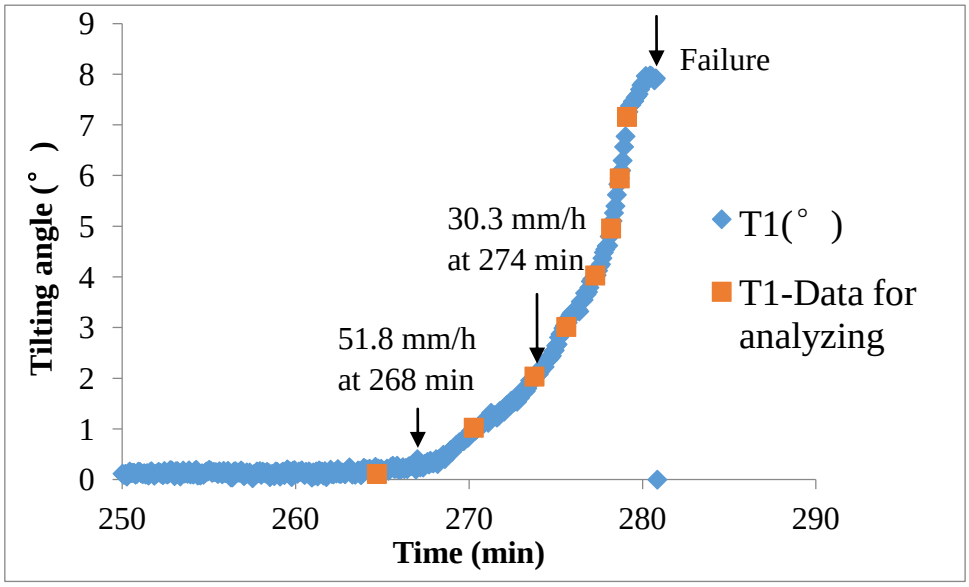

Fig. 7-19 The time history of tilting and the data for analyzing for T1

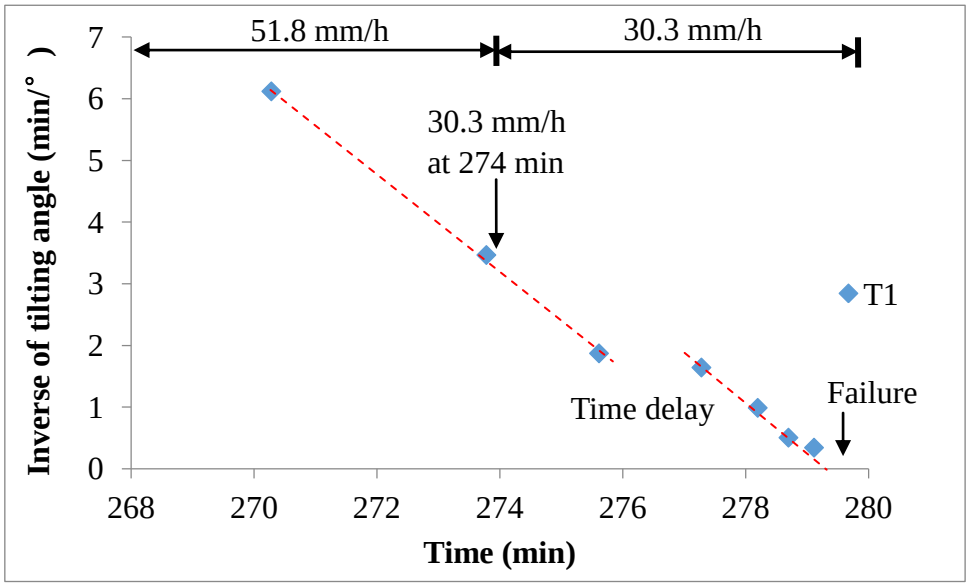

Fig.7-20 The reciprocal of tilting rate against time in Test 2

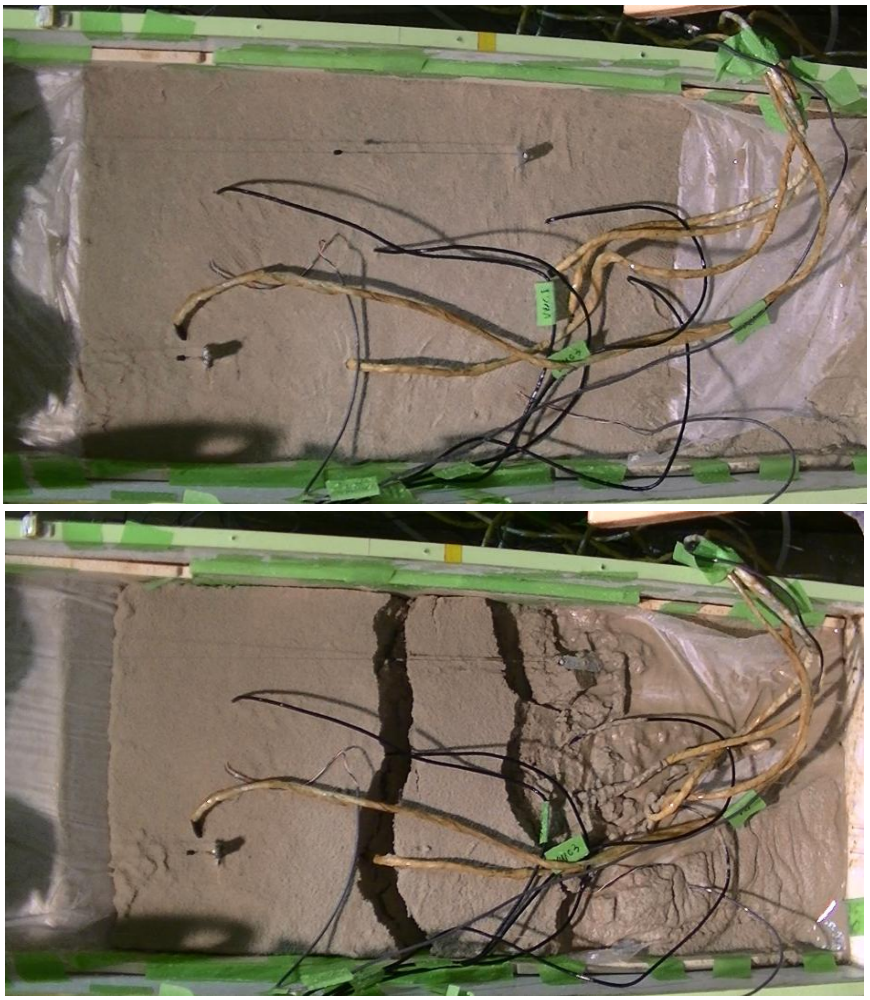

Fig. 7-21 The image before and after the slope failure in Test 2

2) Test 2 using inconstant rainfall

Compared with Test 1 using inconstant rainfall in this part, although the testing condition of these two tests are similar (Fig. 7-22), the time history of rainfall intesity in this test is much more complicated as shown in Fig. 7-23. In this test, two tilt sensors, T1 and T2 were used, and T2 installed in the bottom part of the slope was also damage by errossion (Fig. 2-24). During the test, before the major deformation occurred, the slope deformed slightly and stabled agained after the rainfall stopped for long period (around 230 minute). The time history of tilting of T1 as well as the selected data for analyzing are given in Fig. 7-25. Fig. 7-26 shows the time history of reciprocal tilting rate of T1. In this test, three stages are defined. In stage 1, small deformation occurred and the reciprocal tilting angle reducted with the time, which indicates the slope was unstable. Although the rainfall stopped in stage 1, the slope still slided with a high tilting rate for serveral minutes and the time delay may be caused by the water infiltration after the rainfall stopped. The slope became stable again and the reciprocal tilting rate increase in stage 2. In stage 3, large deformation occurred under the frequently changed rainfall intensity as shown in Fig. 7-27. As shown in Fig. 7-27, linear trends corresponding to different rainfall intensity are indicated. Linear trend 1 is corresponding to the rainfall intensity 46.6 mm/h, and linear trend 2 is related to 39.8 mm/h, while linear trend 3 results from the the rainfall intensity, 39.8 mm/h. The time delay caused by the rainfall intensity change is also indicated in Fig. 7-27. For example , when the rainfall intensity reduced from 46.6 mm/h to 39.8 mm/h, the trend between the inverse number of tilting rate and began to change after several minutes, and these phenomenon are also shown in the later stage. Fig. 7-27 also presents that the slope of the linear trend is related to the rainfall intensity, and the heavier rainfall intensity is corresponding to the steeper slope of the linear trend.

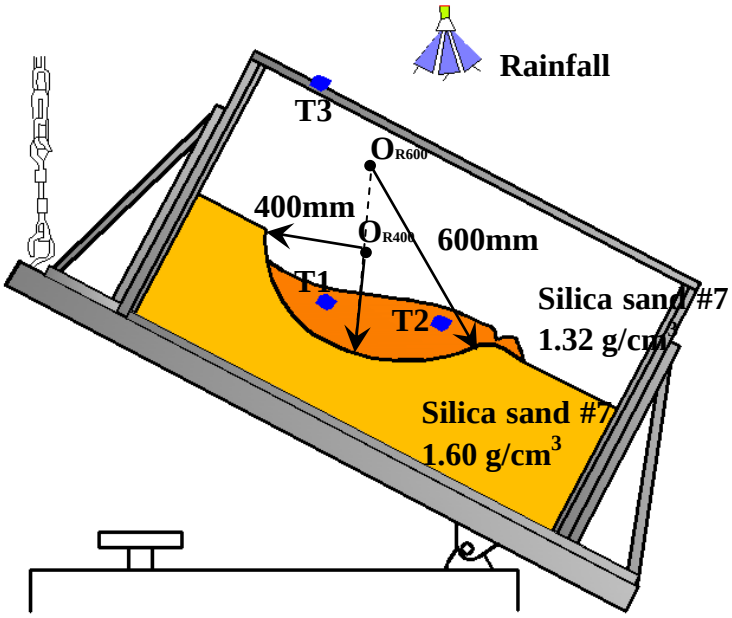

Fig. 7-22 The illustration of slope model and apparatus setup in the test

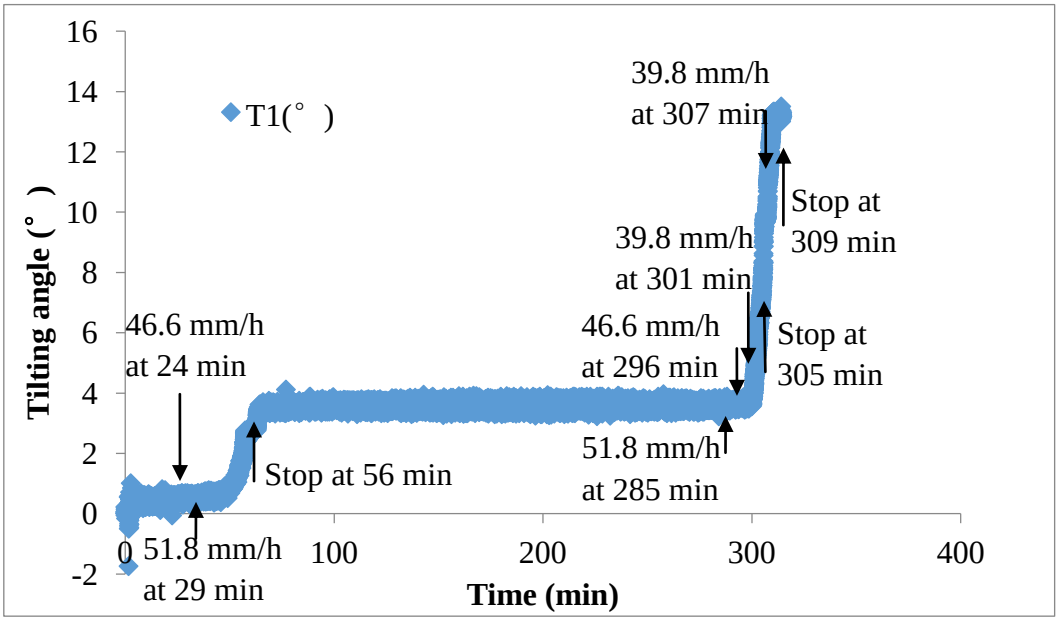

Fig. 7-23 The time history of rainfall and tilting of T1

Fig. 7-24 The image of T2 damaged by errosion

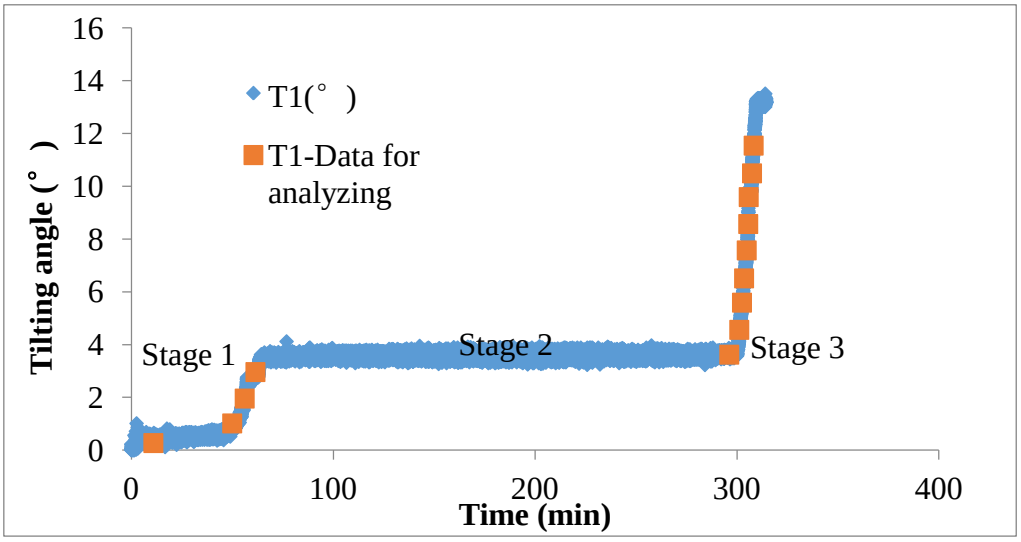

Fig. 7-25 The time history of tilting and the data for analyzing of T1

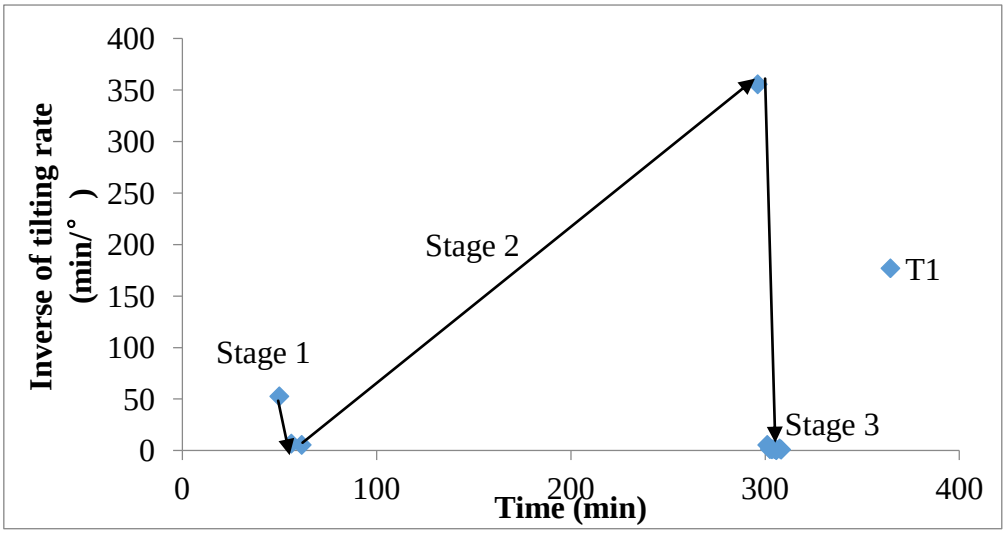

Fig.7-26 The reciprocal of tilting rate against time for T1

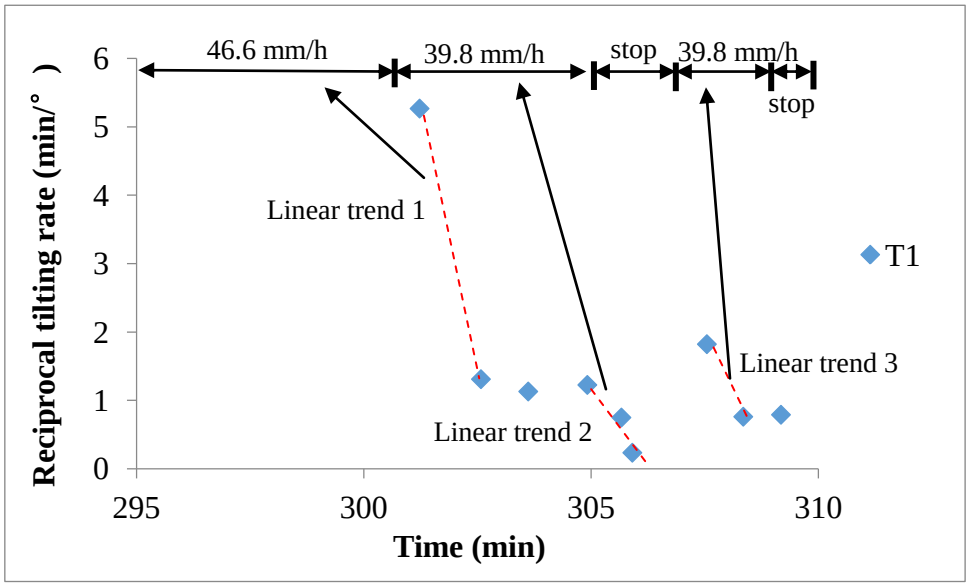

Fig.7-27 The reciprocal of tilting rate against time for T1 in stage 3

3) Field landslide event with inconstant rainfall

A field landslide event monitored using tilt sensors is shown in Fig. 7-28. The time history of accumulated rainfall and the rainfall intensity during monitoring period are presented in Fig. 7-29. The pre-failure behaviour of landslide was record by tilt sensor K-2 in the upper part of the slope and the time history of tilting angle as well as data for analyzing are shown in Fig. 7-30. In Fig. 7-31, the inverse number of tilting rate is plotted againt time. A linear relationship is indicated between the reciprocal tilting angle rate and time. Furthermore, the predicted slope failure time using the new proposed method is around 1236 minutes corresponding to the actual failure time at 1277 minutes. Furthermore, the influence of rainfall intensity change on the slope deformation is also shown in Fig. 7-31. The trends ①, ②, and ③ in Fig . 7-31 are related to the rainfall intensity presented in Fig. 7-29.

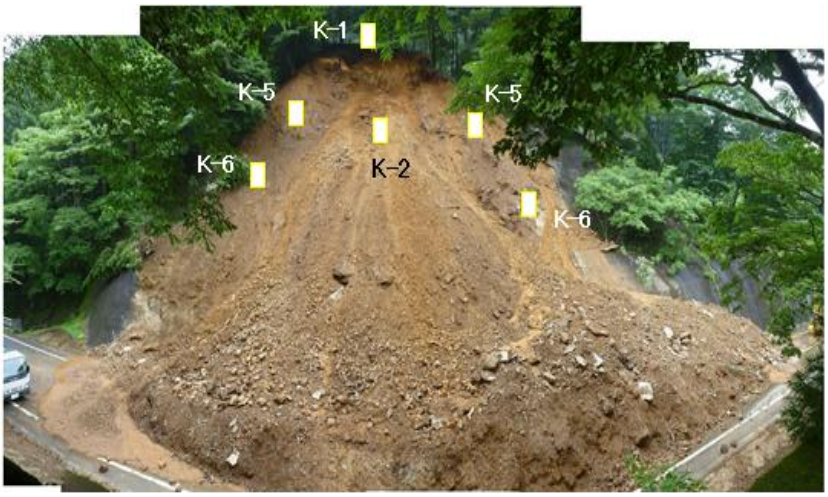

Fig. 7-28 The image of the field event after the slope failure

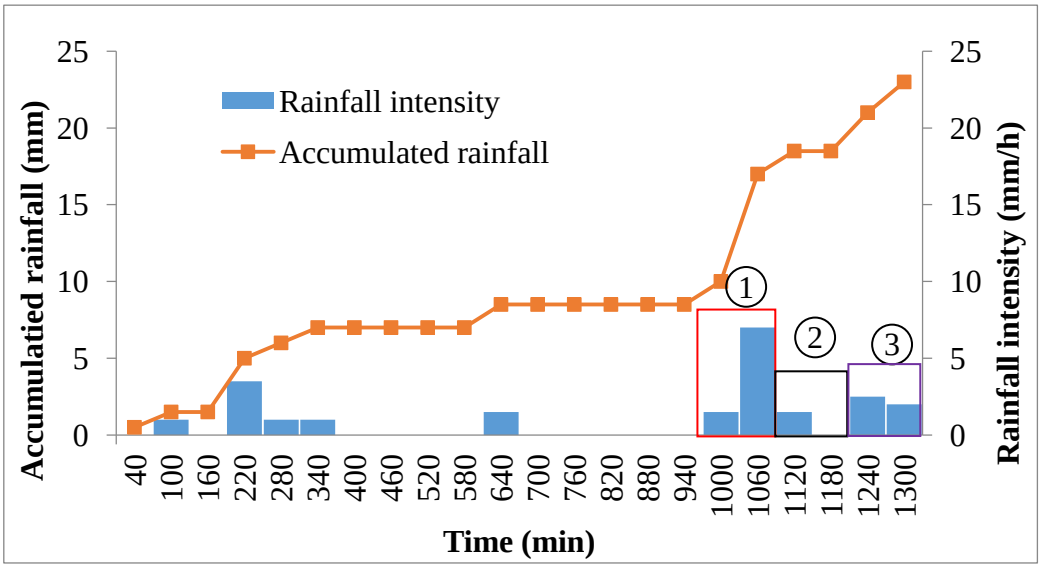

Fig. 7-29 The time history of accumulated rainfall

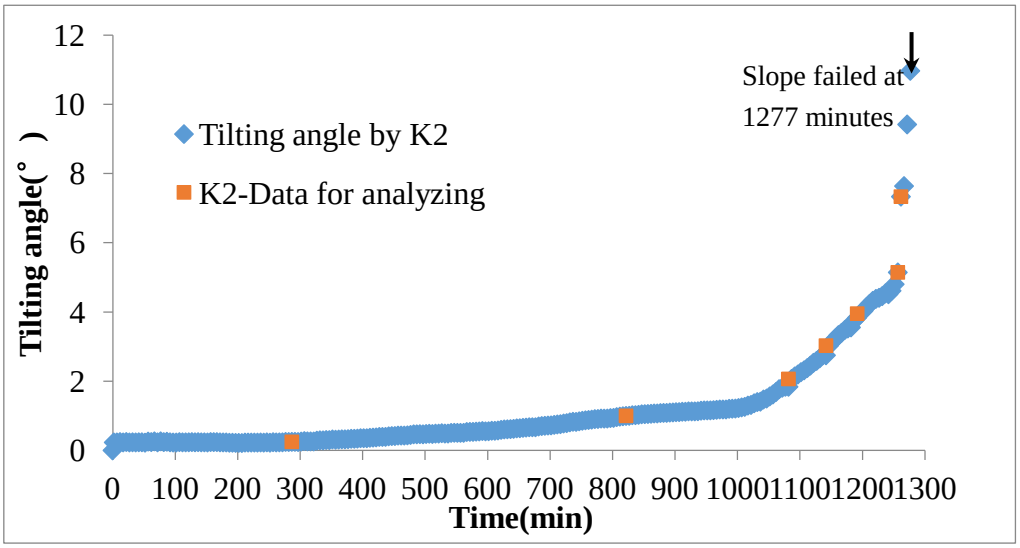

Fig. 7-30 The time history of tilting and the data for analyzing of K-2 in the field event

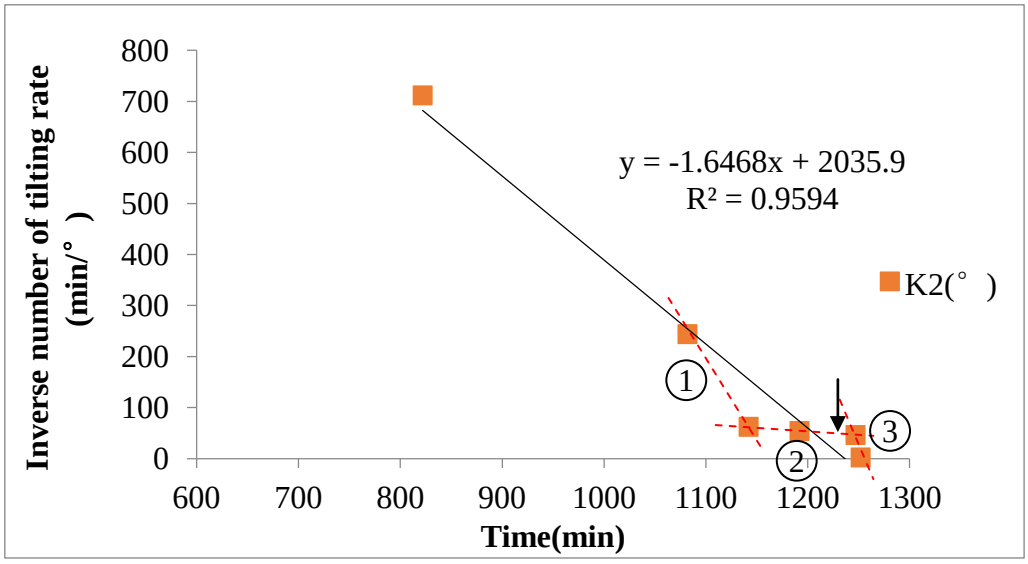

Fig. 7-31 The reciprocal of tilting rate against time for K-2 in the field event

7.4. The influence of data selection on the proposed method

Considering the data noise and fluctuation in slope accelerating stage, the data for analyzing is selected every 1° . In this section, the influence of data selection on the new proposed method is discussed.

1) Case 1- field landslide event

In previous section, the time history of tilting as well as the data selected for analyzing every 1° are presented in Fig. 7-30, and the relationship between the reciprocal tilting angle rate and time is indicated in Fig. 7-31. In this part, the data for analyzing is selected every 2° , 0.5° and 0.2° as shown in Fig. 7-32, Fig. 7-33 and Fig. 7-34 respectively.

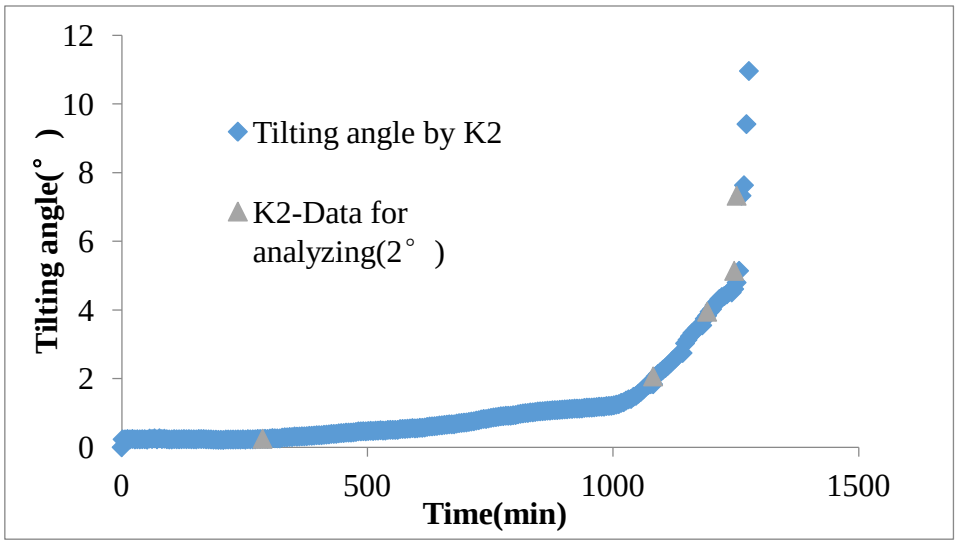

Fig. 7-32 The time history of tilting and the data for analyzing of K-2 every 2°

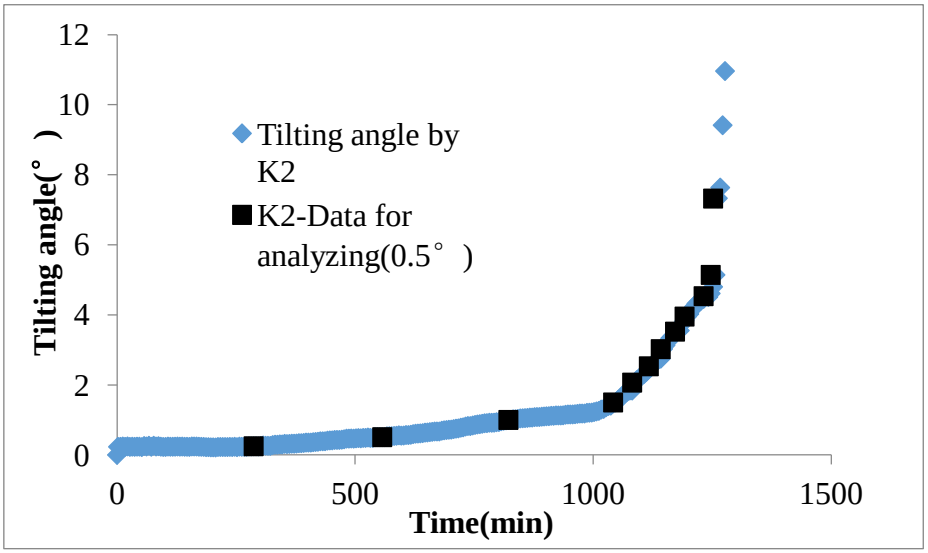

Fig. 7-33 The time history of tilting and the data for analyzing of K-2 every 0.5°

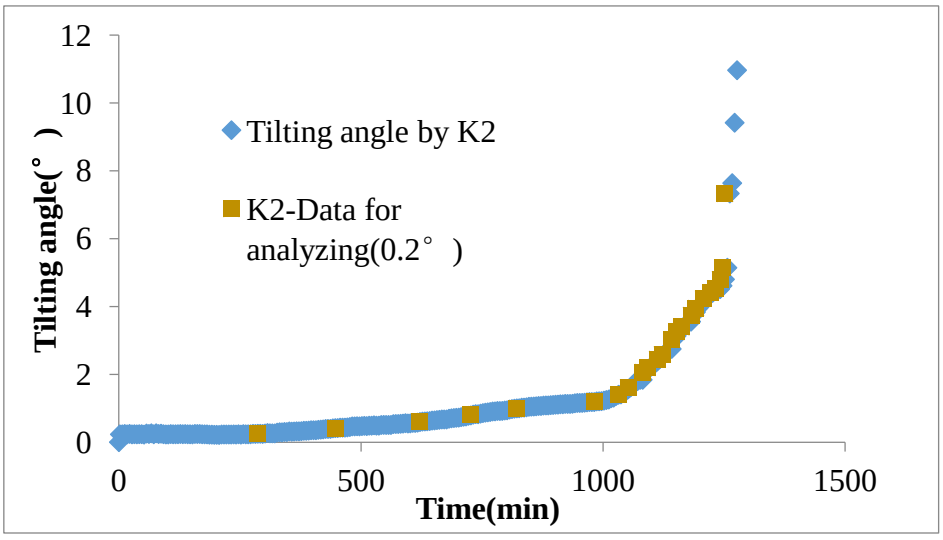

Fig. 7-34 The time history of tilting and the data for analyzing of K-2 every 0.2°

The reciprocal tilting rate approached based on the selected data with different interval angle are plotted together, and then the trend for reciprocal tilting rate against time obtained from each data set are presented in Fig. 7-35 to Fig. 7-38.

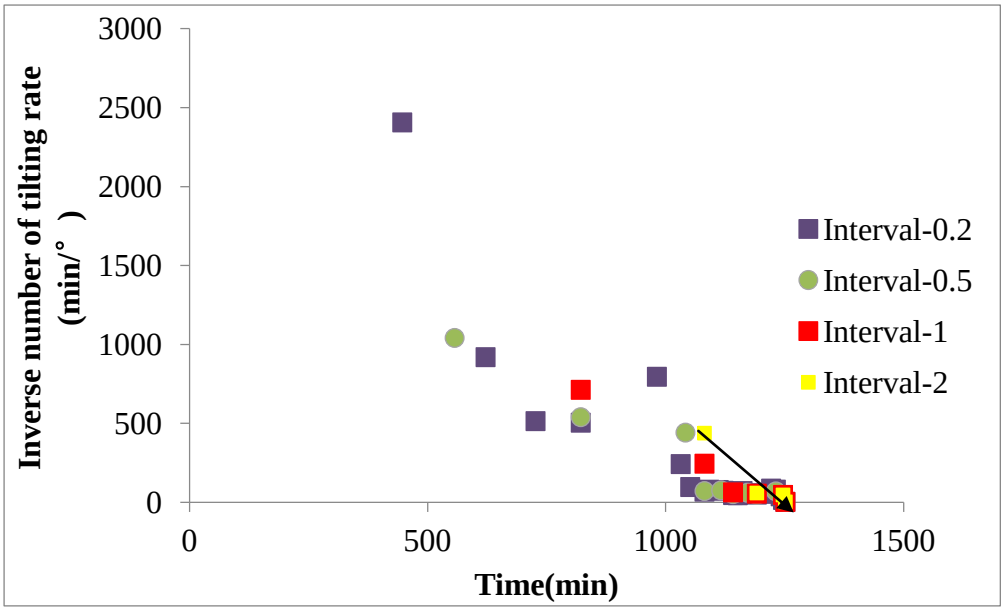

Fig. 7-35 The reciprocal tilting rate against time and the trend for data set every 2°

The equation of the fit line for the data selected every 2° is

$$\frac{dt}{d\theta} = -2.464 \cdot t + 3076.3 \tag{7-9}$$

The correlation coefficient is 0.925, and the predicted failure time based on the linear trend is 1248.5 minutes.

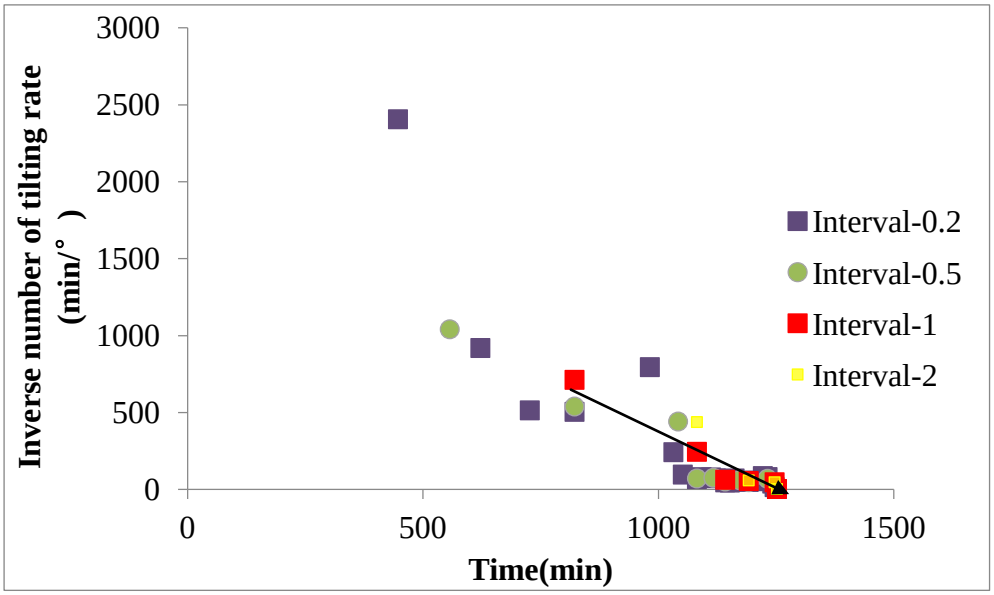

Fig. 7-36 The reciprocal tilting rate against time and the trend for data set every 1°

The predicted failure time based on the data selected every 1° is 1236 minutes as mentioned before.

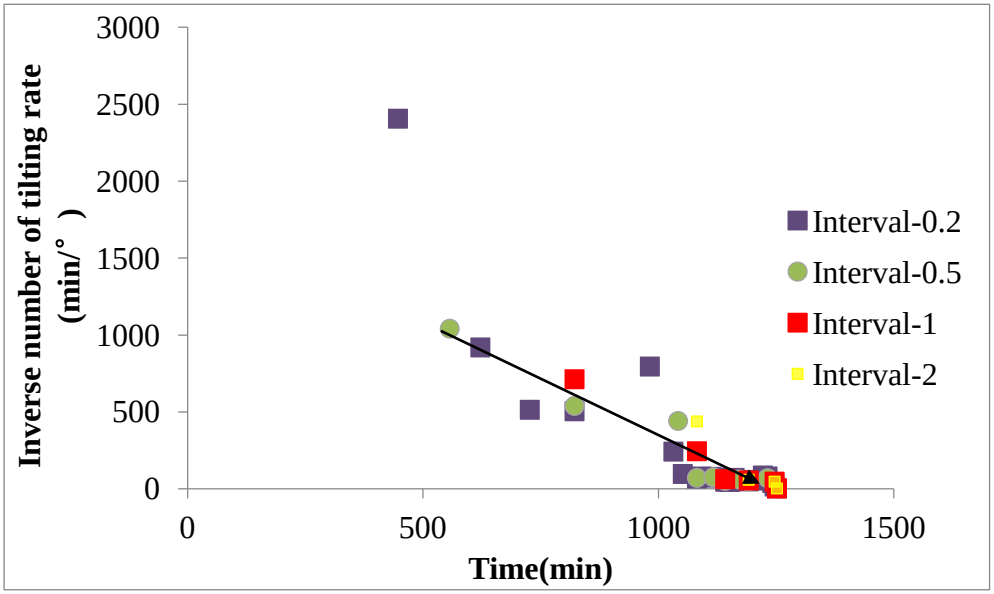

Fig. 7-37 The reciprocal tilting rate against time and the trend for data set every 0.5°

The equation of the fit line for those data selected every 0.5° is

$$\frac{dt}{d\theta} = -1.479 \cdot t + 1814.1 \tag{7-10}$$

The predicted failure time based on the linear trend is 1226 minutes.

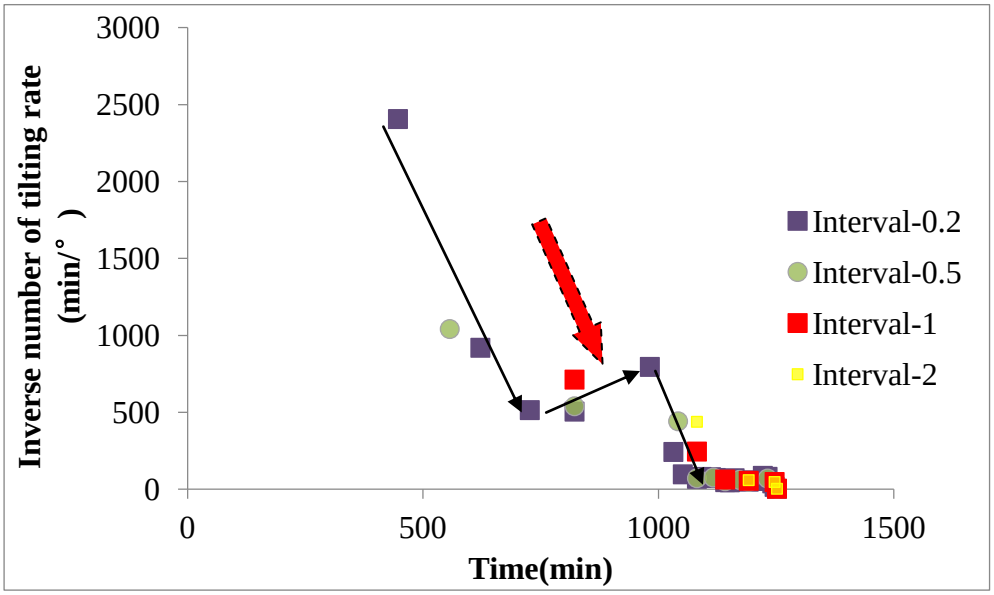

Fig. 7-38 The reciprocal tilting rate against time and the trend for data set every 0.2°

When the data for analyzing selected every 0.2° , as shown in Fig. 7-38, a decreasing trend between the reciprocal tilting rate and time with a notable fluctuation is

indicated.

In addition, the relationship between reciprocal tilting rate and time is also checked for every data point from the original monitoring data as well as the error-processing data as shown in Fig. 7-39. The results for the original data and error-processing data are presented in Fig. 7-40 and Fig. 7-41 respectively. Fig. 7-40 shows that there is no clear trend between the reciprocal tilting rate and time. The relationship between the reciprocal tilting rate and time is covered by the data noise and fluctuation. On the other hand, Fig. 7-41 indicates a clear trend between the reciprocal tilting rate and time using the error-processing data with the error elimination method attached in Appendix 1.

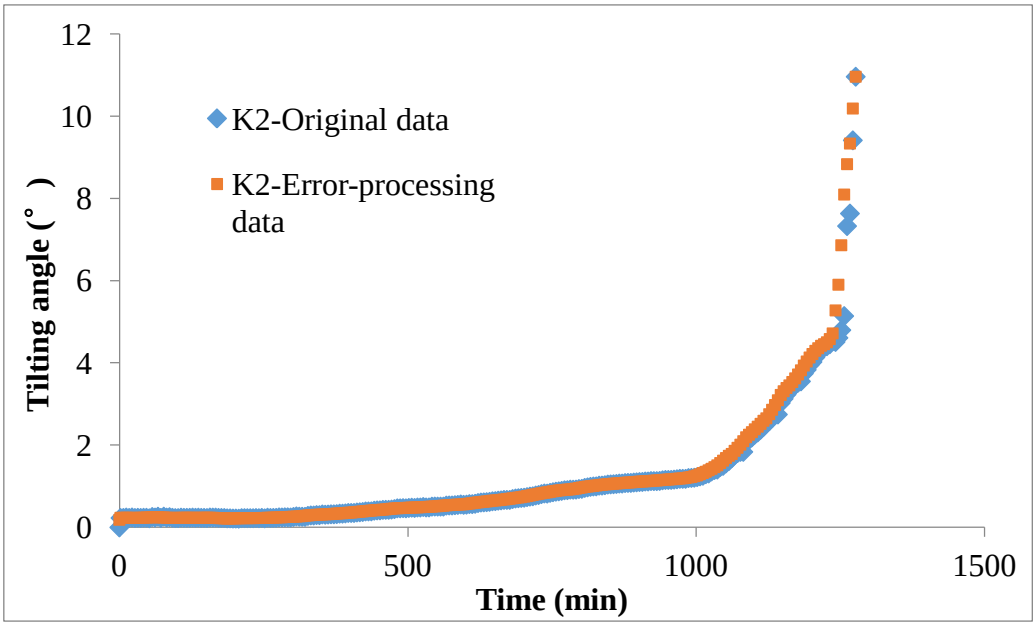

Fig. 7-39 The original data and error-processing data against time

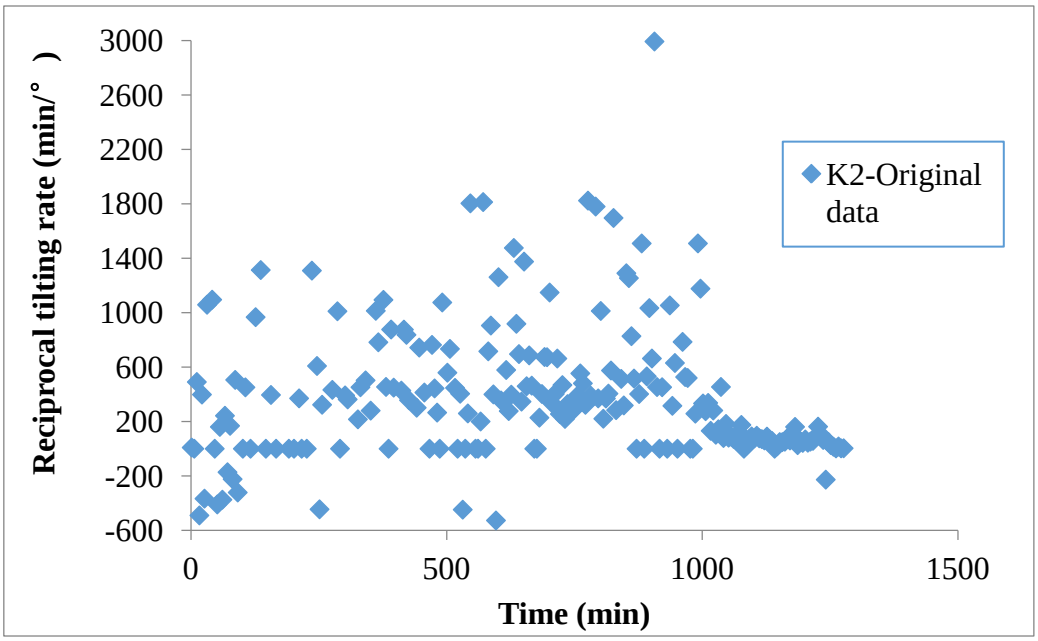

Fig. 7-40 The time history of reciprocal tilting rate using original monitoring data

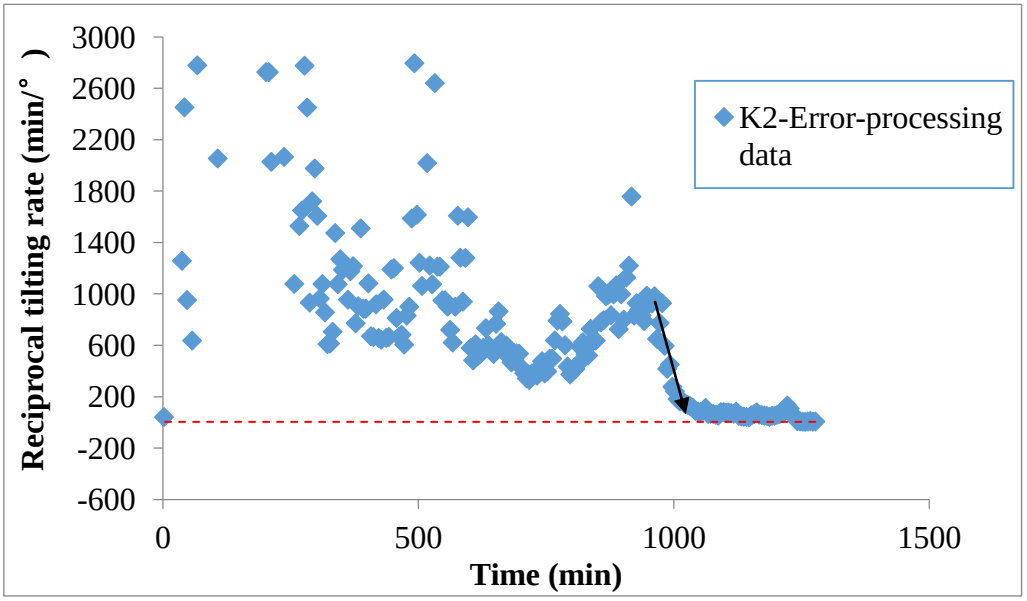

Fig. 7-41 The time history of reciprocal tilting rate using error-processing data

2) Case 2- Field test 2

The relationship between reciprocal tilting rate and time of field test 2 is also checked for every data point from the original monitoring data as well as the error-processing data as shown in Fig. 7-42. The results for the original data and error-processing data are presented in Fig. 7-43 and Fig. 7-44 respectively. Similar as the results of the field landslide event case, Fig. 7-43 shows that there is no clear trend between the

reciprocal tilting rate and time, while Fig. 7-44 indicates a clear trend in the final stage of slope failure as marked in the figure.

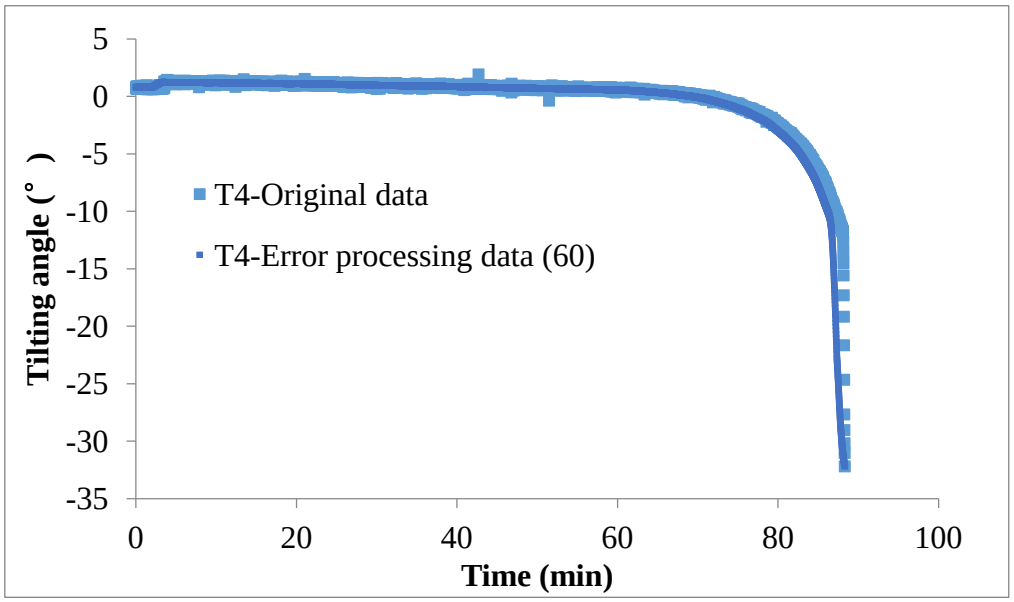

Fig. 7-42 The original data and error-processing data against time

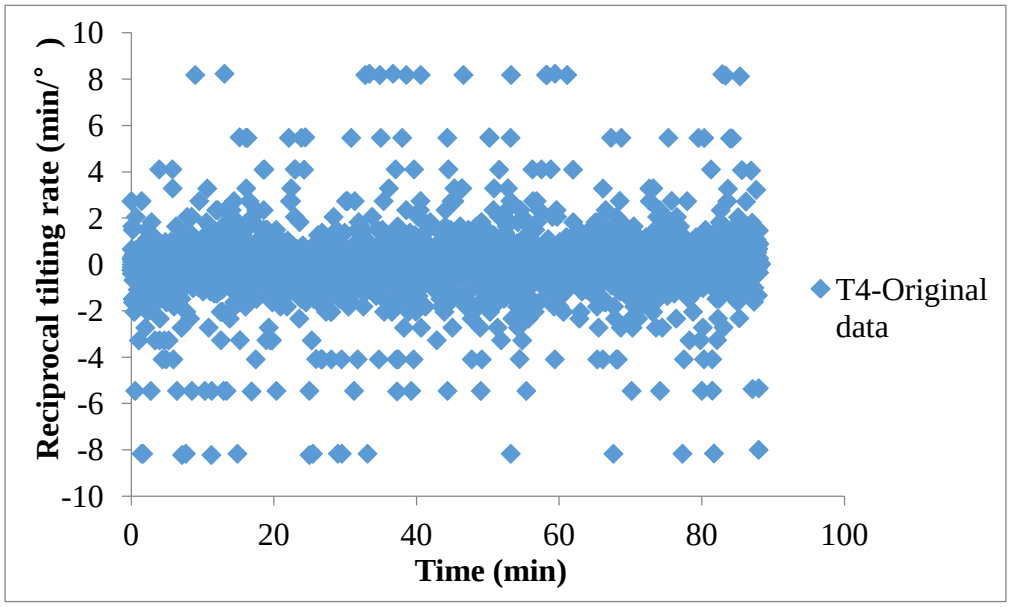

Fig. 7-43 The time history of reciprocal tilting rate using original monitoring data

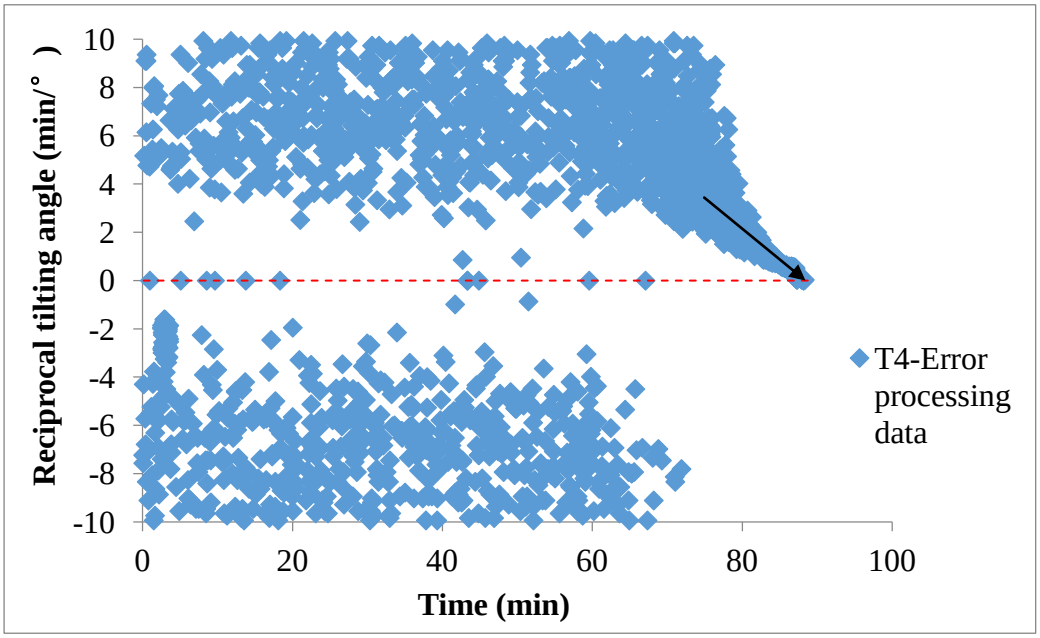

Fig. 7-44 The time history of reciprocal tilting rate using error-processing data

7.5. Field application of this method for landslide early-warning

The criteria for landslide early-warning should comprise the government policy, the economic impact, the safety of local residents and so on. It is reported that currently there is no criterial valid, and most of the criteria for landslide early-warning is on the conservative side because the timming of landslides is very difficult to forecast accurately.

In previous study, the linear trend between the reciprocal tilting angle rate and time has been validated by model tests as well as field cases in the accelerating stage of slope failure. Test results also indicate that it is difficult to predict the slope failure time accurately based on the time history of tilting using the proposed method because of the influence of data noise and flucturation. Considering this situation, the criteria of landslide early-warning for field application based on the new method is developed. As shown in Fig. 7-45, if a linear trend can be approached based on historical data and current data, the future data may locate in three regions, I, II or III as illustrated in the figure. If the future data locates in region I, which means the slope failure may occur earlier than the predicted failure time based on current linear trend, for this situation, we suggest to use the new trend (red dot line) to predict the slope

failure time as shown in the figure. On the other hand, if the future data locates in region II, the slope failure may be postponed. For this case, we suggest to predicted failure time using the current linear trend on the conservative side. Finally, if the future data locates in III region, and follows Trend 1, the slope becomes stable again and no warning will be issued. Otherwise, if the future data locates in III region, and follows Trend 2, the failure time will be predicted based on Trend 2.

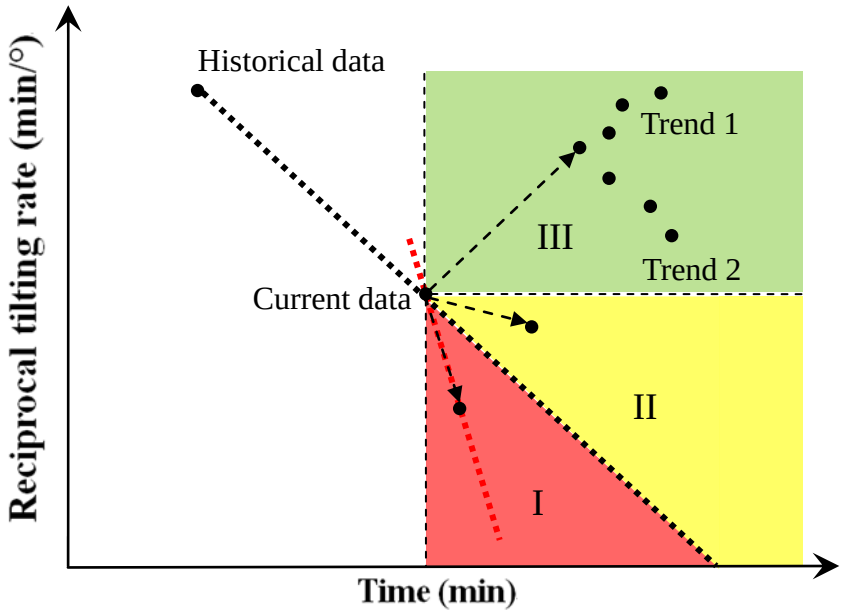

Fig. 7-45 The strategy for landslide early-warning using the proposed method

7.6. The limitation of this method

This new method for landslide prediction based on the time history of tilting of slope surface is applicable for the landslide events with a clear accelerating stage when slope slipping.

However, sometimes the slope failure occurs without a clear accelerating process, as shown in Fig. 7-46. This kind of failure modes may be caused by the fluctuation of rainfall intensity, the soil properties, or other reasons, and the correlation between the triggering factors and failure modes of slopes is still under consideration. As for the slope failure without a clear accelerating stage, the new proposed method is not suitable.

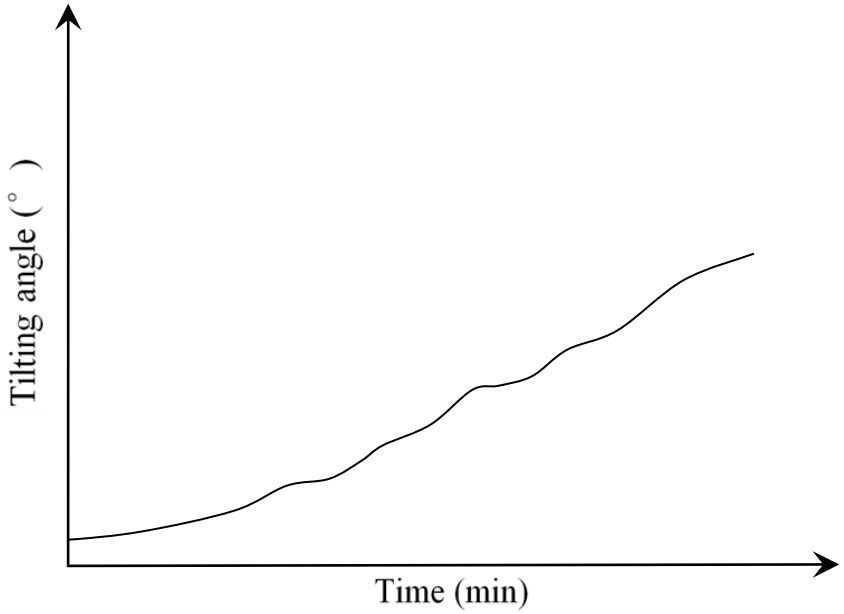

Fig. 7-46 The slope failure without a accelerating stage

For the limitation of the new proposed method, a supplementary method is proposed using the relationship between duration time before slope failure and tilting rate as shown in Fig. 7-47, and the results from more than twenty cases are presented in Fig. 7-48.

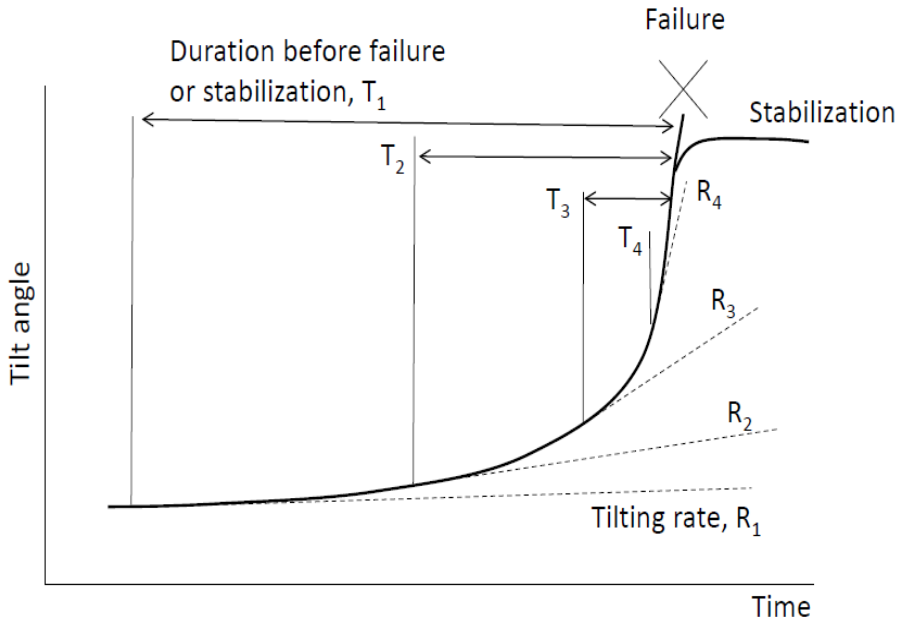

Fig. 7-47 The time history of tilting of slope

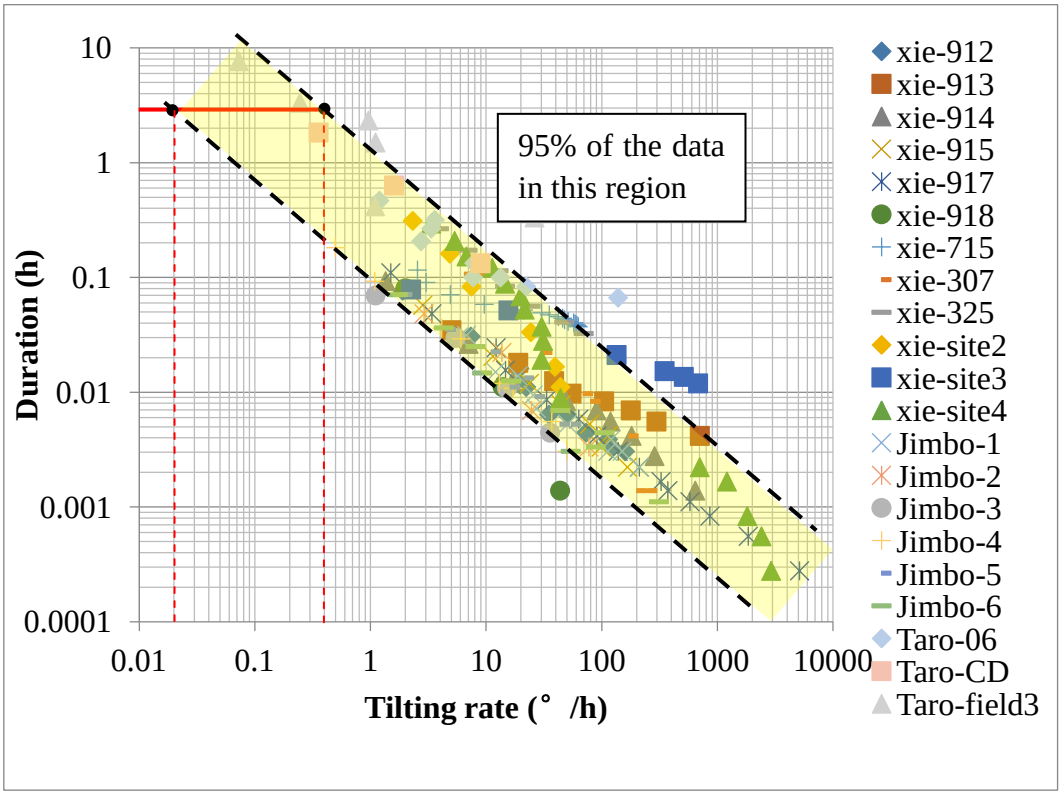

Fig. 7-48 The relationship between tilting rate and duration

Fig. 7-48 indicates that most of the data points located in a region with clear boundary and the tilting rate ranges from 0.02° /h to 0.4° /h when the duration time is 3h. These two tilting rate can be used for precausion and warning of landslides in which no clear accelerating stage ocurres.

Although the supplementary method is easy to use, this method also has some limitation.

1) In the supplimentary method, the tilting rate for precaution and warning are set as 0.02° per hour and 0.4° per hour for all slopes without considering the individual slope conditions, such as the size or the time history of tilting.
2) It is easy to issue the false alarm by using this supplementary method. For example, as for Test 3 shown below.

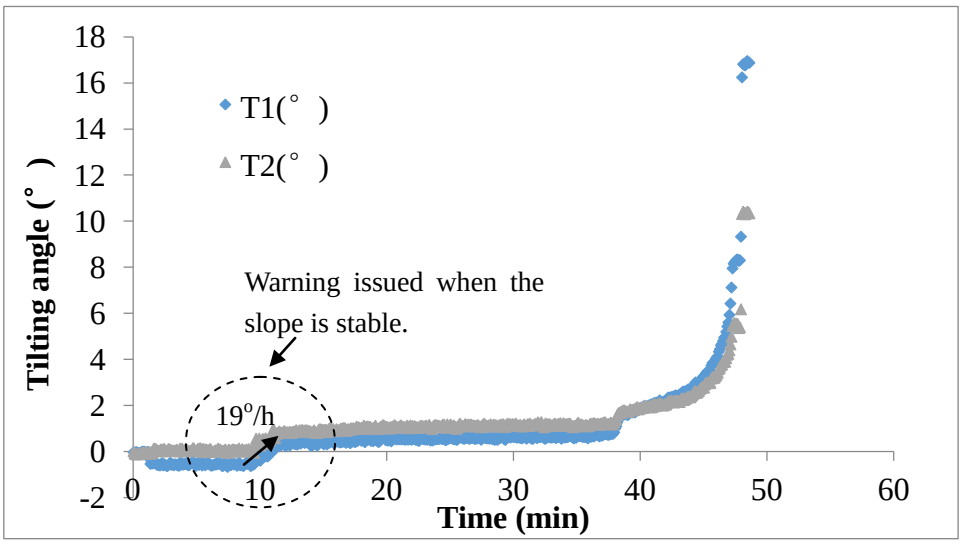

Fig. 7-49 False alarm for a model test

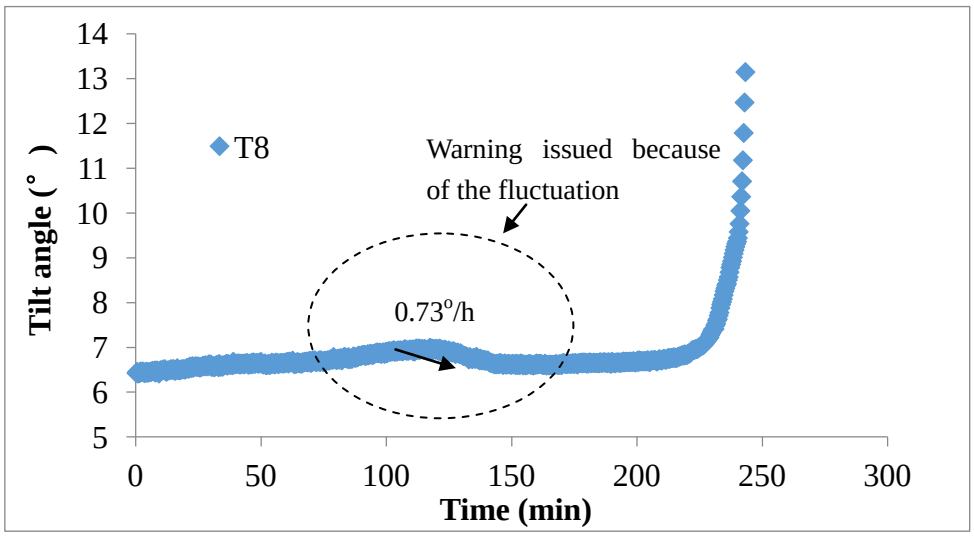

Fig. 7-50 False alarm for a field test

To sum up, if the slope sliding with a clear accelerating stage, the new method based on the time history of tilting of slope can be used to predicted the landslide. On the other hand, if the landslide without a acceleting stage, the warning for landslides can be issued when tilting rate exceeds 0.4° /h or 2.5h /° (300min/°) on a conservative side.

7.7. Summary

In this chapter , a new landslide predicting method using the time history of tilting of slope surface is presented, and the formular is expressed as

$$\frac{dt}{|d\theta|} = -\frac{t}{B} + \frac{t_r}{B} \tag{7-6}$$

Where $B = \frac{1}{r}\left[A \cdot (\alpha - 1)\right]^{\frac{-1}{\alpha - 1}}$, and $\frac{dt}{|d\theta|}$ is the reciprocal of tilting angle rate. t and t_r represent for the current time and failure time respectively.

This new method is validated against laboratory tests as well as field tests. Furthermore, the limitation of this method is also discussed in this part, and a supplementary method based on the data statistical analysis is proposed.

7.8. References

Federico, A., Popescu, M., Murianni, A. (2015). "Temporal prediction of landslide occurrence: a possibility or a challenge?" Italian Journal of Engineering Geology and Environment, 1, 41-60.

Fukuzono, T. (1985). "A new method for predicting the failure time of a slope." Proc. IV, International Conference and Field Workshop on Landslides, Tokyo, 145-150.

Petley, D. N., Petley, D. J., Bulmer, M. H., Carey, J. (2005). "Development of progressive landslide failure in cohesive materials." Geology, 33(3), 201-204.

Saito M. (1965). "Forecasting the time of occurrence of a slope failure." Proceedings of the Sixth International Conference on Soil mechanics and Foundation Engineering, 537-541.

Voight, B. (1989). "A relation to describe rate-dependent material failure." Science,246, 200-203.

CHAPTER 8
CONCLUSIONS AND RECOMMENDATIONS FOR FUTURE RESEARCH

8.1. Introduction

Landslide disasters mainly caused by heavy rainfall and strong earthquakes, are a major threat to human lives and infrastructures. To forecast the failure time of landslides is an essential goal of landslide, and a reasonably accurate prediction of failure time would reduce the quantity of fatalities as well as the cost of property damaged by slope failure.

Nowadays, most of the prediction methods are based on the relationship between failure time and the rate of displacement measured by extensomers. However, as for the installation of extensometers, skillful engineers are required and the stable part of slope to install one end of the extensometers are difficult to be decided in fields. To overcome these shortages, tilting sensors with easy installation and lower costs have been employed in landslides monitoring in recent decades, but some problems for the usage of tilt sensors in slope failure monitoring, such the tilting direction of these sensors and so on are still under consideration. In this study, the three following objectives are investigated by model tests as well as field tests.

1) The tilting directions of tilt sensors are investigated.
2) The relationship between surface displacement of slopes and tilting angle are investigated.
3) A new method to forecast landslides based on time history of tilting of slopes is

investigated.

8.2. Principal conclusions

In this section, the principal conclusions of this study for three objectives are presented repectively.

8.2.1 The investigation for tilting directions of tilt sensors

To investigate the tilting direction of tilt sensors, different types of model tests with the pre-defined slip surface as well as field tests were conducted. In these tests, tilt sensors attached to different length of rods were installed in the slopes, and conclusions are presented in following,

1) Tilt sensors with no rods or short rods located above the slip surface will tilt backward when slope sliding along the slip surface, even though the testing materials and the triggering factors for landslide such as rainfall or tilting the container are different.
2) Tilt sensors with long rods reaching to the slip surface will tilt forward regardless of different testing materials and landslip triggering factors.
3) The tilt sensors installed above the slip surface move together with the slope, and can be used to measure the moving path of the sliding slope.

8.2.2 The investigation for relationship between surface displacement of slopes and tilting angle

The relationship between surface displacement and tilting angle was investigated by conducting small-scaled model tests with pre-defined slip surface. In these model tests, slope models were constructed with different shapes of pre-defined slip surfaces, and tilting angle as well as displacement, were measured during the tests. The tilting angle was measured by tilt sensors embedded into the slopes, while the displacement was obtained with the application of image analysis technique to trace the moving paths of marked points on the slope surface. Then, correlation between slope displacement and tilting angle in the process of slope sliding was studied in these small-scaled model

tests. Additionally, field tests were also carried out to verify the conclusions drew in model tests. In field tests, the extensometers were used for the displacement monitoring and the tilting sensors were employed for measuring the tilting angle of slopes. Principle findings are summarized as following,

1) A linear relationship between the displacement and tilting angle of slopes was found in model tests as well as in field tests regardless of the different testing conditions.
2) Test results shows that the tilt sensors located over the slip surface of slope move together with the sliding part and behave like a pendulum rotating around the center point of the slip surface, while the tilt sensor with long rods reaching the slip surface behave like the inclinometers rotating around the tip point of rods. Although the tilting behaviour of these two type of tilt sensors are different, the linear relationship between the displacement and tilting angle is existed, and can be defined as

$$\Delta s_i = r_i \cdot \left|\Delta \theta_i\right|$$

Where Δs_i is the displacement of slope. r_i represents for the distance between sensors and centers of corresponding slip surfaces, while $\left|\Delta \theta_i\right|$ means the absolute value of tilting angle.

3) Test results shows that the actual distance between the location of tilt sensors and corresponding centers of slip surfaces is close to the rate of fit lines for displacement and tilting angle of slopes. This conclusion indicates that the soil particles in the unstable part of slope rotates around the centers of corresponding slip surfaces, and also indicates that the sliding parts of slopes are similar to semirigid blocks when sliding along the slip surface.

8.2.3 The investigation for the new prediction method of landslides based on the tilting of slope surface

A new method for slope failure prediction with slope tilt angle measurement is proposed based on the failure time and tilting angle rate using the relationship

between surface displacement and tilt angle presented in Chapter 6. Validation of this new method is also carried out against the laboratory tests as well as field tests. Conclusions for this objectives are shown in the following.

1) A new method for landslide prediction based on the time history of tilting of slope surface is presented, and the equation is expressed as follows,

$$\frac{dt}{|d\theta|} = -\frac{t}{B} + \frac{t_r}{B}$$

Where $\frac{dt}{|d\theta|}$ is the reciprocal of tilting rate. t and t_r are the current time and failure time respectively. B is the constant parameter.

2) The new prediction method has been validated against the model tests as well as field tests, and also verified by a field monitoring case using tilting sensors. The validation indicates that this method is suitable to predict the failure time of slope failure with clear accelerating stage.
3) The test results also indicates that rainfall intensity is one of the factors inducing slope deformation, and there is a time delay caused by rainfall intensity change on the slope deformation.
4) For the landslide events without an accelerating stage, a supplementary method based on a data statistic analysis was proposed. In this supplementary method, the value of tilting rate for precausion and warning are set as 0.02^o/h and 0.4^o/h. This method is conservative and possible to issue false warning. Considering these occassions, the supplymentary method combining with the new method to trace the time history of reciprocal of tilting rate can be used to issue the warning for landslides.

8.3. Recommendations for future research

Based on this study, recommendations are made for future research to advance the knowledge on the landslide prediction:

1) The detailed mechanisms and physical explaination for the relationship between

failure time and slope deformation are still under consideration. Some researchers proposed that the acceleting stage of slope can be clarified based on the frictional weakening law which assumes that the frictional rate of materials decreases with the increase of sliding velocity. For this assumption, more laboratory tests should be conducted to explore.

2) The prediction method should be combined with the probability method. Because it is very hard to forecast the timming of landslides precisely.
3) A bigger database should be built for the relationship between duration time and tilting rate, then more precise value for landslides precausion and warning can be proposed.

Appendix 1

The equation for error elimination method is

$$x_i^{'} = \left(\sum_{i-m-1}^{i} x_n \right) / m$$

Where $x_i^{'}$ is the error-processing data, and x_n is the original data, m is the number of data points.

The results are presented in the following figure.

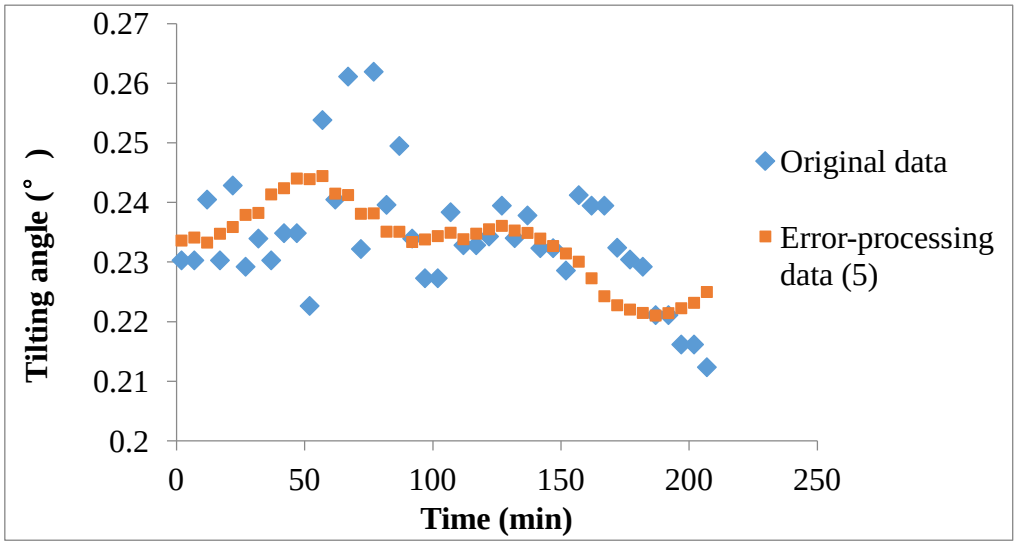

Fig. Appendix-1 The orignial data set and error-processing data set when m=5